

Mining Science and Technology

Горные науки
и технологии

Vol. **8** № **1**
2023



<https://mst.misis.ru/>



Activities of the *Mining Science and Technology (Russia) (Gornye nauki i tekhnologii)* international journal are aimed at developing international scientific and professional cooperation in the field of mining.

The journal target audience comprises researchers, specialists in the field of mining, representatives of academic and professional communities.

The journal publishes original papers describing research findings, experience in the implementation of projects in mining industry, review publications.

The journal seeks to develop interdisciplinary areas that contribute to progress in mining, for example, technological and environmental safety, project organization and management in mining industry, development of territories, legal aspects of natural resource use, and other areas studied by researchers and practitioners. The journal always welcomes new developments. Papers are accepted in English or Russian.

EDITOR-IN-CHIEF

Vadim L. Petrov, Prof., Dr.Sci.(Eng.), National University of Science and Technology MISIS, Moscow, Russian Federation

DEPUTIES EDITOR-IN-CHIEF

Oleg I. Kazanin, Prof., Dr.Sci.(Eng.), National Mineral Resources University "University of Mines", St. Petersburg, Russian Federation

Svetlana A. Epshtein, Dr.Sci.(Eng.), National University of Science and Technology MISIS, Moscow, Russian Federation

EDITORIAL BOARD

Zach Agioutantis, Prof., Ph.D., University of Kentucky, Lexington, Kentucky, USA

Maksim Bogdasarou, Prof., Dr.Sci.(Geol. and Min.), Brest State A. S. Pushkin University, Brest, Belarus

Xuan Nam Bui, Prof., Dr.Sci., Hanoi University of Mining and Geology, Duc Thang – Bac Tu Liem, Hanoi, Vietnam

Carsten Drenstedt, Prof., Ph.D., Freiberg University of Mining and Technology, Freiberg, Germany

Faramarz Doulati Ardejani, Prof., Ph.D., Colledge of Engineering, University of Tehran, Tehran, Iran

Mikhail Ershov, Prof., Dr.Sci.(Eng.), National University of Oil and Gas "Gubkin University", Moscow, Russian Federation

Akper Feyzullaev, Prof., Dr.Sci.(Geol. and Min.), Institute of Geology and Geophysics of the National Academy of Sciences of Azerbaijan, Baku, Azerbaijan

Ochir Gerel, Prof., Dr.Sci.(Geol. and Min.), Geoscience Center, the Mongolian University of Science and Technology, Ulaanbaatar, Mongolia

Zoran Gligorić, Prof., Dr.Sci. (Mining-Underground Mining), University of Belgrade, Belgrade, Republic of Serbia

Monika Hardygora, Prof., Ph.D., Wroclaw University of Technology, Wroclaw, Poland

Nikolae Ilias, Prof., Dr.Sci.(Eng.), University of Petrosani, Petrosani, Romania

Vladislav Kecojevic, Prof., Ph.D., Benjamin M. Statler College of Engineering and Mineral Resources, West Virginia University, Morgantown, West Virginia, USA

Aleksey A. Khoreshok, Prof., Dr.Sci.(Eng.), Gorbachev Kuzbass State Technical University, Kemerovo, Russian Federation

Vladimir I. Klishin, Prof., Dr.Sci.(Eng.), Institute of Coal, Siberian Branch, Russian Academy of Sciences, Kemerovo, Russian Federation

Vladimir N. Koshelev, Prof., Dr.Sci.(Chem.), National University of Oil and Gas "Gubkin University" (Gubkin University), Moscow, Russian Federation

Jyant Kumar, Prof., Ph.D-Geotech.Eng., Indian Institute of Science, Bengaluru, India

Vladimir A. Makarov, Prof., Dr.Sci.(Geol. and Min.), Siberian Federal University, Krasnoyarsk, Russian Federation

Sergey Malafeev, Prof., Dr.Sci.(Eng.), Vladimir State University named after Alexander and Nikolay Stoletovs, Vladimir, Russia

Oleg S. Misnikov, Prof., Dr.Sci.(Eng.), Tver State Technical University, Tver, Russian Federation

Valery V. Morozov, Prof., Dr.Sci.(Eng.), National University of Science and Technology MISIS, Moscow, Russian Federation

Igor Petrov, Dr.Sci.(Eng.), Infomine Research Group LLC, Moscow, Russian Federation

Bakhadirzhan R. Raimzhanov, Prof., Dr.Sci.(Eng.), Uzbekistan Research, Design and Survey Institute for Geotechnology and Nonferrous Metallurgy – O'zGEORANGMETLITI, Tashkent, Uzbekistan

Bayan R. Rakishev, Prof., Dr.Sci.(Eng.), Kazakh National Research Technical University named after K.I. Satpayev, Alma-Ata, Kazakhstan

Oscar Jaime Restrepo Baena, Prof., Ph.D., National University of Colombia, Medellín, Colombia

Alexander N. Shashenko, Prof., Dr.Sci.(Eng.), National Mining University, Dnipro, Ukraine

Vadim P. Tarasov, Prof., Dr.Sci.(Eng.), National University of Science and Technology MISIS, Moscow, Russian Federation

Denis P. Tibilov, Prof., Dr.Sci.(Econ.), Moscow State Institute of International Affairs (University) under the Ministry of Foreign Affairs of Russia, Moscow, Russian Federation

Niyaz Valiev, Prof., Dr.Sci.(Eng.), The Ural State Mining University, Ekaterinburg, Russian Federation

Natalia Zhuravleva, Prof., Dr.Sci.(Eng.), West Siberian Testing Center JSC (WSTCenter JSC), Novokuznetsk, Russian Federation

EDITORIAL COUNCIL

Yuri G. Agafonov, Assoc. Prof., Cand.Sci.(Eng.), National University of Science and Technology MISIS, Moscow, Russian Federation

Michael R. Filonov, Prof., Dr.Sci.(Eng.), National University of Science and Technology MISIS, Moscow, Russian Federation

Leonid A. Plaschansky, Prof., Cand.Sci.(Eng.), National University of Science and Technology MISIS, Moscow, Russian Federation

Yuri I. Razorenov, Prof., Dr.Sci.(Eng.), Platov South-Russian State Polytechnic University, Novocherkassk, Russian Federation

EXECUTIVE SECRETARY

Daria P. Galushka, National University of Science and Technology MISIS, Moscow, Russian Federation

QUARTERLY

FOUNDED in 2016

REGISTRATION

The journal science and applied research journal is registered by the Federal Service for Communication, IT and Mass Communication Control on August 10, 2015. Registration Certificate E-No. ФС77-62652

INDEXATION

Scopus, CAS, EBSCO, DOAJ, РИНЦ, ВИНТИ РАН, Dimensions, BASE, J-Gate, Jisc Library Hub Discover.

FOUNDER AND PUBLISHER



MISIS
UNIVERSITY

The National University of Science and Technology MISIS (NUST MISIS)

CONTACT

4 Leninsky Prospect, Moscow 119049, Russian Federation

Phone: +7 (495) 955-00-77

e-mail: send@misis.ru



This work is licensed under a
Creative Commons Attribution 4.0 License.



Деятельность научно-практического журнала «Горные науки и технологии» (Mining Science and Technology (Russia)) направлена на развитие международного научного и профессионального сотрудничества в области горного дела.

Целевая аудитория журнала – исследователи, специалисты в области горного дела, представители академического и профессионального сообществ.

В журнале публикуются оригинальные статьи, описывающие результаты исследований, опыт реализации проектов в горнопромышленном комплексе, обзорные публикации.

Журнал стремится развивать такие междисциплинарные направления, как технологическая и экологическая безопасность, организация и управление проектами в горной промышленности, развитие территорий, правовые аспекты использования природных ресурсов и другие, которые способствуют прогрессу в горном деле и реализуются исследователями и практиками.

ГЛАВНЫЙ РЕДАКТОР

Петров Вадим Леонидович, проф., д.т.н., НИТУ «МИСиС», г. Москва, Российская Федерация

ЗАМЕСТИТЕЛИ ГЛАВНОГО РЕДАКТОРА

Казанин Олег Иванович, проф., д.т.н., Санкт-Петербургский горный университет, г. Санкт-Петербург, Российская Федерация

Эпштейн Светлана Абрамовна, д.т.н., НИТУ «МИСиС», г. Москва, Российская Федерация

РЕДАКЦИОННАЯ КОЛЛЕГИЯ

Агиутантис Зак, проф., д-р наук, Университет Кентукки, г. Лексингтон, Кентукки, США

Богдасаров Максим Альбертович, проф., д.г.-м.н., Брестский государственный университет им. А.С. Пушкина, г. Брест, Беларусь

Буи Суан Нам, проф., д-р наук, Ханойский университет горного дела и технологии, г. Ханой, Вьетнам

Валиев Нияз Гадым оглы, проф., д.т.н., Уральский государственный горный университет, г. Екатеринбург, Российская Федерация

Герел Очир, проф., д.г.-м.н., Центр геолого-геофизических исследований, Монгольский университет науки и технологии, г. Улан-Батор, Монголия

Глигорич Зоран, проф., д-р наук, Белградский университет, г. Белград, Республика Сербия

Дребенштедт Карстен, проф., д-р наук, Технический университет Фрайбургская горная академия, г. Фрайберг, Германия

Дулати Ардежани Фарамарз, проф., д-р наук, Инженерный колледж, Тегеранский университет, г. Тегеран, Иран

Ершов Михаил Сергеевич, проф., д.т.н., Российский государственный университет нефти и газа (национальный исследовательский университет) им. И.М. Губкина, г. Москва, Российская Федерация

Журавлева Наталья Викторовна, проф., д.т.н., АО «Западно-Сибирский испытательный центр» (АО «ЗСИЦентр»), г. Новокузнецк, Российская Федерация

Илиаш Николае, проф., д.т.н., Университет Петрошани, г. Петрошани, Румыния

Кецоджевич Владислав, проф., д-р наук, Институт инженерного дела и минеральных ресурсов им. Бенджамина М. Статлера Университета Западной Вирджинии, г. Моргантаун, Западная Вирджиния, США

Клишин Владимир Иванович, проф., д.т.н., Институт угля Сибирского отделения Российской академии наук, г. Кемерово, Российская Федерация

Кошелев Владимир Николаевич, проф., д.х.н., Российский государственный университет нефти и газа им. И.М. Губкина, г. Москва, Российская Федерация

Кумар Джьянт, проф., д-р наук (геотехнический инжиниринг), Индийский институт науки (Indian Institute of Science), г. Бангалор, Индия

Макаров Владимир Александрович, проф., д.г.-м.н., Сибирский федеральный университет, г. Красноярск, Российская Федерация

Малафеев Сергей Иванович, проф., д.т.н., Владимирский государственный университет имени А.Г. и Н.Г. Столетовых, г. Владимир, Российская Федерация

Мисников Олег Степанович, проф., д.т.н., Тверской государственный технический университет, г. Тверь, Российская Федерация

Морозов Валерий Валентинович, проф., д.т.н., НИТУ «МИСиС», г. Москва, Российская Федерация

Петров Игорь Михайлович, д.т.н., ООО «Исследовательская группа «Инфолайн»», г. Москва, Российская Федерация

Раимжанов Бахадиржан Раимжанович, проф., д.т.н., Узбекский научно-исследовательский и проектно-испытательский институт геотехнологии и цветной металлургии «O'zGEORANGMETLITI», г. Ташкент, Узбекистан

Ракишев Баян Ракишевич, проф., д.т.н., Казахский национальный исследовательский технический университет им. К.И. Сатпаева, г. Алма-Ата, Казахстан

Рестрепо Баэна Оскар Хайме, проф., д-р наук, Национальный университет Колумбии, г. Медельин, Колумбия

Тарасов Вадим Петрович, проф., д.т.н., НИТУ «МИСиС», г. Москва, Российская Федерация

Тиболов Денис Петрович, проф., д.э.н., Московский государственный институт международных отношений (Университет) Министерства иностранных дел России, г. Москва, Российская Федерация

Фейзуллаев Акпер оглы, проф., д.г.-м.н., Институт геологии и геофизики (ИГТ) Национальной Академии Наук Азербайджана, г. Баку, Азербайджан

Хорешок Алексей Алексеевич, проф., д.т.н., Кузбасский государственный технический университет им. М.С. Горбачева, г. Кемерово, Российская Федерация

Шашенко Александр Николаевич, проф., д.т.н., Национальный горный университет, г. Днепр, Украина

Хардигора Моника, проф., д-р наук, Вроцлавский технологический университет, г. Вроцлав, Польша

РЕДАКЦИОННЫЙ СОВЕТ

Агафонов Юрий Григорьевич, доц., к.т.н., НИТУ «МИСиС», г. Москва, Российская Федерация

Плащанский Леонид Александрович, проф., к.т.н., НИТУ «МИСиС», г. Москва, Российская Федерация

Разоренов Юрий Иванович, проф., д.т.н., Южно-Российский государственный политехнический университет (НПИ) им. М. И. Платова, г. Новочеркасск, Российская Федерация

Филонов Михаил Рудольфович, проф., д.т.н., НИТУ «МИСиС», г. Москва, Российская Федерация

ОТВЕТСТВЕННЫЙ СЕКРЕТАРЬ

Галушка Дарья Петровна, НИТУ «МИСиС», г. Москва, Российская Федерация

ПЕРИОДИЧНОСТЬ 4 раза в год

ОСНОВАН в 2016 году

РЕГИСТРАЦИЯ

Зарегистрирован Федеральной службой по надзору в сфере связи, информационных технологий и массовых коммуникаций 10 августа 2015 года.

Свидетельство о регистрации Эл № ФС77-62652.

ИНДЕКСИРОВАНИЕ

Scopus, CAS, EBSCO, DOAJ, РИНЦ, ВИНТИ РАН, Dimensions, BASE, J-Gate, Jisc Library Hub Discover.



Журнал открытого доступа.

УЧРЕДИТЕЛЬ И ИЗДАТЕЛЬ



Национальный исследовательский технологический университет «МИСиС» (НИТУ «МИСиС»)

АДРЕС УЧРЕДИТЕЛЯ И ИЗДАТЕЛЯ

119049, г. Москва, Ленинский проспект, д. 4

КОНТАКТЫ РЕДАКЦИИ

Адрес: 119049, г. Москва, Ленинский проспект, д. 4

Телефон: +7 (495) 955-00-77

e-mail: send@misis.ru



Контент доступен под лицензией Creative Commons Attribution 4.0 License.



CONTENTS

MINERAL RESOURCES EXPLOITATION

- The engineering and geological substantiation of the resource potential of the bed of the South China Sea 5
Yu. V. Kirichenko, T. T. Q. Ngo, M. V. Shchyokina

MINING ROCK PROPERTIES. ROCK MECHANICS AND GEOPHYSICS

- Amplitude-frequency response of a helically-wound fiber distributed acoustic sensor (DAS) 13
A. V. Chugaev, M. V. Tarantin

- Effect of strain amplitude and confining pressure on the velocity and attenuation of *P* and *S* waves in dry and water-saturated sandstone: an experimental study 22
E. I. Mashinskii

- Influence of random parameter joint length on rock electrical conductivity 30
P. E. Sizin, A. S. Voznesenskii, L. K. Kidima-Mbombi

BENEFICIATION AND PROCESSING OF NATURAL AND TECHNOGENIC RAW MATERIALS

- The effect of clay minerals on in-situ leaching of uranium 39
O. F. Petukhov, I. U. Khalimov, V. P. Istomin, N. M. Karimov

SAFETY IN MINING AND PROCESSING INDUSTRY AND ENVIRONMENTAL PROTECTION

- Study of gas hazard pattern in underground workings after blasting 47
D. V. Olkhovskiy, O. S. Parshakov, S. A. Bublik

MINING MACHINERY, TRANSPORT, AND MECHANICAL ENGINEERING

- Effect of operating conditions of mine monorail locomotives on the durability of drive wheel polymeric rims 59
E. M. Arefiev, K. A. Ryabko

- Behaviour pattern of rock mass haulage energy intensity in deep pits 68
A. G. Zhuravlev, I. A. Glebov, V. V. Chernykh

POWER ENGINEERING, AUTOMATION, AND ENERGY PERFORMANCE

- Equivalent circuit for mine power distribution systems for the analysis of insulation leakage current 78
A. V. Pichuev, V. L. Petrov

EXPERIENCE OF MINING PROJECT IMPLEMENTATION

- The assessment of the level of digitalization and digital transformation of oil and gas industry of the Russian Federation 87
V. V. Yurak, I. G. Polyanskaya, A. N. Malyshev



СОДЕРЖАНИЕ

РАЗРАБОТКА МЕСТОРОЖДЕНИЙ ПОЛЕЗНЫХ ИСКОПАЕМЫХ

Инженерно-геологическое обоснование ресурсного потенциала
дна Южно-Китайского моря

5

Ю.В. Кириченко, Ч.Т.К. Нго, М.В. Щёкина

СВОЙСТВА ГОРНЫХ ПОРОД. ГЕОМЕХАНИКА И ГЕОФИЗИКА

Амплитудно-частотный отклик распределенного акустического сенсора DAS
со спиральной намоткой волокна

13

А.В. Чугаев, М.В. Тарантин

Влияние амплитуды деформации и всестороннего давления на скорость и затухание

P- и *S*-волн в сухом и водонасыщенном песчанике: экспериментальное исследование.....

22

Э.И. Машинский

Влияние длины трещин со случайными параметрами

на электрическую проводимость горных пород

30

П.Е. Сизин, А.С. Вознесенский, Л.К. Кидима Мбомби

ОБОГАЩЕНИЕ, ПЕРЕРАБОТКА МИНЕРАЛЬНОГО И ТЕХНОГЕННОГО СЫРЬЯ

Влияние глинистых минералов на процесс подземного выщелачивания урана

39

О.Ф. Петухов, И.У. Халимов, В.П. Истомин, Н.М. Каримов

ТЕХНОЛОГИЧЕСКАЯ БЕЗОПАСНОСТЬ В МИНЕРАЛЬНО-СЫРЬЕВОМ КОМПЛЕКСЕ И ОХРАНА ОКРУЖАЮЩЕЙ СРЕДЫ

Исследование динамики газовой обстановки подземных выработок
после проведения взрывных работ

47

Д.В. Ольховский, О.С. Паршаков, С.А. Бублик

ГОРНЫЕ МАШИНЫ, ТРАНСПОРТ И МАШИНОСТРОЕНИЕ

Влияние условий эксплуатации шахтных монорельсовых локомотивов
на долговечность полимерных ободьев приводных колес

59

Е.М. Арефьев, К.А. Рябко

Закономерности изменения энергоемкости транспортирования

горной массы транспортом глубоких карьеров

68

А.Г. Журавлев, И.А. Глебов, В.В. Черных

ЭНЕРГЕТИКА, АВТОМАТИЗАЦИЯ И ЭНЕРГОЭФФЕКТИВНОСТЬ

Обоснование схемы замещения шахтной подземной электрической сети
для анализа режимов утечки тока через изоляцию

78

А.В. Пичуев, В.Л. Петров

ОПЫТ РЕАЛИЗАЦИИ ПРОЕКТОВ В ГОРНОПРОМЫШЛЕННОМ СЕКТОРЕ ЭКОНОМИКИ

Оценка уровня цифровизации и цифровой трансформации нефтегазовой отрасли РФ

87

В.В. Юрак, И.Г. Полянская, А.Н. Малышев



MINERAL RESOURCES EXPLOITATION


Research paper

<https://doi.org/10.17073/2500-0632-2022-09-14>

UDC 553.068.56:551.462



The engineering and geological substantiation of the resource potential of the bed of the South China Sea

Yu. V. Kirichenko¹ , Tran Thien Quy Ngo² , M. V. Shchyokina¹  ¹ University of Science and Technology MISiS, Moscow, Russian Federation² Vietnam National University Ho Chi Minh City, University of Science, Ho Chi Minh City, Vietnam mshchekina@yandex.ru

Abstract

The program for the development of the national economy based on own mineral raw materials as adopted in the Socialist Republic of Vietnam requires an increase the volumes of minerals. This includes both liquid hydrocarbons, and non-traditional solid minerals. This paper examines the resource base of mineral deposits in the South China Sea. The objective was to determine and scientifically establish classification criteria for zoning (regionalization), as well as to identify prospective areas with deposits of ferromanganese formations and other solid minerals. An analysis was undertaken of placers on the shelf and deposits of ferromanganese formations in the deep areas of the Vietnam Sea. A multiparameter analysis of the hydrological, geophysical, engineering and geological, environmental conditions of the deposit positions was conducted. In addition, criteria for the prospects of the formation and development of deposits of ferromanganese formations were established. These criteria enabled areas with different prospectivity ratings to be identified. Within the South China Sea, zones (areas) with a high, medium, and low potential for the presence of nodules were identified. Similar zoning for the crusts was also identified. The areas of these zones were determined. The results of the research established that the total potential area of ferromanganese nodules is 91,480 km². The area with the potential of ferromanganese crusts is 2,421.6 km², while the area of coexistence of nodules and crusts is 18,777 km². Furthermore, priority regions for future exploration are those with high nodule potential covering an area of 18,110 km² and the regions of high crust potential with an area of 882.6 km². Based on the materials obtained, the bed of the Vietnamese Exclusive Zone of the South China Sea was zoned. Maps of the resource and predictive prospects of the seabed were drawn, and the prospecting and exploration operations can be established within this framework.

Key words

resource potential, shelf, deep water areas, multiple factor analysis, placers, ferromanganese formations, deposit, nodules, crusts, predictive prospects, zoning, South China Sea, Vietnam


For citation

Kirichenko Yu.V., Ngo T.T.Q., Shchyokina M.V. The engineering and geological substantiation of the resource potential of the bed of the South China Sea. *Mining Science and Technology (Russia)*. 2023;8(1):5–12. <https://doi.org/10.17073/2500-0632-2022-09-14>

РАЗРАБОТКА МЕСТОРОЖДЕНИЙ ПОЛЕЗНЫХ ИСКОПАЕМЫХ

Научная статья

Инженерно-геологическое обоснование ресурсного потенциала дна Южно-Китайского моря

Ю. В. Кириченко¹ , Чан Тхиен Кюи Нго² , М. В. Щёкина¹  ¹ Университет науки и технологий МИСИС, г. Москва, Российская Федерация² Вьетнамский национальный университет Хошимина, Университет естественных наук, г. Хошимин, Вьетнам mshchekina@yandex.ru

Аннотация

Принятая в Социалистической Республике Вьетнам программа развития народного хозяйства, базирующегося на собственной минерально-сырьевой базе, требует повышения объемов добычи полезных ископаемых, в том числе жидких углеводородов, вовлечения нетрадиционных видов твердых полезных ископаемых. Исследована ресурсная база месторождений полезных ископаемых Южно-Китайского моря. Идея исследований заключалась в определении и научном обосновании классификационных критериев зонирования (районирования) и выделении перспективных участков с залежами



железомарганцевых образований и других твердых полезных ископаемых. Проведен анализ россыпных месторождений на шельфе и залежей железомарганцевых образований в глубинных районах Вьетнамского моря. Проведен многосторонний анализ гидрологических, геофизических, инженерно-геологических, экологических условий залегания месторождений, определены критерии перспективности образований и развития залежей железомарганцевых образований. Эти критерии позволили произвести выделение участков с различным рейтингом перспективности. В пределах Южно-Китайского моря выделены зоны (участки) с высоким, средним и низким потенциалом нахождения конкреций, а также выявлена аналогичная зональность для корок. Определены площади указанных зон. Результаты исследований показали, что общая потенциальная площадь железомарганцевых конкреций составляет 91 480 км², площадь с потенциалом железомарганцевых корок – 2421,6 км² и площадь сосуществования конкреций и корок – 18 777 км². При этом приоритетными районами для будущих разведок являются районы с высоким потенциалом конкреций площадью 18 110 км² и районы с высоким потенциалом корок площадью 882,6 км². На основании полученных материалов произведено районирование дна Вьетнамской эксклюзивной зоны Южно-Китайского моря и составлены карты ресурсно-прогнозной перспективности морского дна, в пределах которых необходимо организовывать поисково-разведочные работы.

Ключевые слова

ресурсный потенциал, шельф, глубоководные районы, многофакторный анализ, россыпи, железомарганцевые образования, месторождение, конкреции, корки, прогнозная перспективность, районирование, Южно-Китайское море, Вьетнам

Для цитирования

Kirichenko Yu.V., Ngo T.T.Q., Shchyokina M.V. The engineering and geological substantiation of the resource potential of the bed of the South China Sea. *Mining Science and Technology (Russia)*. 2023;8(1):5–12. <https://doi.org/10.17073/2500-0632-2022-09-14>

The program for the development of the national economy based on own mineral raw material, as adopted in the Socialist Republic of Vietnam requires an increase in the volumes of mineral extraction. This includes both liquid hydrocarbons, and solid minerals (SM), deposits of which are virtually not extant on land¹ [1–3].

The country is characterized by the long coastline of the western margin of the Pacific Ocean, the proximity of the northwestern border of the megabelt and the northern subequatorial belt of ferromanganese nodules. The results of the geological studies of the seabed, the positive experience in the development of placers on the coast and shelf, as well as the intensification and claims of China for the development of the South Chinese Sea (SCS) predetermine the relevance of the extension of geological exploration and development of offshore deposits by Vietnam [1–3, 4, 5].

Marine solid minerals (SM) contain the components of strategic importance for the economic and industrial development of Vietnam. They are especially important in the field of high-tech engineering, and include placers of ilmenite, rutile, zircon, monazite, cassiterite, inter alia, ferromanganese concretions and crusts, polymetallic sulfides and, potentially, enriched polymetallic mud [6, 7].

Thus, the exploration and prospecting of marine minerals in Vietnam are of great importance. They will contribute to a focused and rational use of mineral resources for the process of industrialization process, the consolidation of the country's sovereignty in the Exclusive Economic Zone, and the development of Vietnam towards becoming a maritime power. Vietnam adopted the Strategy for Sustainable Maritime Economic Development of the country up to 2020 (starting from 2007), 2030 and further up to 2045².

In order to address the issue of the development of the resource base, engineering and geological substantiation of the prospects for the development of offshore deposits of solid minerals of Vietnam was undertaken. This was based on the use of maps of predictive resource zoning of the seabed. The purpose of the research was to identify and scientifically establish the classification criteria for zoning (regionalization), as well as to identify prospective areas with deposits of ferromanganese formations (FMF) and other solid minerals (SM). Classification attributes were used with regard to the development of zoning maps. This was in accordance with the priority of prospecting for offshore deposits and the development of tools and methods for engineering and geological studies of seabed deposits in the shelf zone and deep areas of the Vietnam Sea (the Exclusive Economic Zone) [2, 3].

¹ Resolution No. 36-NQ/TW (October 22, 2018) "Vietnam's marine economy to 2030 and vision to 2045"

² Resolution No. 36-NQ/TW (October 22, 2018) "Vietnam's marine economy to 2030 and vision to 2045"

For this purpose, we conducted the following studies:

- analysis and assessment of the current level and state of offshore exploration, as well as the extent to which Vietnam has developed shelf zone and deep areas in the South China Sea;

- assessment of the conditions for the formation and accumulation of building materials and placers in the coastal areas as well as the shelf zone, as prerequisites for identifying zones and regions with potential and prospective conditions for the formation and development of ferromanganese deposits in the seas of Vietnam;

- survey and analysis of the potential of solid minerals of the seabed of Vietnam, including the results of studies of deposits of building materials, placers in the Vietnam waters and ferromanganese deposits in the deep areas of the South China Sea;

- a bathymetric map of the bed of the SCS was drawn; other factors influencing the formation and development of ferromanganese deposits in the World Ocean were also summarized and analyzed for the purpose of identifying these features in the Vietnam Sea (Fig. 1);

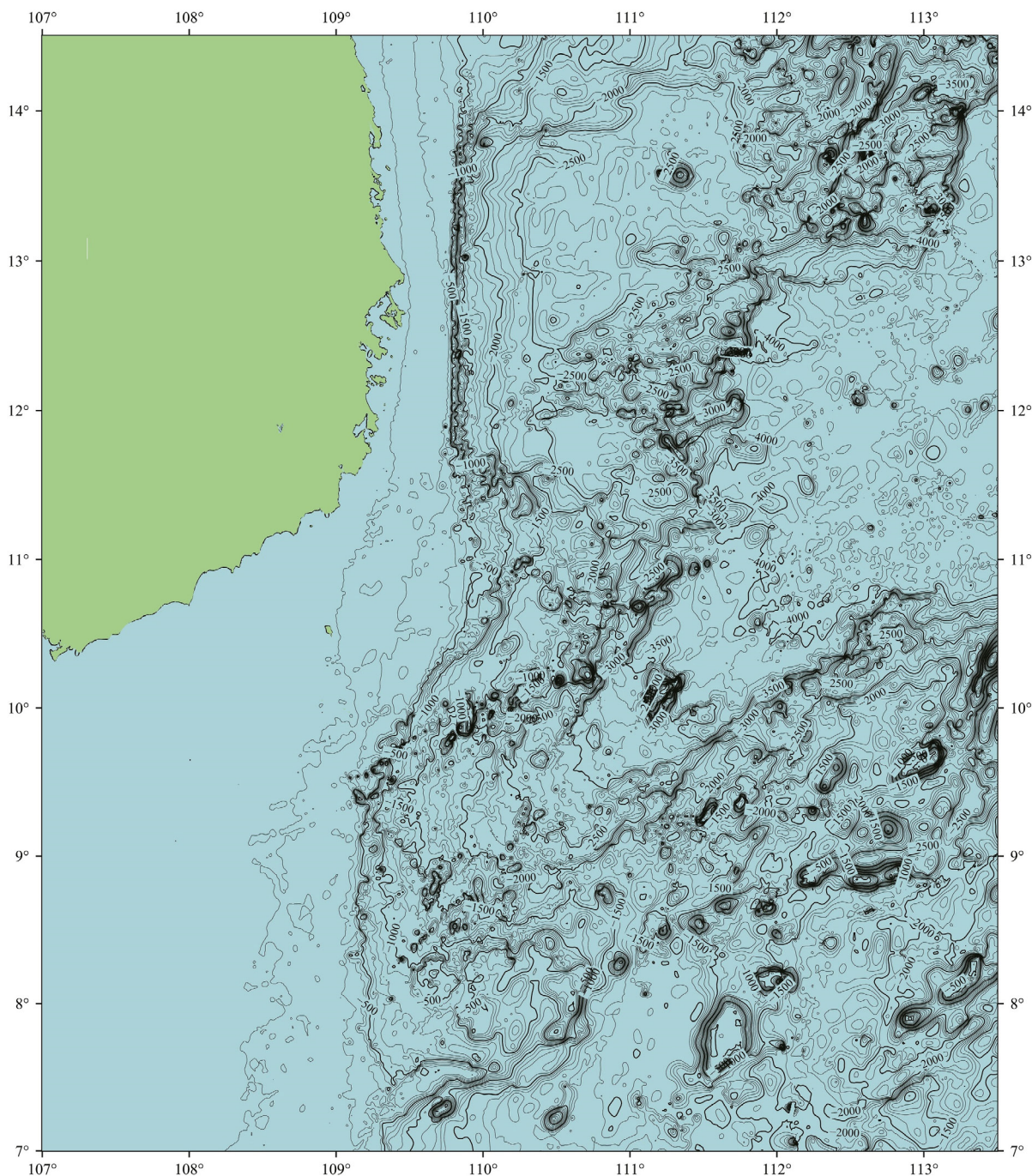


Fig. 1. Bathymetric map of the bed of the South China Sea



– favorable criteria impacting the formation of ferromanganese ores were identified for the purpose of zoning the bed of the SCS. This took into account the potential for their formation in the form of nodules and crusts for future prospecting and exploration.

These studies used a range of results from previous studies in various fields, i.e. geology [4, 5, 8, 9], geophysics [5], petrography [5, 10], geochemistry [6, 7], hydrology [7, 11–13], oceanography [7, 11, 12, 14], geomorphology [6, 7, 9, 13, 15], engineering geology [7, 16–18], mineralogy [19], seabed topography [20], inter alia [21, 22].

Criteria were developed on the basis of multiple factor analysis. They are represented in Tables 1–3.

The zoning criteria are arranged in descending order of prospectivity from 1 to 6. Criteria 1, 2, 3 are essential in the conditions of the SCS and they shall be given priority consideration.

In certain cases, in addition to these criteria, geomorphological criteria are used, in order to assess continental shelves, valleys between seamounts and the topography of seamount tops.

The criteria used to identify the areas unfavorable for the formation and growth of ferromanganese nodules and crusts are presented in Table 4.

Table 1

Criteria for zoning of deposits of ferromanganese nodules

No.	Criterion	Value of the criterion for the rating assigned		
		high	medium	low
1	Sea depth, m	3,000–4,000	> 4,000	2,000–3,000 abyssal plains near continental slope and uplift
2	Seabed slope angles, deg	0–3	0–3	0–3
3	Age of formation of seabed configuration (seamounts/plains), myr	Multiple millions of years (Very favorable conditions – an old seabed: 15.5–24 myr)	Seabed formed 15.5–24 myr ago	Multiple millions of years
4	Presence of nuclei for the formation and development of nodules	Present. The areas being away from submarine volcanoes, seamounts being rich in silica bioclast	Present. Areas away from submarine volcanoes, seamounts rich in silica bioclast	Present
5	Current velocity, cm/s	< 4 for the diagenetic genesis	< 3	No effect
6	Sediments on the seabed surface	Virtually none	Virtually none	Virtually none

Table 2

Criteria for zoning of deposits of ferromanganese crusts

No.	Criterion	Value of the criterion for the rating assigned		
		high	medium	low
1	Sea depth, m	800–1,800	500–800; and > 1,800	500 m to the seabed
2	Seabed slope angles, deg	15–40	15–40	15–40
3	Age of formation of seabed configuration (seamounts/plains), myr	Multiple millions of years (>3). Older age favors to the formation of ores	Multiple millions of years (>3). Older age favors to the formation of ores	Relatively young surface
4	Bedrock surface	No sediment on the basalt surface (very high), on the limestone surface, granite, rhyolite (high)	No sediment	Sediment in some places
5	Current velocity, cm/s	4–5	4–15 (500–800 m); and < 3 (at the depths > 1,800 m)	No need to consider
6	Sediments on the seabed surface	None	None	None



These criteria enable the bed of the Vietnam Sea to be zoned, and a number of areas identified, where it is advisable to undertake prospecting and exploration for the presence of ferromanganese formations (Fig. 2).

The results of studies of the Exclusive Maritime Economic Zone of Vietnam, the potential classification and the corresponding areas of ferromanganese deposits are as follows:

Group of nodules

– The area with a high potential for nodules is 18,110 km², the largest area of which is 13,460 km², located in the central valley in the southwest of the South China Sea.

– The area with a medium potential for nodules is 28,400 km².

– The area with a low potential for nodules is 44,970 km², including 4 regions, the largest of which with an area of 34,110 km² is located in the north of the territory under investigation.

Group of crusts

The total area is 2,421.6 km², including:

- the area with a high potential of 882.6 km²,
- the areas with medium and low potential of 1,539 km².

Group of simultaneous (coexisting) nodules and crusts with an area of 18,777 km².

These maps constitute a basis for the planning of exploration works within the Vietnam Sea, enabling a high extent of detection of the deposits of ferromanganese formations and further planning of mining operations.

Table 3

Criteria for zoning of deposits of ferromanganese nodules and crusts

No.	Criterion	Value of the criterion for the rating assigned	
		medium	low – no
1	Sea depth, m	500–4,000	500–4,000
2	Seabed slope angles, deg	7–15	7–15
3	Age of formation of seabed configuration (seamounts/plains), myr	> 3	< 3
4	Bedrock surface	Nuclei present. Sediment accumulation on the surface is heterogeneous	Nuclei present. Sediment accumulation on the surface is heterogeneous
5	Nucleus for the development of nodules		
6	Current velocity, cm/s	4–15	4–15

Table 4

Areas without potentially perspective conditions for the formation of nodules and crusts

No.	Criterion	Crusts	Nodules
1	Sea depth, m	< 500 m	Continental shelf, depth up to 500 m. Plains exhibit a gentle slope angle (0° – 3°) on continental slopes, seamounts exhibit gentle tops
2	Seabed slope angles, deg	Flat top of seamounts (0–3)	3–7 and > 40
3	Age of formation of seabed configuration (seamounts/plains), myr	Relatively young surface, very young volcanics	No affect
4	Bedrock surface	No need to consider	Does not affect
5	Presence of nuclei for the formation and development of nodules	No affect	Present
6	Current velocity, cm/s	No need to consider	No affect

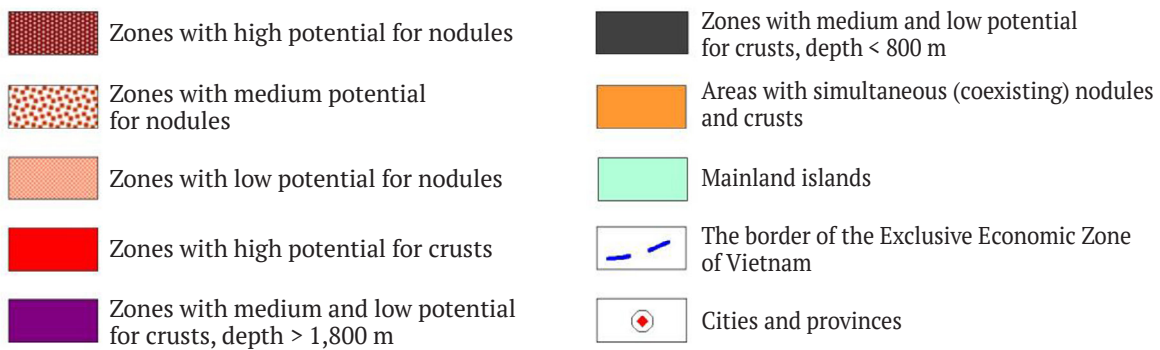
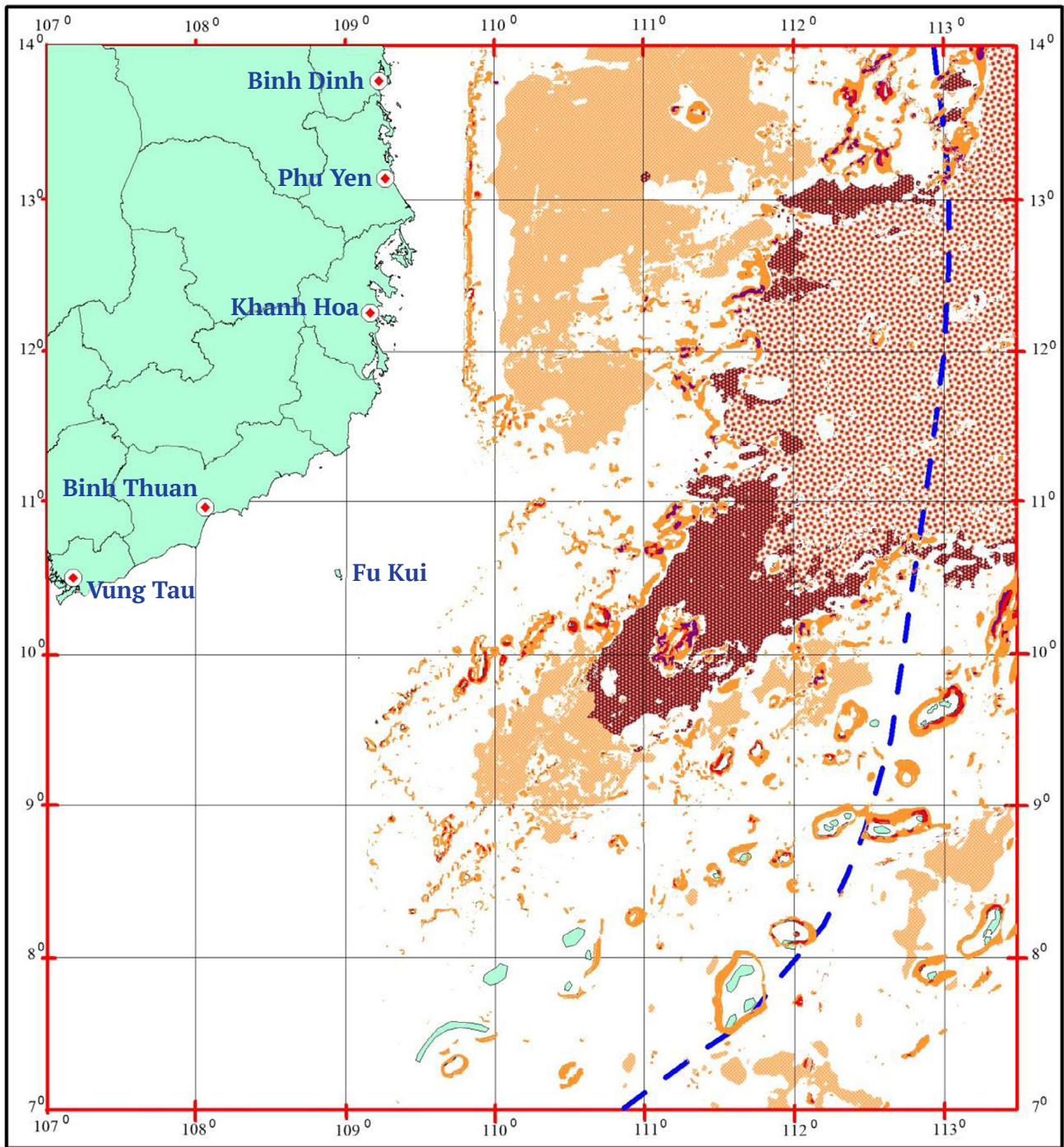


Fig. 2. Map of the zoning of the bed of the SCS according to the potential for finding promising ferromanganese deposits (the area/map of exploration zones)



Conclusions

The Vietnamese Sea represents a typical geological structure of marginal seas. It includes a shelf with placers, abyssal plains with seamounts bearing deposits of ferromanganese formations of various types, all of which considerably enhance the mineral resource and raw material potential of Vietnam.

The predictive zoning of the SCS bed for areas for prospecting and exploration works shall be based on the following factors: classification criteria identified in the results of the multiple factor analysis of known underwater solid minerals (SM) deposits; existing data from geological, hydrological, geophysical, engineering and geological, and other studies.

The zoning areas with different potential for nodules and crusts to be identified in the following

categories: high, medium and low; on the South China Sea bed (as well as within the Exclusive Economic Zone of Vietnam), and for these areas to be defined.

The results of the research revealed that the total potential area of ferromanganese nodules is 91,480 km²; the area with the potential of ferromanganese crusts is 2,421.6 km²; and the area of coexistence of nodules and crusts is 18,777 km². Based on the above, the priority regions for future exploration are the regions of high nodules potential with an area of 18,110 km², and the regions of high crust potential with an area of 882.6 km².

It is recommended that offshore exploration works in the SCS be planned and conducted on the basis of the perspective areas and classification attributes established herein.

References

1. Ngo Tran Thien Quy, Kirichenko Yu.V., Shchyokina M.V. Promising and provable solid mineral resources in the shelf and abyssal deposits in Vietnam. *Mining Informational and Analytical Bulletin*. 2021;(9):103–112. (In Russ.) https://doi.org/10.25018/0236_1493_2021_9_0_103
2. Kirichenko Yu.V., Ngo Tran Thien Quy, Pham Ba Trung et al. Geological characteristics, potential and genesis of iron-manganese ore formation at the bottom of the southwestern part of the South China Sea. Part 1. Geological Characteristics of Subsea Deposits, Exploration Methods and Techniques. *Russian Mining Industry*. (In Russ.) 2022;(1):104–109. <https://doi.org/10.30686/1609-9192-2022-1-104-109>
3. Kirichenko Yu.V., Ngo Tran Thien Quy, Pham Ba Trung et al. Geological characteristics, potential and genesis of iron-manganese ore formation at the bottom of the southwestern part of the South China Sea. Part 2. Results of studying ore samples from the bottom of the South China Sea. *Russian Mining Industry*. 2022;(2):67–75. (In Russ.) <https://doi.org/10.30686/1609-9192-2022-2-67-75>
4. Le D.T. Fundamental Problems. In: *South China Sea*. Vol. 1. Hanoi: Publ. House of Natural Science and Technology; 2009. 317 p.
5. Mai T.T. Geology and Geophysics. In: *South China Sea*. Vol. 3. Hanoi: Publ. House of Natural Science and Technology; 2003. 458 p.
6. Hein J.R., Koschinsky A. Deep-ocean ferromanganese crusts and nodules. In: *Treatise on Geochemistry*. 2nd ed. 2014;13:273–291. <https://doi.org/10.1016/B978-0-08-095975-7.01111-6>
7. Sharma R. (ed.) *Deep sea mining: resource potential, technical and environmental considerations*. Springer Cham; 2017. 548 p. <https://doi.org/10.1007/978-3-319-52557-0>
8. Chao Sh.-Y., Shaw P.-T., Wu S.Y. Deep water ventilation in the South China Sea. *Deep Sea Research Part I: Oceanographic Research Papers*. 1996;43(4):445–466. [https://doi.org/10.1016/0967-0637\(96\)00025-8](https://doi.org/10.1016/0967-0637(96)00025-8)
9. Gillard B., Purkiani K., Chatzievangelou D. et al. Physical and hydrodynamic properties of deep sea mining-generated, abyssal sediment plumes in the Clarion Clipperton Fracture Zone (eastern-central Pacific). *Elementa: Science of the Anthropocene*. 2019;7(1):5. <https://doi.org/10.1525/elementa.343>
10. Long B.H., Thu P.M., Trung N.N. Initial understanding and assessment of role of oceanographic features for ferromanganese crust and nodules in the East Vietnam Sea. *Vietnam Journal of Marine Science and Technology*. 2020;20(4):383–397. <https://doi.org/10.15625/1859-3097/15775>
11. Du D., Ren X., Yan S. et al. An integrated method for the quantitative evaluation of mineral resources of cobalt-rich crusts on seamounts. *Ore Geology Reviews*. 2017;84:174–184. <https://doi.org/10.1016/j.oregeorev.2017.01.011>
12. Hein J.R., Conrad T.A., Dunham R.E. Seamount characteristics and mine-site model applied to exploration- and mining-lease-block selection for cobalt-rich ferromanganese crusts. *Marine Georesources & Geotechnology*. 2009;27:160–176. <https://doi.org/10.1080/10641190902852485>
13. Yeo I.A., Howarth S.A., Spearman J. et al. Distribution of and hydrographic controls on ferromanganese crusts: Tropic Seamount, Atlantic. *Ore Geology Reviews*. 2019;114:103131. <https://doi.org/10.1016/j.oregeorev.2019.103131>



14. Wang P., Li Q. (eds.) *The South China sea: paleoceanography and sedimentology*. Springer Dordrecht; 2009. 516 p. <https://doi.org/10.1007/978-1-4020-9745-4>
15. Yamazaki T., Sharma R. Morphological features of Co-rich manganese deposits and their relation to seabed slopes. *Marine Georesources and Geotechnology, Marine Georesources & Geotechnology*. 2000;18(1):43–76. <https://doi.org/10.1080/10641190009353782>
16. Genov R., Dimitrov T., Kirov B. et al. *Geology and mineral resources of the World Ocean*. Warsaw: Intermorco; 1990. 756 p. (In Russ.)
17. Hein J.R., Konstantinova N., Cherkashov G. et al. Arctic deep water ferromanganese-oxide deposits reflect the unique characteristics of the Arctic ocean. *Geochemistry, Geophysics, Geosystems*. 2017;18(11):3771–3800. <https://doi.org/10.1002/2017GC007186>
18. Emelyanov E. *The barrier zones in the ocean*. Springer Berlin, Heidelberg; 2005. 631 p. <https://doi.org/10.1007/b137218>
19. Hoang N., Trinh P.T. Synthesis of petrographic and geochemical characteristics of Neogene-Quaternary effusives and mantle dynamics of the East Sea and adjacent areas. *Journal of Geology. Series A*. 2009;312(5–6):39–57. (In Vietnamese)
20. Conrad T., Hein J.R., Paytan A., Clague D.A. Formation of Fe-Mn crusts within a continental margin environment. *Ore Geology Reviews*. 2017;87:25–40. <https://doi.org/10.1016/j.oregeorev.2016.09.010>
21. Yang K., Yao H., Ma W. et al. A step-by-step relinquishment method for cobalt rich crusts: a case study on Caiqi Guyot, Pacific Ocean. *Marine Georesources & Geotechnology*, 2022;40(9):1139–1150. <https://doi.org/10.1080/1064119X.2021.1973161>
22. Zhong Y., Chen Zh., González F. J. et al. Composition and genesis of ferromanganese deposits from the northern South China Sea. *Journal of Asian Earth Sciences*. 2017;138:110–128. <https://doi.org/10.1016/j.jseas.2017.02.015>

Information about the authors

Yuriy V. Kirichenko – Dr. Sci. (Eng.), Professor of the Department of Geology and Mine Surveying, University of Science and Technology MISIS, Moscow, Russian Federation; Scopus ID [7007186248](https://orcid.org/0009-0001-7007-186248); e-mail kirichenko.iv@misis.ru

Tran Thien Quy Ngo – PhD-Student, University of Science, Viet Nam National University Ho Chi Minh City, Ho Chi Minh City, Viet Nam; Scopus ID [57222072264](https://orcid.org/0009-0001-5722-2072264); e-mail nttquy@hcmus.edu.vn

Marina V. Shchyokina – Cand. Sci. (Eng.), Associate Professor of the Department of Geology and Mine Surveying, University of Science and Technology MISIS, Moscow, Russian Federation; Scopus ID [57271022000](https://orcid.org/0009-0001-5727-1022000); e-mail mshchekina@yandex.ru

Received 05.09.2022

Revised 08.12.2022

Accepted 15.12.2022



MINING ROCK PROPERTIES. ROCK MECHANICS AND GEOPHYSICS

Research paper

<https://doi.org/10.17073/2500-0632-2022-06-10>

UDC 550.834.08

**Amplitude-frequency response
of a helically-wound fiber distributed acoustic sensor (DAS)**

A. V. Chugaev , M. V. Tarantin

Mining Institute of the Ural Branch of the Russian Academy of Sciences, Perm, Russian Federation chugaev@mi-perm.ru**Abstract**

The goals of this study were to analyze the capabilities of DAS (distributed acoustic sensors) in resolving mining problems, compare them with existing seismoacoustic data collection systems, and prepare the basis for conducting seismoacoustic studies with recording by a fiber optic distributed system. This paper considers the capabilities of recording seismoacoustic responses using fiber optic distributed acoustic systems (DAS). Based on physical and geometrical analysis, the amplitude-frequency responses (characteristics) of recorded longitudinal waves for straight and helically-wound fibers were obtained. In the case of helically-wound fiber, the frequency response depends on several key factors: integrating the measured value along the fiber based on the measurement; the angle of incidence on the cable; and the winding angle of the fiber in the cable. An increase in the winding angle increases the uniformity of the amplitude-frequency characteristics of longitudinal waves both in terms of frequencies and angles of incidence. At the same time, helical winding changes the effective response spacing (gauge length). This makes it possible, by summing the responses of the straight and helically-wound fibers due to the overlap of the spectra, to record frequencies that are suppressed in case of separate recording. Based on the study results, a cable design was proposed to record broadband seismoacoustic responses enabling a wide range of mining and engineering problems to be resolved, and for seismic surveys both in wells and on the surface to be carried out.

Keywords

distributed acoustic sensor, fiber optic sensor, seismic exploration, borehole seismoacoustics, Rayleigh scattering, receiver directivity pattern

Acknowledgments

The reported study was funded by the Russian Foundation for Basic Research and the Perm Territory, Project Number 20-45-596032.

For citation

Chugaev A. V., Tarantin M. V. Amplitude-frequency response of a helically-wound fiber distributed acoustic sensor (DAS). *Mining Science and Technology (Russia)*. 2023;8(1):13–21. <https://doi.org/10.17073/2500-0632-2022-06-10>

СВОЙСТВА ГОРНЫХ ПОРОД. ГЕОМЕХАНИКА И ГЕОФИЗИКА

Научная статья

**Амплитудно-частотный отклик распределенного акустического сенсора DAS
со спиральной намоткой волокна**

А. В. Чугаев , М. В. Тарантин

Горный институт УрО РАН, г. Пермь, Российская Федерация chugaev@mi-perm.ru**Аннотация**

При проведении настоящего исследования была поставлена цель проанализировать возможности распределенных датчиков DAS при решении горнотехнических задач, сравнить с существующими сейсмоакустическими системами сбора данных и подготовить основу для проведения сейсмоакустических исследований с регистрацией оптоволоконной распределенной системой. Рассмотрены возможности регистрации сейсмоакустических сигналов с помощью оптоволоконных распределенных акустических систем. На основании физико-геометрического анализа получены амплитудно-частотные характеристики регистрируемых продольных волн для прямого и спирального волокна. Для спирального волокна амплитудно-частотные характеристики зависят от нескольких ключевых факторов: интегрирования измеряемого значения вдоль волокна на базе измерения, угла падения волны на кабель и угла намотки волокна в кабеле. Увеличение угла намотки повышает равномерность амплитудно-частотной характеристики



продольных волн как по частотам, так и по углам падения. В то же время спиральная намотка меняет эффективную базу измерения сигнала, что позволяет путем суммирования сигналов прямого и спирального волокна за счет перекрытия спектров выполнять регистрацию частот, подавляемых при отдельной записи. По результатам исследования предложена конструкция кабеля для регистрации широкополосных сейсмоакустических сигналов, с помощью которых можно решать обширный круг горнотехнических и инженерных задач, выполняя сейсморазведочные исследования как в скважинах, так и на поверхности.

Ключевые слова

распределенный акустический датчик, оптоволоконный сенсор, сейсморазведка, скважинная сейсмоакустика, рассеяние Рэлея, диаграмма направленности приемника

Благодарности

Исследование выполнено при финансовой поддержке РФФИ и Пермского края в рамках научного проекта №20-45-596032.

Для цитирования

Chugaev A. V., Tarantin M. V. Amplitude-frequency response of a helically-wound fiber distributed acoustic sensor (DAS). *Mining Science and Technology (Russia)*. 2023;8(1):13–21. <https://doi.org/10.17073/2500-0632-2022-06-10>

Introduction

Distributed systems for recording acoustic responses using optical fiber (DAS – distributed acoustic sensing) have been well known for several years [1–3]. However, their reduction to the practice of geophysical research requires certain practical problems related to the physical and geometric features of such systems to be resolved.

The recording of an acoustic response in a DAS system is carried out by analyzing the spectrum of Rayleigh light scattering in an optical fiber. This occurs when a light pulse of a given wavelength and duration passes. Longitudinal deformation of the fiber leads to a change in the amplitude and phase components of the frequency spectra of the reflection optical response [2]. Optical interferometry enables the magnitude of the strain in a certain section to be calculated. The position can be measured from the time of arrival of the backscattered optical pulse at a known velocity of light in the waveguide [4, 5]. The important characteristic of the system is Gauge Length L , which determined by specification of the interrogator. As a result, the stress distribution profile in the fiber at a certain point in time is calculated. The re-interrogation is limited by the time of arrival of the reflection response from the most remote section of the fiber optic cable. The velocity of light propagation in an optical fiber is 2×10^8 m/s. For a 1 km line, the double travel time of a light pulse is 10^{-5} s, and for 100 km it is 10^{-3} s. This is currently the limitation of the recorded response sampling by time.

The goals of this study were to analyze the capabilities of DAS in resolving mining problems, compare them with existing seismoacoustic data collection systems, and prepare the basis for conducting acoustic studies with recording by a fiber optic distributed system.

The frequency content of the responses recorded by fiber-optic sensors with linear fiber is considered

in [6–8]. Since DAS measurements involve averaging the measured parameter based on gauge length L , distortion of the acoustic response spectrum occurs at frequencies above 150–300 Hz [7, 9, 10]. Responses with a frequency not exceeding these values are suitable for resolving problems of oil seismic exploration [3, 11, 12] and monitoring ore deposits [13, 14]. In borehole and seismic exploration of mines, the upper limit of the frequency range of the useful response is 1000 Hz and higher [15–17]. Therefore, the possibility of using distributed fiber optic systems for solving mining problems needs to be considered and compared with existing seismoacoustic data collection systems. In addition, at the present time, the available literature provides no analysis of the amplitude-frequency characteristics of a helically-wound optic cable.

Acoustic pattern of straight fiber

DAS systems measure the deformation of an optical fiber along its axis. Thus, for longitudinal waves, the acoustic pattern is defined as $D_p(\alpha) = A_0 \cos^2 \alpha$, for transverse waves, $D_s(\alpha) = A_0 |\sin 2\alpha|$ [1, 18], where α is the angle between the fiber and the wave propagation vector; and A_0 is the amplitude of the incident wave. The incidence of a seismic wave on a linear section of an optical fiber is considered in [3, 11, 19]. Such a pattern significantly limits the range of possible seismic survey problems to be solved. Particularly, in many standard cases of seismic surveys, the target waves arrive along the normal line to the receiver line.

The use of special cables with non-standard fiber laying can expand the capabilities of fiber-optic systems for solving seismoacoustic problems. The cable design options are given in a patent [20]. For manufacturing, the most accessible way of laying a fiber in a cable is helical winding; field measurements are described in [21, 22].

Influence of winding angle on effective gauge length

With helical winding, the length of the fiber laid in a cable will be greater than the length of the cable. Thus, the effective value L_H (effective gauge length) of the rock mass associated with the cable will also change.

The decrease in the gauge length is proportional to the cosine of the winding angle:

$$L_H = L \cos \theta, \quad (1)$$

where θ is the angle of deviation of the fiber guide from the cable axis (for straight fiber $\theta = 0^\circ$)¹; L is gauge length along the fiber; L_H is gauge length along the cable with helically-wound fiber.

Influence of winding angle on cable sensitivity

When changing the cable directivity pattern due to winding, a single segment of the helix can be represented as a linear section with an equivalent distribution of sensitivity along the axes (Fig. 1). In a parametric form, the response energy will be distributed as follows:

$$E_z = E \cos^2 \theta; \quad (2)$$

$$E_r = E \sin^2 \theta; \quad (3)$$

$$E_{x,y} = \frac{1}{2} E \sin^2 \theta, \quad (4)$$

where E is full sensitivity; E_z , E_r , E_x , E_y are the sensitivities along z axis, in the plane perpendicular to z axis, along x and y axes, respectively.

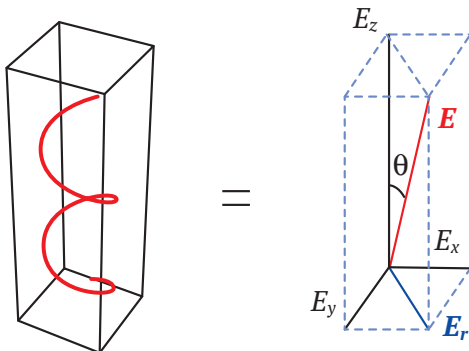


Fig. 1. Sensitivity distribution along the axes at helically-wound fiber

Per unit cable length, an increase in the recorded energy will occur due to an increase in the length of the fiber and the number of channels due to a decrease in the effective gauge length according to formula (1).

¹ In literature, there are two different ways of calculating the winding angle. Kuvshinov, Braid, Innanen et al. take 90° for a straight fiber, while in the study of Egorov, Tertysnikov, and others, 0° corresponds to a straight fiber. We stick to the latter version of the notation.

The algorithm for numerical calculation of the cable directivity pattern due to winding is given in [23, 24].

With an increase in the fiber winding angle, the sensitivity of the system along the normal to the cable axis appears. The directivity pattern for longitudinal waves changes from the pattern of a single-axis sensor towards the pattern of a pressure sensor having a uniform (spherical) pattern.

The sensitivity is evenly distributed between the axes at the value of the winding angle

$$\theta = \arccos\left(\frac{1}{\sqrt{3}}\right) \approx 54.7^\circ \quad [19, 23].$$

Thus, with a uniform directivity pattern (spherical) along one axis, the recorded energy will be 3 times less, and the response amplitude will decrease by $\sqrt{3}$ times.

The total response from the impact of a seismic wave with a helically-wound fiber consists of its interaction with equivalent sections decomposed along orthogonal axes. In the case of longitudinal waves, the responses will be added, and for transverse waves, they will be subtracted (Fig. 2).

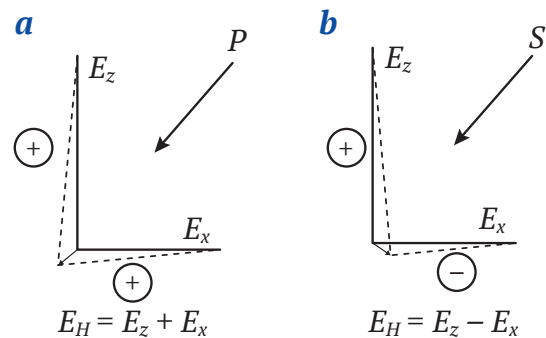


Fig. 2. Scheme of changing the length of the fiber under the influence of longitudinal (a) and transverse (b) waves

The directivity pattern is symmetrical with respect to the cable axis and depends on the angles of winding and seismic wave incidence in accordance with expressions (2–4):

$$D_P(\alpha, \theta) = \cos^2 \alpha \cos^2 \theta + \frac{1}{2} \sin^2 \alpha \cos^2 \theta; \quad (5)$$

$$D_S(\alpha, \theta) = \left| \sin 2\alpha \cos^2 \theta - \frac{1}{2} \sin 2\alpha \sin^2 \theta \right|, \quad (6)$$

where D_P, D_S are directivities for P and S waves, respectively; α is the angle between the cable and the seismic wave beam. Graphically, the patterns are shown in Fig. 3.

Note that the data obtained differs from that presented in study [23], where the polarity of S -wave response varies depending on the direction of propagation of the optical response in the fiber. However, this would mean that measurements on the same cable section when connecting from different ends of the optical line would give different results.

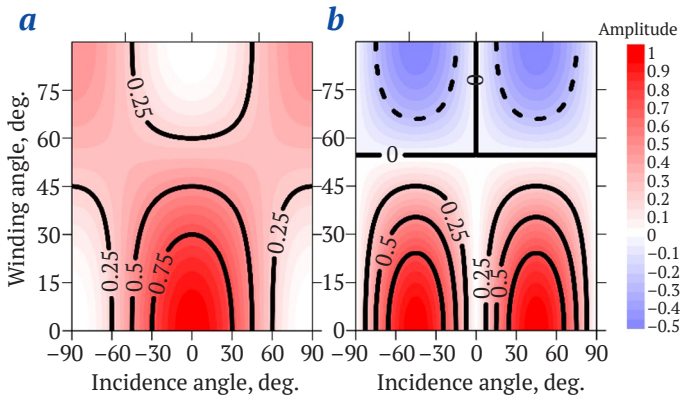


Fig. 3. Dependences of the sensitivity of a cable with helically-wound fiber on the angles of wave incidence and the fiber winding for *P* (a) and *S* (b) waves

Frequency characteristics of the recorded response for direct fiber

Let us consider the moment of time when a monochromatic elastic wave with oscillation frequency f has created longitudinal stresses in a fiber stretched along z axis. In this case, the amplitude of the recorded response will change according to the following expression:

$$A(x) = A_0 \sin(kz),$$

where $k = 2\pi f/V$ is wavenumber; A_0 is maximum response amplitude.

The amplitude of the response measured on a segment of length L is equal to the sum of the amplitudes along this segment:

$$A_L = A_0 \int_0^L \sin(kz) dz = A_0 \frac{V}{2\pi f} \left(1 - \cos\left(\frac{2\pi f L}{V}\right) \right). \quad (7)$$

Here we see that, firstly, as the frequency increases, the response amplitude decreases. Secondly, at points which satisfy the condition $L = n\lambda$, $n \in \mathbb{Z}$, the function takes a null value. As a result, the amplitude-frequency characteristic (AFC) is complicated by the response attenuation sections as a result of the action of a rectangular window filter, which an extended linear receiver appears to be. The AFC for longitudinal waves propagating along the fiber at a velocity $V = 2500$ m/s and spacing $L = 10$ m is shown in Fig. 4.

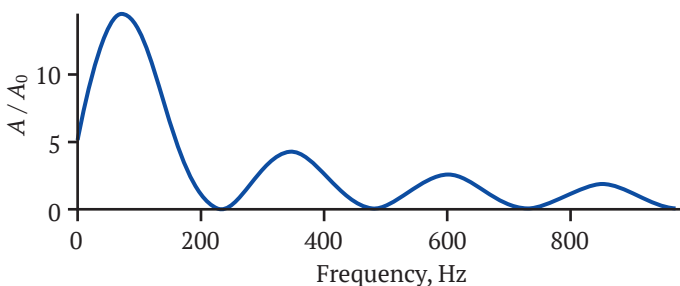


Fig. 4. Amplitude-frequency characteristic of a section of a straight fiber during the passage of a wave along it

The dependence of amplitude-frequency characteristics on the angle of incidence of a wave

When a linear receiver is located in the field of a harmonic wave (Fig. 5), the visible period will increase by increasing the angle α between the direction of wave propagation and the receiver line from 0° to 90° . The apparent frequency, in turn, will decrease:

$$f_a = f |\cos \alpha|. \quad (8)$$

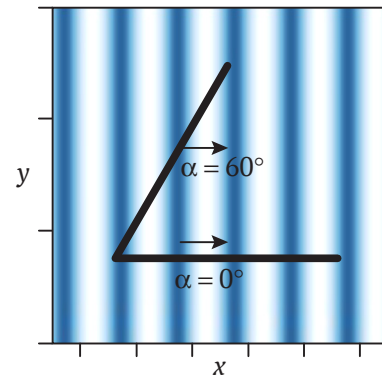


Fig. 5. Change in the visible period at different wave incidence angles

With regard to a section of a straight fiber and an arbitrary angle of incidence of wave α , the dependence of the AFC on the angle of incidence can be found as the product of the amplitude characteristic (7) and the directivity pattern, taking into account the apparent frequency instead of the actual one (8):

$$A_L(\alpha, f) = A_0 \frac{V}{2\pi f_a} \left(1 - \cos\left(\frac{2\pi L f_a}{V}\right) \right) D(\alpha). \quad (9)$$

The image of this dependence for longitudinal and transverse waves at $L = 10$ m, $V_p = 2500$ m/s, $V_s = 1500$ m/s is shown in Fig. 6. The image draws attention to the areas of rejection in the form of “smiles” and low sensitivity at angles close to 90° .

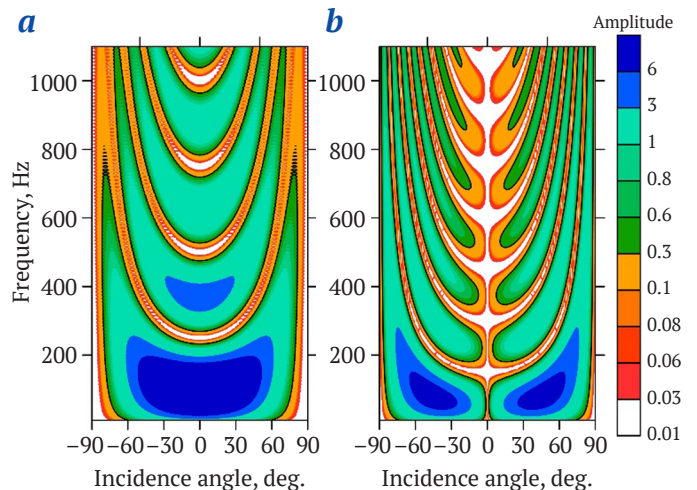


Fig. 6. Amplitude-frequency characteristic of a section of a straight fiber at different angles of incidence of an elastic wave for *P* (a) and *S* (b) waves

Amplitude-frequency response of helically-wound fiber

Next, let us consider a cable of radius r with helically-wound fiber, on which a wave is incident at an angle α . The angle of a wave incidence on separate small sections is equal to $\alpha + \varphi(z)$ (Fig. 7), where $\varphi(z)$ can be found through the derivative of the function describing the helically-wound fiber in plane view (z, x):

$$x(z) = r \sin\left(z \operatorname{tg} \frac{\theta}{r}\right), \quad (10)$$

from where

$$\varphi(z) = \arctg\left(\operatorname{tg} \theta \cos\left(z \operatorname{tg} \frac{\theta}{r}\right)\right). \quad (11)$$

The function $\varphi(z)$ takes values from $-\theta$ to θ , and provided that the wavelength is much larger than the pitch between the turns in the cable, the response will be equal to the sum

$$A_H(f, \theta, \alpha) = \sum_{\varphi=-\theta}^{\theta} A_L(f, \alpha + \varphi(z)) \Delta L(\varphi)/L, \quad (12)$$

where factor $\Delta L(\varphi)/L$ plays the role of a weighting factor depending on the proportion of the sections with a fixed angle φ in the total length of the fiber. The angle distribution can be found by calculating the derivative of function $z(x) = r \operatorname{ctg} \theta \arcsin(x/r)$:

$$\frac{dz}{dx} = \frac{\operatorname{ctg} \theta}{\sqrt{1 - \left(\frac{x}{r}\right)^2}}, \quad (13)$$

for which $x \in [-r, r]$ and the angles vary from $-\theta$ to θ . An example of φ distribution for a winding angle of 45° is shown in Fig. 8.

In the case of longitudinal waves, using formula (12), the amplitude-frequency characteristics were obtained for various winding angles of fiber in a cable (Fig. 9). With an increase in the winding angle, the rejection

bands are smoothed out. As a result, the response becomes more uniform in the angles of incidence. There are sensitivity curve dips in frequencies, although they are less pronounced than those for a straight fiber. This leaves room for spectrum whitening.

An important case here is the wave incidence angle of 90° , the response at which is shown separately in Fig. 10. It can be seen from the graphs that there are frequency bands, in which the response amplitude increases with increasing winding angle, and other bands where such amplification does not take place.

With an increase in the winding angle, the effective gauge length decreases in accordance with formula (1). This, in turn, leads to an increase in the frequency of the first minimum in the total frequency response. This fact makes it possible, when summing the responses from a straight and helically-wound fiber, to obtain a more uniform AFC (frequency response) in a wide range of the angles of wave incidence on the cable (Fig. 11). An exception relates to angles of incidence close to 90° , where the AFC depends only on helically-wound fiber.

Fiber bend radius in helically-wound cable

A standard telecommunication fiber has a certain range of standard sizes and labels. One of the main characteristics is the dependence of the response attenuation constant on the fiber bend radius.

The bend radius is determined in the plane where it is maximum. With uniform helical winding, the radius of bend is constant and coincides with the radius of the minimum curvature of the ellipse formed when the cable is intersected by a plane at the same angle as the winding angle (Fig. 12). Thus, the effective radius of curvature of a fiber will depend on the radius of the fiber in a cable r and the winding angle θ :

$$R_e = \frac{r}{\sin^2 \theta}. \quad (14)$$

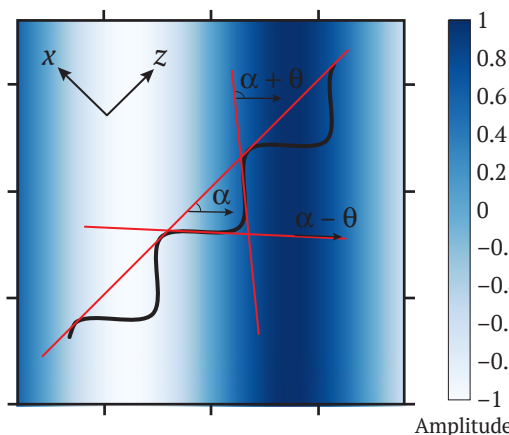


Fig. 7. Helically-wound fiber in the field of a plane elastic monochromatic wave

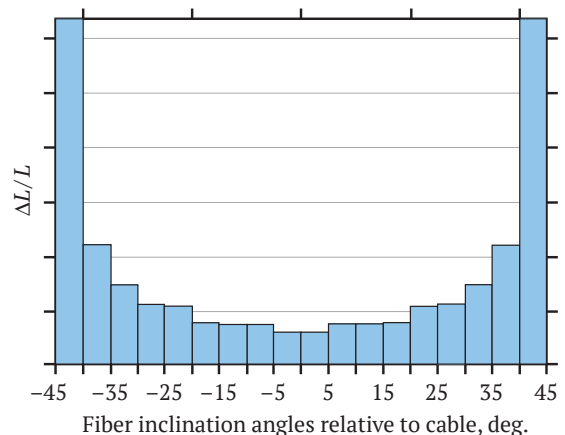


Fig. 8. Distribution of fiber inclination angles relative to cable axis at 45° helical winding

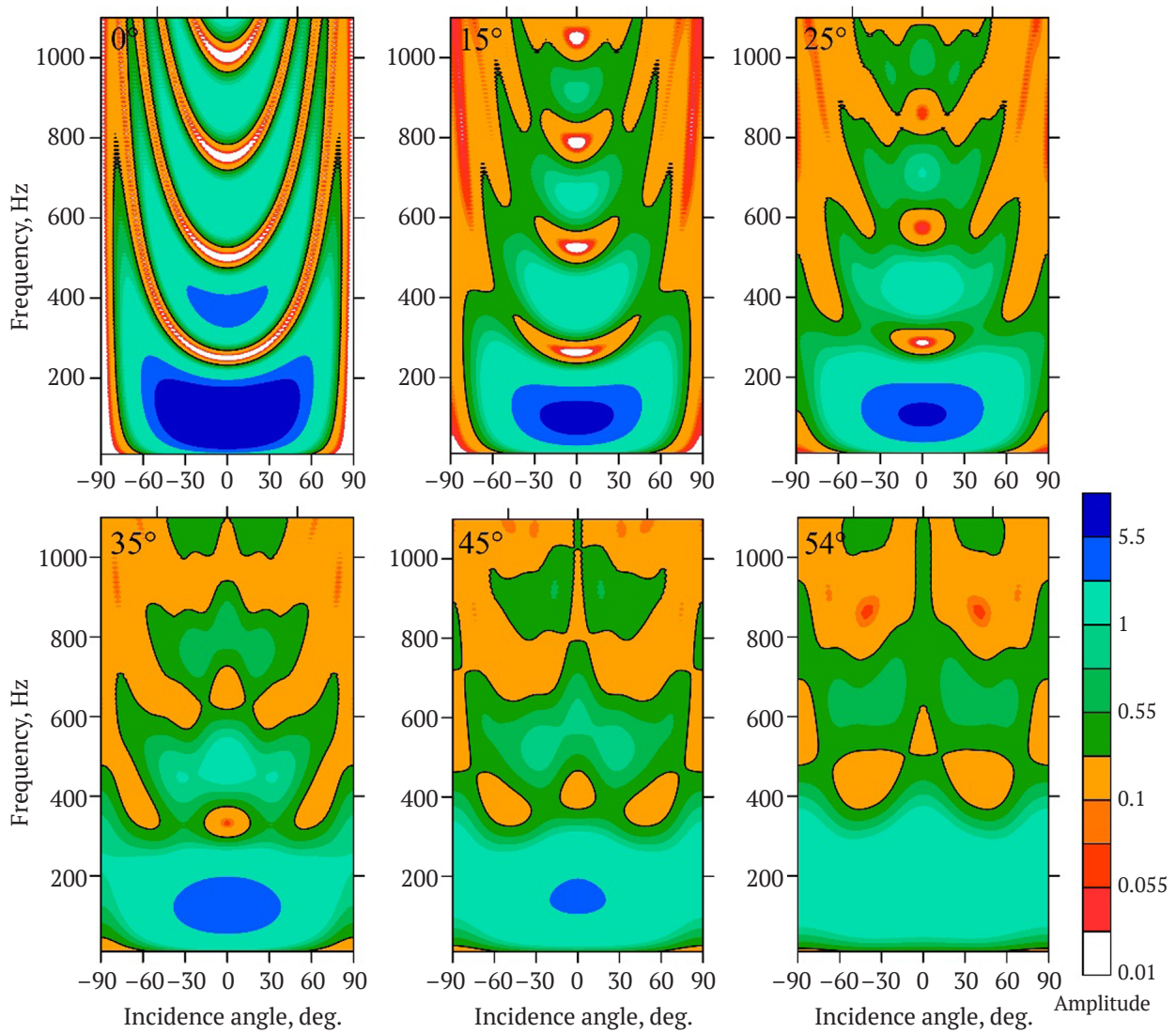


Fig. 9. Amplitude-frequency characteristics of a cable for different fiber winding angles

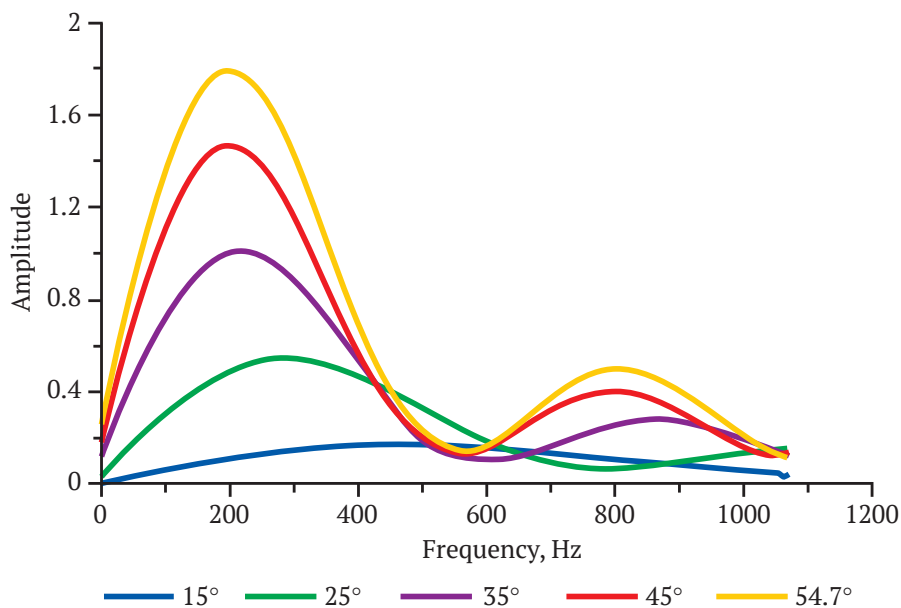


Fig. 10. Cross-sectional sensitivity of helically-wound fiber cable at various winding angles

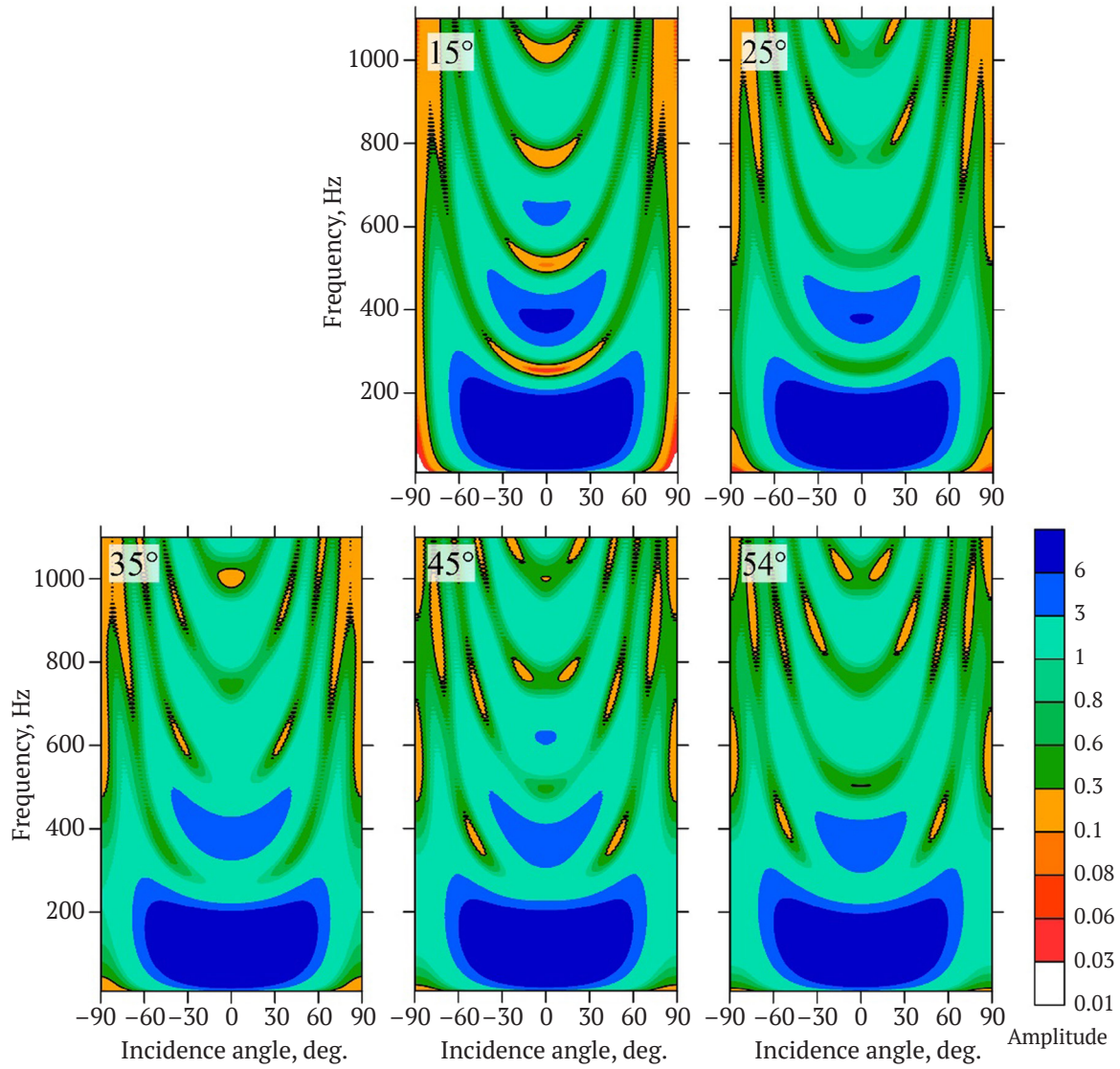


Fig. 11. Amplitude-frequency characteristics of the summed response from a straight and helically-wound fiber with different winding angles

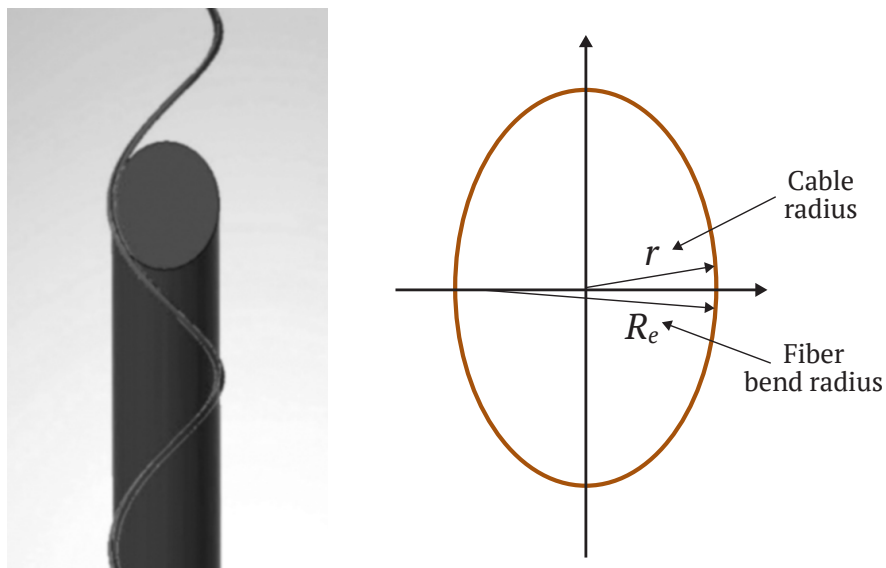


Fig. 12. Scheme for determining effective fiber bend radius



Taking R_c as a fixed value determined by the selected type of fiber, one can obtain the dependence of the cable radius on the winding angle θ : $r = R_c \sin^2 \theta$. The weight of such a cable will be proportional to $\sin^4 \theta$.

In the case of G657.A2 standard fiber, the bend radius at which there are no losses on a significant number of turns is 30 mm. Based on this value of the radius and the winding angle of 45° , a cable was designed containing both straight and helically-wound fibers. The outer diameter of the cable is 32.6 mm, and the weight is 721 kg/km. Such a cable can be used both for land seismic surveys and for downhole ones.

Conclusion

Analysis of the physical and geometric processes of recording acoustic responses by a distributed fiber optic system enabled the spatio-temporal characteristics of such systems to be obtained for straight and helically-wound fibers in a cable. The amplitude-frequency characteristics of the responses re-

corded by a helically-wound fiber depend on several key factors: integration of the measured value along the fiber on the gauge length; the angle of incidence of the wave on the cable; and the angle of winding of the fiber in the cable. It is possible to show that an increase in the winding angle increases the uniformity of the amplitude-frequency characteristic of longitudinal waves both in terms of frequencies and angles of incidence.

At the same time, helical winding changes the effective gauge length. By summing the responses of the straight and helically-wound fibers due to the overlap of the spectra, it is possible to record the frequencies suppressed in the case of separate recording.

Based on the results of the study, a cable design was proposed for recording broadband seismoacoustic responses, the use of which enables a wide range of mining and engineering problems to be resolved and for seismic surveys both in wells and on the surface to be carried out.

References

1. Mateeva A., Mestayer J., Cox B. et al. Advances in distributed acoustic sensing (DAS) for VSP. In: *SEG Technical Program Expanded Abstracts 2012*. Society of Exploration Geophysicists; 2012. <https://doi.org/10.1190/segam2012-0739.1>
2. Parker T., Shatalin S., Farhadiroushan M. Distributed Acoustic Sensing – a new tool for seismic applications. *First Break*. 2014;32(2):61–69. <https://doi.org/10.3997/1365-2397.2013034>
3. Wu X., Willis M.E., Palacios W. et al. Compressional- and shear-wave studies of distributed acoustic sensing acquired vertical seismic profile data. *The Leading Edge*. 2017;36(12):987–993. <https://doi.org/10.1190/tle36120987.1>
4. Hartog A., Kotov O.I., Liokumovich L.B. The optics of distributed vibration sensing. In: *Second EAGE Workshop on Permanent Reservoir Monitoring 2013 – Current and Future Trends*. Netherlands: EAGE Publications BV; 2013. <https://doi.org/10.3997/2214-4609.20131301>
5. Shatalin S.V., Treschikov V.N., Rogers A.J. Interferometric optical time-domain reflectometry for distributed optical-fiber sensing. *Applied Optics*. 1998;37(24):5600–5604. <https://doi.org/10.1364/AO.37.005600>
6. Dean T., Papp B., Hartog A. Wavenumber response of data recorded using distributed fibre-optic systems. In: *3rd EAGE Workshop on Borehole Geophysics*. Netherlands: EAGE Publications BV; 2015. <https://doi.org/10.3997/2214-4609.201412215>
7. Dean T., Cuny T., Hartog A. H. The effect of gauge length on axially incident P-waves measured using fibre optic distributed vibration sensing: Gauge length effect on incident P-waves. *Geophysical Prospecting*. 2017;65(1):184–193. <https://doi.org/10.1111/1365-2478.12419>
8. Bona A., Dean T., Correa J. et al. Amplitude and phase response of DAS receivers. In: *79th EAGE Conference and Exhibition 2017*. Netherlands: EAGE Publications BV; 2017. <https://doi.org/10.3997/2214-4609.201701200>
9. Stork A.L., Baird A.F., Horne S.A. et al. Application of machine learning to microseismic event detection in distributed acoustic sensing data. *Geophysics*. 2020;85(5):KS149–KS160. <https://doi.org/10.1190/geo2019-0774.1>
10. Näsholm S.P., Iranpour K., Wuestefeld A. et al. Array signal processing on distributed acoustic sensing data: Directivity effects in slowness space. *Journal of Geophysical Research: Solid Earth*. 2022;127(2). <https://doi.org/10.1029/2021JB023587>
11. Willis M.E., Barfoot D., Ellmauthaler A., Wu X. et al. Quantitative quality of distributed acoustic sensing vertical seismic profile data. *The Leading Edge*. 2016;35(7):605–609. <https://doi.org/10.1190/tle35070605.1>
12. Sudakova M.S., Belov M.V., Ponimaskin A.O. et al. Features of processing vertical seismic profiling data of offshore shallow wells with fiber-optic distributed systems. *Journal of Geophysics*. 2021;(6):110–118. (In Russ.)



13. Riedel M., Cosma C., Enescu N. et al. Underground Vertical Seismic Profiling with conventional and fiber-optic systems for exploration in the Kylylahti polymetallic mine, eastern Finland. *Minerals (Basel)*. 2018;8(11):538. <https://doi.org/10.3390/min8110538>

14. Bellefleur G., Schetselaar E., Wade D. et al. Vertical seismic profiling using distributed acoustic sensing with scatter-enhanced fibre-optic cable at the Cu–Au New Afton porphyry deposit, British Columbia, Canada. *Geophysical Prospecting*. 2020;68(1):313–333. <https://doi.org/10.1111/1365-2478.12828>

15. Yaroslavtsev A. G., Fatkin K. B. Mine seismic surveys for the control of safety pillars in potash mines. In: *Engineering and Mining Geophysics 2020*. European Association of Geoscientists & Engineers; 2020. <https://doi.org/10.3997/2214-4609.202051043>

16. Sanfirov I. A., Yaroslavtsev A. G., Chugaev A. V. et al. Frozen wall construction control in mine shafts using land and borehole seismology techniques. *Journal of Mining Science*. 2020;56(3):359–369. <https://doi.org/10.1134/S1062739120036641>

17. Chugaev A. V., Sanfirov I. A., Lisin V. P. et al. The integrated borehole seismic surveys at the verkhnekamskoye potassium salt deposit. In: *Lecture Notes in Networks and Systems*. Vol. 342. Cham: Springer International Publishing; 2022. Pp. 255–269. https://doi.org/10.1007/978-3-030-89477-1_25

18. Correa J., Egorov A., Tertyshnikov K. et al. Analysis of signal to noise and directivity characteristics of DAS VSP at near and far offsets – A CO2CRC Otway Project data example. *The Leading Edge*. 2017;36(12):962–1044. <https://doi.org/10.1190/tle36120994a1.1>

19. Kuvshinov B. N. Interaction of helically wound fibre-optic cables with plane seismic waves. *Geophysical Prospecting*. 2016;64(3):671–688. <https://doi.org/10.1111/1365-2478.12303>

20. den Boer J. J., Mateeva A., Pearce J. G. et al. *Detecting broadside acoustic signals with a fiber optical distributed acoustic sensing (DAS) assembly*. Standard Patent WO2013/090544/A1, 2013. URL: <https://patentimages.storage.googleapis.com/6a/52/dc/6513f050b2f66c/AU2012352253C1.pdf>

21. Tertyshnikov K., Bergery G., Freifeld B., Pevzner R. Seasonal effects on DAS using buried helically wound cables. In: *EAGE Workshop on Fiber Optic Sensing for Energy Applications in Asia Pacific*. European Association of Geoscientists & Engineers; 2020. <https://doi.org/10.3997/2214-4609.202070007>

22. Stork A. L., Chalari A., Durucan S. et al. Fibre-optic monitoring for high-temperature Carbon Capture, Utilization and Storage (CCUS) projects at geothermal energy sites. *First Break*. 2020;38(10):61–67. <https://doi.org/10.3997/1365-2397.fb2020075>

23. Baird A. Modelling the response of helically wound DAS cables to microseismic arrivals. In: *First EAGE Workshop on Fibre Optic Sensing*. European Association of Geoscientists & Engineers; 2020. <https://doi.org/10.3997/2214-4609.202030019>

24. Egorov A., Charara M., Alfataierge E., Bakulin A. Realistic modeling of surface seismic and VSP using DAS with straight and shaped fibers of variable gauge length. In: *First International Meeting for Applied Geoscience & Energy Expanded Abstracts*. Tulsa, OK, USA: Society of Exploration Geophysicists; 2021. Pp. 184–193. <https://doi.org/10.1190/segam2021-3576626.1>

Information about the authors

Alexander V. Chugaev – Cand. Sci. (Eng.), Head of the Sector of Shallow Well Research of the Department of Active Seismic Acoustics, Mining Institute of the Ural Branch of the Russian Academy of Sciences, Perm, Russian Federation; ORCID [0000-0002-7494-4042](https://orcid.org/0000-0002-7494-4042), Scopus ID [6602559950](https://scopus.com/authorid/6602559950); e-mail chugaev@mi-perm.ru

Mikhail V. Tarantin – Cand. Sci. (Eng.), Researcher, Department of Active Seismic Acoustics; Mining Institute of the Ural Branch of the Russian Academy of Sciences, Perm, Russian Federation; Scopus ID [36601605800](https://scopus.com/authorid/36601605800); e-mail muxaul20@rambler.ru

Received 04.06.2022

Revised 01.09.2022

Accepted 13.12.2022



MINING ROCK PROPERTIES. ROCK MECHANICS AND GEOPHYSICS

Research paper

<https://doi.org/10.17073/2500-0632-2022-12-36>

UDC 550.834

**Effect of strain amplitude and confining pressure on the velocity and attenuation of *P* and *S* waves in dry and water-saturated sandstone: an experimental study**E. I. Mashinskii   *Trofimuk Institute of Petroleum Geology and Geophysics of Siberian Branch of Russian Academy of Sciences, Novosibirsk, Russian Federation* *MashinskiiEI@ipgg.sbras.ru***Abstract**

In rock physics, much attention has been paid to the study of the processes of strain of natural materials at small strains. Experiments using high-precision measurements have allowed new knowledge at micro/nano level to be acquired. The microplasticity of solids is studied in materials science, but there is also data regarding some rocks. The property of microplasticity of natural materials is still little studied. The study was carried out on rock samples. The effect of strain amplitude and confining pressure on the velocity and attenuation of *P* and *S* waves in dry and water-saturated sandstone has been studied. The method of reflected waves was used in the frequency range of 0.5–1.4 MHz at four strain amplitudes $(0.5–1.67) \cdot 10^{-6}$. Amplitude cycling causes an open and closed hysteresis effect for wave velocity and attenuation. This has been observed for both dry and water-saturated sandstone. The hysteresis loop overlaps in both states. The amplitude changes in the velocity of *P*-wave in dry sandstone is 1.12 %, and the attenuation of *P*-wave in dry sandstone is 5.43 %. As for *S*-wave, its maximum attenuation in dry sandstone reaches 8.81 %. The behavior of a wave velocity and attenuation can be explained by the combined effect of viscoelasticity and microplasticity. Elastoplastic transition strongly depends on the details of the microstructure, its defectiveness, and other parameters. The characteristics of the complications of wave parameters can be the signs of the internal structure of the subject.

Keywords

rock physics, amplitude-dependent wave velocity and attenuation, open hysteresis of wave velocity and attenuation, effect of water saturation on wave velocity and attenuation, microplastic strain, stepwise inelasticity, elastic modulus

Acknowledgments

The study was carried out within the framework of the research project “Mechanisms of the impact of natural and man-made factors on processes in the geospheres based on the results of monitoring natural geophysical fields”. Project number FWZZ-2022-0019 in the ISGZ of Ministry of Education and Science.

For citation

Mashinskii E. I. Effect of strain amplitude and confining pressure on the velocity and attenuation of *P* and *S* waves in dry and water-saturated sandstone: an experimental study. *Mining Science and Technology (Russia)*. 2023;8(1):22–29. <https://doi.org/10.17073/2500-0632-2022-12-36>

СВОЙСТВА ГОРНЫХ ПОРОД. ГЕОМЕХАНИКА И ГЕОФИЗИКА

Научная статья

Влияние амплитуды деформации и всестороннего давления на скорость и затухание *P*- и *S*-волн в сухом и водонасыщенном песчанике: экспериментальное исследованиеЭ. И. Машинский   *Институт нефтегазовой геологии и геофизики им. А.А. Трофимука Сибирского отделения Российской академии наук, г. Новосибирск, Российская Федерация* *MashinskiiEI@ipgg.sbras.ru***Аннотация**

В физике горных пород большое внимание уделяется изучению процессов деформирования природных материалов на малых деформациях. Эксперименты проводятся с помощью высокоточных измерений, которые позволяют получить новые знания на микро/нано уровне. Микропластичность твердых тел изучают в материаловедении, но имеются также данные, полученные для некоторых гор-



ных пород. Свойство микро-пластичности природных материалов пока мало изучено. Исследование проводилось на образцах пород. Изучено влияние амплитуды деформации и всестороннего давления на скорость и затухание P - и S -волн в сухом и водонасыщенном песчанике. Использовался метод отраженных волн в диапазоне частот $(0,5–1,4)$ МГц при четырех амплитудах деформации $(0,5–1,67) \cdot 10^{-6}$. Циклическое изменение амплитуды вызывает эффект открытого и закрытого гистерезиса для скорости волны и затухания. Это наблюдается как для сухого, так и водонасыщенного состояния песчаника. В обоих состояниях имеет место перехлест петель гистерезиса. Амплитудное изменение скорости P -волны в сухом песчанике составляет 1,12 %, а для затухания P -волны в сухом песчанике – 5,43 %. На S -волне максимальное затухание в сухом песчанике достигает 8,81 %. Поведение скорости и затухания волны можно объяснить совместным действием процессов вязко-упругости и микро-пластичности. Упругопластический переход сильно зависит от деталей микроструктуры, ее дефектности и других параметров. Характеристики осложнений параметров волн могут являться признаками внутреннего строения исследуемого объекта.

Ключевые слова

физика горных пород, амплитудно-зависимые скорость волны и затухание, открытый гистерезис скорости и затухания волны, влияние водонасыщения на скорость волны и затухание, микропластическая деформация, скачкообразная неупругость, упругий модуль

Благодарности

Работа выполнялась в рамках проекта НИР «Механизмы воздействия природных и техногенных факторов на процессы в геосферах по результатам мониторинга естественных геофизических полей». Номер проекта в ИСГЗ Минобрнауки FWZZ-2022-0019.

Для цитирования

Mashinskii E. I. Effect of strain amplitude and confining pressure on the velocity and attenuation of P and S waves in dry and water-saturated sandstone: an experimental study. *Mining Science and Technology (Russia)*. 2023;8(1):22–29. <https://doi.org/10.17073/2500-0632-2022-12-36>

Introduction and challenges

The current development of earth sciences is based on new fundamental knowledge in the physics of rock strain, in order to increase performance of seismic and acoustic methods in geological surveys and exploration. New knowledge has been obtained about the mechanism of natural material strain under various loads. These are inelastic step-like, discontinuous strains recorded at micro/nano level. The property of rock microplasticity, which is rather exotic in geophysics, can manifest itself even at small and very small strains. Accounting for this factor is important in practice, since seismic and acoustic methods use a range of small strains. The interest in this effect has emerged as a result of previous studies. The study of seismic non-linearity has led to the need for a deep understanding of the physics of rock strain [1–3]. The possibility of non-linearity at very small strains was confirmed, thus extending the applicability of inelastic processes [4, 5]. Theoretical studies in seismic improve the classical visco-elastic model of a standard body. The model well describes dispersion, relaxation, and related inelastic processes.

Theoretical and experimental studies confirm the presence of the microplasticity effect [6, 7]. The influence of strain amplitude on a wave velocity and attenuation is ambiguous, since in some cases it leads to an increase in the parameters, while in the others, to

a decrease. In the same way, the modulus of elasticity changes, affecting the curvature of the stress-strain relationship [8, 9]. This non-standard behavior of rocks is caused by the joint effect of elastic and microplastic strain [10–11]. This effect is presented as a “stress plateau” and “stress drop” on a stress–strain diagram and in an acoustic response record [12, 13]. The property of microplasticity of rocks allows for irregular short-term “switching on” of the plasticity process with the simultaneous effect of elastic strain. There are also theoretical confirmations [14–16]. The mechanical properties of rocks differ to a greater extent in their inelastic characteristics. They are more related to the dynamic parameters of waves than to the elastic characteristics. The current approach involves the use of new data which can be used to resolve geological problems. This is confirmed by high-precision experimental and theoretical studies [17, 18].

Research in solid state physics has shown that a viscoelastic model can be supplemented with an inelastic element of a discontinuous nature, involved in the deformation process. An elastic-viscoplastic model with the participation of a plastic component represents an amplitude-frequency-dependent dynamic modulus. In this model, the general stress tensor is determined by the sum of three components, elastic, elastic-plastic, and viscoelastic moduli of a material [19–21]. In solid state physics and materials

science, much attention is paid to the study of step-like strain [22–24]. There is a sharp transition from elastic strain to plastic flow. Such a strain jump is accompanied by a stress drop and depends in a complex way on the properties of a material and its loading conditions [25, 26]. The development of a mechanical model of a geological medium takes into account the data obtained on discontinuous inelasticity. Some data for rocks and minerals (sandstone, clay loam, quartz, silica, muscovite, stishovite, mica, sapphire, diorite, graphite) are described in [27, 28].

This paper describes a laboratory study of the effect of strain amplitude and pressure on the behavior of velocity and attenuation of P -wave and S -wave in dry and water-saturated sandstone at room temperature. This study is of great interest for understanding micro-strain mechanisms in rocks. The mechanism of microplasticity of rocks is still poorly understood, but it seems reasonable to say that it is close to a mechanism known in solid state physics. Microplastic behavior occurs when mobile dislocations are activated in the form of an avalanche phenomenon. The first sign of this process is the appearance of the “stress plateau” and “stress drop” effects. The results obtained in this experiment can be useful not only as a fundamental knowledge, but also for their application in solving practical problems. New knowledge about the microplasticity property of rocks allows the standard viscoelastic model used in seismic surveys to be improved. This can be achieved by including a microplastic strain component into the standard model. A complex viscoelastic-plastic model can more realistically describe strain processes in rocks. In the practical application of the knowledge acquired, for example, in seismic and acoustics, the amplitude-dependent effect that affects the velocity and attenuation of longitudinal and transverse waves in rocks needs to be taken into account. Accounting for this effect improves the measurement accuracy and the interpretation of the obtained data.

Research techniques and factual material

In the experiment, samples of fine-grained sandstone from a core taken from a depth of 2,545 m were used. The density of sandstone is 2.45 g/cm³, the content of fine-grained sand fraction is 82 % and that of siltstone is 18 %, the total porosity is 12 %. The measurements of the velocity and attenuation of P and S waves depending on the strain amplitude were carried out at a constant hydrostatic pressure of 20 MPa. In addition, the behavior of P and S wave velocities at constant amplitude was studied depending on the hydrostatic pressure in the range

from 10 to 50 MPa. The cylindrical specimens used had the following dimensions: 40 mm in diameter and 16 mm in length. A standard three-layer installation was used in the experiment [29, 30]. The first and third layers provided identical wave reflection at the interfaces. The first layer is the delay line and the third layer is the acoustic load. A rock sample is located between these layers. The excitation and reception of acoustic responses were provided by piezoceramic sensors at frequency of 1 MHz, which were set to polarize P and S waves. The attenuation decrement was calculated as follows [11, 31, 32]:

$$Q^{-1} = \frac{\alpha V}{8.686\pi f} = \frac{\alpha \lambda}{8.686\pi}, \quad (1)$$

where α is absorption coefficient, dB · m⁻¹,

$$\alpha(\omega) = \frac{8,686}{L} \ln \left[\frac{|R_{25}| A_{top}(f)}{|R_{12}| A_{bot}(f)} (1 - R_{12}^2(f)) \right], \quad (2)$$

where L is double length of the sample, m; $A_{top}(f)$ is Fourier amplitude of the reflected pulse from the upper boundary of the sample; $A_{bot}(f)$ is Fourier amplitude of the reflected pulse from the lower boundary of the sample; $R_{12}(f)$ is coefficient of reflection from the upper boundary; $R_{25}(f)$ is coefficient of reflection from the lower boundary. In our case, the boundaries are identical and therefore $R_{12}(f) = -R_{25}(f)$. Reflection coefficient

$$R(f) = \frac{\rho_r V_r(f) - \rho_b V_b(f)}{\rho_r V_r(f) + \rho_b V_b(f)}, \quad (3)$$

where ρ_r and ρ_b are densities of the rock and beryllium bronze, kg · m⁻³, respectively; $V_r(f)$ and $V_b(f)$ are the wave velocities, m · s⁻¹; V is the phase velocity, m · s⁻¹; f is frequency, Hz.

When measuring a wave velocity and attenuation, the strain amplitude changed in a closed cycle. First, the amplitude increased from the minimum to the maximum value (upward course), then decreased through the same values (downward course). The full course: $\varepsilon_1 \approx 0,5 \times 10^{-6} \rightarrow \varepsilon_2 \approx 1,0 \times 10^{-6} \rightarrow \varepsilon_3 \approx 1,3 \times 10^{-6} \rightarrow \varepsilon_4 \approx 1,67 \times 10^{-6} \rightarrow \varepsilon_3 \approx 1,3 \times 10^{-6} \rightarrow \varepsilon_2 \approx 1,0 \times 10^{-6} \rightarrow \varepsilon_1 \approx 0,5 \times 10^{-6}$. The increase and subsequent decrease in the amplitude are marked with arrows in all Figures. The pulse recording was carried out with the accumulation of signals (responses). This provided improved noise immunity.

Research Findings

Figs. 1 and 2 show the dependence of P and S wave velocities on the strain amplitude in dry and water-saturated (50 %) sandstone at a constant pressure of 20 MPa. In Fig. 1, in dry sandstone, on the ascending and descending courses of the strain

amplitude, P-wave velocity increases by 1.12 %. In water-saturated sandstone, the change in wave velocity under the same conditions is 0.28 %. The velocity diagrams represent open hysteresis loops (marked with brackets). The open hysteresis of dry and water-saturated sandstone is 1.41 and 0.28 %, respectively. The change in S-wave velocity under the same measurement conditions did not exceed 0.35 %. The open part of the hysteresis loop for dry and water-saturated sandstone is 0.54 and 0.35 %, respectively.

Fig. 3 shows the attenuation of P-wave as a function of the strain amplitude in dry and water-saturated sandstone at constant pressure. In dry sandstone, when the amplitude changes from the minimum to the maximum value, the attenuation of the wave increases in a non-linear way by 5.43 %. When the amplitude returns to the minimum value, the attenuation decreases to the initial value. As a result, the attenuation hysteresis loop is closed. In water-saturated sandstone, an increase in amplitude has little effect on attenuation. On the reverse course of the amplitude, the attenuation decreases by 4.93 %. This leads to the appearance of an open hysteresis loop. The water-saturated sandstone attenuation curve is above that for dry sandstone.

Fig. 4 shows the attenuation of S-wave as a function of the strain amplitude in dry and

water-saturated sandstone at constant pressure. The curves for dry and water-saturated sandstone are significantly spaced apart. The value of wave attenuation in dry sandstone is much less than in water-saturated sandstone. In both cases, as the amplitude increases, the attenuation decreases. In dry and water-saturated sandstone, the attenuation reduction is 8.81 % and 2.71 %, respectively. Both hysteresis loops are open. The value of the open hysteresis loop in both cases does not exceed 0.8 %.

Fig. 5 shows P-wave velocity as a function of confining pressure in dry and water-saturated sandstone at constant strain amplitude. With an increase in the confining pressure from the minimum to the maximum value both in dry and water-saturated sandstone, the wave velocity increases in a non-linear way by 15.06 and 26.35 %, respectively. In both cases, an open hysteresis loop is observed: for dry sandstone, 9.77 %, and for water-saturated one, 15.93 %. Fig. 6 shows S-wave velocity as a function of confining pressure in dry and water-saturated sandstone at a constant strain amplitude. Here, the increase in the wave velocity proceeds in the same way as in the case of P-wave, and amounts to 12.42 % for dry sandstone, and 15.81 % for water-saturated sandstone. The open hysteresis for dry sandstone is 0.67 %, and water-saturated is 3.45 %.

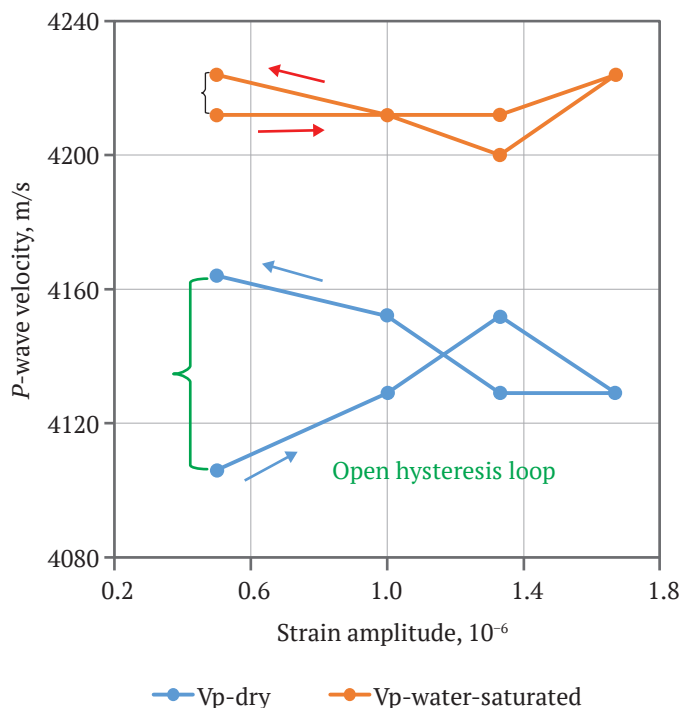


Fig. 1. P-wave velocity versus strain amplitude in dry and water-saturated sandstone

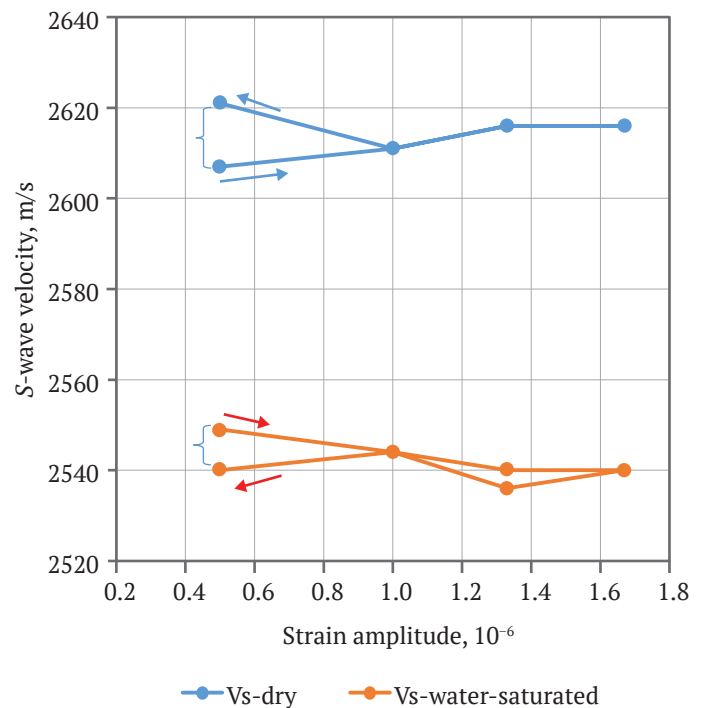


Fig. 2. S-wave velocity versus strain amplitude in dry and water-saturated sandstone

Findings Discussion

The conducted study shows the complex effect of strain amplitude, pressure, and sandstone state on the behavior of the velocity and attenuation of *P* and *S* waves. Wave attenuation is more sensitive to amplitude deviation and sandstone wetness than wave velocity. The behavior of the velocity

of a longitudinal wave differs significantly from that of a transverse one. The measurements of *P*-wave velocity show that the change in the state of sandstone affects the shape of the hysteresis and the magnitude of its opening. The open part of the hysteresis for a longitudinal wave is 1.41 % in dry sandstone and 0.28 % in water-saturated one, i.e.

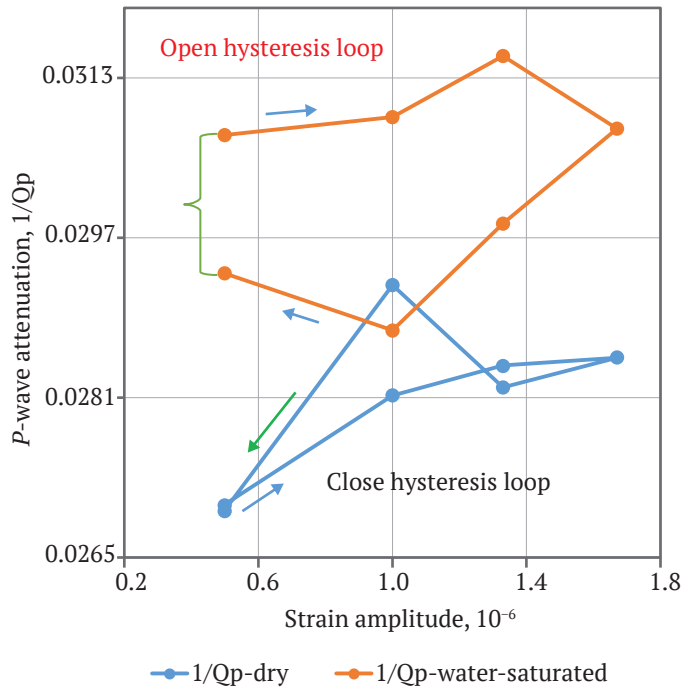


Fig. 3. Attenuation of *P*-wave depending on strain amplitude in dry and water-saturated sandstone

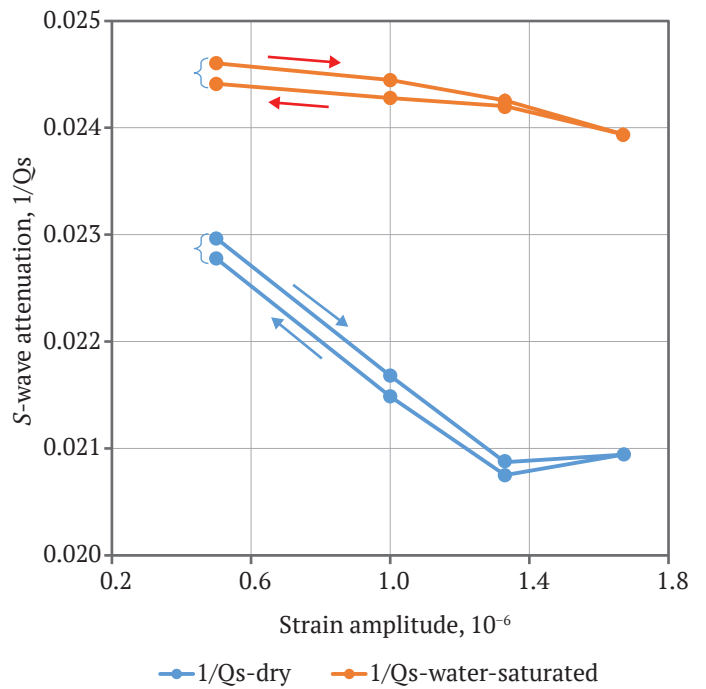


Fig. 4. Attenuation of *S*-wave depending on strain amplitude in dry and water-saturated sandstone

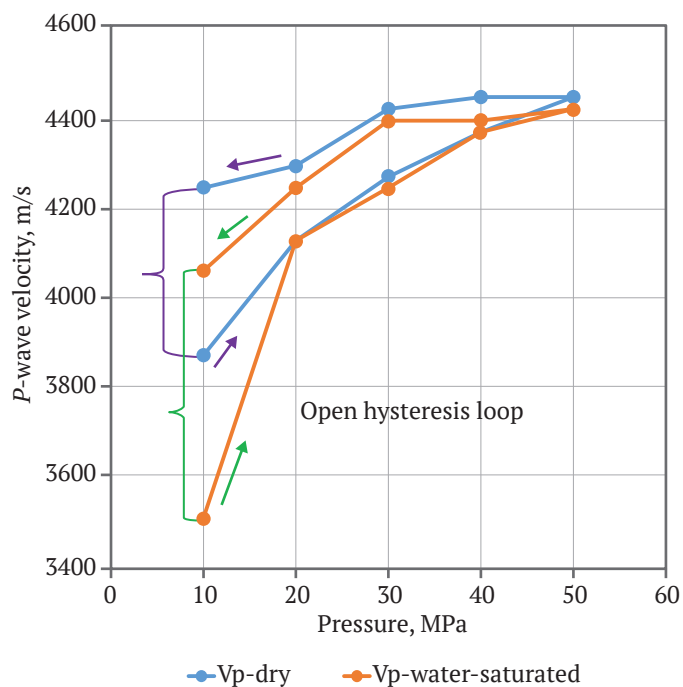


Fig. 5. *P*-wave velocity as a function of confining pressure in dry and water-saturated sandstone

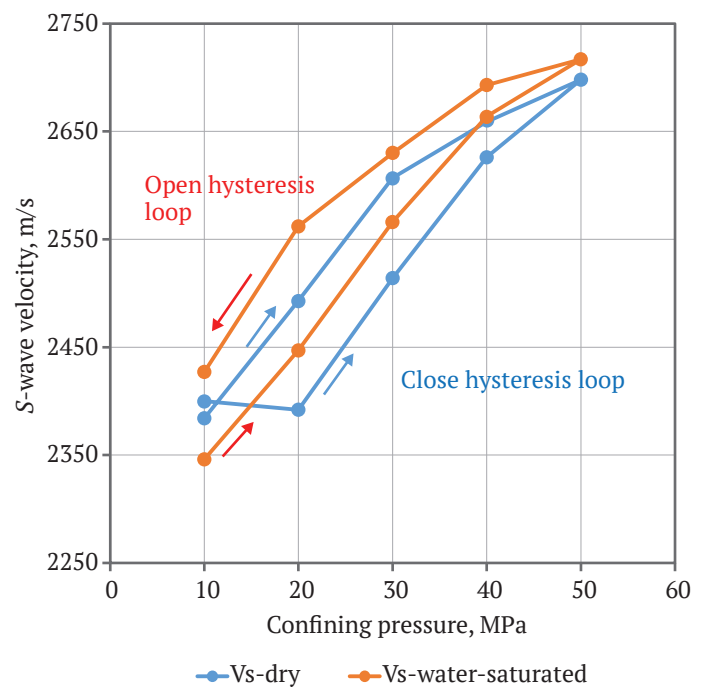


Fig. 6. *S*-wave velocity as a function of confining pressure in dry and water-saturated sandstone



there is a great difference between them. S-wave velocity in both dry and water-saturated sandstone responds weakly to amplitude deviation.

The greatest change in the attenuation of a longitudinal wave due to the strain amplitude was obtained in dry sandstone (5.43 %), the same as that of a transverse wave at the same sandstone state (8.81 %). The change in the attenuation of a transverse wave in water-saturated sandstone due to the amplitude reaches 2.71 %. For a longitudinal wave, an open hysteresis was recorded in the water-saturated sandstone (4.5 %), while it is not manifested in the dry one. For a transverse wave, both in dry and water-saturated sandstone, the manifestation of open hysteresis is insignificant. A change in the confining pressure in a closed regime for both longitudinal and transverse waves leads to a non-linear increase in the velocity and the appearance of an open hysteresis loop. It should be noted that the velocities of longitudinal and transverse waves at both states of sandstone respond to the changes in the value of the confining pressure.

Conclusion

An analysis of the new data obtained in the experiment shows the complex nature of the behavior of the velocity and attenuation of longitudinal and transverse waves depending on the strain amplitude and wetness of the sandstone. Changing the strain amplitude and confining pressure within a closed cycle (i.e. its increase and adequate decrease) leads to a significant change in the dynamic characteristics of the recorded

response. This transformation takes place for wave velocity and attenuation. The strain amplitude affects the open and closed type hysteresis both for a wave velocity and attenuation. In both dry and water-saturated sandstone, an open hysteresis loop is observed in most cases. There are cases of the manifestation of a closed hysteresis loop and also the effect of overlapping hysteresis loops. The greatest change in wave velocity due to strain amplitude was obtained for a longitudinal wave in dry sandstone. However, the attenuation parameter exceeds the achievements of the wave velocity. The highest result for the amplitude-dependent attenuation was obtained in dry sandstone with the propagation of a longitudinal wave, 5.43 %, and with the propagation of a transverse wave, 8.81 %.

In our study, the signs of the manifestation of microplasticity include the following: open and closed hysteresis found in amplitude-dependent velocity and attenuation in dry and water-saturated sandstone; non-linear nature and overlap of the ascending and descending amplitude courses. Their divergence may be caused by the effect of microplasticity. The complex and peculiar behavior of both hysteresis loops suggests the possibility of contribution of a non-standard mechanism in the sandstone strain. The diverse behavior of wave velocity and attenuation at rock strain can be caused by the combined effect of viscoelasticity and microplasticity processes. The qualitative and quantitative characteristics of the complications of dynamic parameters can be the signs of the internal structure of the subject.

References

1. Gushchin V.V., Pavlenko O.V. Study of nonlinear elastic properties of rocks based on seismic data. In: *Modern seismology. Achievements and Challenges*. Vol. 13. Moscow; 1998. (In Russ.)
2. Egorov G.V. Variation of nonlinear parameters of a consolidated water-saturated porous specimen depending on the degree of gas saturation. *Fizicheskaya Mezomekhanika*. 2007;10(1):107–110. (In Russ.)
3. Kondratyev O.K. *Seismic waves in absorbing media*. Moscow: Nedra Publ.; 1986, 176 p. (In Russ.)
4. Nikolaev A.V. *Problems of nonlinear seismic*. Moscow: Nauka Publ.; 1987. 288 p. (In Russ.)
5. Diallo M.S., Prasad M., Appel E. Comparison between experimental results and theoretical predictions for P-wave velocity and attenuation at ultrasonic frequency. *Wave Motion*. 2003;37(1):1–16. [https://doi.org/10.1016/S0165-2125\(02\)00018-5](https://doi.org/10.1016/S0165-2125(02)00018-5)
6. Duret T., Souche A., Borst R., Le Pourhiet L. The benefits of using a consistent tangent operator for viscoelastoplastic computations in geodynamics. *Geochemistry, Geophysics, Geosystems*. 2018;19(12):4904–4924. <https://doi.org/10.1029/2018GC007877>
7. Golovin I.S., Pavlova T.S., Golovina S.B. et al. Effect of severe plastic deformation on internal friction of an Fe–26at.% Al alloy and titanium. *Materials Science and Engineering: A*. 2006;442(1–2):165–169.
8. Guyer R.A., Johnson P.A. Nonlinear mesoscopic elasticity: Evidence for a new class of materials. *Physics Today*. 1999;52(4):30–36. <https://doi.org/10.1063/1.882648>



9. Mashinskii E. I. Difference between static and dynamic elastic moduli of rocks: Physical causes. *Russian Geology and Geophysics*. 2003;44(9):953–959.
10. Derlet P. M., Maaß R. *Micro-plasticity and intermittent dislocation activity in a simplified micro structural model*. arXiv:1205.1486v2. Condensed Matter – Materials Science. 8 February 2013. <https://doi.org/10.48550/arXiv.1205.1486>
11. Mashinskii E. I. Amplitude-frequency dependencies of wave attenuation in single-crystal quartz: experimental study. *Journal of Geophysical Research. Solid Earth*. 2008;113(B11). <https://doi.org/10.1029/2008JB005719>
12. Mashinskii E. I. Seismo-micro-plasticity phenomenon in the rocks. *Natural Science*. 2010;2(3):155–159. <https://doi.org/10.4236/ns.2010.23025>
13. Mashinskii E. I. Jump-like inelasticity in sandstone and its effect on the amplitude dependence of P-wave attenuation: An experimental study. *Wave Motion*. 2020;97:102585. <https://doi.org/10.1016/j.wavemoti.2020.102585>
14. Huang J., Zhao M., Du X. et al. An elasto-plastic damage model for rocks based on a new nonlinear strength criterion. *Rock Mechanics and Rock Engineering*. 2018;51:1413–1429. <https://doi.org/10.1007/s00603-018-1417-1>
15. Vodenitcharova T., Zhang L. C. A new constitutive model for the phase transformations in mono-crystalline silicon. *International Journal of Solids and Structures*. 2004;41(18–19):5411–5424. <https://doi.org/10.1007/s00603-018-1417-1>
16. Liu Y., Dai F., Feng P., Xu N.-W. Mechanical behavior of intermittent jointed rocks under random cyclic compression with different loading parameters. *Soil Dynamics and Earthquake Engineering*. 2018;113:12–24. <https://doi.org/10.1016/j.soildyn.2018.05.030>
17. Nourifard N., Lebedev M. Research note: the effect of strain amplitude produced by Ultrasonic waves on its velocity. *Geophysical Prospecting*. 2019;67(4):715–722. <https://doi.org/10.1111/1365-2478.12674>
18. Nourifard N., Mashinskii E., Lebedev M. The effect of wave amplitude on S-wave velocity in porous media: an experimental study by Laser Doppler Interferometry. *Exploration Geophysics*. 2019;50(6):683–691. <https://doi.org/10.1080/08123985.2019.1667228>
19. Baud P., Vajdova V., Wong T. Shear-enhanced compaction and strain localization: Inelastic deformation and constitutive modeling of four porous sandstones. *Journal of Geophysical Research. Solid Earth*. 2006;111(B12). <https://doi.org/10.1029/2005JB004101>
20. Gurmani S. F., Jahn S., Brasse H., Schilling F. R. Atomic scale view on partially molten rocks: Molecular dynamics simulations of melt-wetted olivine grain boundaries. *Journal of Geophysical Research. Solid Earth*. 2011;116(B12). <https://doi.org/10.1029/2011JB008519>
21. Olsson A. K., Austrell P.-E. A fitting procedure for viscoelastic-elastoplastic material models. In: *Proceedings of the Second European Conference on Constitutive Models for Rubber*. Hannover, Germany, 10–12 September 2001.
22. Golovin Yu. I., Dub S. N., Ivolgin V. I. et al. Kinetic features of strain of solids in nano-microvolumes. *Physics of the Solid State*. 2005;47(6):961–973. (In Russ.)
23. Peschanskaya N. N., Smirnov B. I., Shpeizman V. V. Steplike micro-strain in nano-structural materials. *Physics of the Solid State*. 2008;50(5):815–819.
24. Zhou C., Biner S. B., LeSar R. Discrete dislocation dynamics simulations of plasticity at small scales. *Acta Materialia*. 2010;58:1565–1577.
25. Luo Sh.-N., Swadener J. G., Ma Ch., Tschauer O. Examining crystallographic orientation dependence of hardness of silica stishovite. *Physica B: Condensed Matter*. 2007;399(2):138–142. <https://doi.org/10.1016/j.physb.2007.06.011>
26. Yin H., Zhang G. Nanoindentation behavior of muscovite subjected to repeated loading. *Journal of Nanomechanics and Micromechanics*. 2011;1(2):72–83. [https://doi.org/10.1061/\(asce\)nm.2153-5477.0000033](https://doi.org/10.1061/(asce)nm.2153-5477.0000033)
27. Mashinskii E. I., Dynamic micro-plasticity manifestation in consolidated sandstone in the acoustical frequency range. *Geophysical Prospecting*. 2016;64:1588–1601. <https://doi.org/10.1111/1365-2478.12368>
28. Nishino Y., Kawaguchia R., Tamaokaa S., Idea N. Amplitude-dependent internal friction study of fatigue deterioration in carbon fiber reinforced plastic laminates. *Materials Research*. 2018;21(2):e20170858. <https://doi.org/10.1590/1980-5373-MR-2017-0858>



29. Johnston D.H., Toksoz M.N. Thermal cracking and amplitude dependent attenuation. *Journal of Geophysical Research. Solid Earth*. 1980;85(B2):937–942. <https://doi.org/10.1029/JB085iB02p00937>

30. Jones S.M. Velocity and quality factors of sedimentary rocks at low and high effective pressures. *Geophysical Journal International*. 1995;123(3):774–780. <https://doi.org/10.1111/j.1365-246X.1995.tb06889.x>

31. Mavko G.M. Frictional attenuation: an inherent amplitude dependence. *Journal of Geophysical Research. Solid Earth*. 1979;84(B9):4769–4775. <https://doi.org/10.1029/JB084iB09p04769>

32. Winkler K.W. Frequency dependent ultrasonic properties of high-porosity sandstones. *Journal of Geophysical Research. Solid Earth*. 1983;88(B11):9493–9499. <https://doi.org/10.1029/JB088iB11p09493>

Information about the author

Eduard I. Mashinskii – Dr. Sci. (Geol. and Min.), Trofimuk Institute of Petroleum Geology and Geophysics of Siberian Branch of Russian Academy of Sciences, Novosibirsk, Russian Federation; ORCID [0000-0001-8621-0719](https://orcid.org/0000-0001-8621-0719), Scopus ID [8886240600](https://scopus.com/authorid/8886240600); e-mail MashinskiiEI@ipgg.sbras.ru

Received 01.12.2022

Revised 07.02.2023

Accepted 08.02.2023



MINING ROCK PROPERTIES. ROCK MECHANICS AND GEOPHYSICS

Research paper

<https://doi.org/10.17073/2500-0632-2022-07-11>

UDC 622.83:550.83

**Influence of random parameter joint length on rock electrical conductivity**

P. E. Sizin , A. S. Voznesenskii , L. K. Kidima-Mbombi

University of Science and Technology MISIS, Moscow, Russian Federation al48@mail.ru**Abstract**

Rock joint hollowness coefficient is an important parameter when resolving practical mining problems. Geophysical methods used to resolve this problem are indirect. Thus the interpretation of their results may cause certain difficulties as a result of the uncertainty of the physical relationships between the parameters of joints and the measurement results. One of the ways to resolve this problem is to combine experimental research methods with analytical and numerical simulation. The studies were aimed at investigating the electrical conductivity of a two-dimensional medium in the presence of thin insulating (non-conducting) joints. This paper proposes an analytical method for assessing the dependence of the specific conductivity of a medium with inclusions in the form of elliptical joints on their half-length. This dependence is shown to have the form of an exponent depending on the square of the length of the maximum semi-axis as an argument. The simulation method is based on the assumption of the elliptical shape of a joint when the length of the minor semi-axis of the ellipses tends to zero. A review of publications and their results presented in this paper showed that this method for determining the specific conductivity of the medium with thin joints is one of the best in terms of compliance with experimental data. Its predictions are close to those of the Effective Media Approximation (EMA). However, the proposed method is distinguished by the simplicity of the formulas and their physical visibility essential for the use in interpreting the data of a physical experiment. In two-dimensional formulation, numerical simulation of the specific electrical conductivity of a sample of a medium measuring 1×1 m with elliptical joints of conductivity less than that of the matrix was carried out in the COMSOL Multiphysics environment. A square sample of unit sizes with unit conductivity was considered in which 25 joints with uniform distribution along the length occurred. 40 models were built wherein the maximum length of the joints varied from 0.01 to 0.4 sample size in increments of 0.01 m. The satisfactory concordance of the results of numerical and analytical models, both visual and confirmed by statistical estimates, has been shown. It was noted that when the size of the joints changes to achieve the value of the maximum semi-axis $a = 0.15$ m, the influence of single joints that do not extend beyond the boundaries of the sample prevails. Above this value, at $a > 0.15$ m, the influence of joint coalescence, as well as their extension to and beyond the sample boundaries begins to affect. Comparison of the proposed theoretical model of electrical conductivity, depending on the square of the length of the maximum semi-axis of a joint, with a similar model in the form of an exponent with a linear dependence showed a better concordance of the proposed model with observations at the stage of the lack of joint coalescence and their extension to the sample boundaries at $a < 0.15$ m. At $a > 0.15$ m. The proposed model has a lower coefficient of determination compared to the full range including both intervals, but higher than that of the model with a linear dependence in the exponent argument. This indicates the universal nature of the proposed model.

Keywords

electrical resistance, joint length, numerical, analytical, simulation, COMSOL Multiphysics

For citation

Sizin P.E., Voznesenskii A.S., Kidima-Mbombi L.K. Influence of random parameter joint length on rock electrical conductivity. *Mining Science and Technology (Russia)*. 2023;8(1):30–38. <https://doi.org/10.17073/2500-0632-2022-07-11>

СВОЙСТВА ГОРНЫХ ПОРОД. ГЕОМЕХАНИКА И ГЕОФИЗИКА

Научная статья

Влияние длины трещин со случайными параметрами на электрическую проводимость горных пород

П. Е. Сизин , А. С. Вознесенский , Л. К. Кидима Мбомби

Университет науки и технологий МИСИС, г. Москва, Российская Федерация al48@mail.ru**Аннотация**

При решении практических задач горного производства возникает необходимость оценки трещинной пустотности горных пород. Геофизические методы при решении данной задачи являются косвенными, поэтому интерпретация результатов может вызывать определенные трудности, обу-



словенные непрозрачностью физических связей между параметрами трещин и результатами измерений. В этой связи одним из путей решения данной проблемы является сочетание экспериментальных методов исследования с аналитическим и численным моделированием. Исследования были направлены на изучение электрической проводимости двумерной среды при наличии тонких изолирующих трещин. В статье предложен аналитический метод оценки зависимости удельной проводимости среды с включениями в виде эллиптических трещин от их полудлины. Показано, что данная зависимость имеет вид экспоненты, зависящей от квадрата длины максимальной полуоси в качестве аргумента. Метод моделирования основан на допущении эллиптической формы трещины при устремлении к нулю длины малой полуоси эллипсов. Анализ публикаций и результаты, изложенные в статье, показали, что такой метод нахождения удельной проводимости среды с тонкими трещинами один из наилучших в плане соответствия экспериментальным данным. Его предсказания близки к предсказаниям метода эффективной среды (ЕМА), но он отличается простотой формул и их физической наглядностью, что существенно для использования при интерпретации данных физического эксперимента. В двумерной постановке проведено численное моделирование в среде COMSOL Multiphysics удельной электрической проводимости образца среды размером 1×1 м с эллиптическими трещинами меньшей, чем у матрицы, проводимости. Рассмотрен квадратный образец единичных размеров с единичной проводимостью, в котором помещалось 25 трещин, имевших равномерное распределение по длине. Было построено 40 моделей, в которых максимальная длина трещин менялась от 0,01 до 0,4 размера образца, с шагом 0,01 м. Показано удовлетворительное соответствие результатов численной и аналитической моделей как визуальное, так и подтвержденное с помощью статистических оценок. Отмечено, что при изменении размера трещин до значения максимальной полуоси $a = 0,15$ м преобладает влияние одиночных трещин, не выходящих за границы образца. Выше этого значения при $a > 0,15$ м начинает сказываться влияние слияния трещин, а также их выхода на границы и за пределы образца. Сравнение предложенной теоретической модели электрической проводимости, зависящей от квадрата длины максимальной полуоси трещины, с похожей моделью в виде экспоненты с линейной зависимостью показало лучшее соответствие предложенной модели на стадии отсутствия слияния трещин и их выхода на границы образца при $a < 0,15$ м. При $a > 0,15$ м предложенная модель имеет меньший коэффициент детерминации по сравнению с полным диапазоном, включающим оба участка, но более высокий, чем у модели с линейной зависимостью в аргументе экспоненты, что говорит об универсальном характере предложенной модели.

Ключевые слова

электрическое сопротивление, длина трещины, численный, аналитический, моделирование, COMSOL Multiphysics

Для цитирования

Sizin P.E., Voznesenskii A.S., Kidima-Mbombi L.K. Influence of random parameter joint length on rock electrical conductivity. *Mining Science and Technology (Russia)*. 2023;8(1):30–38. <https://doi.org/10.17073/2500-0632-2022-07-11>

Introduction

The relevance of the problem of assessing rock joint hollowness coefficient emerges from the need to address problems of strength [1–4] and stability of rocks around mine workings [5–7], hydraulic fracturing of rock mass [8–10], fluid filtration through a rock mass [11, 12], the calculation of drilling and blasting parameters [13–15], as well as other practical problems of mining. Geological [16–18], surveying [19–21], video methods [22, 23] are used to determine rock jointing. A special place here is occupied by geophysical methods [24–26]. A significant place is given to electromagnetic [27] and electric [28] methods. Despite the significant advantages of electrical methods for studying rock jointing, they also have a number of disadvantages. The geophysical methods are indirect, so the interpretation of their results may cause certain difficulties due to the uncertainty of the physical relationships between the parameters of joints and the measurement results. In this regard, one

of the ways of resolving this problem is to combine experimental research methods with analytical and numerical simulation. As an example, we can cite study [29] which shows the theoretical feasibility of analytical calculation of the relationship between rock jointing and electrical resistance.

The problem of sample resistance with joints ultimately comes down to the problem of the conductivity of a two-component medium consisting of a continuum (matrix) and a component represented by individual inclusions. At low concentration of the inclusions, such conductivity is easily calculated [30]. It is connected with the concentration of inclusions according to the linear law. In the case of high concentrations, the best method is considered to be the Effective Media Approximation (EMA) [31–33]. Initially designed for “volumetric” inclusions (spheres in three-dimensional space, circles, squares, etc. in two-dimensional problems), it was then modified for the case of “disembodied” inclusions, such as infinitely thin disks in the



three-dimensional case and “scratches” in the two-dimensional case [34]. This approach enables the electrical conductivity of rocks containing joints to be simulated. At the same time, in actual rocks, joints can be empty or containing low-conducting liquids (oil). They can also be filled with a solution of salts (high-conductive fluid) [35]. In the former case, the joints should be considered insulating, while in the latter one, almost perfectly conductive when the fluid conductivity is several orders of magnitude higher than the conductivity of the host rock [29]. In this paper, a model of “dry” or fluid-filled joints with a conductivity of 10-4 of the conductivity of a rock matrix is used. It should also be noted that at some rather high concentration of inclusions, coalescence occurs when they overlap, forming a continuous conductive or insulating cluster [36–38]. However, in the first place, such high concentrations of joints will not be considered, since when approaching the coalescence threshold, disintegration of a sample occurs.

The purpose of this study is to develop analytical and numerical models of the dependencies of the electrical resistance of a rock sample on the size of joints, and compare the results of simulating by these methods with each other, as well as with the results of testing rock samples.

2. Research techniques

2.1. Analytical method

Let us consider the problem of conductivity of a two-dimensional medium with thin joints (in the limit, scratches of zero thickness). For the case of low concentration of scratches perpendicular to the gradient of the applied voltage (and the direction of the electric current), we get [34]

$$\sigma = \sigma_0 \left(1 - \pi \left(\frac{l}{2} \right)^2 N \right), \quad (1)$$

where σ_0 is conductivity of a medium without joints; $l/2$ is the “radius” of a joint, equal to half of its length; N is two-dimensional concentration of joints. In the case of chaotic orientation of the joints (uniform distribution by angle), the contribution of these joints to the conductivity is halved:

$$\sigma = \sigma_0 \left(1 - \frac{\pi l^2}{8} N \right).$$

The reason is that when the conductivity is averaged by a statistical ensemble of joints, one of the two coordinate axes does not make a contribution: the insulating joints oriented parallel to the current do not significantly affect conductivity.

Note that if there is exactly a single joint in a square sample with a side L and a conductivity of σ_0 , perpendicular to the field, the concentration $N = 1/L^2$, and the sample conductivity is:

$$\sigma = \sigma_0 \left(1 - \frac{\pi l^2}{4L^2} \right).$$

Let us suppose now a square sample with a side L contains n joints perpendicular to the applied voltage and has a conductivity of σ . Let us place another similar joint into this sample. In this case, the increment of the sample conductivity

$$\Delta\sigma = -\sigma \frac{\pi l^2}{4L^2}.$$

Thus, we obtain a differential equation ($\Delta n = 1$)

$$\frac{\Delta\sigma}{\Delta n} = -\sigma \frac{\pi l^2}{4L^2}, \quad (2)$$

the solution of which is

$$\sigma = \sigma_0 e^{-\frac{\pi l^2}{4L^2} n},$$

where the obvious initial condition is used: the conductivity in the absence of joints is σ_0 . Given the two-dimensional concentration of joints, this solution can be written in the form:

$$\sigma = \sigma_0 e^{-\frac{\pi l^2}{4} N}. \quad (3)$$

Let the lengths of the joints now be distributed evenly in the range from 0 to l . In this case, the average value of the square of the joint length is $l^2/3$. This value will determine the average contribution of an individual joint to the change in conductivity. Then the initial differential equation should be replaced with

$$\frac{\Delta\sigma}{\Delta n} = -\sigma \frac{\pi l^2}{12L^2},$$

and we get for the sample conductivity

$$\sigma = \sigma_0 e^{-\frac{\pi l^2}{12L^2} n},$$

or taking into account the concentration of joints in the two-dimensional case $N = n/L^2$

$$\sigma = \sigma_0 e^{-\frac{\pi l^2}{12} N}. \quad (4)$$

It is often beneficial to use half the length of a joint $a = l/2$ (similar to the radius of a circular inclusion), and then

$$\sigma = \sigma_0 e^{-\frac{\pi a^2}{3} N}. \quad (5)$$

If we denote $A = \pi N/3$, formula (3) takes on form

$$\sigma = e^{-Aa^2}. \quad (6)$$

The parameter A has the physical meaning of the effective concentration of joints and can be found from a numerical simulation or a physics experiment.

It should be noted that in [36], use of the EMA method for conductivity of a two-dimensional medium with parallel insulating joints, the following expression was obtained:

$$\sigma = \sigma_0 \left(\sqrt{1 + \frac{1}{4} \left(\frac{\pi l^2}{4} N \right)^2} - \frac{1}{2} \frac{\pi l^2}{4} N \right)^2 \quad (7)$$

This expression at not very high concentrations of joints, up to

$$\frac{\pi l^2}{4} N \approx 1,$$

is very close to (3), but (3) is much simpler, more convenient for analysis, and has a quite transparent physical meaning.

2.2. Numerical method

The methodology for constructing geometry and setting the properties and boundary conditions of a model when using this method is explained in [39]. A feature of this approach was the construction of geometry, properties, and boundary conditions of the model using program scripts. Changing the joint parameters in each specific model was achieved by changing the values of the variables used to set the length, position, and the angle of inclination of the ellipses which simulated the joints. These parameters were changed within the specified limits using a random number generator with a uniform distribution.

The simulation was carried out using the COMSOL Multiphysics environment in conjunction with Matlab. The script was written and the changes were made in accordance with the required joint parameters. Figure 1 shows a drawing of one of the models as an example. The simulation was carried out in dimensionless relative units. Since the results for electrical conductivity and resistance are most conveniently represented in relative values, the following technique was used in the simulation. A rock sample was selected in the form of a square with a side of 1 m, with a specific conductivity of 1 Cm/m. A voltage of 1 V was applied to the two opposite sides. In the absence of joints, the current in the sample was 1 A. When joints were added, the current became less than 1 A. By virtue of Ohm's law, numerically coinciding with both the conductivity and the specific conductivity of a fractured rock.

A total of 40 models were used when changing the half-lengths of the joints from 0.01 to 0.4 m. One

more model was jointless and corresponded to the case $a/2 = 0$. The minor semi-axis of the joints was 0.01 m, and the major semi-axis in accordance with the uniform distribution varied from 0.01 m to the value assigned in the series of experiments, ranging from 0.01 to 0.4 m. The joint angle varied within $\pm 20^\circ$. The number of joints in the sample was 25. The maximum displacements of the centers of the ellipses from the regular grid horizontally and vertically with their uniform distribution amounted to $\pm 0.2DX$ and $\pm 0.5DY$, respectively, where DX , DY were the average distances between the centers of joints along X and Y axes, respectively. With some combinations of joint sizes and displacements relative to their centers, they could partially or completely extend beyond the contour of a sample, while their total number was less than the specified value. In addition, the coalescence of joints led to a decrease in their equivalent number. Several interconnected joints led to an effect equivalent to the effect of one joint of greater length. The specific conductivity of the rock matrix was 1 cm/m, and that of the joint material, 10–4 cm/m. The boundary conditions were as follows: on the upper edge, the potential V was set at $V_0 = 1$ V, and on the lower edge $V_0 = 0$ V (“earth”). On the side edges, zero conductivity was set $\sigma = 0$ cm/m (insulation).

For finding solutions in the COMSOL Multiphysics system, a static problem solver was used in the simulation, which allowed obtaining the distribution of currents and voltages in steady state.

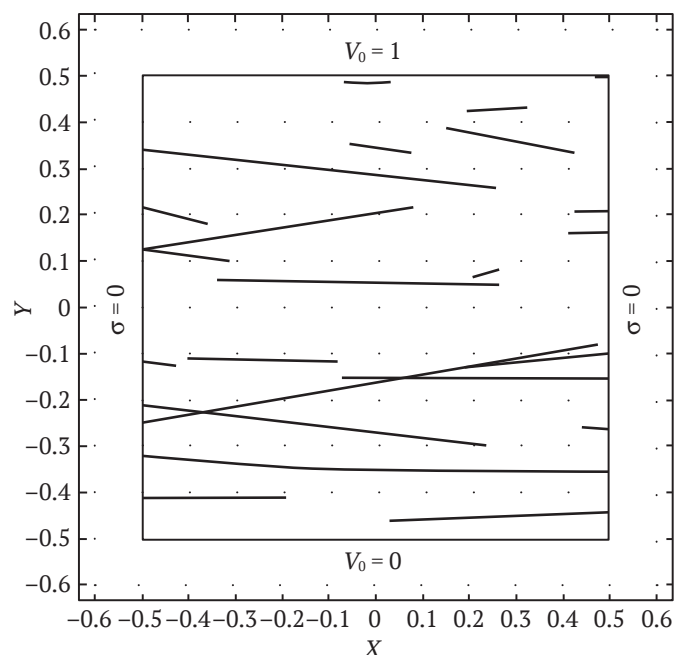


Fig. 1. Example of a 2D model scheme for a numerical experiment

3. Findings

Figure 2 presents examples of the results of simulation of current flow through a sample without joints (*a*), with elliptical joints of half-length from 0.01 to 0.1 m (*b*), from 0.01 to 0.2 m (*c*), from 0.01 to 0.5 m (*d*). The red current lines clearly demonstrate the effect of joints, acting as “dams” for current.

On the graph in Fig. 3, the sample conductivity dependencies obtained by finite element calculations are represented in the form of separate points. The formula (6) was used to approximate the results obtained.

As can be seen the satisfactory mutual convergence of the theoretical and experimental attracts them to each other. The quantitative estimates of this convergence are given below.

4. Findings Discussion

If there are no joints in a sample, the current lines (Fig. 2, *a*) are evenly distributed over the sample along its horizontal axis, and the electrical potential demonstrates a uniform change along the vertical axis. In the graph in Fig. 3, this case corresponds to the joint half-length $a/2 = 0$. The presence of joints of horizontal direction in Fig. 2, *b* increases the length of the current lines. This is the reason for the decrease in conductivity with an increase in $a/2$. With a significant increase in the joints length up to the complete intersection of the sample in Fig. 2, *e*, the length of the current lines increases significantly with a significant change in their configuration as compared to the intact sample in Fig. 2, *a*. In this

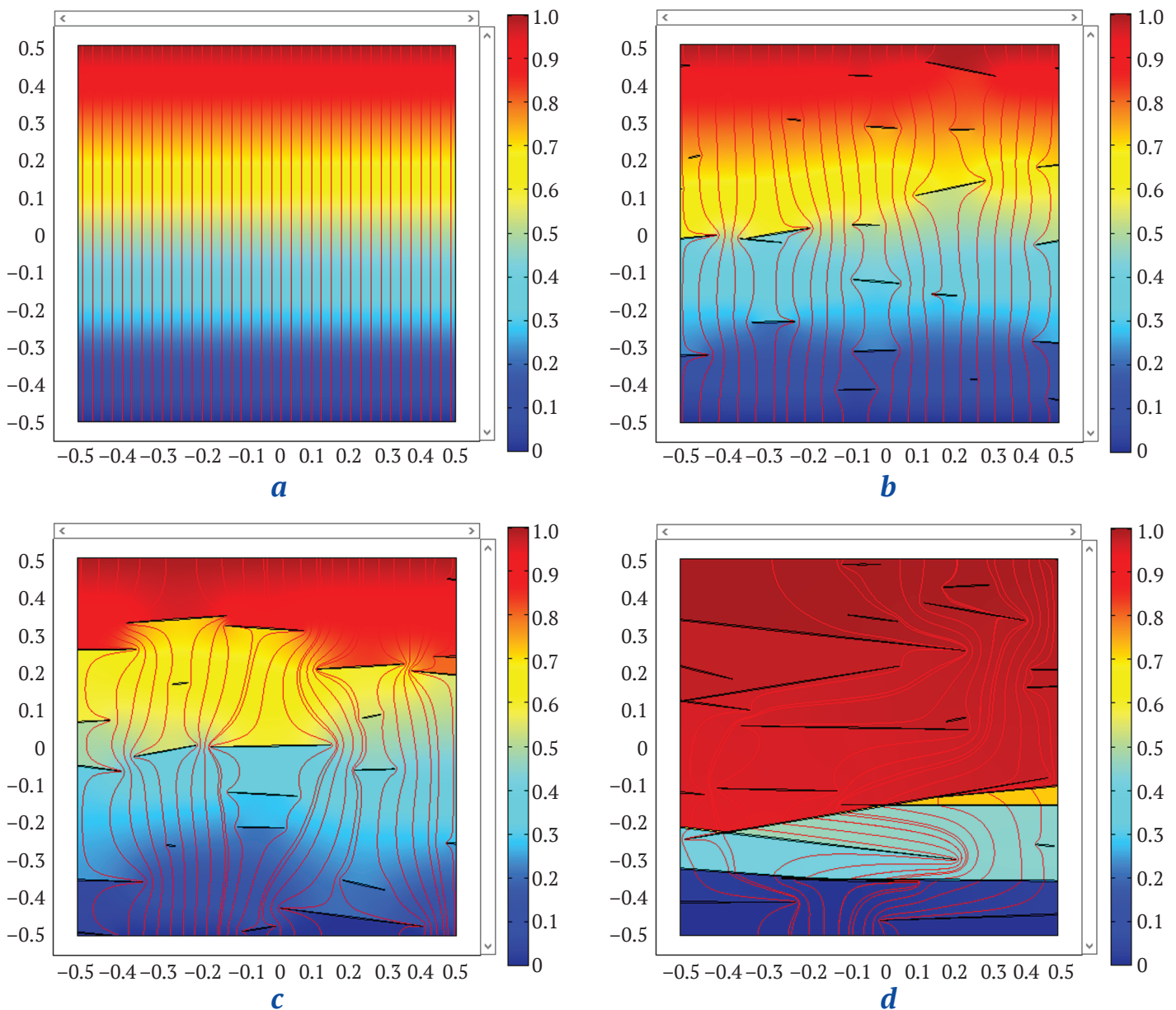


Fig. 2. Current lines (red lines) and the distribution of electrical potential relative to the lower boundary according to the scales on the right

case, the electric potential demonstrates a jump-like change in the places of joints. Since the numerical model includes a probabilistic distribution of joint parameters, the experimental points in Fig. 3 have random deviations from the analytical curve. At the same time, up to the value of $a/2 = 0.15$ (m), the points are located closer to the analytical curve than with larger values of $a/2$. This is due to the fact that the extent of high-impedance joints beyond the boundaries of the sample begins to take affect also owing to their coalescence leading to significant curvatures of the current lines.

The experimental points are well described by dependency (6), in which the parameter A is selected using the Statistica package according to the least-squares criterion

$$y = \exp(-21.23x^2),$$

where $x = a/2$ is the maximum value of the major semi-axis of an elliptical joint. The value varied from 0.01 to 0.4; $y = \sigma/\sigma_0$ is the relative conductivity of the sample; σ_0 is the conductivity of the sample without joints. In this case, the parameter is $A = 21.33$, which corresponds to the equivalent number of joints $N_{eq} = 3A/\pi = 20.4$. This number is noticeably less than 25, the true number of joints in the sample. This is explained by the fact that with considerable sizes of joints, some of them merge with each other or occur on the boundaries of the sample. The determination coefficient of the numerical simulation results at approximation $R^2 = 0.977$, the root-mean-square deviation (RMSD) = 0.0494 cm/m, reflecting the random nature of the joint parameters and less than 10 % of the average conductivity value of 0.5 cm/m in the experiment. For the initial section of the curve, where the influence of edge effects and coalescence of joints does not affect, this value is much lower.

Accordingly, for a more detailed analysis, the whole range of joint half-length values a was divided into two sections: $0 \leq a < 0.15$ m (section 1) and $0.15 \leq a \leq 0.40$ m (section 2), for which statistical estimates were carried out separately.

It is interesting to compare the results obtained with the experimental results. In [40], the findings of the conductivity study for the Chayandinsky deposit reservoir rock samples are considered. The dependence of the change in specific electrical conductivity on the proportion of fracture porosity was approximated by an exponent

$$y = a_0 \exp(-a_1 x), \tag{8}$$

where a_0, a_1 are the exponential dependency parameters. The graph of the dependence according to formula (8) in comparison with the numerical simulation results is shown in Fig. 4. In this case, $a_0 = 1.179$; $a_2 = 5.251$.

As follows from the comparison of Fig. 4 with Fig. 3, visually, the approximation by dependence (8) is worse than that by dependence (6). If the experimental data curve in the first section is curved upwards, then the dependence (8) is curved downwards. In the second section, the curve (8) passes above the experimental points, although in this section the curvature of the course of both curves coincides.

Table 1 shows the results of approximation of the data obtained according to formulas (6) and (8). For formula (6), the values of parameter A and the calculated values of the equivalent number of joints N_{eq} are also given. It should be noted that the calculations according to formula (7) gave results close to the results of formula (6), so they are not given separately in Table 1. For formula (8), the values of parameter A were not calculated, because this model differed from model (6) in essence.

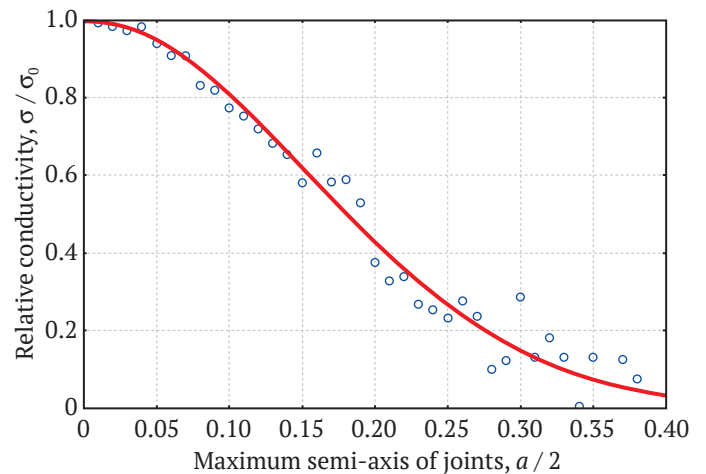


Fig. 3. Dependencies of sample conductivity on joint length obtained by a numerical method (hollow circles) and the approximation by formula (6) (solid line)

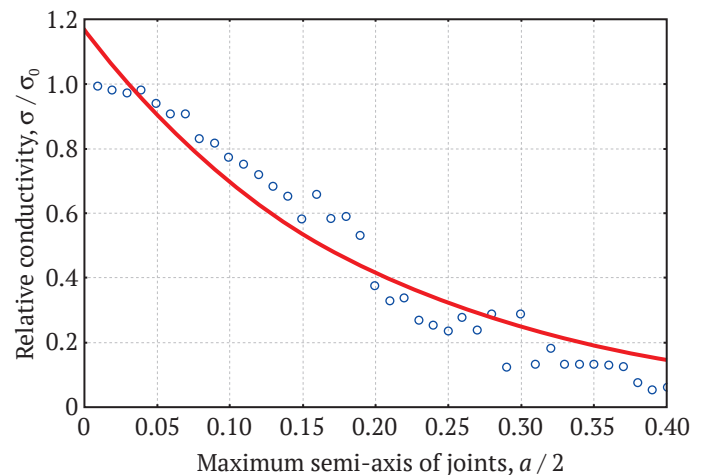


Fig. 4. Approximation of experimental points by dependence (8)



Table 1
Statistical parameters of numerical simulation results approximation according to formulas (6) and (8)

Formula number	Section	R^2	RMSD	A	N_{eq}
(6)	1+2	0.979	0.014	20.34	21.30
	1	0.987	0.00014	23.32	24.42
	2	0.901	0.016	19.96	20.90
(8)	1+2	0.935	0.044	–	–
	1	0.932	0.0036	–	–
	2	0.922	0.012	–	–

As follows from Table 1, formula (8) gives worse results compared to formula (6). Thus, for the complete curve (8) and for its first section, the determination coefficient R^2 is lower, and the RMSD is higher than for curve (6). For the second section, where joints overlap and their extension beyond the sample limits begin to affect, this difference is lower, but still significant.

In paper [40], the author explains that the dependence of type (8) is used to approximate joints in actual samples. Such samples have a rather developed system of joints, which in large part overlap with each other, and also demonstrate an extent beyond the sample. This factor is predominant in the description of the dependencies in question, and dependence (8) is acceptable for this case.

Thus, it can be concluded that formula (6) is acceptable for describing the relationship between the size of joints and the conductivity of a rock sample in the case of "dry" or low-conductive fluid-filled joints at their low concentration before the manifestation of joint coalescence phenomena.

Conclusion

1. An analytical method for assessing the dependence of the specific electrical conductivity of a medium with inclusions in the form of thin elliptical joints on their half-length is proposed. It was shown that this dependence has the form of an exponent depending on the square of the length of the maximum

semi-axis as an argument. The simulation method is based on the assumption of the elliptical shape of a joint when the length of the minor semi-axis of the ellipses tends to zero. The review of publications and the results presented in this paper showed that this method for determining the specific conductivity of the medium with thin joints is one of the best in terms of the compliance with experimental data. Its predictions are close to those of the Effective Media Approximation (EMA), while the proposed method is distinguished by the simplicity of the formulas and their physical visibility essential for use in interpreting the data of a physical experiment.

2. In a two-dimensional formulation, a numerical simulation of the specific electrical conductivity of a sample of a medium measuring 1×1 m with elliptical joints of conductivity less than that of the matrix was carried out using the COMSOL Multiphysics environment. Satisfactory concordance of the results of numerical and analytical models, both visual and confirmed by statistical estimates, was shown. It was noted that when the size of the joints changes to the value of the maximum semi-axis $a = 0.15$ m, the influence of single joints which do not extend beyond the boundaries of the sample prevails. Above this value, the influence of joint coalescence as well as their extension to and beyond the sample boundaries begins to affect.

3. Comparison of the proposed theoretical model of electrical conductivity, depending on the square of the length of the maximum semi-axis of an elliptical joint, with a similar model in the form of an exponent with a linear dependence on the half-length of a joint showed a better concordance of the proposed model with the observations at the stage of the lack of joint coalescence and their extension to the sample boundaries at $a < 0.15$ m. At $a > 0.15$ m, the proposed model has a lower coefficient of determination compared to the full range including both intervals, but higher than that of the model with a linear dependence in the exponent argument. This indicates the universal nature of the proposed model.

References

1. Feng P., Zhao J., Dai F. et al. Mechanical behaviors of conjugate-flawed rocks subjected to coupled static–dynamic compression. *Acta Geotechnica*. 2022;17(5):1765–1784. <https://doi.org/10.1007/s11440-021-01322-6>
2. Feng P., Dai F., Shuai K. et al. Dynamic mechanical behaviors of pre-fractured sandstone with noncoplanar and unparallel flaws. *Mechanics of Materials*. 2022;166:104219. <https://doi.org/10.1016/j.mechmat.2022.104219>
3. Yan Z., Dai F., Liu Y. et al. Experimental investigation of pre-flawed rocks under combined static-dynamic loading: Mechanical responses and fracturing characteristics. *International Journal of Mechanical Sciences*. 2021;211:106755. <https://doi.org/10.1016/j.ijmecsci.2021.106755>
4. Qi C., Xia C., Dyskin A. et al. Effect of crack interaction and friction on the dynamic strength of rock-like materials with many cracks. *Engineering Fracture Mechanics*. 2021;257:108006. <https://doi.org/10.1016/j.engfracmech.2021.108006>



5. Gao M., Xie J., Gao Y. et al. Mechanical behavior of coal under different mining rates: A case study from laboratory experiments to field testing. *International Journal of Mining Science and Technology*. 2021;31(5):825–841. <https://doi.org/10.1016/j.ijmst.2021.06.007>
6. Lu J., Jiang C., Jin Z. et al. Three-dimensional physical model experiment of mining-induced deformation and failure characteristics of roof and floor in deep underground coal seams. *Process Safety and Environmental Protection*. 2021;150:400–415. <https://doi.org/10.1016/j.psep.2021.04.029>
7. Li T., Chen G., Li Y. et al. Study on Progressive Instability Characteristics of Coal-Rock Composite Structure with the Different Height Ratios. *Geotechnical and Geological Engineering*. 2022;40(3):1135–1148. <https://doi.org/10.1007/s10706-021-01947-0>
8. Serdyukov S., Patutin A., Rybalkin S.L. et al. Directional hydraulic fracturing based on tensile loading. In: *International Multidisciplinary Scientific GeoConference Surveying Geology and Mining Ecology Management – SGEM. International Multidisciplinary Scientific Geoconference*. 2017;17(13):269–274. <https://doi.org/10.5593/sgem2017/13/S03.034>
9. Ingles J., Lamouroux C., Soula J.C. et al. Nucleation of ductile shear zones in a granodiorite under greenschist facies conditions, Neouvielle massif, Pyrenees, France. *Journal of Structural Geology*. 1999;21(5):555–576. [https://doi.org/10.1016/S0191-8141\(99\)00042-5](https://doi.org/10.1016/S0191-8141(99)00042-5)
10. Economides M.J., Mikhailov D.N., Nikolaevskiy V.N. On the problem of fluid leakoff during hydraulic fracturing. *Transport in Porous Media*. 2007;67(3):487–499. <https://doi.org/10.1007/s11242-006-9038-7>
11. Khramchenkov M.G., Korolev E.A. Dynamics of fractures growth in oil saturated carbonate beds of the Republic of Tatarstan. *Neftyanoe Khozyaistvo*. 2017;(4):54–57. <https://doi.org/10.24887/0028-2448-2017-4-54-57>
12. Petrov V.A., Lespinasse M., Poluektov V.V. et al. Rescaling of fluid-conducting fault structures. *Doklady Earth Sciences*. 2017;472(2):130–133. <https://doi.org/10.1134/S1028334X17020027>
13. Matray J.M., Savoye S., Cabrera J. Desaturation and structure relationships around drifts excavated in the well-compacted Tournemire’s argillite (Aveyron, France). *Engineering Geology*. 2007;90(1–2):1–16. <https://doi.org/10.1016/j.enggeo.2006.09.021>
14. Andrievskij A.P. Design procedure of optimal parameters of drilling and blasting operations certificate under drilling with straight slot tier cut. *Fiziko-Tekhnicheskie Problemy Razrabotki Poleznykh Iskopaemykh*. 1992;(5):71–76.
15. Kononenko M., Khomenko O., Savchenko M. et al. Method for calculation of drilling-and-blasting operations parameters for emulsion explosives. *Mining of Mineral Deposits*. 2019;13(3):22–30. <https://doi.org/10.33271/mining13.03.022>
16. Krstic S., Ljubojev M., Ljubojev V. et al. Monitoring the stability of the rock mass excavating of underground premises in the ore body t1, jama bor. In: *International Multidisciplinary Scientific GeoConference Surveying Geology and Mining Ecology Management – SGEM. International Multidisciplinary Scientific Geoconference*. 2014;2(1):613–619. <https://doi.org/10.5593/sgem2014/b12/s2.078>
17. Sudarikov A.E., Merkulova V.A. Specifics of calculating the stability of mine workings when applying drilling and blasting. *ARP Journal of Engineering and Applied Sciences*. 2017;12(21):6192–6196. URL: https://arjournals.org/jeas/research_papers/rp_2017/jeas_1117_6471.pdf
18. Abaturova I., Savintsev I., Korchak S. Assessment of risk of development of contingency situations on railway tracks. In: *Engineering and Mining Geophysics 2018 – 14th Conference and Exhibition. European Association of Geoscientists and Engineers*. 2018. P. 137600. <https://doi.org/10.3997/2214-4609.201800545>
19. Nurpeisova M.B., Kirgizbayeva D.M., Kopzhasaruly K. Innovative methods of the rock massif fractures survey and treatment of its results. *Naukovyi Visnyk Natsionalnoho Hirnychoho Universytetu*. 2016;(2):11–18.
20. Levytskyi V., Sobolevskiy R., Zawieska D. et al. The accuracy of determination of natural stone cracks parameters based on terrestrial laser scanning and dense image matching data. In: *International Multidisciplinary Scientific GeoConference Surveying Geology and Mining Ecology Management, SGEM*. 2017;17(23):255–262. <https://doi.org/10.5593/sgem2017/23/S10.031>
21. Golik V., Stas G., Morkun V. et al. Study of rock structure properties during combined stopping and development headings. In: *The International Conference on Sustainable Futures: Environmental, Technological, Social and Economic Matters (ICSF 2020)*. 2020;166:03006. <https://doi.org/10.1051/e3sconf/202016603006>
22. Tian W.L., Yang S.Q., Dong J.P. et al. An experimental study on triaxial failure mechanical behavior of jointed specimens with different JRC. *Geomechanics and Engineering*. 2022;28(2):181–195. <https://doi.org/10.12989/gae.2022.28.2.181>
23. Fan X., Yu H., Deng Z. et al. Cracking and deformation of cuboidal sandstone with a single nonpenetrating flaw under uniaxial compression. *Theoretical and Applied Fracture Mechanics*. 2022;119:103284. <https://doi.org/10.1016/j.tafmec.2022.103284>
24. Ren S., Han T., Fu L. et al. Pressure effects on the anisotropic velocities of rocks with aligned fractures. *Acta Geophysica Sinica*. 2021;64(7):2504–2514. (In Chinese) <https://doi.org/10.6038/cjg202100318>



25. Anderson I., Ma J., Wu X. et al. Determining reservoir intervals in the Bowland Shale using petrophysics and rock physics models. *Geophysical Journal International*. 2022;228(1):39–65. <https://doi.org/10.1093/gji/ggab334>
26. Wu J., Goto T., Koike K. Estimating fractured rock effective permeability using discrete fracture networks constrained by electrical resistivity data. *Engineering Geology*. 2021;289:166–178. <https://doi.org/10.1016/j.enggeo.2021.106178>
27. Attya M., Hachay O., Khachay O. New method of defining the geotechnical parameters from CSEM (controlled source electromagnetic method) monitoring data at the 15th May City, Egypt. *Methods and Applications in Petroleum and Mineral Exploration and Engineering Geology*. 2021;371–388. <https://doi.org/10.1016/b978-0-323-85617-1.00022-9>
28. Grib N.N., Uzbekov A.N., Imaev V.S. et al. Variations in the geoelectric properties of the rock masses as a result of the seismic effects of industrial explosions. In: IOP Conference Series: Earth and Environmental Science. *World Multidisciplinary Earth Sciences Symposium (WMESS 2019)*. 9–13 September 2019, Prague, Czech Republic. 2019;362(1):012120. <https://doi.org/10.1088/1755-1315/362/1/012120>
29. Sizin P.E., Shkuratnik V.L. Theoretical estimation of microcracks influence on rocks conductivity with maxwell approximation. *Mining Informational and Analytical Bulletin*. 2015;(3):212–218.
30. Landau L.D., Lifshits E.M. *Theoretical physics: At 10 parts. T. VIII. Electrodynamics of continuous media*. Moscow: Fizmatlit; 2005. 656 p. (In Russ.)
31. Bruggeman D.A.G. Berechnung verschiedener physikalischer Konstanten von heterogenen Substanzen. I. Dielektrizitätskonstanten und Leitfähigkeiten der Mischkörper aus isotropen Substanzen. *Annalen der Physik*. 1935;416(8):665–679. (In German) <https://doi.org/10.1002/andp.19354160802>
32. Landauer R. Conductivity of cold-worked metals. *Physical Review*. 1951;82(4):520–521. <https://doi.org/10.1103/PhysRev.82.520>
33. Landauer R. High-field magnetoresistance of point defects. *Journal of Physics F: Metal Physics*. 1978;8(11):L245–L250. <https://doi.org/10.1088/0305-4608/8/11/001>
34. Balagurov B. Ya. *Electrophysical properties of composites: Macroscopic theory*. Moscow: LENAND; 2015. 752 p. (In Russ.)
35. Kasakhara K. *Earthquake Mechanics*. Moscow: Mir; 1985. 264 p. (In Russ.)
36. Shklovskii B.I., Éfros A.L. Percolation theory and conductivity of strongly inhomogeneous media. *Soviet Physics Uspekhi*. 1975;18(11):845–862. <https://doi.org/10.1070/PU1975v018n11ABEH005233>
37. Pride S.R., Berryman J.G., Commer M. et al. Changes in geophysical properties caused by fluid injection into porous rocks: analytical models. *Geophysical Prospecting*. 2017;65(3):766–790. <https://doi.org/10.1111/1365-2478.12435>
38. Tan X., Konietzky H. Numerical simulation of permeability evolution during progressive failure of Aue granite at the grain scale level. *Computers and Geotechnics*. 2019;112:185–196. <https://doi.org/10.1016/j.compgeo.2019.04.016>
39. Voznesensky A. S., Kidima-Mbombi L.K. Formation of synthetic structures and textures of rocks when simulating in COMSOL Multiphysics. *Mining Science and Technology (Russia)*. 2021;6(2):65–72. <https://doi.org/10.17073/2500-0632-2021-2-65-72>
40. Zhukov V.S. Influence of intergranular and fractured porosity on the electrical resistivity of reservoirs of the Chayandinsky field (Eastern Siberia). *Geophysical Research*. 2022;23(2):5–17. (In Russ.) <https://doi.org/https://doi.org/10.21455/gr2022.2-1>

Information about the authors

Pavel E. Sizin – Cand. Sci. (Phis. and Math.), Associate Professor of the Department of Mathematics, University of Science and Technology MISIS, Moscow, Russian Federation; ORCID [0000-0001-8156-4972](https://orcid.org/0000-0001-8156-4972), Scopus ID [6506196727](https://scopus.com/authorid/6506196727); e-mail sizin.pe@misis.ru

Alexander S. Voznesenskii – Dr. Sci. (Eng.), Professor of the Department of Physical Processes of Mining and Geocontrol, University of Science and Technology MISIS, Moscow, Russian Federation; ORCID [0000-0003-0926-1808](https://orcid.org/0000-0003-0926-1808), Scopus ID [57210211383](https://scopus.com/authorid/57210211383), ResearcherID [C-3863-2015](https://orcid.org/C-3863-2015), SPIN 5976-3030; e-mail al48@mail.ru

Lemuel Ketura Kidima-Mbombi – PhD student, Department of Physical Processes of Mining and of Geocontrol, University of Science and Technology MISIS, Moscow, Russian Federation; Scopus ID [57226447408](https://scopus.com/authorid/57226447408)

Received 12.07.2022

Revised 08.08.2022

Accepted 15.12.2022




BENEFICIATION AND PROCESSING OF NATURAL AND TECHNOGENIC RAW MATERIALS

Research paper

<https://doi.org/10.17073/2500-0632-2022-10-20>

UDC 553.495.061.4

**The effect of clay minerals on in-situ leaching of uranium**O.F. Petukhov¹, I.U. Khalimov¹   , V.P. Istomin², N.M. Karimov¹ ¹ NavoiState Mining and Technological University, Navoi, Uzbekistan² Navoi Mining and Metallurgical Complex, Navoi, Uzbekistan halimov_i@bk.ru**Abstract**

In recent years, with the development of techniques and methods for in-situ leaching (ISL), additional uranium extraction from previously worked-out blocks is becoming not only relevant, but also quite achievable. In this case, the extraction of residual uranium reserves from previously worked-out blocks does not require additional costs for the necessary infrastructure. One of the most important factors in the formation of residual uranium reserves in worked-out blocks is the presence of clay minerals in the ore horizon. In this regard, we conducted a number of studies on the adverse and positive effects of clay minerals on ISL process. Water permeability and relatively good filtration (not less than 0.5–1 m/day) of ores and rocks of a productive horizon (aquifer) is the most important hydrogeological factors affecting the performance of uranium ISL. The second most important hydrogeological factor is the lack of fluid communication between the productive aquifer and non-productive aquifers, i.e., the obligatory presence of aquicludes. The role of clays in these hydrogeological factors is twofold. On the one hand, the presence of clays negatively affects both the solutions filtration rate and uranium extraction. On the other hand, the presence of clay minerals (forming an aquiclude) enhances the effect of ISL. The study findings allowed the role of clay minerals in uranium ISL to be assessed. The diffusion coefficients of nitrate ions in the clays were determined, and the protective effect of aquicludes was calculated. The effect of the clay content in the ore sand horizon on the solutions filtration coefficients was also established. The static uranium exchange capacity of clays was determined by studying the process of uranium sorption by clay samples from sulfate and bicarbonate solutions. The studies established the diffusion coefficients of nitrate ions in montmorillonite and kaolinite clays, which amounted to $3.34 \cdot 10^{-6}$ and $2.14 \cdot 10^{-6}$ cm²/s. Taking into account the calculated values of diffusion coefficients, the protective time of the clayey aquiclude for nitrate ions was 43 years. At 20 % clay minerals content, the solution filtration coefficient decreases to values where ISL conditions become unfavorable. It was found experimentally that the sorption of uranium by clay minerals depends on both the nature of the clays and the composition of the solution. Uranium sorption from sulfate solutions proceeds noticeably better than that from bicarbonate solutions. The highest values of the static uranium exchange capacity were obtained for bentonite (104 mg/g).

Keywords

uranium, ISL, clay, filtration, diffusion coefficient, water permeability, sorption

For citationPetukhov O.F., Khalimov I.U., Istomin V.P., Karimov N.M. The effect of clay minerals on in-situ leaching of uranium. *Mining Science and Technology (Russia)*. 2023;8(1):39–46. <https://doi.org/10.17073/2500-0632-2022-10-20>**ОБОГАЩЕНИЕ, ПЕРЕРАБОТКА МИНЕРАЛЬНОГО И ТЕХНОГЕННОГО СЫРЬЯ**

Научная статья

**Влияние глинистых минералов
на процесс подземного выщелачивания урана**О. Ф. Петухов¹, И. У. Халимов¹   , В. П. Истомина², Н. М. Каримов¹ ¹ Навоийский государственный горно-технологический университет, г. Навои, Узбекистан² Навоийский горно-металлургический комбинат, г. Навои, Узбекистан halimov_i@bk.ru**Аннотация**

В последние годы с развитием техники и технологии подземного выщелачивания (ПВ) доизвлечение урана из ранее отработанных блоков становится не только актуальной, но и вполне достижимой задачей, так как извлечение остаточного запаса урана из ранее отработанных блоков не требует дополнительных расходов на необходимую инфраструктуру. Одним из важнейших факторов фор-



мирования остаточного запаса урана в отработанных блоках является присутствие глинистых минералов в рудном горизонте. В связи с этим нами был проведен ряд исследований по изучению отрицательного и положительного влияния глинистых минералов на процесс ПВ. Водопроницаемость и относительно хорошая фильтрация (не менее 0,5–1 м/сут) руд и пород продуктивного горизонта занимают первое место в ряду гидрогеологических факторов, влияющих на эффективность ПВ урана. Вторым по значимости гидрогеологическим фактором является отсутствие гидрологической связи продуктивного водоносного горизонта с непродуктивными горизонтами, то есть обязательное наличие водоупоров. При этом роль глин в указанных гидрогеологических факторах – двоякая. В первом случае наличие глин негативно сказывается как на скорости фильтрации растворов, так и на извлечении урана. Во втором – наличие глинистых минералов (в качестве водоупоров) усиливает эффект ПВ. В результате исследования дана оценка роли глинистых минералов в процессе подземного выщелачивания урана; определены коэффициенты диффузии нитрат-ионов в глинах и рассчитано защитное действие водоупоров; установлено влияние содержания глин в рудном песчаном горизонте на коэффициенты фильтрации растворов; определены статические обменные емкости глин по урану путем исследования процесса сорбции урана на глинистых образцах из сернокислых и бикарбонатных растворов. Проведенными исследованиями установлены коэффициенты диффузии нитрат-ионов в монтмориллонитовых и каолинитовых глинах, которые составили $3,34 \cdot 10^{-6}$ и $2,14 \cdot 10^{-6}$ см²/с. С учетом полученных расчетами значений коэффициентов диффузии защитное время глинистого водоупора для нитрат-ионов составило 43 года. При 20%-ном содержании глинистых минералов коэффициент фильтрации растворов снижается до значений, когда условия ПВ становятся неблагоприятными. Экспериментально установлено, что сорбция урана глинистыми минералами зависит как от природы глин, так и от состава раствора. Из сернокислых растворов сорбция урана протекает заметно лучше, чем из бикарбонатных растворов. При этом наибольшие значения статической обменной емкости по урану получены для бентонита (104 мг/г).

Ключевые слова

уран, подземное выщелачивание, глина, фильтрация, коэффициент диффузии, водопроницаемость, сорбция

Для цитирования

Petukhov O.F., Khalimov I.U., Istomin V.P., Karimov N.M. The effect of clay minerals on in-situ leaching of uranium. *Mining Science and Technology (Russia)*. 2023;8(1):39–46. <https://doi.org/10.17073/2500-0632-2022-10-20>

Introduction

In-situ leaching (ISL) mining methods find large-scale implementation and ensure the effective operation of mining industry in many countries [1–4]. The properties of the rocks and minerals involved in ISL processes determine its performance. Therefore, research aimed at studying the key physical and chemical processes in ISL process is of great importance.

In our opinion, insufficient attention has been paid in historical studies to the influence of clay properties on the ISL process [5–8]. For example, in [5, 6], the emphasis was placed on the influence of clays on the filtration of solutions through an ore horizon, while quantitative characteristics of the filtration coefficients were not presented. In [7], for the first time, the role of clayey aquicludes was included in the list of the classification factors for deposit developed by ISL method. However, the numerical values of the diffusion coefficients of elements were not presented, and no examples of calculating the thickness of the protective aquiclude were given. In [8], the influence of clays on the water permeability of an ore layer was described, but similar to [5–7], nothing was said about the influence of clay minerals on the sorption of uranium from pregnant solutions, leading to losses of leached metal.

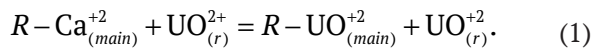
The purpose of our study was: a) to estimate the coefficients of diffusion in clay minerals and calculate the thickness of a protective aquiclude; b) to study the effect of the content of clay minerals on the solutions filtration coefficient; and c) to study the sorption of uranium by clay minerals.

Positive effect of the properties of clay minerals on ISL processes

In order to establish the thickness (height) of a clayey aquiclude as a screen to protect against the harmful effects of leaching solutions on natural waters, we conducted studies to determine the diffusion coefficients of some chemical components in clays. Since clay aquicludes are mainly represented by montmorillonite (bentonite), less often kaolinite, these clay minerals were considered in the study. First, it was taken into account that the rate of penetration of chemical components through clays is limited by diffusion [9]. Second, a relatively toxic NO₃⁻ anion (MPC = 45 mg/L) present in the pregnant solutions of uranium ISL was selected as the chemical component to be studied.

It is incorrect to use metal cations (e.g., UO₂²⁺) as chemical components in diffusion studies, since the diffusion process is accompanied by cation-exchange

sorption of metals by clays (in exchange for Ca^{2+} , Mg^{2+} , Na^+) by reaction:



As for anions, according to data of [9] and our studies [10], NO_3^- anions are not sorbed by bentonite and kaolinite.

Samples of intact bentonite and kaolinite clays were used in the experimental studies. The identification of constituent minerals of the clays was carried out using a “Dron-3.0” X-ray diffractometer with a tube 03BSV – 25-Cu. The content of exchangeable forms of cations and the total cation-exchange capacity (CEC) of the clays were determined based on their interaction with a 0.1N solution of ammonium acetate at $\text{pH} = 7.0$ [11]. The composition of the clay samples is presented in Table 1. It shows that alkaline-earth bentonite contains 93 % of montmorillonite, while the content of the main mineral in the kaolinite clay sample is 88.2 %.

The studies to determine the diffusion coefficients in the clays were carried out according to the technique described in [12, 13] in a laboratory setup, the schematic of which is shown in Fig. 1.

An intact clay sample with known area S and thickness h was placed in a glass tube. Gauze swabs were placed on both sides of the sample for stability and destruction prevention. The tube containing the

clay sample was connected to the vessels through the rubber stoppers. Vessel A was filled with a solution of volume V_A with known concentration NO_3^- . Vessel B was filled with distilled water of volume V_B . The same level of the liquids in the vessels was maintained on both sides. Magnetic stirrers were used to stir the solutions, in order to create a uniform concentration of NO_3^- throughout the whole volume. The conditions of the experiments were constant: $t = 200^\circ\text{C}$, stirring solutions at a rate of $n = 50$ rpm; $V_A = V_B = 1$ L.

The diffusion coefficients were calculated based on the experimental data obtained using Fick's first law equation:

$$D = \Delta m(h/\tau)S(C_A - C_B), \quad (2)$$

where D is diffusion coefficient, cm^2/s ; Δm is weight of substance transferred during diffusion, mg, $\Delta m = C_B V_B$; h is thickness of clay sample, cm; τ is diffusion time, s; S is area of clay sample, cm^2 ; C_A is equilibrium concentration in vessel A , mg/cm^3 ; C_B is equilibrium concentration in vessel B , mg/cm^3 .

The conditions and findings of the experiments and the calculated diffusion coefficients of NO_3^- – ions in the clays are presented in Table 2.

As can be seen from Table 2, the values of the diffusion coefficients obtained agree well with the findings of [14, 15]. In particular, according to [15], the diffusion coefficient of Cl^- in bentonite was $3,0 \cdot 10^{-6} \text{ sm}^2/\text{s}$.

Table 1

Clay composition

Clay sample	Mineral composition, %				Content of counterions, g/kg				CEC, g-eq/kg
	Montmorillonite	Kaolinite	Sericite	Quartz	Ca^{2+}	Mg^{2+}	Na^+	K^+	
Alkali-earth bentonite	93.0	2.0	5.0	–	6.32	0.60	0.05	0.15	0.372
Kaolinite	–	88.2	5.8	6.0	1.85	0.19	0.07	0.12	0.113

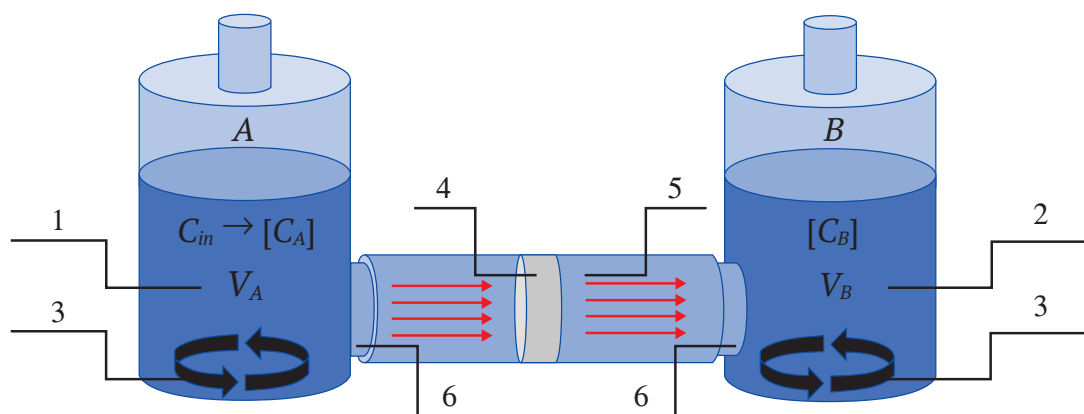


Fig. 1. Schematic of the laboratory setup for determining the diffusion coefficients in clays: 1 – vessel A with initial concentration C_{in} , equilibrium concentration C_A and volume V_A ; 2 – vessel B with equilibrium concentration C_B and volume V_B ; 3 – stirring devices; 4 – intact clay sample; 5 – glass tube connecting the vessels; 6 – rubber stoppers

Secondly, the diffusion coefficient in bentonite is about 1.5 times higher than that in kaolinite. This is explained by the fact that kaolinite has a strong, fixed lattice, the interpacket distance in which is 0.71–0.72 nm. In montmorillonite, the crystal lattice packet is movable, three-layered; the interpacket distance is 1.5 nm and can expand up to 14 nm. The difference in the lattices of these clays can be clearly seen in Fig. 2.

The established values of diffusion coefficients are of great practical importance, as they allow calculating the clay aquiclude protective action time. For example, the concentration of NO_3^- -ions in the pregnant solutions of the ore horizon $C_{in} = 2,0 \text{ g/l}$ (2 mg/cm^3) and does not change in the process due to flow renewal. The concentration of NO_3^- -ions in natural waters should not exceed $C_B = 0.045 \text{ g/l}$ (0.045 mg/cm^3). The area of the bentonite aquiclude $S = 1000 \text{ m}^2$ ($1 \cdot 10^7 \text{ cm}^2$), and the thickness $h = 10 \text{ m}$ ($1 \cdot 10^5 \text{ cm}$). The volume of natural water is taken to be

2000 m^3 ($2 \cdot 10^9 \text{ cm}^3$). The weight of NO_3^- , transferred by diffusion to natural waters, $\Delta m = 9 \cdot 10^7 \text{ mg}$. According to formula (2), the time of the protective action of the aquiclude is determined as follows:

$$\begin{aligned} \tau &= m(h/D)S(C_A - C_B) = \\ &= 9 \cdot 10^7 \cdot 1 \cdot 10^5 / 3,34 \cdot 10^6 \cdot 1 \cdot 10^7 \cdot (2,0 - 0,045) = \\ &= 1,37 \cdot 10^9 \text{ s or } 10 \text{ years.} \end{aligned}$$

However, right there the positive effect of clays on the ISL process ends.

Negative effect of the properties of clay minerals on ISL processes

The other three properties of clay minerals: extremely low filtration coefficient ($K_f = 10^{-4} - 10^{-6} \text{ m/day}$ [15, p. 3–6]), noticeable sorption properties in relation to metal cations [10], and the tendency to form colloidal solutions have a negative impact on the process of uranium ISL.

Table 2

Diffusion coefficients determination results

Clay sample	Experimental conditions				Findings				
	$h, \text{ cm}$	$S, \text{ cm}^2$	$C_{\text{NO}_3} (\text{in}), \text{ mg/cm}^3$	$\tau, \text{ s}$	$[C_A], \text{ mg/cm}^3$	$[C_B], \text{ mg/cm}^3$	$C_A - C_B, \text{ g/cm}^3$	$\Delta m, \text{ mg}$	$D, \text{ cm}^2/\text{s}$
Bentonite	0.5	7.0	1.0	$2.6 \cdot 10^5$	0.65	0.35	0.30	350	$3.34 \cdot 10^{-6}$
Kaolinite	0.5	7.0	1.0	$2.6 \cdot 10^5$	0.70	0.30	0.40	300	$2.14 \cdot 10^{-6}$

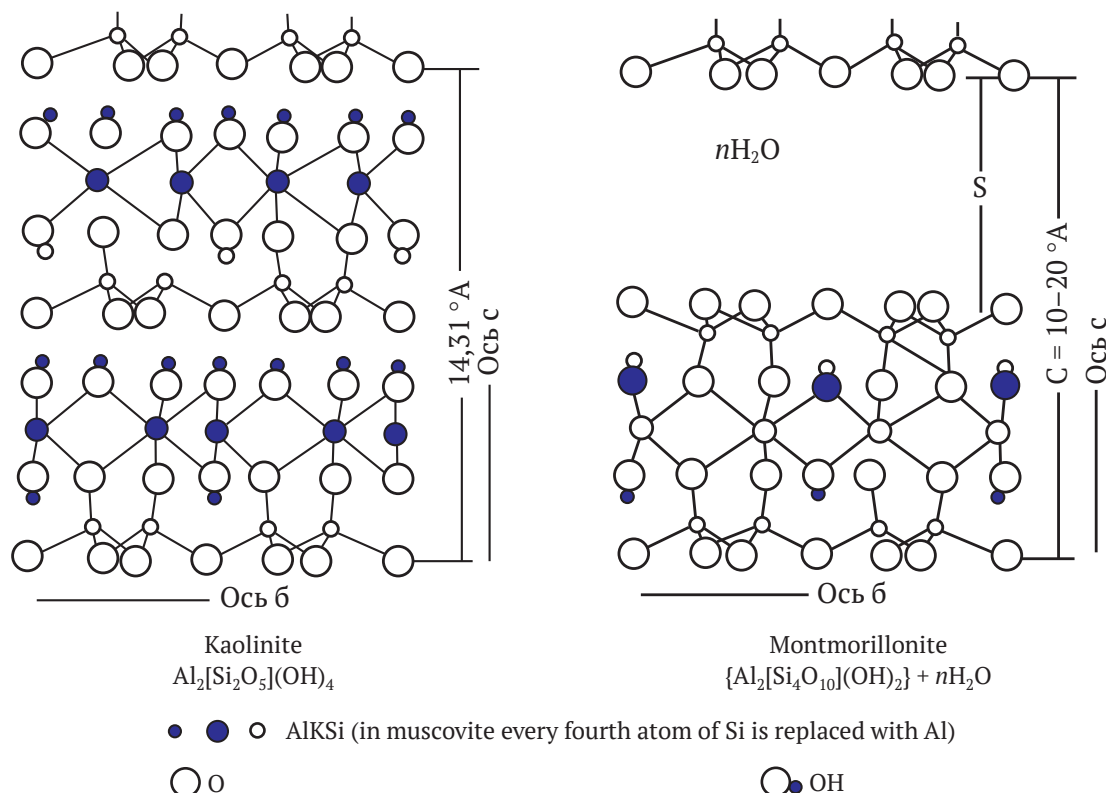


Fig. 2. Crystal lattices of clay minerals



Table 3

Effect of clay content in sand on water and solution filtration coefficients

Clay content in sand, %	K_f in the presence of bentonite, cm/s · 10 ⁻²			K_f in the presence of kaolinite, cm/s · 10 ⁻²		
	H ₂ O	10 g/l H ₂ SO ₄	1 g/l NaHCO ₃	H ₂ O	10 g/l H ₂ SO ₄	1 g/l NaHCO ₃
0.0	2.2	2.2	2.2	2.2	2.2	2.2
3.0	1.2	1.1	1.0	1.3	1.3	1.1
6.0	0.9	0.8	0.6	1.1	1.0	0.9
15.0	0.4	0.3	0.2	0.6	0.5	0.4
20.0	0.2	0.1	0.05	0.3	0.2	0.1

First, let us elaborate on low filtration coefficients of clays. Permeable ore horizons mainly consist of sand. In addition to sand, an ore horizon often contains clay minerals that cement the sand (hence the name “sandstone-type deposits” has arisen [16]). The content of clay minerals limits the rate of solution filtration through the ore horizon.

We performed experimental studies, in order to determine the coefficients of filtration of water and solutions through sand and a mixture of sand with different content of clay minerals (bentonite and kaolinite). The studies were conducted in steady-state regime (the filtering material layer was unchangeable in all experiments) at a constant head gradient according to GOST 25584–2016¹. In the experiments, a thoroughly washed sand of 0.25–0.50 mm fraction and powdered clays were used (see Table 1). Samples of the sand with the given clay content were thoroughly mixed before being loaded into the cylinder of the filtration unit. Water and solutions of 10 g/l H₂SO₄ and 1 г/л NaHCO₃ were used as filtering liquids. Filtration coefficient K_f was calculated by Darcy equation based on the experimental data obtained (using the determined filtration rate).

$$v = K_f (\Delta P / h), \tag{3}$$

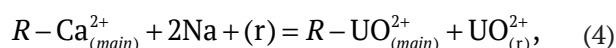
where K_f is filtration coefficient, cm/s; v is filtration rate, cm/s, $v = V/S\tau$; V is volume of filtered liquid, cm³; S is filtration area, cm²; τ is filtration time, s; $\Delta P/h$ is pressure gradient in the layer (slope ratio of the filtration rate versus filtration time plot); ΔP is water pressure fall, cm; h is thickness of filtering layer, cm.

The findings of the studies to determine the filtration coefficients are shown in Table 3.

The data presented in Table 3 shows that K_f of the liquids decreases markedly with increasing the clay content. Notice that K_f in the presence of bentonite

¹ GOST–2016 25584. Soils. Methods for laboratory determination of filtration coefficient. Moscow: Standardinform; 2016.

is lower than in the presence of kaolinite. This is due to the different swelling properties of the clays, as mentioned above. The use of sulfate and sodium bicarbonate solutions also affects the K_f , and the use of NaHCO₃ solution (even at a lower concentration than that of the sulfate solution) has a stronger effect. This is explained by the fact that, due to the cationic exchange of Na⁺ ions for Ca²⁺ counterions in the clays,



clay swelling takes place. At the content of clay of 20 % K_f decreases to the values, at which the conditions become unfavorable for ISL [6, p. 405].

c) Next, let us focus on the sorption properties of clays, which produce adverse impact on uranium ISL process. Table 4 presents the data on CEC values of some clay minerals [17].

As shown in Table 4, vermiculite and montmorillonite (the main mineral of bentonite clays, being the most characteristic of uranium ISL conditions), have the highest CEC values.

Table 4

Cation exchange capacities of clay minerals

Clay type	Mineral	CEC, g-eq/kg
Kaolinite group	Kaolinite	0.02–0.10
	Muscovite	0.105
Illite group	Illite	0.13–0.42
	Attapulgitite	0.18–0.22
Fibrous clay	Nontronite	0.57–0.64
	Saponite	0.69–0.81
	Montmorillonite	0.8–1.5
Resinous derivatives	Biotite	0.03
	Vermiculite	1.0–1.5



We have conducted studies specifically on the sorption of uranium from different solutions by bentonite and kaolinite clays. The studies were performed under static conditions with the use of a thermostatically controlled stirred reactor at a temperature of 20 °C, Solid / Liquid ratio of 1000, and the agitation time of 1 h (saturation regime) [17]. After agitation, the suspension was filtered, the sediment was washed with water, dried, and analyzed for uranium by X-ray spectral analysis at a ARF-7 spectrometer. The experiments used actual production solutions taken from sulfate and bicarbonate uranium ISL sites. The composition of the solutions is presented in Table 5. Table 6 presents the experimental data on the uranium static exchange capacity (SCEC) of the clays.

The data presented in Table 6 shows that the sorption of uranium by clays depends significantly on the nature of both the clay and the test solution. Uranium SCEC of bentonite is markedly higher than that of kaolinite. This can be explained by the higher values of bentonite CEC (see Table 1). The uranium sorption from sulfate solutions is also markedly higher than that from bicarbonate solutions. This is because the stability constants of sulfate anionic uranyl complexes ($K = 76-2500$) is much lower than those of the carbonate complex ($K = 2,0 \cdot 10^{18}$). It is very likely that the sorption of uranium from bicarbonate solutions proceeds not by the ion-exchange mechanism, but as adsorption.

Clayey rocks of sedimentary strata often contain carbonaceous organic matter, which is also a good sorbent for uranium.

It should be noted that laboratory studies do not fully simulate natural conditions. The differences between the laboratory experimental conditions and the natural processes consist in the lack of rock pressure and the associated changes in the values of porosity, moisture, and anisotropic component of the artificially prepared clay layer.

The simulation of rock pressure during the research requires the use of special installations. As for the isotropy of samples, it is clear that the quantitative relationships between individual parameters can be established only when the composition is homogeneous and its characteristics are known.

In any case, in natural ISL conditions, along with the process of uranium leaching, a parallel process of partial sorption of uranium by clay minerals ensues. This is both by the boundary surface of clay aquicludes, and by the clays contained in a sandy ore horizon.

In conclusion, let us consider three other properties of clay minerals which produce an adverse impact on the ISL process. First of all, this is the ability of clays to form colloidal species. When clays interact with a large volume of solutions that takes place at ISL, peptization, the process of forming clay colloidal species (gels) proceeds. The gels entrained by the flow of pregnant solutions, move towards extraction wells. Some of the gels are sorbed on the surface of the host rock, some are deposited on filters, and some are pumped out with the pregnant solution for sorption uranium extraction. In order to prevent the gels and other solids from entering the sorption columns, at the ISL mines, settling sumps are provided. However, in those cases where the concentration of colloidal species is high (turbid opalescent solutions are formed), the area of settling sumps is not enough, a clogging of the sorption resin with these species happens. This leads to reducing the performance of sorption columns, and sometimes to their shutdown. In this case, the uranium sorbed by colloidal species of clay is lost with the sediments at the bottom of the sumps.

When drilling and constructing ISL process boreholes, clay layers and interlayers are often intersected in the stratigraphic sequence. During the drilling process, the clay drowning takes place, causing them to swell inside the borehole, resulting in reducing the specified borehole diameter. This, in turn, prevents the casing from descending. In practice, we have to use technical means to eliminate this problem that leads to additional labor costs when casing boreholes.

Drilling, including the penetration of a productive horizon, is carried out with the use of clay mud as a washing fluid, creating a clay crust on the borehole

Table 5

Composition of ISL production solutions

Solution	Concentration, mg/l						pH
	U	SO ₄ ²⁻	HCO ₃ ⁻	Fe ³⁺	Fe ²⁺	Al ³⁺	
Sulfate	40.4	12750	–	730	240	544	1.2
Bicarbonate	36.2	67	665	30	–	–	9.3

Table 6

The findings of determining static uranium exchange capacity of clays

Clay sample	Uranium SCEC of clays, mg/g	
	from sulfate solution	from bicarbonate solution
Bentonite	104	15
Kaolinite	32	5



walls. In the filter installation interval, claying of the near-filter zone also takes place. Preflushing the borehole with clean water and pumping after casing are carried out for the filter cake removal. These measures do not allow the near-filter zone to be completely cleared from clays which subsequently adversely affect the borehole productivity. It is especially difficult to clean a borehole from clays in the conditions of low groundwater head on the productive horizon roof.

When constructing the process sumps, a special attention is paid to waterproofing of their bottoms. The bottom is waterproofed using bentonite clays, which, as mentioned above, also sorb uranium that leads to its losses.

Conclusions

1. Clay minerals have a great deal of both positive and adverse effects on uranium ISL process.
2. Clay minerals are very effective as aquicludes, preventing the flow-out of pregnant and extracting solutions. The studies conducted enabled the diffusion coefficients of nitrate ions in montmorillonite

and kaolinite clays to be determined, amounting to $3,34 \cdot 10^{-6}$ and $2,14 \cdot 10^{-6}$ cm²/s.

3. Taking into account the calculated values of the diffusion coefficients, the protective time of the clayey aquiclude for nitrate ions was 43 years.

4. Clay minerals present in a sand ore horizon adversely affect the filtration coefficient of the solutions. The decrease in the filtration coefficients of the solutions with increasing the content of montmorillonite and kaolinite clays in a sand ore horizon has been experimentally established. At 20 % content of the clay minerals, the solution filtration coefficient decreases to values at which the conditions become unfavorable for the ISL.

5. Exhibiting cation-exchange sorption abilities, clay minerals also adversely affect uranium extraction. It was found experimentally that the sorption of uranium by clay minerals depends on both the nature of the clays and the composition of the solution. The uranium sorption from sulfate solutions proceeds noticeably better than from bicarbonate solutions. The highest values of the static uranium exchange capacity were obtained for bentonite (104 mg/g).

References

1. Ahrens V.Zh. *Physical and chemical geotechnology*. Moscow: MGGU Publ.; 2001. 656 p. (In Russ.)
2. Rudenko A.A., Troshkina I.D., Danileyko V.V. et al. Prospects for selective-and-advanced recovery of rhenium from pregnant solutions of in-situ leaching of uranium ores at Dobrovolnoye deposit. *Mining Science and Technology (Russia)*. 2021;6(3):158–169. <https://doi.org/10.17073/2500-0632-2021-3-158-169>
3. Golik V.I., Komashchenko V.I., Razorenov Yu.I., Valiev N.G. Experience of underground leaching of metals from balance reserves of ores. *News of the Ural State Mining University*. 2017;(2):57–62. (In Russ.) <https://doi.org/10.21440/2307-2091-2017-2-57-62>
4. Podrezov D.R. Issues of improving control and increasing efficiency of production blocks at an ISL uranium mine. *Mining Science and Technology (Russia)*. 2020;5(2):131–153. (In Russ.) <https://doi.org/10.17073/2500-0632-2020-2-131-153>
5. Beletsky V.I., Dolgikh P.F., Petrov R.P., et al. *Handbook of uranium geotechnology*. Moscow: Energoatomizdat Publ.; 1997. Pp. 127–132. (In Russ.)
6. Petukhov O.F., Istomin V.P., Rudnev S.V., Khasanov A.S. *Uranium*. Tashkent: Turon Zamin-ziyo; 2015. Pp. 437–453. (In Russ.)
7. Petukhov O.F., Kurbanov M.A., Ahadov H.R., Khalimov I.U. The classification of uranium deposits, suitable for practicing the method of in-situ leaching. *Gorniy Vestnik Uzbekistana*. 2021;(2):16–21. (In Russ.) URL: <http://gorniyvestnik.uz/assets/uploads/pdf/2021-aprel-iyun.pdf>
8. Alikulov Sh.Sh., Khalimov I.U. Intensification of in situ uranium leaching from impermeable ore: A case-study of uranium deposits in Uzbekistan. *Mining Informational and Analytical Bulletin*. 2021;(3):37–48. (In Russ.) <https://doi.org/10.25018/0236-1493-2021-3-0-37-48>
9. Zatenatskaya N.P., Safokhina I.A. *Diffusion leaching of clays*. Moscow: Nauka Publ.; 1968. Pp. 54–58. (In Russ.)
10. Grim R. *Mineralogy and practical use of clays*. Moscow: Mir Publ. House; 1967. Pp. 47–53. (In Russ.) (Orig. ver.: Grim R.E. *Applied clay mineralogy*. NY, Toronto, London: McGraw-Hill Book Company, Inc.; 1962)
11. Latyshev V.E., Grutsinov V.A., Petukhov O.F. Sorption of heavy metals by natural inorganic minerals. *Gorniy Vestnik Uzbekistana*. 2002;(4):24–29. (In Russ.) URL: <http://gorniyvestnik.uz/assets/uploads/pdf/2002-oktyabr-dekabr.pdf>
12. Drever J. *The geochemistry of natural waters*. Moscow: Mir Publ. House; 1985. Pp. 97–100. (In Russ.) (Orig. ver.: Drever J.I. *The geochemistry of natural waters*. Englewood Cliffs, NJ: Prentice Hall, Inc.; 1982)



13. Akselrud G.A., Lysyansky V.M. *Extraction: solid-liquid system*. Leningrad: Khimiya Publ.; 1974. Pp. 167–176. (In Russ.)
14. Tovbina Z.M., Strazhko D.N. Diffusion of dissolved substances in silica gels. *Ukrainian Chemical Journal*. 1968;34(9):876–880. (In Russ.)
15. Goldberg V.M., Skvortsov N.P. *Permeability and filtration in clays*. Moscow: Nedra Publ.; 1986. P. 143. (In Russ.)
16. Tolstov E.A., Tolstov D.E. *Physical and chemical geotechnologies for the development of uranium and gold deposits in Kyzylkum region*. Moscow: Geoinformtsent Publ.; 2002. Pp. 9–28. (In Russ.)
17. Amphlett C.B. *Inorganic ion exchangers*. Amsterdam–London–NY: Elsevier Publ. House; 1964.

Information about the authors

Oleg F. Petukhov – Dr. Sci. (Eng.), Professor, the Department of Rare and Radioactive Metals, Navoi State Mining and Technology University, Navoi, Uzbekistan

Ilkhom U. Khalimov – Cand. Sci. (Eng.), Associate Professor, Head of the Department of Rare and Radioactive Metals, Navoi State Mining and Technology University, Navoi, Uzbekistan; ORCID [0000-0002-4552-556X](https://orcid.org/0000-0002-4552-556X), Scopus ID [57222556259](https://scopus.org/57222556259); e-mail halimov_i@bk.ru

Vladimir P. Istomin – Leading Geologist, Navoi Mining and Metallurgical Company, Navoi, Uzbekistan

Nurkhan M. Karimov – Assistant of the Department of Rare and Radioactive Metals, Navoi State Mining and Technology University, Navoi, Uzbekistan; ORCID [0000-0001-7552-072X](https://orcid.org/0000-0001-7552-072X)

Received 04.10.2022

Revised 08.11.2022

Accepted 31.10.2022



SAFETY IN MINING AND PROCESSING INDUSTRY AND ENVIRONMENTAL PROTECTION



Research paper

<https://doi.org/10.17073/2500-0632-2022-08-86>

UDC 622.817.4

Study of gas hazard pattern in underground workings after blasting

D. V. Olkhovskiy , O. S. Parshakov , S. A. Bublik 

Mining Institute of the Ural Branch of the Russian Academy of Sciences, Perm, Russian Federation

 demexez@gmail.com

Abstract

Determining the sources of hazardous and toxic substances released into mine air, their gas composition, as well as providing each such source of pollution with the required amount of fresh air are important issues in terms of ensuring normal healthy and safe working conditions for miners. This paper studies blasting as one of the most dangerous sources of mine air pollution. The study was carried out for a long dead-end exploration working, and a development (preparatory) working of a copper-nickel mine. In accordance with the federal rules and regulations (FNiP), a number of requirements, including monitoring of gas hazard at a face, is applied to blasting operations.

The study examined the behavior of gas-air mixture in dead-end mine workings after blasting. The findings are based on the experimental data obtained in the conditions of two dead-end workings at an operating copper-nickel mine. A technique for the experimental studies of gas release after blasting in a dead-end working was developed. The main technical characteristics of the instruments involved in the in-situ measurements are given. Time dependences of the concentrations of toxic gases after blasting at the blasted working mouth, at the return ventilation current, and near a booster were established. In order to assess the reliability of the data obtained, the volume of released carbon oxides was calculated based on the data of gas analyzers and chemical reactions of explosives decomposition during detonation, depending on the types and weights of the explosives. A model of gas-air mixture transfer was described, constructed, and calibrated allowing for longitudinal dispersion. The Voronin model was used to simulate the gradual removal of toxic gases from the working face and solving the problem of boundary conditions. Based on experimental data, the coefficients of longitudinal dispersion, ventilation efficiency, and volume concentration of the considered gas admixture in the mixing zone at initial time were determined for a long dead-end mine working.

The constructed gas-dynamic model and longitudinal dispersion coefficients obtained as a result of the analysis enabled the time required for long dead-end mine workings ventilation to be analysed and estimated. Based on the model, the algorithm for calculating the velocity of spreading the combustion products in a mine ventilation network in emergency situations is being improved. The value of longitudinal dispersion coefficient for different operating conditions is also being refined.

Based on the gas distribution simulation within the interval of 1,500 m from a working face, the time required for the ventilation of a dead-end mine working was determined.

Keywords

mine ventilation, gas distribution, toxic gases, blasting, monitoring, mathematical model, ventilation of a long dead-end working, longitudinal dispersion coefficient, ventilation time

Acknowledgments

The research was carried out with the financial support of the Russian Science Foundation under the project No. 19-77-30008.

For citation

Olkhovskiy D. V., Parshakov O. S., Bublik S. A. Study of gas hazard pattern in underground workings after blasting. *Mining Science and Technology (Russia)*. 2023;8(1):47–58. <https://doi.org/10.17073/2500-0632-2022-08-86>



ТЕХНОЛОГИЧЕСКАЯ БЕЗОПАСНОСТЬ В МИНЕРАЛЬНО-СЫРЬЕВОМ КОМПЛЕКСЕ И ОХРАНА ОКРУЖАЮЩЕЙ СРЕДЫ

Научная статья

Исследование динамики газовой обстановки подземных выработок после проведения взрывных работ

Д. В. Ольховский  , О. С. Паршаков , С. А. Бублик 

Горный институт Уральского отделения РАН, г. Пермь, Российская Федерация

 demexez@gmail.com

Аннотация

Определение источников выделения опасных и ядовитых веществ в рудничную атмосферу, их газового состава, а также обеспечение каждого такого источника загрязнения требуемым количеством свежего воздуха – важные вопросы с точки зрения обеспечения нормальных санитарно-гигиенических и безопасных условий труда горнорабочих. В настоящей работе на примере протяженной тупиковой разведочной выработки и подготовительной разрезной выработки медно-никелевого рудника проводится исследование одного из наиболее опасных источников загрязнения – взрывных работ, к которым в соответствии с Федеральными нормами и правилами (ФНП) предъявляется ряд требований, в том числе осуществление контроля газовой обстановки в забое.

В работе проведено исследование динамики газовой смеси в тупиковых горных выработках после проведения в них взрывных работ. Исследования выполнены с учетом экспериментальных данных, полученных в условиях двух тупиковых выработок действующего медно-никелевого рудника. Разработана методика проведения экспериментальных исследований газовой обстановки после взрывных работ в тупиковой выработке. Даны основные технические характеристики инструментальной базы, задействованной при проведении натурных измерений. Выявлены зависимости изменения концентраций ядовитых газов после взрывных работ в устье взрываемой выработки, на исходящей струе воздуха и у вентилятора местного проветривания. Для оценки достоверности полученных данных произведен расчет объема выделившихся окислов углерода по данным газоанализаторов и химическим формулам разложения взрывчатых веществ при детонации в зависимости от типа и массы взрывчатых веществ. Описана, построена и откалибрована модель переноса газовой смеси с учетом продольной дисперсии. Для моделирования постепенного выноса ядовитых газов из забоя выработки и задачи граничного условия применяется модель Воронина. На основе экспериментальных данных определены коэффициенты продольной дисперсии, эффективности проветривания и объемная концентрация рассматриваемой газовой примеси в зоне перемешивания в начальный момент времени для протяженной тупиковой выработки.

Построенная газодинамическая модель и полученные в результате анализа коэффициенты продольной дисперсии позволяют выполнять анализ времени проветривания протяженных тупиковых выработок. На основе полученной модели ведется усовершенствование алгоритма расчета скорости распространения в вентиляционной сети рудника продуктов горения при аварийных ситуациях, а также уточнение коэффициента продольной дисперсии для различных условий ведения работ.

Определено время проветривания тупиковой выработки по результатам моделирования газораспределения при удалении забоя выработки на 1500 м.

Ключевые слова

рудничная вентиляция, газораспределение, ядовитые газы, взрывные работы, мониторинг, математическая модель, проветривание протяженной тупиковой выработки, коэффициент продольной дисперсии, время проветривания

Благодарности

Исследование выполнено при финансовой поддержке РФФ в рамках проекта № 19-77-30008.

Для цитирования

Olkhovskiy D.V., Parshakov O.S., Bublik S.A. Study of gas hazard pattern in underground workings after blasting. *Mining Science and Technology (Russia)*. 2023;8(1):47–58. <https://doi.org/10.17073/2500-0632-2022-08-86>

Introduction

Determining the sources of hazardous and toxic substances released into mine air, their gas composition, as well as providing each such source of pollution with the required amount of fresh air are the important issues in terms of ensuring normal healthy and safe working conditions for miners [1]. Mine air gas composition depends on a number of factors (man-made and natural sources of pollution) [2]:

- rock breaking method;
- blasting;
- applying mining machinery and equipment;
- rock gas content;
- rock gas-dynamic characteristics.

This paper studies blasting as one of the most dangerous sources of mine air pollution. The study was carried out for the case of a long dead-end exploration mine and a development (preparatory) working of a copper-nickel mine. In accordance with the federal rules and regulations (FNiP), a number of requirements, including monitoring of gas hazard at a face, is applied to blasting operations¹.

The study objectives included:

- in-situ measuring the mine air gas composition at different distances from a working face over time;
- simulation of gas-dynamic processes in a long dead-end mine working after blasting;
- determination of the coefficients of longitudinal dispersion and ventilation efficiency;
- determination of changing the required time of a long dead-end working ventilation as its driving proceeds on the basis of the simulation results.

Based on experimental data, the coefficients of longitudinal dispersion, ventilation efficiency, and volume concentration of the considered hazardous gas in the mixing zone at initial time were determined for a long dead-end working. As a result, the rate of decreasing toxic gases concentrations was determined, taking into account the actual parameters of a working ventilation, the flow rate of air supplied to the face, and the time of its ventilation. Based on the measurements, the amount of gases released after blasting was determined. The results of theoretical studies allowed the performance of a working ventilation to be assessed, taking into account the prospective development of mining, on the basis of the developed and verified gas-dynamic model of a working.

¹ Federal norms and rules in the field of industrial safety “Safety rules for the production, storage and use of explosive materials for industrial use”: approved by order of the Federal Service for Environmental, Technological and Nuclear Supervision dated December 03, 2020 No. 494.

Experimental studies in a development (preparatory) working

The general pattern of the measurements was as follows: prior to blasting in dead-end workings at predetermined points, portable gas analyzers were installed in the mode of recording readings, and the ventilation air flow rates were measured prior to and after blasting. In most workings the measurement points were located as follows (Fig. 1):

- point 1 – at a booster fan;
- point 2 – at the mouth of a working;
- point 3 – at the return ventilation current from a dead end.

The location of a gas analyzer at point 1 enabled the presence of toxic gases and the degree of influence of the toxic gases recirculation on the face ventilation to be assessed. The gas analyzer at point 2 enabled the time required to ventilate a dead-end working, as well as the volume of the released gases to be determined. The gas analyzer at point 3 enabled the time of removal of the toxic gases and the degree of dilution of the toxic gases by return ventilation current to be assessed, taking into account the additional fresh air intake.

According to this pattern, the measurements were carried out in a development (preparatory) working (Stope drift 26-20-1). Dräger X-am 5600 portable gas analyzers were used for the measurements (their technical specifications are presented in Table 1).

The volume of air was determined by an APR-2 propeller-type anemometer and a Leica Disto X310 laser rangefinder. The main technical characteristics of the devices are given in Table 2.

The blasting of any industrial explosive produces toxic gases in varying quantities [3]. The main products of industrial explosives blasting are: carbon oxides CO and CO₂, sulfur dioxide SO₂, and nitrogen oxides NO, NO₂ [4]. The concentration of sulfur dioxide SO₂ was not measured in this study, due to the strong influence on the readings of the nitrogen dioxide (NO₂) gas analyzer sensors.

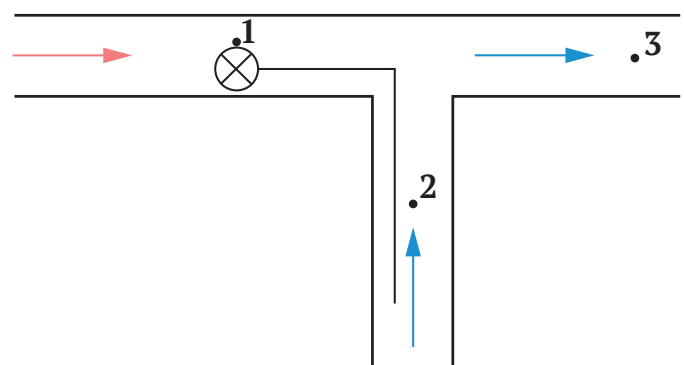


Fig. 1. Locations of portable gas analyzers

Processing of the portable gas analyzers data for each measuring point enabled graphs presenting the toxic gas concentrations in a working mine to be constructed as a function of time elapsed. Figs. 2–4 show graphs of carbon monoxide CO and nitrogen dioxide NO₂ concentrations as functions of time.

Fig. 5 presents the carbon dioxide CO₂ concentrations as functions of time. No significant changes in the concentrations of oxygen O₂ and methane CH₄ were recorded (were not shown in the graphs).

The time of working ventilation required to achieve a concentration decrease below the Maximum Permissible Concentration (MPC) was 130 minutes—much longer than the time permitted by the federal

rules and regulations (FNiP) (30 minutes)². The results of the monitoring of the toxic gases concentrations after blasting suggest that the booster fan was turned off prior to blasting and was launched only at 22:50. This means that the working was not ventilated by active air current for 110 minutes. This assumption is supported by the curve in Fig. 3, where the concentration of toxic gases begins to sharply decrease after switching on the booster fan. In the return

² Federal rules and regulations in the field of industrial safety “Safety rules for mining and processing of minerals”: approved by Order No. 505 of the Federal Service for Ecological, Technological and Nuclear Supervision dated 08.12.2020, 524 p.

Table 1

Technical specifications of a Dräger X-am 5600 gas analyzer

Measured gas	Measuring range	Sensor lower detection limit	Measurement error	Sensor response time
Methane CH ₄	0–100 % LEL	0.1 % LEL	± 5 % LFL	Up to 15 s
Carbon dioxide CO ₂	0–5 vol. %	0.01 vol. %	± 10 %	Up to 15 s
Oxygen O ₂	0–25 vol. %	0.1 vol. %	± 5 %	5–90 s
Carbon monoxide CO	0–2000 ppm	1 ppm	± 15 %	5–90 s
Nitric oxide NO	0–200 ppm	0.1 ppm	± 10 %	5–90 s
Nitrogen dioxide NO ₂	0–50 ppm	0.1 ppm	± 15 %	5–90 s

Table 2

Technical specifications of the anemometer and rangefinder

Measured value	Measuring range	Measurement error
APR-2		
Airflow velocity	0.2–40 m/s	± (0.1 + 0.05·V) m/s
Leica Disto X310		
Length	0.05–120 m	± 1.0 mm

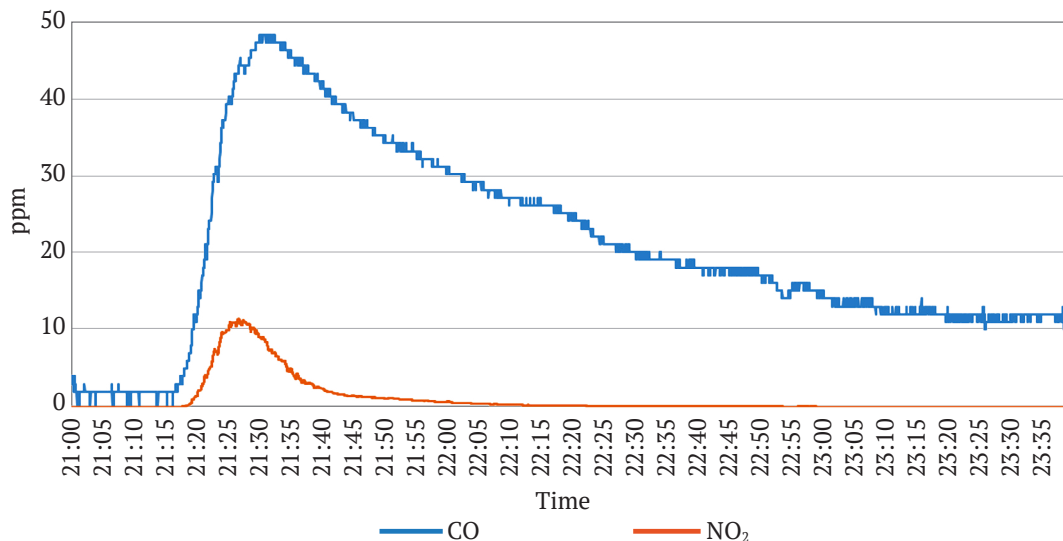


Fig. 2. Toxic gas concentrations at the booster fan (point 1) as functions of time

ventilation current (see Fig. 4), the concentration of the toxic gases, on the contrary, sharply increased. This suggested the rapid removal of the toxic gases from the dead-end working and evidenced the activation of the booster fan. In 20 minutes after booster fan activation, the concentration of the toxic gases reached the background values. This indicated a sufficient level of ventilation under the condition of a permanently operating booster fan.

In addition, the experimental data analysis allows certain conclusions to be drawn. In Figs. 2 and 4, an increase in the concentrations (in $\approx 21:30$) is seen, indicating the arrival of toxic gases after blasting from other workings. This is the result of the sequential

ventilation of working zones causing increased gas hazard in some workings of a mine due to non-optimum ventilation. The carbon dioxide concentration peaks in Fig. 5 after 23:20 are presumably caused by starting operation of ICE equipment in the workings. The concentration of nitrogen dioxide at the blasted working mouth exceeded the effective measuring range of the portable gas analyzer (50 ppm).

In order to assess the reliability of the data obtained, the calculation of the volume of the carbon oxides released was performed based on the data of gas analyzers and the chemical reactions of the explosives' decomposition during detonation, depending on the types and weights of the explosives.

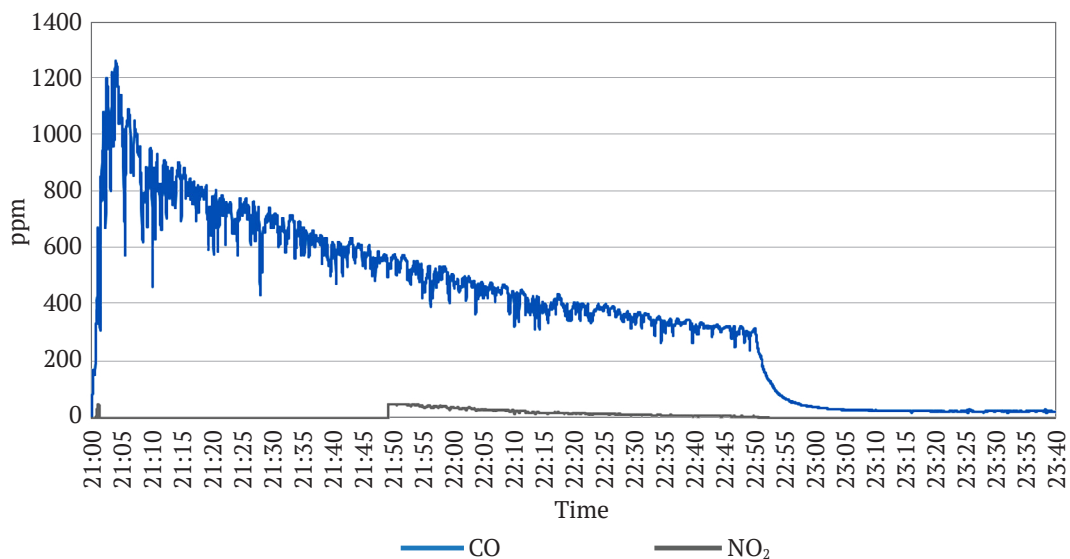


Fig. 3. Toxic gas concentrations at the blasted working mouth (point 2) as functions of time

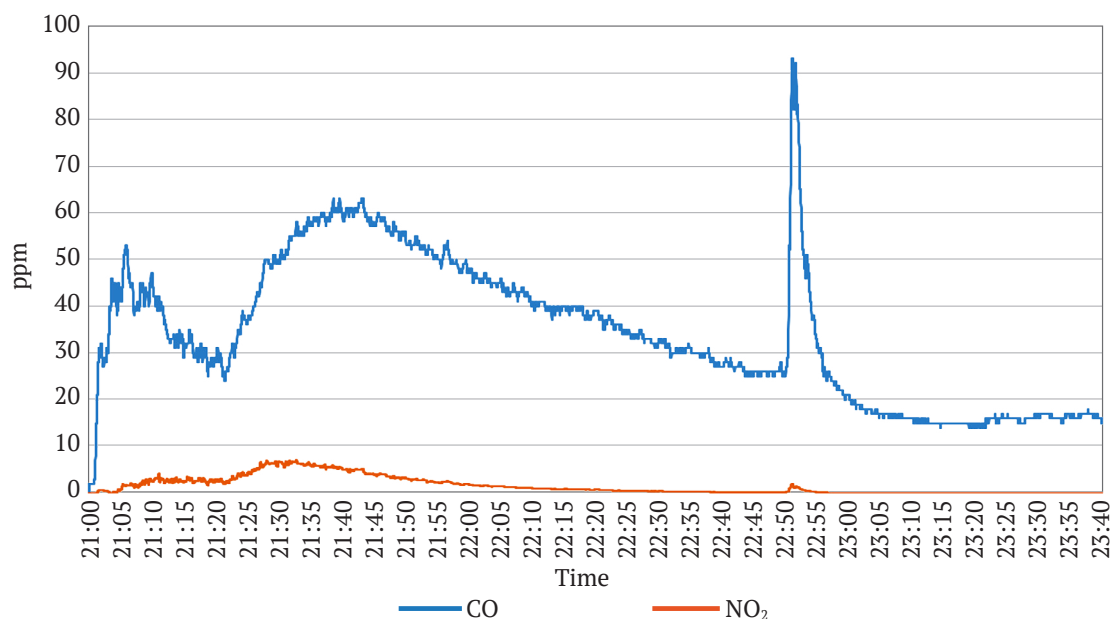


Fig. 4. Toxic gas concentrations at the return ventilation current (point 3) as functions of time

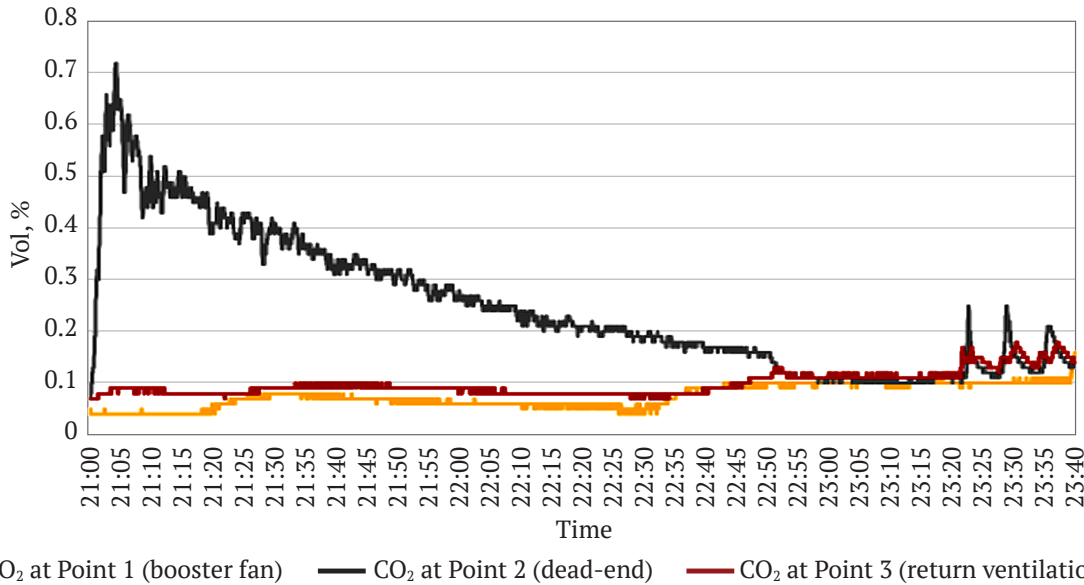


Fig. 5. Carbon dioxide concentrations at the booster fan (point 1), at the blasted working mouth (point 2), at the return ventilation current (point 3) as functions of time

The volumes of the released carbon oxide CO and dioxide CO₂, m³ were calculated from the data of gas analyzers by determining the average concentrations from the moment of starting the increase in the concentration to the moment of the decrease to the background values:

$$V_{co} = (\varphi_{av} - \varphi_{back})Qt, \quad (1)$$

(for the case of CO), where φ_{av} is average gas concentration from the moment of starting the increase in the concentration to the moment of the decrease to the background values, m³/m³; φ_{back} is background gas concentration, m³/m³; Q is air flow rate in the point, m³/s; t is time from the moment of starting the increase in the concentration to the moment of the decrease to the background values, s.

The results of the calculations of the released volume of carbon monoxide and carbon dioxide (hereinafter referred to as carbon oxides) are presented in Table 3.

At point 2, it was impossible to reliably determine the volume of the carbon oxides due to the fact that the booster fan was switched off.

Table 3
Results of calculations of the released volume of carbon oxides after blasting in the development (preparatory) working

Point No.	Air flow rate, m ³ /s	Volume of released CO, m ³	Volume of released CO ₂ , m ³
2	23.2	–	–
3	35.4	4.78	19.65

In addition, the volume of releasing other toxic gases depending on the types and weights of explosives used has been estimated.

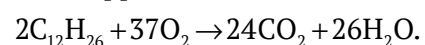
A mixture consisting of Granulit AS-7 and Ammonit 6 ZhV explosives was used for blasting in the working. The weight of Granulit AS-7 was 280 kg, and that of Ammonit 6 ZhV, 68 kg. The oxygen balance of both explosives is positive.

Granulit AS-7 consists of ammonium nitrate (~90 %), aluminum powder (~7 %), and mineral oil (~3 %). When ammonium nitrate detonates, nitrogen N₂, water H₂O, and oxygen O₂ are released, and the oxygen balance is positive. In addition to the components listed above, nitrogen oxides are also generated during the detonation. Nitrogen oxides (nitrogen oxide NO and nitrogen dioxide NO₂) are released due to the incomplete reduction of ammonium nitrate NO₃, and also originate at high temperatures. The formula for the decomposition of ammonium nitrate at detonation is as follows [5]:



Aluminum powder and oil are added to ammonium nitrate, in order to increase the detonation energy and compensate for the excess oxidizer. Aluminum powders do not release toxic gases during detonation.

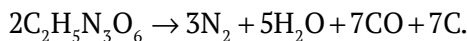
In order to calculate carbon dioxide release, the chemical formula of mineral oil is taken as C₁₂H₂₆ according to [5]. Then the chemical reaction of oil combustion will appear as follows:



The oil combustion produces carbon dioxide CO_2 and, in the case of the shortage of oxygen, carbon monoxide CO . In addition, the oil often contains sulfur, combustion of which produces sulfur dioxide SO_2 . Estimating its quantity is problematic.

Ammonit 6 ZhV consists of ammonium nitrate (~79 %) and TNT (trinitrotoluene), ~21 %. The detonation of TNT produces nitrogen N_2 , water H_2O , carbon monoxide CO and carbon C.

The formula for the trinitrotoluene decomposition during detonation is as follows [5]:



Trinitrotoluene has a negative oxygen balance, compensated by the positive balance of ammonium nitrate. Thus, the main source of carbon monoxide CO is trinitrotoluene in Ammonit 6 ZhV and oil contained in Granulit AS-7.

With the known weight of an explosive, the maximum volume of the released carbon oxides (CO_x) m^3 , is estimated by the following formula:

$$V_{\text{co}} = \frac{m_{\text{expl}} k}{M_{\text{TNT}}} \text{mol}_C V_{\text{mol}}, \quad (2)$$

where m_{expl} is the weight of an explosive, g; k is the weight fraction of the carbon-containing component in the explosive; M_{TNT} is molar mass of the carbon-containing component (TNT), g/mol; mol_C is the number of moles of carbon (including those contained in CO and CO_2) released during detonation; V_{mol} is the volume of one mole of gas, 0.0224 m^3 .

As a result, the detonation of 68 kg of Ammonit 6 ZhV can release 9.86 m^3 of carbon oxides CO_x . When detonating 280 kg of Granulit AS-7 and the mineral oil contained in it, the maximum possible volume of the released carbon oxides amounts to 13.24 m^3 . Thus, during blasting of a mixture of 280 kg of Granulit AS-7 and 68 kg of Ammonit 6 ZV, 23.1 m^3 of carbon oxides can be released, corresponding to the total volume of carbon oxides measured by the portable gas analyzers at point 3 (24.44 m^3). This suggests the credibility of the experimental data measured by the portable gas analyzers.

Experimental studies in a long dead-end working

RV-1, a long exploration working (more than 800 m long at the time of measurements, with a mouth close to the ventilation shaft; fresh air was supplied to the working directly from the surface through a ventilation pipeline) required corrections in the measurement techniques. In order to conduct the field (in-situ) studies after blasting, the sensors (gas analyzers) were installed along the length of a long dead-end working at three points. Point 1 was as close to the blasted face as possible, point 2 was in the middle of the working, and point 3 was located at the working's mouth. The layout of the sensors is shown in Fig. 6.

The layout of measuring points along the working length is due to significant air leaks (about 50 %) along the length of the ventilation duct, laid along the working. In this case, the degree of dilution of toxic gases along the length of the long working and the influence of the longitudinal dispersion of gas impurities are of interest. In this context, the installation of the sensors at the booster fan and in the main return ventilation current is not important due to the lack of possible recirculation of air and the delivery of all the return air through the ventilation shaft directly to the surface.

Fig. 7 shows the experimentally determined time dependences of the toxic gas concentrations in the mouth of the working. The mouth of the working is characterized by the lowest gas concentrations due to their maximum dilution.

The nitrogen dioxide concentrations above 50 ppm were obtained by approximation.

It should be noted that nitrogen dioxide NO_2 concentrations at other points exceeded the measuring ranges of the instruments, so for other measurement points, the data is given only for carbon monoxide CO and carbon dioxide CO_2 . The plots of the concentrations of carbon monoxide CO at points 1, 2, and 3 and carbon dioxide CO_2 at points 1 and 3 as functions of time are shown in Figs. 8 and 9, respectively.

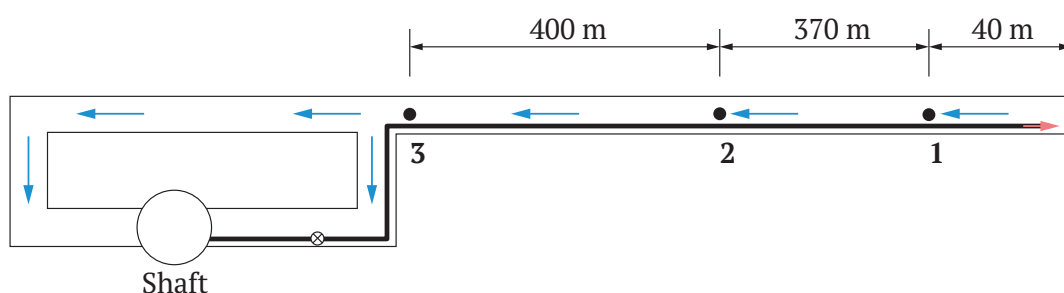


Fig. 6. Layout of measuring points in RV-1 working

According to the data obtained, the concentration of toxic gases decreases as the air flows along the working, while the time of exceeding the maximum permissible concentration increases. This is due to the leaks in the ventilation duct and longitudinal dispersion [6, 7] which do not allow simplified models [8] to be applied.

In Table 4, the data on the distance of the points from the working face, the time of exceeding MPC at them, the air flow rate, and the volume of carbon monoxide CO passing through them are presented.

In order to assess the reliability of the obtained results of the toxic gases concentrations monitoring in the mine working after blasting, the volume of the released toxic gases depending on the types and weights of the explosives used was assessed.

For blasting purposes, a mixture consisting of Granulit AS-7 and Ammonit 6 ZhV explosives was used in the working. The weight of Granulit AS-7 was 200 kg, and the weight of Ammonit 6 ZhV was 34 kg. As a result, the detonation of 34 kg of Ammonit 6 ZhV can release 4.92 m³ of carbon oxides CO_x. When

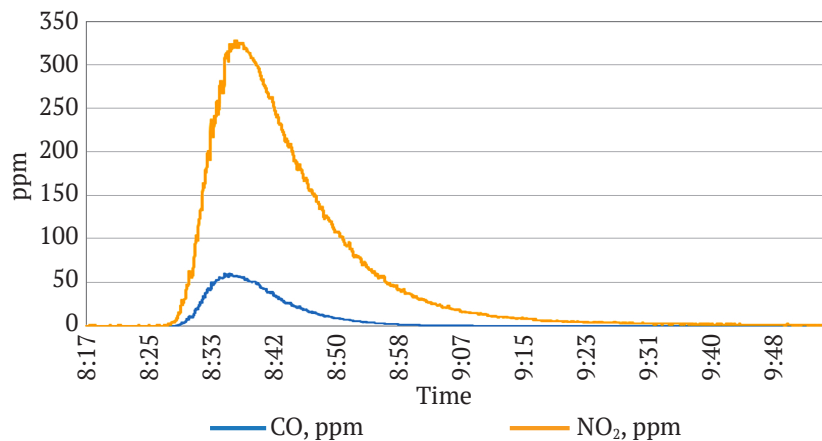


Fig. 7. Time dependences of the concentrations of toxic gases after blasting in point 3

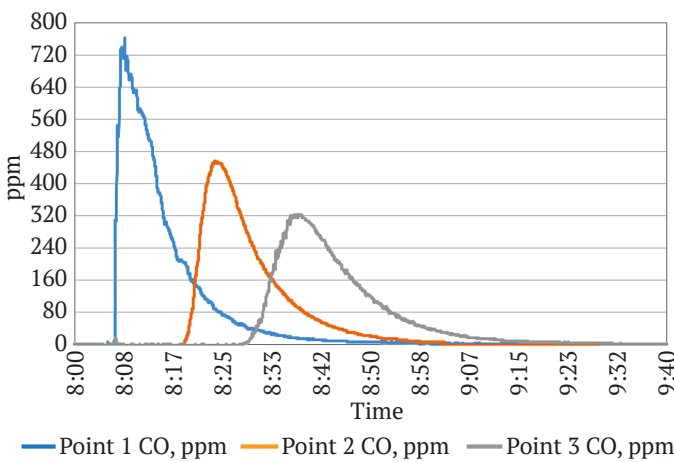


Fig. 8. Time dependences of carbon monoxide CO concentrations in the working after blasting

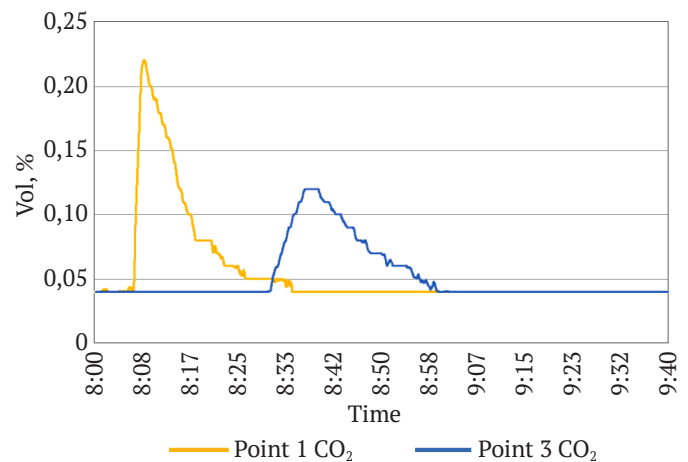


Fig. 9. Time dependences of carbon dioxide CO₂ concentrations in the working after blasting

Table 4

Results of the study of the gas hazard in the working after blasting

Measuring point number	Distance from the face to the measuring point	Start time of exceeding MPC (17 ppm)	End time of exceeding MPC (17 ppm)	Required duration of ventilation	Air flow rate at the measuring point	Volume of released CO	Volume of released CO ₂
RV-1 working							
1	40 m	8:06	8:38	63 min	m ³ /s	4.0 m ³	9.1 m ³
2	410 m	8:20	8:53		–	–	–
3	810 m	8:32	9:09		m ³ /s	4.8 m ³	10.6 m ³



detonating 200 kg of Granulit AS-7 and the mineral oil contained in it (6 kg), the maximum possible volume of the released carbon oxides amounts to 9.46 m³. Thus, blasting of a mixture of 200 kg of Granulit AS-7 and 36 kg of Ammonit 6 ZV can release 14.38 m³ of carbon oxides which corresponds to the total volume of carbon oxides measured by the portable gas analyzers at Points 1 (13.1 m³) and 3 (15.4 m³). This suggests the reliability of the experimental data obtained with due consideration of the instrument accuracy and the sensor response delay in the gas concentration measurements. The resulting volume of the released carbon oxides was used for the mathematical simulation of the gas distribution in the ventilation network of the mine workings after blasting.

The ventilation time required in the long working, in order to achieve the concentration decrease below the Maximum Permissible Concentration (MPC) was 63 minutes – much longer than the time permitted by the federal rules and regulations (FNiP) (30 minutes)⁵.

Theoretical Studies

In order to analyze the temporal dynamics of toxic gas impurities blow-away from the RV-1 working face depending on the distance of the face from the mouth, a non-stationary gas-dynamic model was developed.

The following assumptions were taken in the model:

- the volumetric concentrations of gases are small, so the difference in the density of the gas-air mixture they create in different parts of the dead-end working cannot result in a significant gas depression and/or convective stratification of the flows along a working cross-section;

- the concentration of toxic gases is uniform in the cross-section of a mine workings;

- all physical processes are determined only by time and the longitudinal coordinate of a working. This assumption allows considering workings geometrically as one-dimensional objects;

- the Ox coordinate system is selected in such a way that the longitudinal x -axis is directed in the direction of air flow in a dead-end working, and the origin of coordinates O is in the face of a working;

- the zone of irregular vortex air motion near the face is negligibly small compared to the total length of a working;

- the model takes into account the process of mixing harmful gas impurities with fresh air by setting the contact boundary of the vortex mixing

zone with the zone of unidirectional and steady air movement in the model.

Analyzing the time dependences of CO concentrations in the working (see Fig. 10), one can observe the concentration dispersion with increasing distance from the face. This indicates that gas dispersion takes place in the workings. According to [8], dispersion includes both “dissipation” of admixtures due to the airflow velocity non-uniformity across the cross-section, and longitudinal turbulent diffusion due to eddy turbulent pulsations of the flow velocity at each of its points. The molecular diffusion of a dust and air mixture is generally considered negligible when considering the turbulent air flows in mine workings. It correlates with turbulent diffusion in the same way as molecular viscosity with turbulent, i.e. it is lower than the latter by one-three orders of magnitude [9, 10]. The main factor that leads to the dispersion of admixtures at the straight runs of the working is the non-uniform cross-sectional airflow velocity. It is important to note that the effect of airflow dispersion, caused by the turbulent diffusion and nonuniformity of the velocity field across the cross-section, is true primarily for the one-dimensional models of mine workings within the ventilation network.

The convection-diffusion transfer equation was solved to describe a gas admixture transfer in mine workings [11]:

$$\frac{\partial c}{\partial t} + \frac{\partial(vc)}{\partial x} = D \frac{\partial^2 c}{\partial x^2}, \quad (3)$$

where $c = c(t, x)$ is volume concentration of the considered gas impurity, m³/m³; $v = v(x)$ is airflow velocity in a working, m/s; D is longitudinal dispersion coefficient, m²/s [12, 13]; x is longitudinal coordinate, m; t is time, s. Taking into account the dependence of airflow velocity v on the longitudinal coordinate enables the air leaks in the ventilation duct to be explicitly calculated.

The contact boundary with the mixing zone and the mouth of the working are taken as the boundaries of the calculation area. The following boundary conditions are set on these boundaries:

$$c(t, x_{\text{mixing}}) = c_{\text{mixing}}; \quad (4)$$

$$\frac{\partial c}{\partial t}(t, x_{\text{mouth}}) = 0, \quad (5)$$

where x_{mixing} is contact boundary with the mixing zone, m; x_{mouth} is boundary of the working mouth, m; $c_{\text{mixing}} = c_{\text{mixing}}(t)$ is volume concentration of gas in the mixing zone, m³/m³.

The position of the contact boundary with the mixing zone is determined by the following formula [14]:

⁵ Federal rules and regulations in the field of industrial safety “Safety rules for mining and processing of minerals”: approved by Order No. 505 of the Federal Service for Ecological, Technological and Nuclear Supervision dated 08.12.2020, 524 p.



$$x_{mouth} = x_p + 4d_{eff}, \tag{6}$$

where x_p is distance from the face to the end of the ventilation duct, m; d_{eff} is equivalent diameter of the working, m.

The equivalent diameter is calculated using the following formula:

$$d_{eff} = 4 \frac{S}{P}, \tag{7}$$

where S is cross-sectional area of the working, m²; P is the working perimeter, m.

The Voronin model [15] is used to determine the volume concentration in the mixing zone c_{mixing} :

$$c_{mixing} = c_0 \exp\left(-k \frac{Q_p}{V_{mixing}} t\right), \tag{8}$$

where c_0 is volume concentration of the considered gas impurity in the mixing zone at the initial time, m³/m³; k is ventilation efficiency coefficient; Q_p is rate of airflow leaving the duct, m³/m³; $V_{mixing} = x_{mouth} S$ is mixing zone volume, m³.

At the initial time, in the calculation area, zero concentration of a harmful gas impurity is set:

$$c(0, x) = 0. \tag{9}$$

As a result, equations (2)–(8) constitute a mathematical gas-dynamic model of harmful gas admixtures removal from a working during ventilation after gas release at a face. It is worth noting that the values of D , c_0 and k for each working and gas must be determined by backward analysis [16], using the results of field (experimental) measurements, like those obtained for CO in Fig. 7.

The numerical solution of the problem of convection-diffusion transfer of a gas admixture in workings was sought using finite-difference method by means of splitting by physical processes, convection and diffusion [17] (if necessary, taking into account the action of a mass source of a harmful admixture).

It should be noted that the calculation of gas concentrations and calibration of the model were performed based on the carbon monoxide CO concentrations measured during the experimental studies at the time of blasting in three points along the length of mine workings (see Fig. 10). Of all three measuring points, the measuring results at point 3 are considered to be the most reliable. This is justified by the fact that due to the longitudinal dispersion, the entire gas volume passes through point 3 without sharp changes in the concentrations. In this case, the sensitive element of a sensor (gas analyzer) has time to measure the concentration of gas passing through it more accurately, i.e. the influence of the sensor time response decreases.

However, in order to determine the concentration in the mixing zone at the initial time c_0 the results of the measurements at point 1 are required, because this point is within the mixing zone, therefore, the maximum CO concentration at point 1 will determine the value of c_0 .

The ventilation efficiency coefficient k and the longitudinal dispersion coefficient D are determined by backward analysis using the results of the measurements at point 3 [18]. The backward analysis consists in the following:

1. Knowing the value of c_0 , the value of k is selected so that the gas mass balance between point 3 and the boundary of the mixing zone is maintained.

2. Having fully determined the parameters of the boundary condition on the boundary of the mixing zone, simulation is carried out with different values of the longitudinal dispersion coefficient D . Finally the D value is found by the selection, at which the simulated dispersion of gas (decreasing its concentration) over time in point 3 coincides with the experimental measurement data.

The obtained values of parameters c_0 , k , and D for the RV-1 are given in Table 5.

Table 5

Value of longitudinal dispersion coefficient and parameters in Voronin mixing model

$D, m^2/s$	c_0	k
RV-1 working		
2.5	765	0.11

The results of the simulation of gas distribution in the working at point 3 are shown in Fig. 10. In addition, the Figure shows the results of the experimental measurements, the time dependence of the gas concentration.

Comparative analysis of the results of the simulation and measurements (Fig. 10) showed that the developed gas distribution model, when calibrated by the field (in-situ) measurements, enabled an acceptable agreement to be obtained with the time dependence of the measured gas concentrations at point 3. The existing differences between the simulated and measured dependences can be explained by a number of reasons: due to the rapid transfer of CO through the sensor at point 1 and the sensor time lag (see Table 1), it is impossible to correctly determine the time dependence of the gas concentration that leads to a slight shift of the experimental dependence to the right and less accurate estimate of c_0 ; value; the lack of accurate data on the distribution of air leaks along workings; use of a constant coefficient of longitudinal dispersion; applying a simplified model of air mixing at a face. It is important to note that,

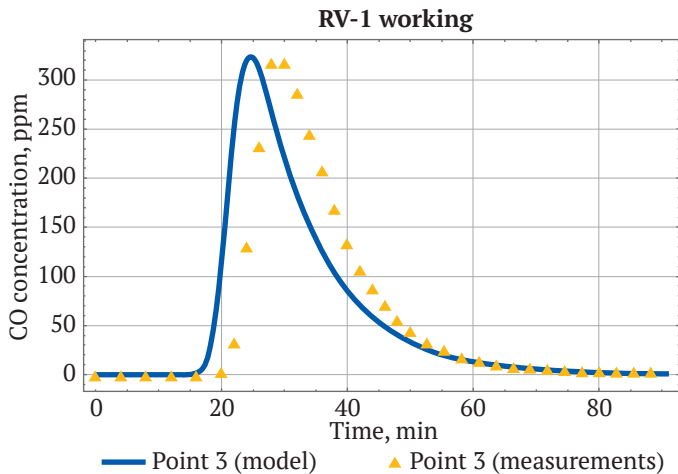


Fig. 10. Comparative analysis of the time dependences of CO concentration at measuring point 3 in the working

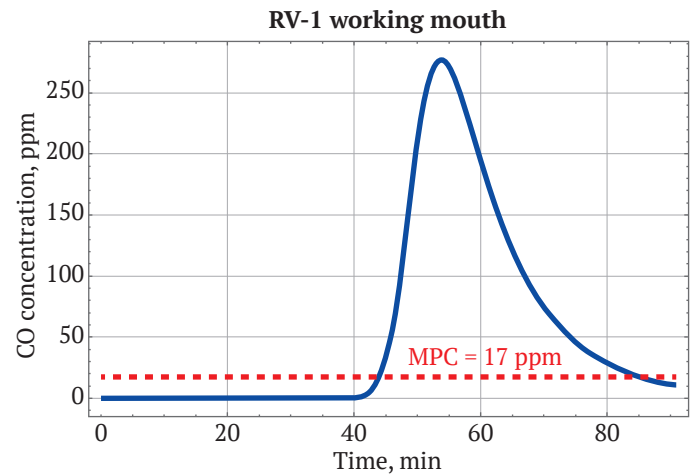


Fig. 11. Time dependence of CO concentration at the working mouth at 1500-m distance between the face and the mouth

through selecting the effective simulated airflow rate in a working, it is possible to achieve almost perfect coincidence of the theoretical curve and the measurement point data.

Based on the values of carbon monoxide CO concentrations obtained in the model, it was found that the MPC level at the mouth of the working is achieved in 18 minutes after blasting. Then, the concentration of CO at the mouth decreases to the MPC only after 52 minutes of the working ventilation after blasting.

In addition, after the calibration and verification of the model, the simulation of the working ventilation was carried out for the case of increasing its length up to 1,500 m. It was assumed that the airflow rate in the working from the mouth to the previous position of the face corresponds to the previous initial parameters, and the minimum airflow rate of 9 m³/s was accepted for the newly driven part of the working. The simulation results are shown in Fig. 11.

When increasing the working length up to 1,500 m, it was established that the time after blasting for the concentration of CO to reach MPC at the mouth increased to 87 min (38 % more than for the shorter working length).

The constructed gas-dynamic model and the longitudinal dispersion coefficients obtained as a result of the analysis enable the time required for long dead-end mine workings ventilation to be analyzed and estimated. Based on the model developed, the

algorithm for calculating [8] the velocity of spreading the combustion products in the mine ventilation network in emergency situations is being improved, and the longitudinal dispersion coefficient for different operating conditions is being refined.

Conclusions

The experimental (measurement) data obtained from the study of blasting operations in RSH-26-20-1 and RV-1 mine workings enabled the actual time of ventilation of a dead-end working and the amount of carbon monoxide CO_x released to be determined. The results obtained were analyzed for the correspondence to the total amount of gas released after blasting, depending on the types and weights of the explosives used.

Based on the obtained graphs of the time dependences of the concentrations of toxic gases along the length of RV-1 working, a mathematical model of the dynamics of a gas-air mixture was built and calibrated, taking into account the convection-diffusion transfer. Based on the experimental data, the coefficients of longitudinal dispersion, ventilation efficiency, and the volume concentration of the considered gas admixture in the mixing zone at initial time were determined for a long dead-end mine working (RV-1). The time required for the ventilation of long dead-end workings since its driving proceeds was determined on the basis of the simulation results.

References

1. Grishin E.L. Gas behavior in the modern concept of mine ventilation. *Gornoe Ekho*. 2021;(4):101–104. <https://doi.org/10.7242/echo.2021.4.20>
2. Ushakov K.Z., Burchakov A.S., Puchkov L.A., Medvedev I.I. *Aerology of mining enterprises*. Moscow: Nedra Publ.; 1987. 420 p. (In Russ.)
3. Dubnov L.V., Bakharevich N.S., Romanov A.I. *Industrial explosives*. 3rd ed. Moscow: Nedra Publ.; 1988. 358 p. (In Russ.)



4. Ganapolsky M.I., Baron V.L., Belin V.A., et al. *Methods of blasting operations. Special blasting operations*. Textbook. Moscow: Moscow State Mining University Publ.; 2007. 563 p. (In Russ.)
5. Gushin V.I. *Set of problems on blasting*. Moscow: Nedra Publ.; 1990. 174 p. (In Russ.)
6. Semin M.A., Isaevich A.G., Trushkova N.A. et al. Calculating dispersion of air pollutants in mines. *Fiziko-Tekhnicheskiye Problemy Razrabotki Poleznykh Iskopaemykh*. 2022;(2):82–93. (In Russ.) <https://doi.org/10.15372/FTPPI20220208>
7. Widiatmojo A., Sasaki K., Widodo N.P., Sugai Y. Numerical simulation to evaluate gas diffusion of turbulent flow in mine ventilation system. *International Journal of Mining Science and Technology*. 2013;23(3):349–355. <https://doi.org/10.1016/j.ijmst.2013.05.004>
8. Levin L. Yu., Kormshchikov D.S., Semin M.A. Rapid determination of combustion gas distribution in mine workings. *Mining Informational and Analytical Bulletin*. 2013;(12):179–184. (In Russ.) URL: https://giab-online.ru/files/Data/2013/12/179-184_Levin_-_6_str.pdf
9. Vengerov I.R. *Thermophysics of underground mines and open pits. Mathematical models. Vol. 1. Paradigm analysis*. Donetsk: Nord-Press Publ.; 2008. 632 p.
10. Vardy A.E., Brown J.M.B. Transient turbulent friction in smooth pipe flows. *Journal of Sound and Vibration*. 2003;259(5):1011–1036. <https://doi.org/10.1006/jsvi.2002.5160>
11. Zhou A., Wang K. A transient model for airflow stabilization induced by gas accumulations in a mine ventilation network. *Journal of Loss Prevention in the Process Industries*. 2017;47:104–109. <https://doi.org/10.1016/j.jlp.2017.02.014>
12. Arpa G., Widiatmojo A., Widodo N.P., Sasaki K. Tracer gas measurement and simulation of turbulent diffusion in mine ventilation airways. *Journal of Coal Science and Engineering (China)*. 2008;14(4):523–529. <https://doi.org/10.1007/s12404-008-0401-x>
13. Kim D.Y., Lee S.H., Jeong K.H., Lee C.W. Study on the turbulent diffusion coefficients of contaminants in an underground limestone mine with large cross section using tracer gas. *Geosystem Engineering*. 2013;16(2):183–189. <https://doi.org/10.1080/12269328.2013.806051>
14. Kolesov E.V., Kazakov B.P. Efficiency of ventilation of dead-end development headings after blasting operations. *Bulletin of the Tomsk Polytechnic University. Geo Assets Engineering*. 2020;(7):15–23. (In Russ.) <https://doi.org/10.18799/24131830/2020/7/2715>
15. Voronin V.N. *Fundamentals of Mine Aerogas dynamics*. Moscow-Leninrad: Ugletekhizdat Publ.; 1951. 491 p. (In Russ.)
16. Isaevich A., Semin M., Levin L. et al. Study on the dust content in dead-end drifts in the potash mines for various ventilation modes. *Sustainability*. 2022;14(5):3030. <https://doi.org/10.3390/su14053030>
17. Voevodin A.F., Goncharova O.H. Method of splitting into physical processes for numerical investigation of convection problem. *Matematicheskoe Modelirovanie*. 2001;13(5):90–96. (In Russ.) URL: https://www.mathnet.ru/php/archive.phtml?wshow=paper&jrnid=mm&paperid=717&option_lang=rus
18. Nakaryakov E.V., Semin M.A., Grishin E.L., Kolesov E.V. Analysis of the regularities of accumulation and removal of the exhaust gases from the combustion-engined vehicles in the dead-end chamber-like mine workings. *Occupational Safety in Industry*. 2021;(5):41–47. (In Russ.) <https://doi.org/10.24000/0409-2961-2021-5-41-47>

Information about the authors

Dmitriy V. Olkhovskiy – Engineer, Mining Production Development Laboratory, Mining Institute of the Ural Branch of the Russian Academy of Sciences, Perm, Russian Federation; Scopus ID [57225125993](https://orcid.org/0000-0002-5722-5125); e-mail demexez@gmail.com

Oleg S. Parshakov – Cand. Sci. (Eng.), Researcher, Mining Production Development Laboratory, Mining Institute of the Ural Branch of the Russian Academy of Sciences, Perm, Russian Federation; Scopus ID [57202379375](https://orcid.org/0000-0002-5720-2379); e-mail olegparshakov@gmail.com

Sergey A. Bublik – Engineer, Laboratory of Mathematical Modeling of Geotechnical Processes, Mining Institute of the Ural Branch of the Russian Academy of Sciences, Perm, Russian Federation; Scopus ID [57223084283](https://orcid.org/0000-0002-5722-3084); e-mail serega-bublik@mail.ru

Received	04.08.2022
Revised	04.10.2022
Accepted	31.10.2022




MINING MACHINERY, TRANSPORT, AND MECHANICAL ENGINEERING

Research paper

<https://doi.org/10.17073/2500-0632-2022-11-34>

UDC 622.625.6

**Effect of operating conditions of mine monorail locomotives on the durability of drive wheel polymeric rims**E. M. Arefiev¹  , K. A. Ryabko²  ¹ Saint Petersburg State Institute of Technology, Saint Petersburg, Russian Federation² Rostov State University of Railway Transport (Voronezh Branch), Voronezh, Russian Federation elcross@mail.ru**Abstract**

An increase in the rate of coal mining and a reduction of its prime cost can be ensured by comprehensive mechanization and automation of the system of mine auxiliary transport through the widespread introduction of overhead monorail tracks. The potential use of mine monorail tracks are conditioned by the following factors: low payload ratio of the train; reduction of the mine workings cross-section area due to transfer of auxiliary transport to the upper part of the workings; high operational safety; as well as the possibility of dismantling the track in the unused sections and subsequently installing it in new mine workings. The use of rubberized rollers in the drives of mine monorail locomotives enables the coefficient of adhesion of the wheel with the monorail to be increased. It also reduces dynamic loads and the noise level during operation. The purpose of this research is to assess the durability of polymeric rims of drive wheels for mine monorail locomotives, taking into account their operating conditions. Stress distribution over the contact area of the wheel rim with the monorail was determined, enabling the development of measures to increase the service life of drive wheels of mine monorail locomotives to be developed. It was established that the effect of the monorail track deformation has no significant impact on the durability of drive wheel rims of mine monorail locomotives. A mathematical model was obtained to determine the durability of drive wheel polymeric rims, taking into account the maximum dynamic forces arising during the contact of drive wheels with the monorail. The durability of wheel polymeric rims of mine monorail locomotives was assessed in accordance with the Bailey criterion with regard to the maximum values of dynamic contact loads arising during the monorail train movement. It was also established that an increase in the carriage mass from 20 to 47 kN leads to 32 % less durability of a monorail locomotive drive wheel rim (from 8700 to 5900 hours).

Keywords

mine monorail track, monorail locomotive, durability, service life, drive, polymeric rim, overhead monorail, undercarriage, dynamic loads

For citation

Arefiev E. M., Ryabko K. A. Effect of operating conditions of mine monorail locomotives on the durability of drive wheel polymeric rims. *Mining Science and Technology (Russia)*. 2023;8(1):59–67. <https://doi.org/10.17073/2500-0632-2022-11-34>

ГОРНЫЕ МАШИНЫ, ТРАНСПОРТ И МАШИНОСТРОЕНИЕ

Научная статья

Влияние условий эксплуатации шахтных монорельсовых локомотивов на долговечность полимерных ободьев приводных колесE. M. Арефьев¹  , K. A. Рябко²  ¹ Санкт-Петербургский государственный технологический институт (технический университет), г. Санкт-Петербург, Российская Федерация² Ростовский государственный университет путей сообщения (филиал в г. Воронеже), г. Воронеж, Российская Федерация elcross@mail.ru**Аннотация**

Увеличение темпов добычи угля и снижение ее себестоимости может быть обеспечено путем комплексной механизации и автоматизации системы шахтного вспомогательного транспорта за счет широкого внедрения подвесных монорельсовых дорог. Перспективность использования шахтных монорельсовых дорог обусловлена низким коэффициентом тары состава; снижением площади сечения выработок за счет вынесения вспомогательного транспорта в верхнюю часть выработок; высокой безопасностью



эксплуатации; возможностью демонтажа дороги на неиспользуемых участках и последующего монтажа в новых выработках. Использование обрешеченных роликов в приводе шахтных монорельсовых локомотивов позволяет повысить коэффициент сцепления колеса с монорельсом, снизить динамические нагрузки и уровень шума в процессе эксплуатации. Целью исследований является оценка долговечности полимерных ободьев приводных колес шахтных монорельсовых локомотивов с учетом условий их эксплуатации. Получено распределение напряжений по пятну контакта обода колеса с монорельсом, что позволит разработать мероприятия по повышению срока службы приводных колес шахтных монорельсовых локомотивов. Установлено, что влияние деформации монорельсового пути не оказывает существенного влияния на долговечность ободьев приводных колес шахтных монорельсовых локомотивов. Получена математическая модель для определения долговечности полимерных ободьев приводных колес с учетом максимальных динамических усилий, возникающих при контакте приводных колес с монорельсом. Проведена оценка долговечности полимерных ободьев колес шахтных монорельсовых локомотивов в соответствии с критерием Бейли с учетом максимальных значений динамических контактных нагрузок, возникающих при движении монорельсового состава. Установлено, что увеличение массы тележки с 20 до 47 кН приводит к снижению долговечности обода приводного колеса монорельсового локомотива на 32 % (с 8700 до 5900 ч).

Ключевые слова

шахтная монорельсовая дорога, монорельсовый локомотив, долговечность, срок службы, привод, полимерный обод, подвесной монорельс, ходовая тележка, динамические нагрузки

Для цитирования

Arefiev E. M., Ryabko K. A. Effect of operating conditions of mine monorail locomotives on the durability of drive wheel polymeric rims. *Mining Science and Technology (Russia)*. 2023;8(1):59–67. <https://doi.org/10.17073/2500-0632-2022-11-34>

Introduction

One way to increase coal production is to increase labor productivity. One important fact in this regard is the connectivity, comprehensive mechanization and automation of the mine auxiliary transport system by means of wide introduction of overhead monorail tracks becomes of great importance.

The potential of the use of monorail tracks in mines are conditioned by a number of essential advantages of this transport type: low payload ratio of the train; transfer of auxiliary transport to the upper part of the workings, enabling a substantial decrease in the section area and thus the capital expenditures for their construction; high safety of operation both at high and low speeds; simple automation; as well as possibility of dismantling the track in the unused sections and subsequently installing it in new mine workings.

The use of rubberized rollers in the drive of mine monorail locomotives enables the coefficient of adhesion with the monorail to be increased. It also enables a reduction in the dynamic loads and the noise level during operation. Therefore, the issue of the effect of mine monorail locomotives operating conditions on the durability of drive wheel polymeric rims is relevant.

Review of researches and publications

A number of papers of scientific-research and design organizations are dedicated to the design and upgrading of drives for monorail locomotives used in mines. The methods of calculating the

main parameters and operating conditions for drive wheels of mine overhead monorail locomotives, as considered in scientific publications, do not fully reflect the effect of the interaction of the drive wheels with the monorail with regard to their durability. The synthesising of multipurpose methods on the effect of operating conditions of mine monorail locomotives on the durability of drive wheel polymeric rims is a very complex scientific task. Analysis of computational and theoretical bases aimed at developing drives for overhead monorail locomotives shows the necessity of assessing the effect of their operating conditions on the durability of drive wheel polymeric rims.

Results of studies of the winch wheel rolling process aimed at increasing the draft force when driving on slopes are presented in [1]. The authors substantiate the possibility of increasing the tangential draft force by means of increasing the coefficient of adhesion between the wheels and the monorail by making winch wheels out of friction materials. This paper, however, does not address the issues of assessing the durability of drive wheel polymeric rims.

The study in [2] proposes a design of the mine locomotive drive which provides increased draft and braking properties due to the use of additional rubberized rollers kinematically connected with the drive wheels. The use of friction materials for roller lining allows the draft force and coefficient of adhesion to be increased up to 0.35...0.45 and the braking distance to be reduced. The above studies



refer to the draft-braking properties of monorail locomotives, but do not cover the very relevant issue of studying the effect of increasing the coefficient of adhesion of additional rubberized rollers with a monorail on durability.

The results of studying the process of interaction between the drive carriage and the monorail using the original simulation model are presented in [3, 4]. The additional deformations of the monorail track due to inertial components arising in the process of the monorail train movement have been assessed, and the maximum dynamic loads arising in the "carriage-rail" system have been determined. The main provisions of the work under study do not reflect the effect of dynamic loads on the drive wheels.

Significant works are dedicated to the simulation of loads and justification of design parameters of tough elastic elements, justification of geometrical parameters of rubber-polymeric drive drums of a belt conveyor, prediction of complex failure of rubber materials, as well as the effect of increased speeds of monorail locomotives on the dynamic parameters of the locomotive–monorail system. Paper [5] provides a simulation of the loads arising in the rubber-cord elastic coupling. An epure of equivalent stresses of the elastic element was obtained. These results are valid for rubber-cord elements working in shear, while not taking into account the nature of loading of mine monorail locomotive drive wheels. Paper [6] describes the forces occurring in rubber linings of the belt conveyor drive drums. The stress-strain state of digital solid models was simulated. In paper [7] a comprehensive method of determining the parameters of rubber fracture is given. The proposed method allows a quantitative assessment of rubber strength depending on the applied mechanical impacts. However, it does not fully take into account the features of loading the rims of drive wheels of mine monorail locomotives. Papers [8, 9] present the results of numerical simulation of the locomotive impact on the overhead monorail track, aimed at improving the safety of mine monorail locomotives. However, the models obtained do not take into account the effect of dynamic loads on the truck of hauling carriages.

The main provisions of the studies under consideration do not fully determine the effect of operating conditions of mine monorail locomotives on the durability of drive wheel polymeric rims, so they require additions and clarifications.

Operation of a wheel drive for overhead monorail locomotives in mines is characterized by several parameters: formation of draft force; creation of the necessary coefficient of adhesion of a wheel with

a monorail; perception of alternative dynamic impacts from track roughness; as well as influence of braking forces and condition of interaction surfaces between a monorail and drive wheels. All these parameters have been well studied for ground-based motor road and railway vehicles, but they do not fully reflect the assessment of the influence of mine monorail locomotives operating conditions on the durability of drive wheel polymeric rims.

Purpose of research

During use, the drive wheels of a mine monorail locomotive, drive wheel polymeric rims experience periodic contact stresses due to the contact of the rim elements with the monorail. The relationship of rim durability to operating conditions determines the economically justified parameters. Thus, the assessment of durability of drive wheel polymeric rims of mine monorail locomotives is of scientific and practical interest.

Research methods

Studies aimed at determining the effect of operating conditions of mine monorail locomotives on the durability of drive wheel polymeric rims were carried out using the methods of differential and integral calculus, mathematical analysis and graphic interpretation.

The durability of polymeric and rubber rims of drive wheels for monorail tracks under dynamic contact loads can be determined in accordance with the Bailey criterion [10]:

$$N \int_0^{\Theta} \frac{dt}{L(\sigma, T)} = 1, \quad (1)$$

where N is the number of pulses to fracture; $L = L(\sigma, T)$ is the durability of rubber and polymeric products under the static loading mode; σ is the law of stress change; T is the absolute temperature of rim material (temperature of mine atmosphere); $\Theta = l_c/V$ is the pulse duration (time of contact of the rim fragment with a monorail); V is the average speed of train movement; here l_c is the length of the rim contact patch with the monorail (Fig. 1) determined by the Hertz formula [11]:

$$l_c = \sqrt{\frac{4F_d r_{red}}{\pi E_{red}}}, \quad (2)$$

where F_d is the force of contact interaction between the monorail locomotive carriage wheel and the monorail; E_{red} is the reduced modulus of elasticity:

$$E_{red} = \frac{E_1 E_2}{E_1 + E_2},$$

where E_1, E_2 are the moduli of elasticity of the wheel rim and the monorail, respectively; r_{red} is the reduced radius of curvature,

$$\frac{1}{r_{red}} = \frac{1}{r_1} + \frac{1}{r_2},$$

where r_1, r_2 are the radii of curvature of the wheel rim and monorail.

When the carriage moves at constant speed V , the monorail deflects in the vertical plane by value z under the action of carriage mass m . This deflection is caused by the action of both static load and vertical forces of inertia (Fig. 2).

The mass of the carriage with the load is much greater than the mass of the monorail section, so the mass of the monorail can be neglected. The force with which the carriage acts on the monorail can be represented by the dependence:

$$F_d = mg - m \frac{d^2z}{dt^2}.$$

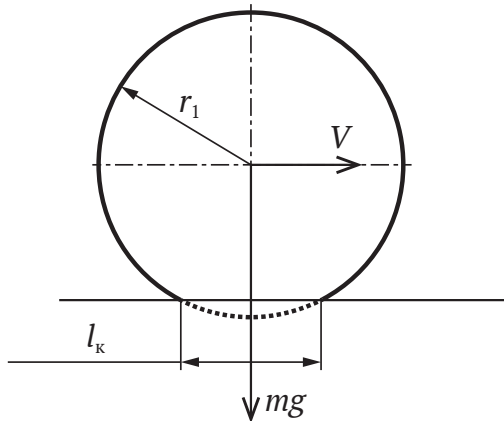


Fig. 1. Establishing the contact patch length of the wheel rim with the monorail

Given that coordinate $x = Vt$:

$$\frac{dz}{dt} = \frac{dz}{dx} \frac{dx}{dt} = V \frac{dz}{dx}.$$

Hence:

$$\frac{d^2z}{dt^2} = V^2 \frac{d^2z}{dx^2}. \tag{3}$$

Given equation (3), the force with which the carriage acts on the monorail:

$$F_d = m \left(g - V^2 \frac{d^2z}{dx^2} \right). \tag{4}$$

The monorail can be seen as a beam (see Fig. 2) acting on the curve; then, the deflection of the beam can be described by equation:

$$z(x) = \frac{F_d}{E_2 J} \frac{x(L-x)^2}{3L},$$

where L is the distance between monorail hangers (section length); J is the moment of inertia of the monorail cross section.

Given equation (4) we obtain:

$$z(x) = m \left(g - V^2 \frac{d^2z}{dx^2} \right) \frac{x^2(L-x)}{3LE_2J}. \tag{5}$$

The maximum dynamic load at the wheel contact with the monorail will occur in the middle of the span between the monorail hangers $L = x/2$, then, taking into account formula (5), we get:

$$F_{d_{max}} = mg \left(1 - V^2 \frac{mL}{3EJ} \right). \tag{6}$$

The monorail for modern mine monorail tracks is made of a hot-rolled steel I-beam with a section height of 160 mm and the following parameters: $E_2 = 20.6 \cdot 10^7$ kN/m² and $J = 8.72 \cdot 10^{-6}$ m⁴.

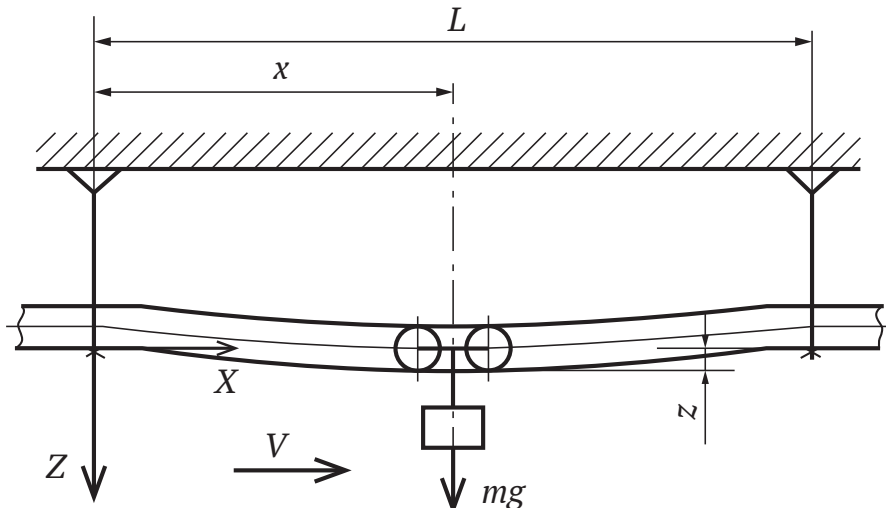


Fig. 2. Diagram of deformation of the overhead monorail track under the moving carriage

According to studies [3, 12], the maximum dynamic forces arising at the contact of a monorail with a drive wheel, depending on the carriage mass, change from 20 to 47 kN, and the maximum longitudinal bending varies from 7 to 15 mm (Table 1).

Table 1

Maximum dynamic forces arising from the contact of the monorail with the drive wheel and values of maximum longitudinal bending of the monorail depending on the carriage mass

Carriage mass <i>m</i> , t	Maximum dynamic forces, $F_{d_{max}}$, kN	Maximum longitudinal bending of monorail z_{max} , mm
2	20	6.3
2.5	25	7.5
4	42	13
4.5	47	15

Durability of rim material under static loading mode [13–15]:

$$L(\sigma) = \tau_0 \ln \left(\frac{\Delta p_\infty}{\Delta p_\infty - \Delta p_{cr}} \right) \exp \left(\frac{U_0 - \gamma \sigma}{k' T} \right), \quad (7)$$

where τ_0 is the vibrational period of atoms in molecules; Δp_∞ is an increment of bond excessive stresses accumulation caused by thermal fluctuations; Δp_{cr} is the critical concentration of bond excessive stresses accumulation; U_0 is the energy of rim material chemical bond breaking activation; k' is the Boltzmann constant; and γ is the structure-sensitive parameter [16, 17].

As a rule, mine monorail locomotive haulage is used for the transportation of auxiliary cargo within one mine horizon where the temperature of the mine atmosphere is practically constant. Thus the influence of temperature change on the rim durability can be neglected.

The stress in the contact of two cylindrical surfaces can be determined by the Hertz formula. Taking into account the maximum dynamic forces arising from the contact between the monorail and the drive wheel, a stress occurs in the rubber or polymeric rim. The average value across the contact patch is as follows:

$$\sigma_{av} = \sqrt{\frac{E_{red} E_{d_{max}}}{\pi(1 - \mu^2) r_{red} B}}, \quad (8)$$

where μ is the Poisson ratio of the rim material; B is the width of the wheel.

The change in stress pulses in time is well described by a parabola of the form:

$$\sigma(t) = A_1 t^2, \quad (9)$$

where A_1 is the coefficient, which is determined by the shape of the stress pulse.

Coefficient A_1 can be determined by taking into account the average value of stress (8) and the duration of cycle Θ of the wheel rim fragment contact with the monorail:

$$A_1 = \frac{3\sigma_{av}}{\Theta^3}.$$

Let us suppose that the monorail deflects along a circular arc. Then the radius of the arc when the carriage is in the middle of the span can be determined by the following dependence:

$$r_2 = \frac{L^2}{8z_{max}} + \frac{z_{max}}{2}.$$

In this case, at the places where the monorail hangs on the fastening sections (see Fig. 2), the sections of the monorail can be considered horizontal, $r_2 \rightarrow \infty$.

The results of calculations show that the number of cycles before failure when the carriage is at the places of monorail suspension ($r_2 \rightarrow \infty$) and in the middle of the span

$$\left(r_2 = \frac{L^2}{8z_{max}} + \frac{z_{max}}{2} \right)$$

differs by no more than 1 %. This conclusion was obtained on the basis of calculations performed according to equation (1), taking into account the durability of rubber and polymeric products under static loading mode L .

This allows us to conclude that the effect of monorail deflection can be disregarded when calculating the durability of drive wheel rims for mine monorail locomotives.

Taking into account equations (1), (7) and (9), we can determine rim durability T_r , h:

$$T_r = \frac{1,74 \cdot 10^{-3}}{\int_0^\Theta \frac{dt}{\tau_0 \ln \left(\frac{\Delta p_\infty}{\Delta p_\infty - \Delta p_{cr}} \right) \exp \left(\frac{U_0 - \gamma \sigma(t)}{k' T} \right)}}. \quad (10)$$

According to the results of simulating the working process of carriage interaction with the overhead monorail [3, 18, 19] the range of values of maximum dynamic forces arising from the contact of the monorail with the drive wheel was obtained: 20...47 kN per carriage. At the same time, there is a load of $F_{d_{max}} = 10 \cdot 10^3 \dots 2.35 \cdot 10^5$ N per carriage wheel, respectively. For this range of contact forces, the rim can take from $1.1 \cdot 10^7$ to $6.7 \cdot 10^6$ interactions.

Using equation (10), we obtained a graphical dependence of wheel rim durability on the load

(Fig. 3), a hyperbolic dependence for the following conditions: $F_{d_{max}} = 10...23$ kN; $T = 305.15$ K; $V = 3$ m/s; $r_1 = 0.08$ m; $B = 0.04$ m.

Analysis of the dependences obtained shows that when the carriage mass increases from 20 to 47 kN, the durability of polymeric rims of mine monorail locomotives decreases by 32 % (from 8700 to 5900 h).

The formation of stress pulses is determined by the complex nature of interaction between the wheel rim and the monorail, as well as by the train speed and the current distance from the monorail suspension point to the fastening sections to the carriage [3, 20, 21]. This makes it difficult to obtain an analytical dependence describing the value of stress pulses. At the same time, the pulse shape is described quite well by a paraboloid of the following form:

$$\sigma(x', y') = A_2(x')^2 + B_2(y')^2,$$

where A_1, B_1 are coefficients determined by the stress pulse shape. Coefficient $B_1 = l_c$, taking into account the ratio of the length and width of the contact patch for the rim with the monorail, $A_2 = 1/2 B_2$; x', y' are relative dimensions of the contact patch of the wheel rim with the monorail.

Based on the dependences calculated, the distribution of stresses over the contact patch of the wheel rim with the monorail was obtained. This has the shape of an elliptic paraboloid (Fig. 4). Graphic interpretation of stresses shows that the maximum stresses are concentrated at the top of the paraboloid.

Since the durability of the material is inversely proportional to stresses, the greatest wear will be on the rim surface along the line passing through the middle of its generators.

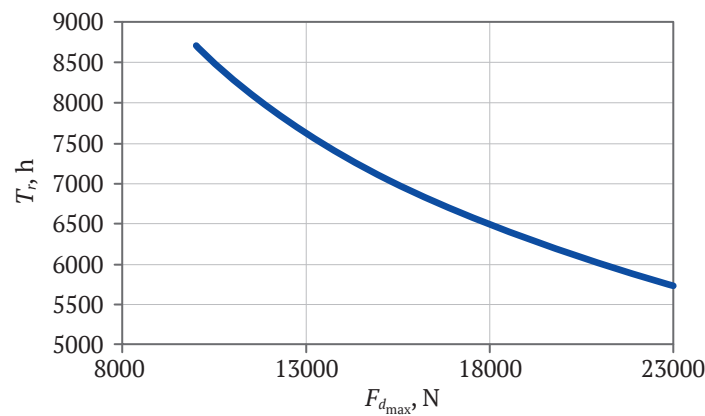


Fig. 3. Dependence of durability of monorail locomotive drive wheels on the force acting on one wheel

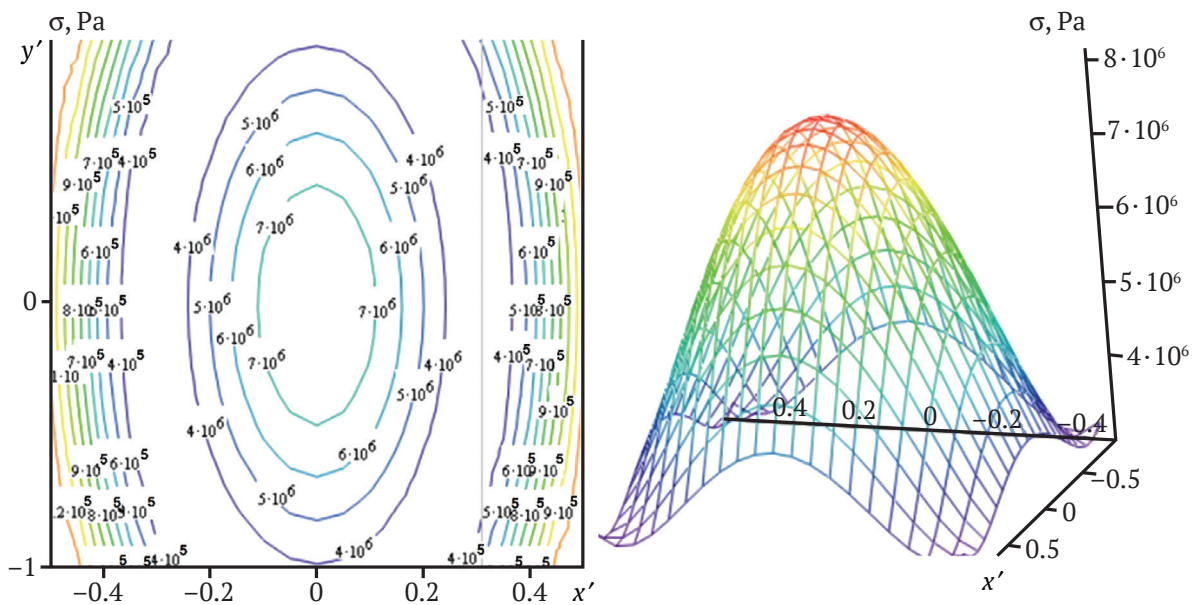


Fig. 4. Distribution of stresses along the contact patch of the wheel rim with the monorail: y', x' are relative dimensions of the contact patch

Practical use

Based on these dependencies, an algorithm was obtained to determine the parameters of drive wheels of monorail locomotives (wheel radius and rim material), in order to ensure the required durability T_{req} of their rims (Fig. 5).

The algorithm takes into account the parameters of the monorail track and the locomotive, enabling the maximum contact dynamic forces in the polymeric rim of drive wheels to be determined. Using the above methodology, it is possible to establish the parameters of the shape of the stress pulse change in time, as well as to calculate the durability of the

rim, taking into account the parameters of the mine atmosphere and its material.

The results obtained can be used both in the process of developing technical assignments and designing the drive wheels of mine monorail locomotives, as well as in studies aimed at improving the design of drives for the rolling stock of the overhead monorail track. Also, the algorithm and calculation methods described above can be useful for engineers and technicians of mining enterprises interested in durability and increasing performance indicators of mine monorail locomotives running gears.

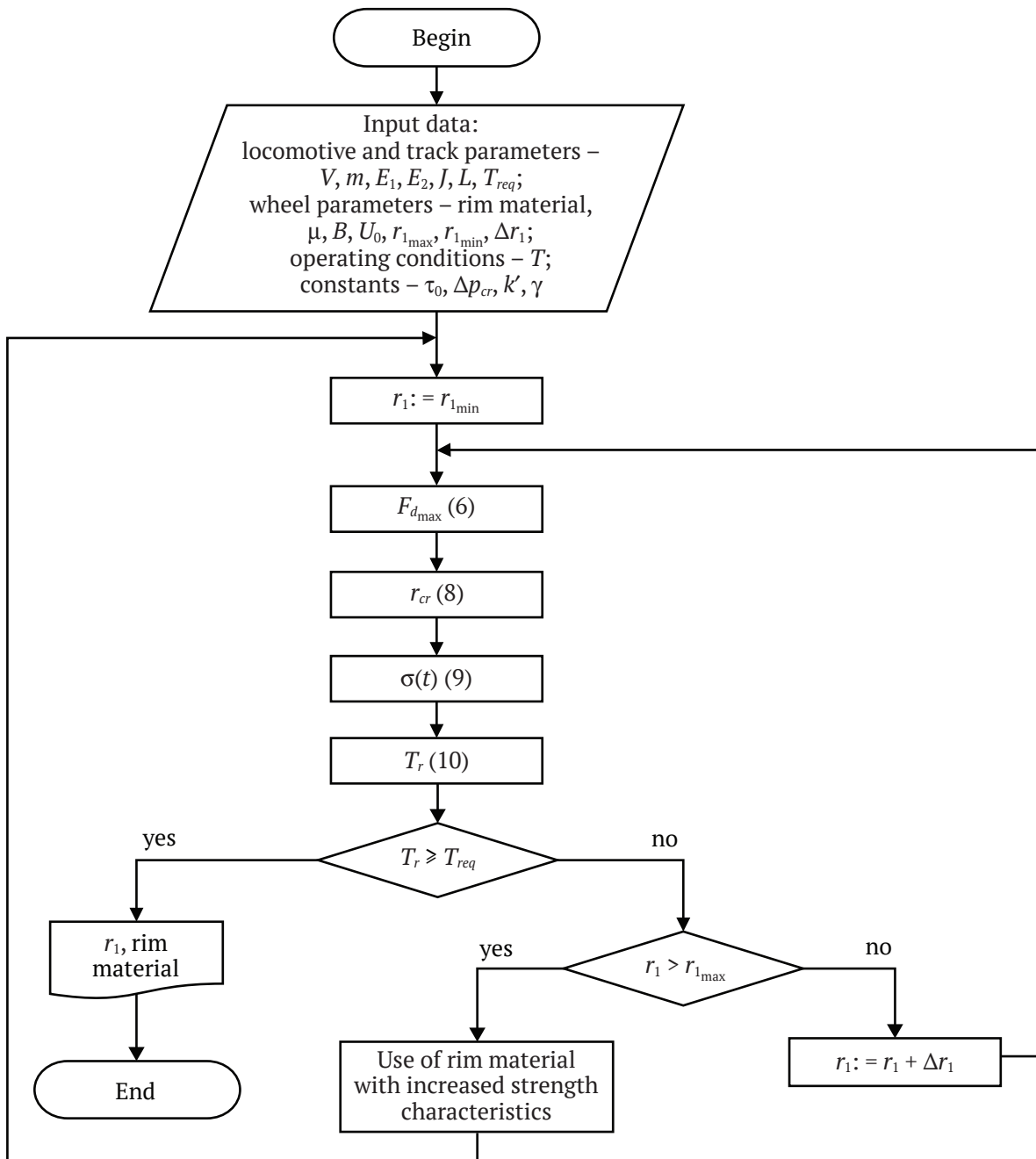


Fig. 5. Algorithm of determining the parameters of drive wheels of monorail locomotives to ensure required durability T_{req} of their rims



Conclusions and further research

A mathematical model was obtained to determine the durability of drive wheel polymeric rims, taking into account the maximum dynamic forces arising during the contact of drive wheels with the monorail. It was also established that the effect of the monorail track deformation has no significant impact on the durability of drive wheel rims of mine monorail locomotives.

An algorithm of determining the parameters of drive wheels of monorail locomotives to ensure the required durability T_{req} of their rims was determined.

The durability of wheel polymeric rims of mine monorail locomotives was calculated, taking into account the dynamic loads arising during the movement of the monorail train. Stress distribution over the contact area of the wheel rim with the monorail was obtained. This enables measures to increase the service life of drive wheels of mine monorail locomotives to be developed. An increase in the carriage mass from 20 to 47 kN leads to 32 % less durability of a monorail locomotive drive wheel rim (from 8700 to 5900 hours). Further research will be aimed at developing a comprehensive model to assess the durability of the drive wheel of mine monorail locomotives.

References

1. Kol'ga A.D., Agliullin A.S. Railway transport of mining enterprises: ways of efficiency improvement. *Gornoe Oborudovanie i Elektromekhanika*. 2016;(5):23–28. (In Russ.)
2. Aleksandrov S.N., Bereginский V.I., Budishevskiy V.A., Melnikov S.A. Creation of mine locomotives for delivery of cargoes by the ways with the inconsistent and overrated profile. *Mining Informational and Analytical Bulletin*. 2009;(16):215–229. (In Russ.)
3. Gutarevych V.O. Dynamic loading of monorail bogies and suspended railway. *Bulletin of Higher Educational Institutions. North Caucasus Region. Technical Sciences*. 2015;(4):85–88. (In Russ.) <https://doi.org/10.17213/0321-2653-2015-4-85-88>
4. Gutarevych V.O., Kondrakhin V.P. Reduction of dynamic loads from suspended monorail tracks on mine working support. *Vestnik Donetsk National Technical University*. 2016;(6):7–11. (In Russ.)
5. Melezhik R.S., Vlasenko D.A. Load simulation and substantiation of design values of a pin flexible coupling with a flexible disk-type element. *Mining Science and Technology (Russia)*. 2021;6(2):128–135. (In Russ.) <https://doi.org/10.17073/2500-0632-2021-2-128-135>
6. Ziborova E.Yu., Mnatsakanyan V.U. Justification of geometrical parameters of lining plates for a belt conveyor drive drum. *Mining Science and Technology (Russia)*. 2022;7(2):170–179. <https://doi.org/10.17073/2500-0632-2022-2-170-179>
7. Stoček R., Stěnička M., Zádřapa P. Future trends in predicting the complex fracture behaviour of rubber materials. *Continuum Mechanics and Thermodynamics*. 2021;33(2):291–305. <https://doi.org/10.1007/s00161-020-00887-z>
8. Szewerda K., Tokarczyk J., Wiczorek A. Impact of increased travel speed of a transportation set on the dynamic parameters of a mine suspended monorail. *Energies*. 2021;14(6):1528. <https://doi.org/10.3390/en14061528>
9. Herbus K., Szewerda K., Swider J. Virtual prototyping of the suspended monorail in the aspect of increasing the permissible travel speed in hard coal mines. *Eksploatacja i Niezawodność*. 2020;4:610–619. <https://doi.org/10.17531/ein.2020.4.4>
10. Kondrakhin V., Arefyev E., Khitsenko N. Assessment of impact made by vibration cleaning on the conveyor-belt service life. *Bulletin of Kharkov National Automobile and Highway University*. 2012;(57):292–295. (In Russ.)
11. Aleksandrov V.M., Chebakov M.I. *Introduction to the mechanics of contact interactions*. Rostov-on-Don: TsVVR LLC; 2007. 114 p. (In Russ.)
12. Ryabko K.A., Gutarevich V.O. Substantiation of performance indicators of mine monorail locomotives. *Mining Science and Technology (Russia)*. 2021;6(2):136–143. (In Russ.) <https://doi.org/10.17073/2500-0632-2021-2-136-143>
13. Vodolazskaya N.V., Shevchenko D.A. *The problem of increasing the durability of machine parts operating in aggressive environments. Mechanical engineering of Ukraine through the eyes of scientists: progressive ideas – science – production*. Sumy: SumGU; 2010. Pp. 25–27. (In Russ.)
14. Litvinova I.A., Veselov I.V., Gamlitskiy Y.A. Improvement of rubber recipe for massive tires by addition of non-traditional fillers. *Proceedings of the Voronezh State University of Engineering Technologies*. 2019;81(4):196–204. (In Russ.) <https://doi.org/10.20914/2310-1202-2019-4-196-204>
15. Kablov V.F., Gamlitskiy Yu.A., Tyshkevich V.N. *Mechanics of reinforced plastics and rubber-cord composites*. Volgograd: Volgograd State Technical University; 2014. 348 p. (In Russ.)



16. Kartsovnik V.I. Prediction of the creep of elastomers taking into account the forces of entropic elasticity of macromolecules (prediction of creep of elastomers). *Journal of Macromolecular Science, Part B*. 2018;57(6):447–464. <https://doi.org/10.1080/00222348.2018.1470836>

17. Luo R.K. Effective stress criterion for rubber multiaxial fatigue under both proportional and non-proportional loadings. *Engineering Failure Analysis*. 2021;121:105–172. <https://doi.org/10.1016/j.engfailanal.2020.105172>

18. Swider J., Szeferda K., Herbuś K., Jura J. Testing the impact of braking algorithm parameters on acceleration and braking distance for a suspended monorail with regard to acceptable travel speed in hard coal mines. *Energies*. 2021;14:7275. <https://doi.org/10.3390/en14217275>

19. Szeferda K., Krenicky T. Use of the MBS method in mining industry R&D projects. *Mining Machines*. 2022;40(2):110–120. <https://doi.org/10.32056/KOMAG2022.2.6>

20. Gutarevich V.O., Ryabko K.A., Ryabko E.V. Damping of lateral oscillations of the rolling stock of a mine suspended monorail road. In: *Collection of abstracts of reports of the VI international scientific and technical conference “Ways to improve technological processes and equipment of industrial production”*. Alchevsk: DSTU; 2021. Pp. 172–174. (In Russ.)

21. Szeferda K. Supporting development of suspended underground monorails using virtual prototyping techniques. In: *IOP Conference Series: Materials Science and Engineering. Innovative Mining Technologies (IMTech 2019 Scientific and Technical Conference)*. 25–27 March, 2019. Szczyrk, Poland. 2019;545:012018. <https://doi.org/10.1088/1757-899X/545/1/012018>

Information about the authors

Evgeny M. Arefiev – Cand. Sci. (Eng.), Associate Professor, Saint Petersburg State Institute of Technology, Saint Petersburg, Russian Federation; ORCID [0000-0001-5055-2370](https://orcid.org/0000-0001-5055-2370), Researcher ID [B-2261-2016](https://orcid.org/B-2261-2016); e-mail elcross@mail.ru

Konstantin Al. Ryabko – Cand. Sci. (Eng.), Associate Professor, Rostov State University of Railway Transport (Voronezh Branch), Voronezh, Russian Federation; ORCID [0000-0003-4391-506X](https://orcid.org/0000-0003-4391-506X), Scopus ID [57203884218](https://orcid.org/57203884218); e-mail railroader@yandex.ru

Received 20.11.2022

Revised 10.02.2023

Accepted 11.02.2023



MINING MACHINERY, TRANSPORT, AND MECHANICAL ENGINEERING

Research paper

<https://doi.org/10.17073/2500-0632-2022-09-12>

UDC 622.684

**Behaviour pattern of rock mass haulage energy intensity in deep pits**

A. G. Zhuravlev , I. A. Glebov , V. V. Chernykh

*Institute of Mining Engineering of the Ural Branch of the Russian Academy of Sciences,
Yekaterinburg, Russian Federation* chernyh@igduran.ru**Abstract**

A significant portion of mineral deposits developed by open-pit mining is opened to the full depth by road transport ramps without the use of combined transport. In most cases, this is dictated by the high rate of a pit deepening and multi-stage development. In this study, the energy intensity of rock mass (RoM) haulage from the working zone of a pit to the surface is considered at several hierarchical levels. Mineframe software was used to study 3D-models of open pits with different slope angles in order to test the method of analytical calculation of a pit volume that allowed ensuring accuracy under a wide range of mining conditions. The findings of the research are as follows: with an increase in the pit bottom diameter, the zone of stabilization of rock mass lifting (haulage) height shifts to greater target depths. An increase in the pit slope angles entails shifting the weighted average height to deeper elevations. By increasing the pit target depth, combined modes of transport become more economical in comparison with dump trucks due to an increase in the total volume of rock mass. Depending on the comparison purpose, it was proposed to use different types of energy intensity. For a broad estimation of the rationality of the pair “scheme of opening – mode of transport” for open pits, the ratio of potential energy intensities of rock mass haulage of a considered option of a pit opening and its basic option without transport berms was used. The ratio of potential energy intensities as a function of a pit depth was determined. The values of total energy intensity of rock mass haulage from a pit to the surface were also established.

Keywords

energy intensity, open pit haulage system, deep pit, opening scheme, transport berm, pit dump trucks, slope angle

Acknowledgments

The research was performed within the framework of the State Assignment of the Ministry of Education and Science of the Russian Federation No. 075-00412-22 PR

For citationZhuravlev A. G., Glebov I. A., Chernykh V. V. Behaviour pattern of rock mass haulage energy intensity in deep pits. *Mining Science and Technology (Russia)*. 2023;8(1):68–77. <https://doi.org/10.17073/2500-0632-2022-09-12>

ГОРНЫЕ МАШИНЫ, ТРАНСПОРТ И МАШИНОСТРОЕНИЕ

Научная статья

**Закономерности изменения энергоёмкости
транспортирования горной массы транспортом глубоких карьеров**

А. Г. Журавлев , И. А. Глебов , В. В. Черных

*Институт горного дела Уральского отделения Российской академии наук (ИГД УрО РАН),
г. Екатеринбург, Российская Федерация* chernyh@igduran.ru**Аннотация**

Значительная часть месторождений полезных ископаемых, разрабатываемых открытым способом, вскрывается автомобильными транспортными съездами на всю глубину без использования комбинированного транспорта. В большинстве случаев это связано с высокой скоростью снижения уровня горных работ и многоэтапной разработкой. Методы исследований энергоёмкости транспортирования горной массы из рабочей зоны карьера на поверхность рассматриваются в несколько иерархических уровней. Для исследования 3D-моделей карьеров с различными углами откоса использовано программное обеспечение Mineframe с целью забазировать методику аналитического расчета объема карьера, что позволило обеспечить точность при широком охвате диапазона горнотехнических условий. При увеличении диаметра дна карьера зона стабилизации высоты подъема смещается к большим конеч-

ным глубинам, увеличение угла откоса бортов карьера влечет за собой смещение средневзвешенной высоты в глубину, с ростом конечной глубины карьера комбинированные виды транспорта становятся более экономичными в сравнении с автомобильным за счет увеличения суммарного объема горной массы. В зависимости от цели сравнения предложено использовать различные виды энергоёмкости, для укрупненной оценки рациональности пары «схемы вскрытия – вид транспорта» для карьеров возможно использовать отношение потенциальных энергоёмкостей перемещения горной массы рассматриваемого варианта вскрытия карьера и его базовой версии без транспортных берм, установлены закономерности изменения отношения потенциальных энергоёмкостей от глубины карьера, определены значения полной энергоёмкости транспортирования горной массы из карьера до поверхности комбинированными видами транспорта.

Ключевые слова

энергоёмкость, транспортная система карьера, глубокий карьер, схема вскрытия, транспортная берма, карьерные автосамосвалы, угол откоса бортов

Благодарности

Исследования выполнены в рамках Государственного задания Минобрнауки РФ №075-00412-22 ПР

Для цитирования

Zhuravlev A. G., Glebov I. A., Chernykh V. V. Behaviour pattern of rock mass haulage energy intensity in deep pits. *Mining Science and Technology (Russia)*. 2023;8(1):68–77. <https://doi.org/10.17073/2500-0632-2022-09-12>

Introduction

A significant portion of mineral deposits developed by open-pit mining is opened to the full depth by road transport ramps without the use of combined transport. As a rule, this is dictated by the high rate of a pit deepening, multi-stage development (up to 5–6 stages with a cutback at full height at each stage) that does not allow more economical, but capital-intensive modes of transport to be implemented. At the same time, the effective development of these deposits with the fullest possible extraction of reserves is an urgent task [1, 2].

The volume of rock mass within the envelope of a pit depends significantly on its depth and size

in plan view, and, with an increase in its depth, the volume increases parabolically (Fig. 1). At the same time, the distribution of these volumes by bench is uneven. Deepening leads to a decrease in the volume of each underlying horizon, while the distance of haulage increases [3]. The final figures of haulage work while developing a deposit by a deep round pit is described by an ascending-and-descending curve. For instance, Fig. 1, b shows a graph built without taking into account annual smoothing production volumes. It can be seen that the peak value and intensity of the change in the tonne-km work significantly depend on the slope angles of the pit walls.

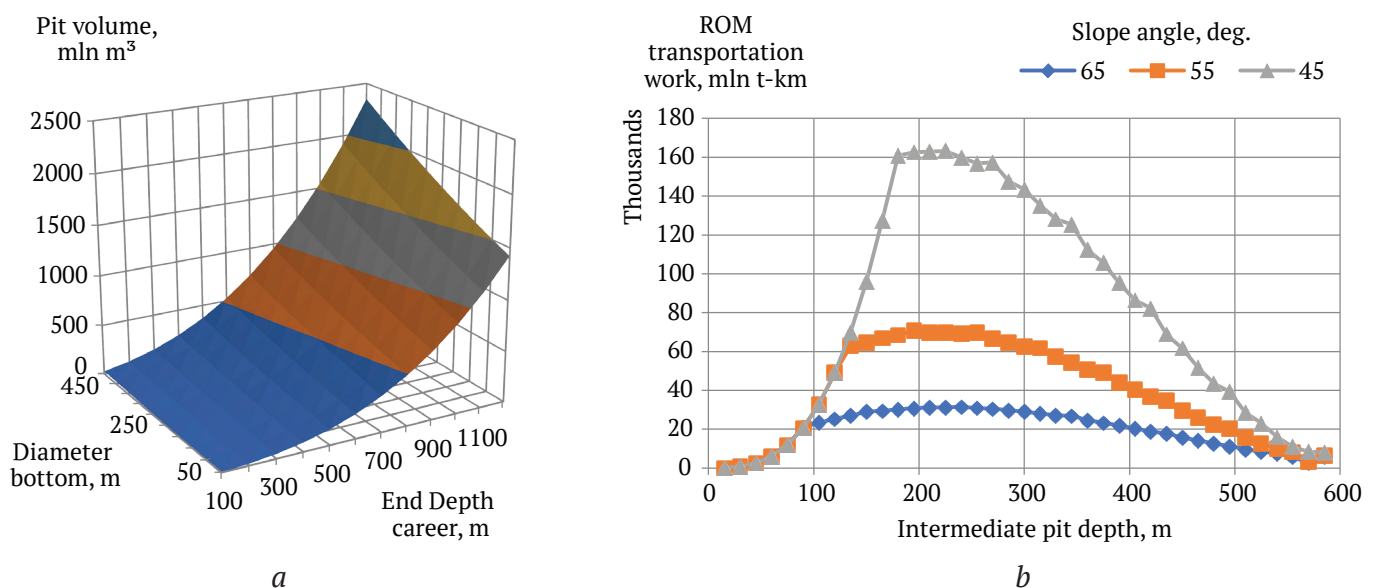


Fig. 1. Dependence of the volume of rock mass and haulage work within a round-shaped pit envelope on the size of the bottom, target depth, and slope angle of the walls:

- a – dependence of the volume of rock mass within a round-shaped pit envelope;
- b – the haulage work depending on a pit depth at the target depth of – 585 m



The way to manage the shape of a pit walls in a final pit envelope, in order to achieve significant slope angles is to optimize the parameters of transport (haulage) lines:

- use of narrow transport berms, including t single-lane roads with separation of the laden and unladen vehicle traffics;
- use of increased road gradients;
- use of appropriate modes of transport located on benches without transport berms (high incline conveyor, skip hoist, freight suspended ropeway, etc.), etc.

In order to compare different schemes of opening of mineral deposits in an open-pit with different modes of transport, certain criteria need to be defined. One such a criterion can be the energy intensity of hauling the entire volume of rock mass from a pit.

The approach which uses energy intensity as an indicator or criterion for evaluating open-pit mining processes or mining machines is used in a number of studies [4–7]. This indicates both the universality of this method and the relevance of the problem under consideration. The topic of energy efficiency has been pressing for the last 20 years. For example, the paper “Substantiating systems of open-pit mining equipment in the context of specific costs” [8] describes the energy efficiency of equipment in coal mines. The study “Energy consumption in open-pit mining operations relying on reduced energy consumption for haulage using in-pit crusher systems” [9] investigates energy efficiency in haulage with the use of in-pit crushing systems. “Smart energy management: a comparative study of energy consumption forecasting algorithms for an experimental open-pit mine” [10] is a paper which reviews the problem of smart energy efficiency management. In the study “Structure of energy consumption and improving open-pit dump truck efficiency” [11], increasing energy efficiency through reducing energy consumption is considered. The paper “An integrated model of an open-pit coal mine: improving energy efficiency decisions” [12] describes an integrated model of a coal mine. The paper “Bulk material transportation system in open pit mines with improved energy efficiency” [13] describes the increase in energy efficiency of bulk material transportation. A generalized approach to assessing transport systems on the whole and the energy efficiency of individual vehicles should be combined.

Research tasks and objectives

1) to structure the energy intensity of rock mass (RoM) haulage, applicable to compare the efficiency of transport modes and opening schemes, by hierarchical level;

2) to establish patterns of change in the relative energy intensity of rock mass haulage from a pit to the surface depending on the parameters of a pit;

3) to determine the energy intensity of rock mass haulage by different modes of transport when opening the working zone by truck transport.

Research techniques

In this study, the energy intensity of rock mass haulage from the working zone of a pit to the surface is considered in several hierarchical levels (Table 1).

Since the study is aimed at identifying general patterns, for simplicity the calculation of the volume of rock mass within a pit envelope is performed as for an inverted truncated cone, the generatrix slope of which corresponds to the average slope angle of the pit walls.

To a certain extent, when searching for a rational scheme of opening and an appropriate mode of transport, an open pit that has no transport berms can be considered as the ultimate optimized option. Only bench sloping (working berms) is implemented on its walls, and the wall slope angles are selected to maintain wall stability. We will conventionally call such pit a “basic” option. A number of 3D models of pits with slope angles of 35, 45, 55 and 65°, on the target envelopes (walls) of which transport berms were positioned, were studied. The simulation was carried out in Mineframe software package [14] for a number of open pit options, in order to test the method of analytical calculation of a pit volume [15], which allowed accuracy to be achieved under a wide range of mining conditions.

The working berm was assumed to be 15 m wide. The width of transport berms was taken as different in accordance with the rational type of dump trucks for a particular size of a pit (taking into account a pit dimensions in plan and depth) which determines the production capacity. The range of variation was as follows:

- for small pits, the width of berms of 24.5 m is designed for 60–90 ton-payload dump trucks;
- for large pits, the width of berms of 34 m is designed for 130–160 ton-payload dump trucks.

Fig. 2 shows the results. They demonstrate that the construction of spiral ramp berms leads to a decrease in the wall slope angles by 2–3° for small basic angles and by 5–7° for large basic angles. The data processing enabled the dependences of the slope angle on the pit depth and the overall pit slope angle (Table 2) to be determined. They were used in further calculations.

In order to cover a set of pits in terms of the stability of walls. the following basic overall slope angles were taken: 35°, 45°, 55°, 65°.

Table 1

Hierarchical levels of hauling energy intensity research

Level of energy intensity consideration	Expression for estimation	Significance
1 Energy intensity of haulage in units of potential energy (conservative forces only), taking into account the volume for pushback for the placement of haulage lines	$\frac{\Delta E_p}{\Delta E_{p0}}$	Effect of pushback for the placement of haulage lines, taking into account their parameters, on the total energy intensity (as a rule, produces the main effect on the total energy intensity)
2 Energy intensity of haulage in units of physical work of external (in relation to vehicles) conservative forces and external dissipative forces	$\frac{A_{(T1)}}{A_{(T2)}} = \frac{\Delta E_{p(T1)} + A_{d(T1)}}{\Delta E_{p(T2)} + A_{d(T2)}}$	When comparing modes of transport: along with the effect of the haulage lines parameters, the energy efficiency of a drive (propelling unit) of a particular mode/modification of transport is taken into account
3 Energy intensity of haulage taking into account the energy carrier indicators	$\frac{Q}{E_{po}} = \frac{(\Delta E_p + A_d)q}{\Delta E_{p0}}$	1. For a particular mode of transport: selection of the optimal shape of the walls of pushbacks and an ultimate pit, determination of rational parameters of openings (slope and width of transport berms, etc.)
	$\frac{Q_{(T1)}}{Q_{(T2)}} = \frac{(\Delta E_{p(T1)} + A_{d(T1)})q_{T1}}{(\Delta E_{p(T2)} + A_{d(T2)})q_{T2}}$	2. When comparing modes of transport: the selection of energy-efficient mode of transport, taking into account the energy carrier indicators (fuel calorific value, coefficient of efficiency of electricity generation and transmission, etc.) and the coefficient of efficiency of the power plant of vehicles

Notes: $\Delta E_p, \Delta E_{p0}$ are energy intensities of rock mass lifting (difference of the mass potential energies on the surface and in situ in a pit) for an open pit with haulage lines (ΔE_p) and the basic pit option (ΔE_{p0}), respectively; A_d is work against dissipative forces when hauling the rock mass; $T1, T2$ are modes/modifications of transport 1 and 2, respectively; Q is total energy inputs for rock mass haulage; q is specific energy intensity of generation and transmission of a unit of energy by a power plant to a vehicle's engine (for example, the lower calorific value of fuel, taking into account the coefficient of efficiency of the internal combustion engine and the transmission).

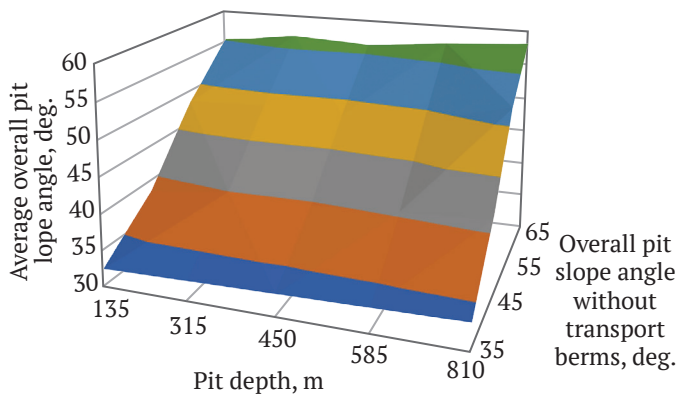


Fig. 2. Changing slope angle of a round-shaped pit when constructing transport berms for spiral ramps on the walls

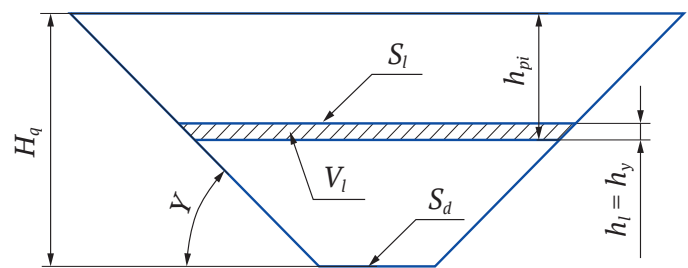


Fig. 3. Scheme for determining the volume of layers to be excavated within a pit envelope: S_l is layer area, m^2 ; S_d is bottom area, m^2 ; V_l is layer volume, m^3 ; h_l is layer height, m ; h_y is bench height, m ; h_{pi} height from the top elevation of a pit (daylight surface) to the bottom elevation of a layer, m ; Y is overall pit slope angle, deg ; H_q is pit wall height

Table 2

Dependencies of slope angle on pit depth (H_k)

Параметры	Overall pit slope angle			
	35°	45°	55°	65°
Dependence of pit slope angle on pit depth y	$0.0018H_k + 32.168$	$0.0035H_k + 38.325$	$0.0052H_k + 46.898$	$0.004H_k + 54.771$
Confidence R^2	0.9967	0.884	0.7647	0.8848

Let us define the theoretical energy intensity as the energy spent for lifting the whole volume of a rock mass within a pit envelope to the surface, described by the change in the potential energy of each elementary volume between the positions “on the surface” and “in situ”. In this case, the calculation shall be performed layer-by-layer, since the material moving in the horizontal plane does not lead to a change in energy intensity taking into account the accepted assumptions (Fig. 3).

Correspondingly, the energy intensity of rock mass haulage from a pit envelope:

$$\Delta E_p = \sum V_{li} \rho h_{pi} g = \int_0^{H_k} g \rho h_{pi} S_l dh_{pi}, \quad (1)$$

where V_{li} is volume of the i -th layer (horizon) within a pit envelope, m^3 ; h_{pi} is height from the bottom of the i -th layer to the surface of the pit (height of rock mass lifting), m ; g is free fall acceleration (9.81), m/s^2 ; ρ is density of rock mass in a pillar, τ/m^3 .

When passing to an integral, a layer height decreases to an infinitesimal value, so the areas of the bottom and the top of the truncated cone, which represents each layer, can be considered to be equal. The corresponding area, m^2 , is defined as follows:

$$S_l = S_d + 2\sqrt{\pi s_d} H_k ctg \gamma - 2\sqrt{\pi s_d} h_{pi} ctg \gamma + \pi H_k^2 ctg^2 \gamma - 2\pi H_k h_{pi} ctg^2 \gamma + \pi h_{pi}^2 ctg^2 \gamma, \quad (2)$$

where S_d is the area of the bottom of a pit, m^2 ; γ is the average overall pit slope angle, deg ; H_k is target depth of a pit, m .

Correspondingly, the formula for determining E_p can be expressed as:

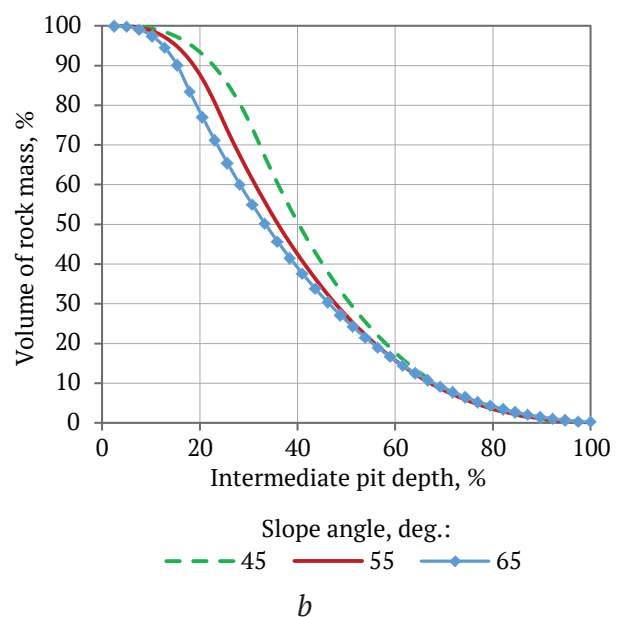
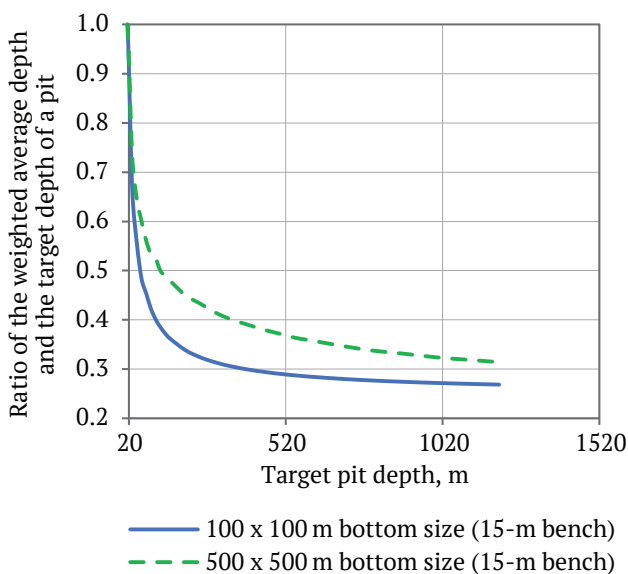
$$\Delta E_p = \int_0^{H_k} \rho g (S_d + 2\sqrt{\pi s_d} H_k ctg \gamma - 2\sqrt{\pi s_d} h_{pi} ctg \gamma + \pi H_k^2 ctg^2 \gamma - 2\pi H_k h_{pi} ctg^2 \gamma + \pi h_{pi}^2 ctg^2 \gamma) dh_{pi}. \quad (3)$$

After all transformations and integration, the formula takes the following form:

$$\Delta E_p = \rho g \left(\frac{\pi ctg^2 \gamma}{12} H_k^4 + \frac{\sqrt{\pi s_d} ctg \gamma}{3} H_k^3 + \frac{S_d}{2} H_k^2 \right). \quad (4)$$

Research Findings

As already mentioned above, the energy intensity of rock mass haulage is determined by two main factors: the distribution of volumes within a pit envelope; and the increase in energy consumption for haulage with extraction deepening. Therefore, in order to explain the patterns of changes in the energy intensity when changing the parameters of open pits, it is important to identify their influence on the location of the “center of mass” of the total volume of rock mass within a pit envelope. It can be seen in Fig. 4, a that, at a bottom diameter of 100 m, with increasing the target depth of a pit above 500–600 m, the average weighted height of rock mass lifting stabilizes at 26–28 % of the target depth, and, at the depth less than 200 m, the height increases sharply, becoming practically equal to the full depth of a pit. As the pit bottom diameter increases, the lifting



a

b

Fig. 4. Pattern of changes in the position of the “center of mass” of the rock mass volume within a pit envelope depending on its parameters:

a – ratio of the average weighted (by the volume of excavated rock mass) depth of a pit to the target depth of a pit; b – reciprocal cumulative graph of the volume of rock mass in a pit envelope as a function of a pit depth

height stabilization zone shifts to greater target depth values. Increasing the pit slope angle entails a shift of the average weighted height towards greater depths (Fig. 4, b).

Calculations showed that the energy intensity of rock mass haulage, based on the difference in the potential energy (see Table 1, p. 1), characterizes the mining and geological conditions and the scheme of opening as a whole. Fig. 5 shows that its increase with the depth of a pit is generally similar to the increase in the volume of pit space. However, as the analysis showed, this is more intense due to increasing energy consumption with depth. Increasing the slope angles naturally leads to decreasing the rock volumes and, consequently, the total energy costs, while increasing the diameter of the bottom leads to the costs increase.

A convenient way to compare alternative opening schemes is to calculate relative energy intensity, as equal to the ratio of the energy intensity of hauling the whole volume of the rock mass within a pit with the considered opening scheme ΔE_p to the energy intensity for a pit without opening berms and ramps ΔE_{p0} . It makes it possible to estimate the contribution of opening berms and ramps to the increase in the volumes and their distribution by depth. Let us consider the results of the calculations in more detail.

Fig. 6 shows that the curves of the dependences of the relative energy intensity on the target depth of a pit have maximums, corresponding to the greatest negative impact of the placement of transport berms

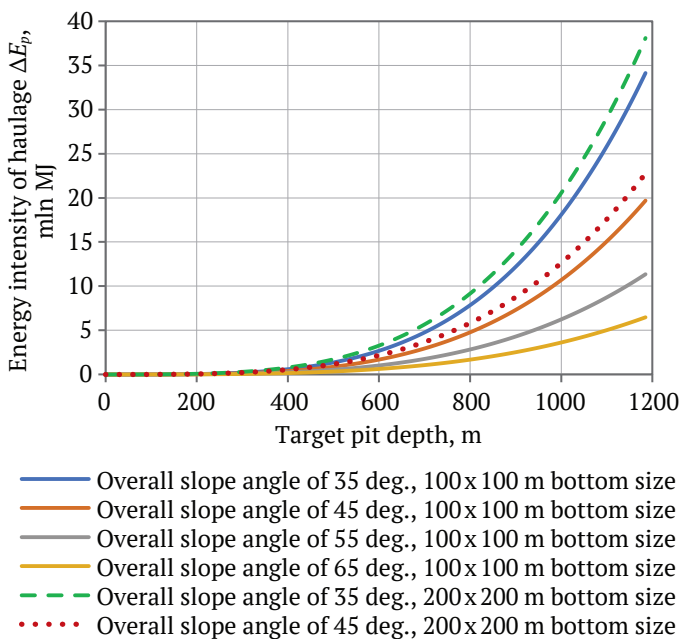


Fig. 5. Theoretical energy intensity of the haulage of the rock mass within a pit envelope |to the surface ΔE_p

on a pit wall cutback. This pattern is “natural”, arising from geometry, so these groups of pits should be subject to mandatory optimization. The decrease in relative energy intensity with further increase in depth can be explained by a decrease in the proportion of wall cutback in the geometric volume of the pit space and a smaller decrease in the slope angles of a pit due to the distribution of transport berms over the increasing perimeter of the outline of a pit. For the same reasons, the specific energy intensity decreases as the size of a pit bottom increases.

Fig. 7 shows that with growth of the basic pit slope angle (without transport berms), which were taken in the study as the limiting stable slope angle, the relative energy intensity increases at all depths. However, the character of this growth changes (see Fig. 7, b): at low depths the intensity of growth decreases; at depths of 400–500 m the graph is almost straight, and then it curves, approaching the parabolic form.

Pit bottom diameter has a significant impact on the relative energy intensity. With a large bottom diameter, the relative energy intensity is generally lower than in the case of a small diameter (Fig. 8). Moreover, if at small bottom sizes, the maximum energy intensity is observed at a depth of the pit of 100–500 m, then at an extensive bottom the intensity shifts to depths of 500–900 m. Consequently, the greatest negative impact from the wall cutback of a pit for the placement of haulage lines on them is observed for pits with relatively small size of the bottom, 50–100 m in diameter at a depth of 100–500 m.

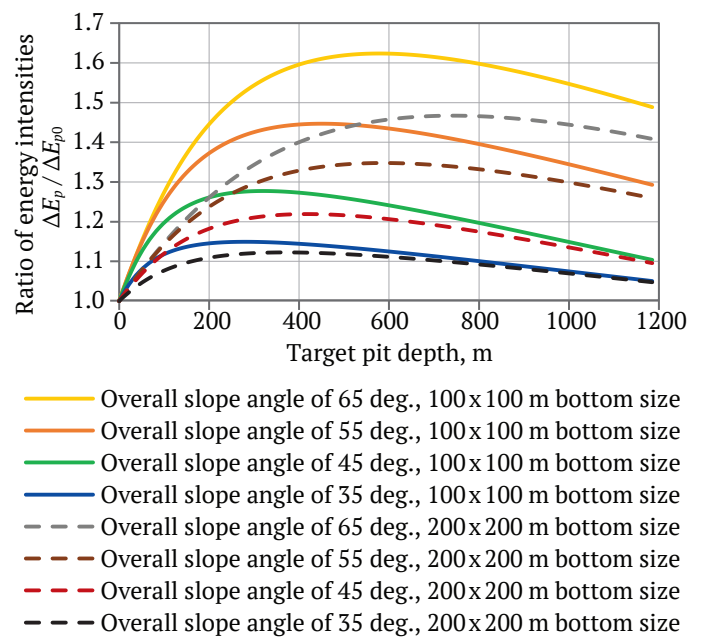


Fig. 6. Changing the relative theoretical energy intensity of rock mass haulage from a pit with depth at different parameters of a pit

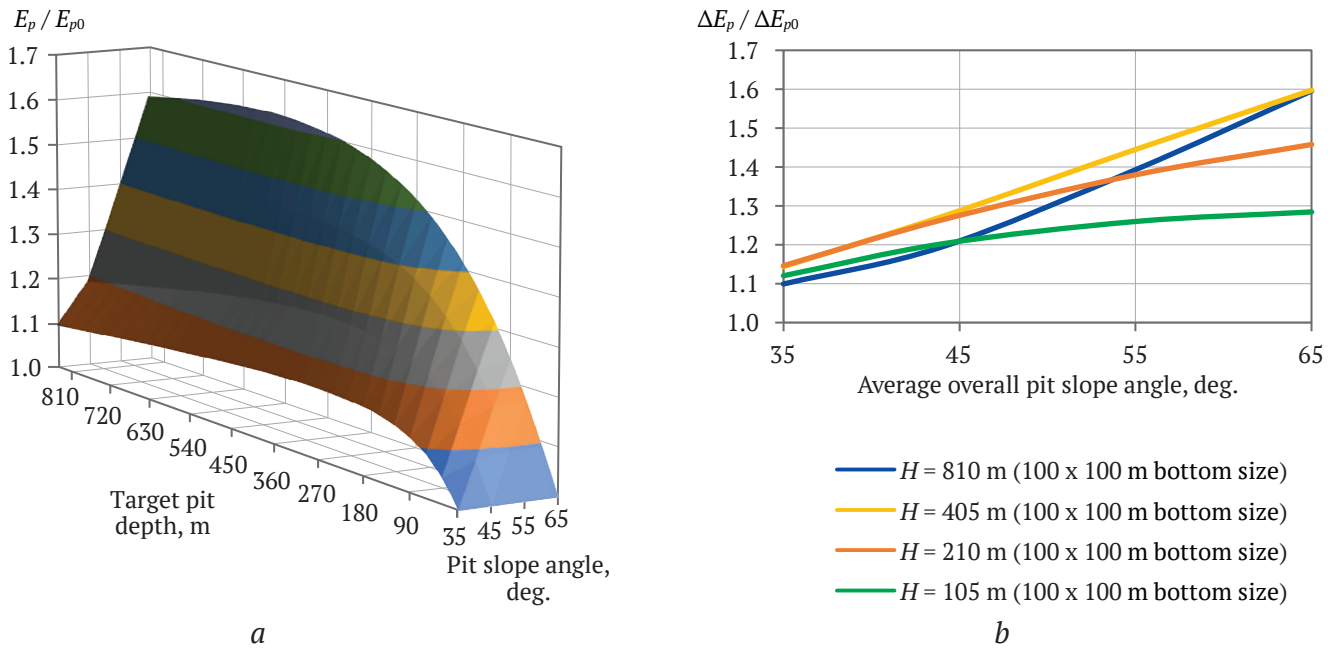


Fig. 7. The ratio of energy intensities $\Delta E_p / \Delta E_{p0}$ depending on the overall slope angle of a basic pit (not taking into account transport berms):
a – summary three-dimensional graph; *b* – graphs for specific depths

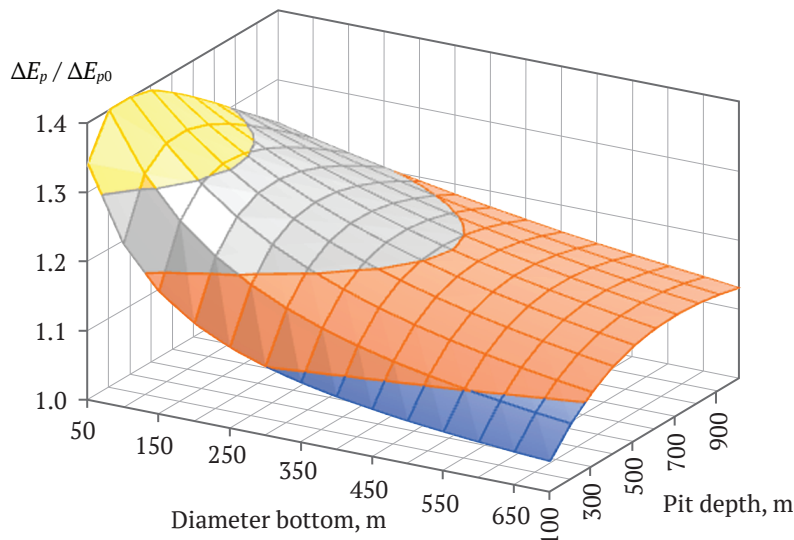


Fig. 8. The ratio of energy intensities $\Delta E_p / \Delta E_{p0}$ depending on the pit depth and diameter of its bottom for the option of the basic pit with an average slope angle of 45°

The patterns described above refer to the theoretical energy intensity. In practice, it is markedly influenced by the mode of transport used, characterized by specific energy consumption. In order to bring different modes of transport with different energy carriers (diesel fuel, electricity) to a comparable type of energy intensity, the following must be used (Table 3):

- the calculated work of conservative and dissipative forces on a vehicle engine;

- the energy of the primary fuel by its calorific value, at the place of its generation (diesel engine of autonomous vehicles or a power plant).

With regards to the second option, the study [6] suggests and describes the method of reducing the energy intensity of a transport mode to the amount of consumed fuel equivalent in g of f.e./(t·m), suitable for practical calculations in natural terms. However, given that it is more convenient to operate with energy units within the framework of this study, in-

cluding for the transition to dimensionless relative units, Table 3 shows the results of the calculations based on: traction calculation, transmission efficiency calculation, averaged reference efficiency of engines, lower calorific value of fuel, and calculation of the losses in power lines. For electrified modes of transport (rail and conveyor), a scheme with electricity generation at a gas turbine mini thermal power plant located in the immediate vicinity of a pit was adopted.

Note that these indicators are averaged and depend on specific mining conditions (weighted aver-

age slope of the route, haulage distance, configuration of haulage lines, etc.).

The capabilities of the approach under consideration were tested by comparing the combined modes of transport: truck+rail and truck+conveyor. The slope angle of a pit with haulage lines on the walls was taken into account, as well as the specific energy intensity of hauling depending on the height of the rock mass lifting (the pit depth). For the sake of convenience, the results of the calculations are given in the form of the ratio of energy intensities (Fig. 9): the smaller this ratio, the more economical

Table 3

Specific energy intensity of generation and transmission of a unit of energy by a power plant to a vehicle's engine

Mode of transport	Specific energy intensity by mode of transport ¹	
	MJ/MJ (work of forces on the wheels of a vehicle)	MJ/MJ (taking into account the heat of combustion, the efficiency of PP and the transmission from the power line to a vehicle)
Ratio to the energy intensity indicator according to Table 1.	$A / \Delta E_p$	$Q / \Delta E_p$
Dump trucks	3.28	9.89
ЖRail / Trucks + Rail ²	2.01 / 2.52–2.64	6.89 / 8.09–8.39
Conveyor / Trucks + Conveyor ²	1.88 / 2.44–2.16 ³	5.98 / 7.37–6.53 ³

¹ In the numerator, the initial consumption of the energy carrier is converted into fuel equivalent.

² In the range of pit depths of 200-1000m, the height of the working zone of dump trucks is accepted: in case of rail transport, 80–400 m, in case of conveyor transport, 80–150 m.

³ Taking into account coarse crushing; PP – power plant.

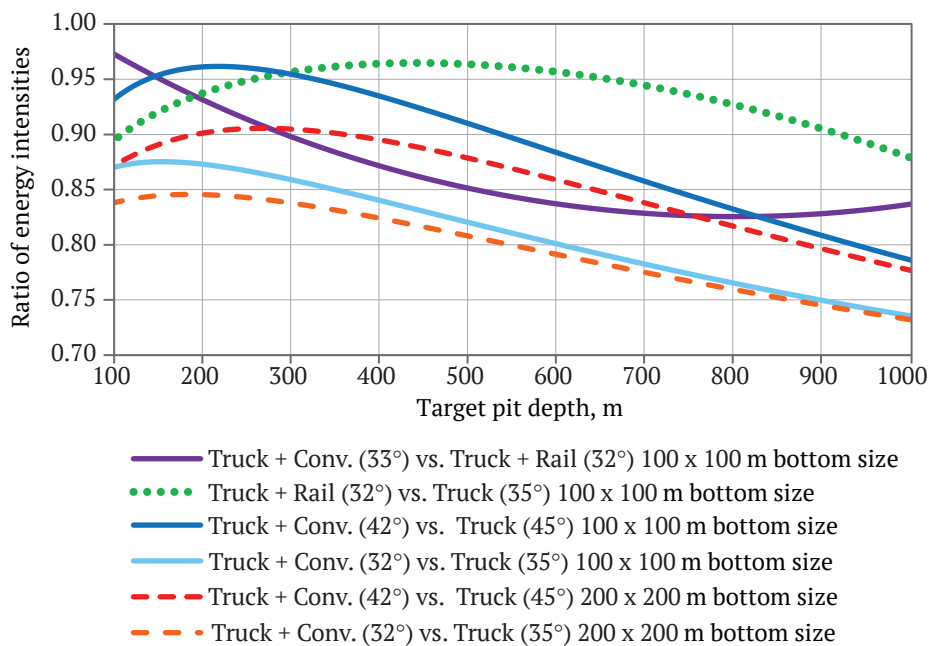


Fig. 9. The ratio of total energy intensities (Q) of hauling rock mass to the surface from a pit, taking into account the heat of combustion of an initial fuel by mode of transport: Truck + Rail – Dump Trucks + Railway transport; Truck + Conv. – Dump Trucks + Conveyor transport. In parentheses, the average pit slope angle is given



the transport mode indicated in the numerator of the fraction. At the given parameters, the truck-conveyor transport mode has less energy intensity in the entire depth range as compared to the truck-rail and truck transport modes. This is achieved due to optimizing the shape of the walls and increasing their slope angle as compared to rail transport, as well as lower specific energy consumption, especially as compared to truck transport. This difference can be increased by optimizing the layout of conveyor lines on the walls of a pit [16, 17]. As a pit target depth and a pit bottom diameter increase, the combined modes of transport become more economical in comparison with dump trucks due to increasing the total volume of rock mass to be hauled.

Conclusions

1. The proposed approach is based on a universal integral indicator, which allows the energy efficiency (in units of natural values) of the options of opening schemes and modes of pit transport to be compared. This approach takes into account the decrease in the volume of extracted rock mass with depth and the increase in energy consumption for its lifting (hauling) to the surface.

Depending on the purpose of the comparison, it is proposed to use relative theoretical energy intensity, the work of conservative and dissipative forces on the drive of a vehicle, or total energy intensity taking into account the efficiency of fuel energy conversion and transmission.

2. The ratio of potential energy intensities $\Delta E_p / \Delta E_{p0}$ of rock mass haulage for a considered option

of a pit opening and its basic option without transport berms can be used for the broad estimation of the rationality of the pair “scheme of opening – mode of transport” for open pits. The closer this indicator is to “1”, the more optimal the adopted design of the walls of a pit.

3. The patterns of changes in the ratio of potential energy intensities $\Delta E_p / \Delta E_{p0}$ depending on pit depth, slope angles, and the bottom diameter were established, indicating that the greatest negative impact from the wall cutback for the placement of haulage lines on them is observed in pits with relatively small size of the bottom, 0–50 m in diameter at a depth of 100–500 m.

4. The total energy intensity of rock mass haulage for deep open pits and open pits with significant size of the bottom (200 m in diameter and more) is most influenced by the energy efficiency of transport mode, while for pits less than 500 m deep with a lower bottom size m (up to 100–150 m in diameter), mainly by optimization of the shape of a pit towards its reduction (while maintaining a given volume of extracted rock mass).

5. The values of the total energy intensity of hauling rock mass from a pit to the surface by combined modes of transport were determined. It was shown that due to the higher energy efficiency of rail and conveyor transport in combination with truck transport, they were more economical when compared to truck transport alone, while truck-conveyor transport combination was more economical than truck-rail transport combination due to the shortest haulage distance.

References

1. Yakovlev V.L., Kornilkov S.V., Sokolov I.V. *Innovative basis of the strategy for integrated development of mineral resources*. Yekaterinburg: UrO RAS Publ.; 2018. 360 p. (In Russ.) URL: <https://igduran.ru/files/eshop/elibrary/2019-inno-bazis.pdf>
2. Zyryanov I.V., Akishev A.N., Bondarenko I.F. *Improvement of mining and processing of diamond-bearing ores*. Yakutsk: SVFU Publ. House; 2020. 720 p. (In Russ.)
3. Zhuravlev A., Budnev A. Influence of the dump truck type and size on the diversity of the quarry sides. *Problems of Subsoil Use*. 2018;(2):20–29. (In Russ.) <https://doi.org/10.25635/2313-1586.2018.02.020>
4. Anistratov Yu.I. Energy theory for calculating the technology of open-pit mining. *Mining Informational and Analytical Bulletin*. 1996;(3):20–29 (In Russ.)
5. Kovalenko V.A., Tangaev I.A. Energy principle of control and optimization of work processes in open pits. *Mining Informational and Analytical Bulletin*. 2008;(2–1):293–301. (In Russ.)
6. Lel Yu.I., Voroshilov G.A., Stenin Yu.V., Nikolaev N. A. Methodology of energy assessment of pit transport systems under market conditions. *Proceedings of the Ural State Mining University*. 2005;(21):129–137. (In Russ.)
7. Kurlenya M.V., Tanaino A.S. Energy analysis of open-pit coal mining. *Journal of Mining Science*. 1997;33(5):453–462. <https://doi.org/10.1007/BF02765621>
8. Symonenko V.I., Haddad J.S., Cherniaiev O.V. et al. Substantiating systems of open-pit mining equipment in the context of specific cost. *Journal of The Institution of Engineers (India): Series D*. 2019;100(2):301–305. <https://doi.org/10.1007/s40033-019-00185-2>



9. Purhamadani E., Bagherpour R., Tudeshki H. Energy consumption in open-pit mining operations relying on reduced energy consumption for haulage using in-pit crusher systems. *Journal of Cleaner Production*. 2021;291:125228. <https://doi.org/10.1016/j.jclepro.2020.125228>
10. El Maghraoui A., Ledmaoui Y., Laayati O. et al. Smart energy management: a comparative study of energy consumption forecasting algorithms for an experimental open-pit mine. *Energies*. 2022;15(13):4569. <https://doi.org/10.3390/en15134569>
11. Koptev V.Y., Kopteva A.V. Structure of energy consumption and improving open-pit dump truck efficiency. In: *IOP Conference Series: Earth and Environmental Science*. 2017;87(2):022010. <https://doi.org/10.1088/1755-1315/87/2/022010>
12. Patterson S.R., Kozan E., Hyland P. An integrated model of an open-pit coal mine: improving energy efficiency decisions. *International Journal of Production Research*. 2016;54(14):4213–4227. <https://doi.org/10.1080/00207543.2015.1117150>
13. Ristić L., Bebić M., Štatkic S. et al. Bulk material transportation system in open pit mines with improved energy efficiency. In: *Proceedings of the 15th WSEAS International Conference on Systems*. Corfu Island, Greece. 14–16 July 2011. Pp. 327–332.
14. Lukichev S.V., Nagovitsyn O.V. Digital simulation in solving problems of surface and underground mining technologies. *Gornyi Zhurnal*. 2019;(6):51–55. (In Russ.) <https://doi.org/10.17580/gzh.2019.06.06>
15. Budnev A.B., Zhuravlev A.G. The estimate of errors of some analytical methods of pit volume calculation. *Problems of Subsoil Use*. 2017;(4):61–70. (In Russ.) <https://doi.org/10.18454/2313-1586.2017.04.061>
16. Bersenev V.A., Karmayev G.D., Semenkin A.V., Sumina I.G. Schemes of cyclic-flow technology by various bedding of mineral deposits (reviewing of existing and proposed schemes of CFT). *Problems of Subsoil Use*. 2018;(4):13–21. (In Russ.) <https://doi.org/10.25635/2313-1586.2018.04.013>
17. Zhuravlev A.G., Semenkin A.V., Cherepanov V.A. et al. The purpose of developing advanced in-pit crushing and conveying technology for deep open pits. *Russian Mining Industry*. 2022;(1S):53–62. (In Russ.) <https://doi.org/10.30686/1609-9192-2022-1S-53-62>

Information about the authors

Artem G. Zhuravlev – Cand. Sci. (Eng.), Head of the Laboratory of Quarry Transport Systems and Geotechnics, Mining Institute of the Ural Branch of the Russian Academy of Sciences, Yekaterinburg, Russian Federation; ORCID [0000-0001-7643-3994](https://orcid.org/0000-0001-7643-3994), Scopus ID [57211343137](https://orcid.org/57211343137); e-mail juravlev@igduran.ru

Igor A. Glebov – Junior Researcher, Mining Institute of the Ural Branch of the Russian Academy of Sciences, Yekaterinburg, Russian Federation; ORCID [0000-0003-4436-3594](https://orcid.org/0000-0003-4436-3594), Scopus ID [57216874834](https://orcid.org/57216874834); e-mail i.glebov@igduran.ru

Vladimir V. Chernykh – Junior Researcher, Mining Institute of the Ural Branch of the Russian Academy of Sciences, Yekaterinburg, Russian Federation; Scopus ID [57760083700](https://orcid.org/57760083700); e-mail chernykh@igduran.ru

Received 27.09.2022
Revised 19.01.2023
Accepted 20.01.2022



POWER ENGINEERING, AUTOMATION, AND ENERGY PERFORMANCE


Research paper

<https://doi.org/10.17073/2500-0632-2023-01-72>

UDC 622:621.311

**Equivalent circuit for mine power distribution systems for the analysis of insulation leakage current**A. V. Pichuev  , V. L. Petrov  

University of Science and Technology MISIS, Moscow, Russian Federation

 allexstone@mail.ru**Abstract**

Successful mining businesses rely heavily on the safety and reliability of their mine power distribution systems. Mine power distribution systems are designed to withstand an aggressive environment with a range of hazards. The harsh operating conditions require improvement to personnel protection systems through the study and simulation of the electric network's normal and emergency operations. The purpose of this study is to assess insulation leakage current using an equivalent circuit of a mine power distribution system. The simulation identified the key properties of the equivalent circuit which can model potential hazardous situations. We also selected the quantitative metrics and the equivalent circuit property ranges. In order to simulate the transients, we recommended using the time constants for the oscillation damping in circuits, the insulation phase resistance properties, and the absorption currents. This paper presents the equations to estimate these values. As an example, we considered the equivalent circuit of a mine power distribution system with an R-L filter in the residual current device line. The equivalent circuit helps analyze the current leakage when a person touches a live phase conductor accounting for low-frequency polarization in the phase insulation. The proposed approach to the simulation and analysis of the insulation current makes it possible to generate an equivalent circuit of the mine power distribution system to analyze phase voltage asymmetry, trip currents of residual current devices, low-frequency polarization of the insulation, and the leakage current effects on the human body.

Keywords

mine power distribution system, leakage current, residual current device, insulation properties, EMF sources, electrical safety

For citationPichuev A. V., Petrov V. L. Equivalent circuit for mine power distribution systems for the analysis of insulation leakage current. *Mining Science and Technology (Russia)*. 2023;8(1):78–86. <https://doi.org/10.17073/2500-0632-2023-01-72>**ЭНЕРГЕТИКА, АВТОМАТИЗАЦИЯ И ЭНЕРГОЭФФЕКТИВНОСТЬ**

Научная статья

Обоснование схемы замещения шахтной подземной электрической сети для анализа режимов утечки тока через изоляциюА. В. Пичуев  , В. Л. Петров  

Университет науки и технологий МИСИС, г. Москва, Российская Федерация

 allexstone@mail.ru**Аннотация**

Характеристики безопасности и надежности шахтных электротехнических комплексов и систем во многом обеспечивают успешность горных предприятий. Сложные технологические условия, особенно при ведении подземных горных работ, многообразии индивидуальных факторов определяют совокупность требований, которые предъявляются к подземным электрическим сетям горных предприятий. Все это определяет необходимость совершенствования систем защиты персонала на основе исследования характеристик сетей, моделирования режимов работы, в том числе аварийных. Основная цель исследований – обоснование схемы замещения шахтной подземной электрической сети путем синтеза ее структуры для последующего анализа режимов утечки тока через изоляцию. На основе методов математического моделирования дано обоснование параметров схемы замеще-



ния шахтной подземной электрической сети с учетом условий возникновения и развития аварийных и травмоопасных ситуаций. Определены количественные показатели и диапазоны изменения параметров элементов схемы замещения электрической сети. Для математического моделирования переходных процессов рекомендовано использование электромагнитных постоянных времени затухания колебаний в контурах, образованных параметрами фазных сопротивлений изоляции, а также абсорбционных составляющих токов утечки, и приведены соответствующие расчетные соотношения. В качестве примера приведена схема замещения шахтной подземной электрической сети с активно-индуктивным фильтром присоединения устройства защитного отключения, позволяющая выполнить анализ утечки тока при однополюсном прикосновении человека к токоведущей фазе, с учетом процесса низкочастотной поляризации в фазной изоляции. Предложенный методический подход к моделированию и анализу режимов утечки тока через изоляцию позволяет осуществить синтез схемы замещения подземной электрической сети для анализа несимметрии фазных напряжений, токов срабатывания устройств защитного отключения, процессов низкочастотной поляризации в изоляции, воздействия тока утечки на человека.

Ключевые слова

шахтная подземная электрическая сеть, режимы утечки тока, защитное отключение, параметры изоляции, источники ЭДС, электробезопасность

Для цитирования

Pichuev A. V., Petrov V. L. Equivalent circuit for mine power distribution systems for the analysis of insulation leakage current. *Mining Science and Technology (Russia)*. 2023;8(1):78–86. <https://doi.org/10.17073/2500-0632-2023-01-72>

Terms and Definitions

Leakage Current: the current that flows from exposed live parts or protective conductors to the ground in normal operation.

Leakage current type: the current that depends on the earth-to-phase voltages for different active resistance and insulation capacitance values.

Absorption current: the amount of current that flows and is absorbed by the dielectric insulation, which is caused by polarization and redistribution of free charges.

Ion conductivity: the movement of charged particles (ions) under voltage applied to the insulation with the charge neutralization on the conductor's insulation layer.

Introduction

Successful mining businesses rely heavily on the safety and reliability of their mine power distribution systems. Mine power distribution systems [1, 3, 4] are designed to withstand aggressive environments [1, 2] with a range of hazards [1, 5, 6]. The harsh operating conditions require improvement to personnel protection systems through the study and simulation of the electric network's normal and emergency operations.

As mine conductors age, their insulation resistance reduces. The insulation resistance of each phase may change either steadily (symmetric leakage current) or abruptly (single-phase and two-phase leakage current) [1–3, 5]. Asymmetric leaks lead to significant phase voltage surges (the undamaged phase voltage raises to the linear voltage). Such

surges may damage the electrical equipment and are an electric hazard, if the exposed phase wire are touched.

The simulation of leakage currents provides a sufficiently accurate definition of the most complicated electric processes (e.g., transients).

Our study included the following stages: selecting the simulation model structure and inputs; definition of the simulation target; definition of the numerical experiment procedure; and the processing of the results.

The core of the simulation model is a system of equations deducted from the equivalent circuit. These equations estimate the effects of voltage and insulation properties on the leakage current.

The literature review identified several approaches to the leakage current studies applicable to specific operating conditions of the electric equipment.

Many researchers use equivalent circuits, in order to simulate the insulation behavior [2, 6, 7]. The key cable insulation properties are *distributed resistance* determined by the quality of the insulating material along the entire conductor length, and *lumped resistance* affected by mechanical damage, aging, moisture ingress, etc. The *ground capacitance* is mainly determined by the length and cross-section of the cables. Note that the insulation resistance and capacitance vary as the mine power distribution system components are powered up or down according to the startup/shutdown procedure. For example, the backbone cable is energized first, and then the branch cables connecting the switchboard to the consumers are powered.

The simulation of leakage currents is challenging because, for more complicated equivalent circuits, it is extremely difficult to model the transients. Conventional simulation methods are not quite suitable, if we need to consider the properties of residual current devices, phase insulation, current leakage circuits, capacitive current compensation devices, and shunt-connected surge protection devices, etc. These components generate transients in the RC oscillator circuits which lack proper mathematical interpretation. A possible solution to this problem is the simulation of the leakage currents which requires an appropriate equivalent circuit and a set of variables.

Goals and Objectives

The purpose of this study is the assessment insulation leakage current using an equivalent circuit of a mine power distribution system.

This paper presents the solutions to the following problems:

- selection of the equivalent circuit structure for a mine power distribution system and its component properties;
- deriving the equations for the time constants of damped EM oscillations in circuits consisting of the insulation and current leakage paths;
- development of an equivalent circuit to solve a specific problem related to insulation monitoring and protective device performance.

Model Structure and Input Variables

We used a circuit equivalent to a typical mine power distribution system up to 1,140 V (Fig. 1).

Let us consider the key components of the equivalent circuit, in order to analyze the leakage current paths through the insulation and a person touching a live phase conductor.

The EMF source (Fig. 1, a) is the secondary winding of the power transformer installed on a mobile substation, 6,000/660 (1,140) V.

A residual current device (RCD) is represented as an RL filter (Fig. 1, b) or an RC filter (Fig. 1, c) (UAKI, AZAK, AZSH, SASU, ASZUS, AZUR models of RCD) [7, 8]. The RCD is defined with the RC filter properties. The phase resistances of the branch lines are $R_{Fa} = R_{Fb} = R_{Fc} = 15 \text{ kOhm}$, $R_{PN} = 1 \text{ kOhm}$, and the capacitance is $L_{PN} = 8$. The measuring instrument is connected between the neutral of the filter and the ground. For RCDs with RL filters: phase resistances are $R_{Fa} = R_{Fb} = R_{Fc} = 0.3 \text{ kOhm}$, phase inductances are $L_{Fa} = L_{Fb} = L_{Fc} = 75 \text{ H}$. The measuring circuit resistance and inductance are $R_0 = 3.9 \text{ kOhm}$, and $L_0 = 8 \text{ H}$, respectively [5].

The impedance components of the phase insulations (Z_a, Z_b, Z_c) vary in the following ranges: resistance $R_I = 10.5...300 \text{ kOhm/phase}$; and capacitance: $C_I = 0.1...1.5 \text{ }\mu\text{F/phase}$ (Fig. 1, d). The resistance and capacitance of the absorption current circuit vary as follows: $R_{ab} = 0.01...10 \text{ MOhm/phase}$, $C_{ab} = 0.01...0.5 \text{ }\mu\text{F/phase}$. The impedance components

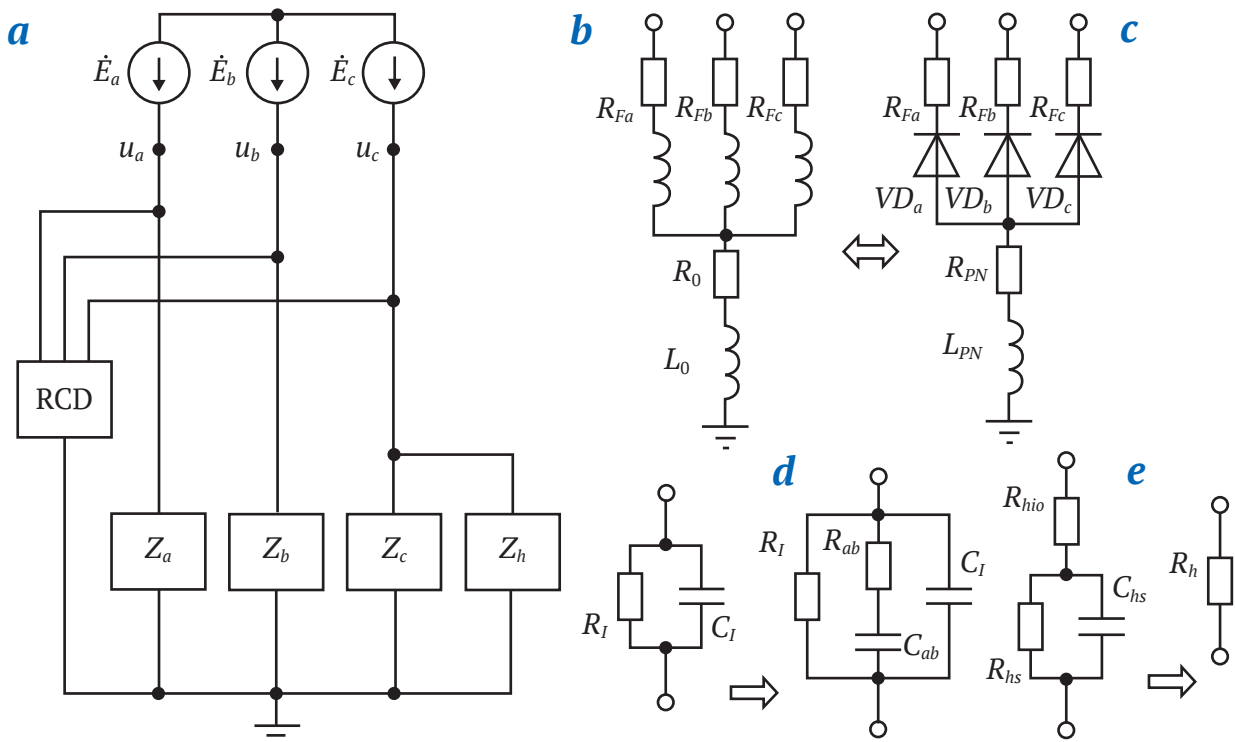


Fig. 1. Equivalent circuit for a current leakage path in a substitution in a mine power distribution system

of the equivalent leakage path through the human body (Z_h): internal body resistance is $R_{hio} = 0.7...1$ kOhm; skin resistance is $R_{hs} = 0.5...3.5$ kOhm; and skin capacitance is $C_{hs} = 0.3...1$ μ F (Fig. 1, e). If the voltage exceeds 380 V, we can simplify the model to $Z_h \approx R_h = R_{hio} = 1$ kOhm, since over 40 V the skin no longer protects from electric shocks, and the leakage path resistance is equal to the internal body resistance [9–11].

The inclusion of RCD in the equivalent circuit of the leakage path significantly complicates both the circuit and the simulation model [12–14]. Note that the introduction of a neutral displacement device and an additional leakage path through the RCD tester into the equivalent circuit results in a noticeable (15...20 %) increase in the insulation leakage current (especially if an RC filter is present) [5, 7, 15].

The symmetric leakage current values in 380 and 660 V networks are fairly well known for zero sequence equivalent circuits [4, 6, 12].

Among the variety of options, the most common are zero sequence substitution circuits, for which the equivalent insulation properties are expressed as:

$$R_I = \frac{R_a R_b R_c}{R_a R_b + R_b R_c + R_c R_a}; C_I = C_a + C_b + C_c, \quad (1)$$

where $R_a, R_b, R_c, C_a, C_b,$ and C_c are the phase resistances and capacitances.

For such circuits, the insulation properties vary within the ranges: $R_I = 3.5...300$ kOhm/phase, $C_I = 0.03...1$ μ F/phase.

The representation of phase insulation with linear lumped capacitance and resistance models provides a more accurate description of the processes in a circuit with asymmetric leakage current.

For such circuits, the phase resistances and ground capacitances are in the range of $R_I = 31.5...300$ kOhm and $C_I = 0.3...3$ μ F.

Since we studied leakage currents during a transient while the RCD trips, it is reasonable to represent the phase insulation as time constants of dumped EM oscillations in RC circuits:

$$T_{Ia} = \frac{X_{Ia}}{R_{Ia}}, T_{Ib} = \frac{X_{Ib}}{R_{Ib}}, T_{Ic} = \frac{X_{Ic}}{R_{Ic}}, \quad (2)$$

where R_{Ia}, R_{Ib}, R_{Ic} are the insulation resistances; X_{Ia}, X_{Ib}, X_{Ic} are the insulation capacitances ($X_I = 1/(\omega_0 C_I)$); T_{Ia}, T_{Ib}, T_{Ic} are the time constants of dumped oscillations.

It was found that the amplitude and damping rate of EM oscillations largely depends on the ratio of the phase resistance and capacitance. The highest values correspond to the insulation resistances up to 60 kOhm/phase and capacitances less than 0.3 μ F/phase. In the resistance range of $R_I = 60...300$ kOhm/phase and capacitances greater than 0.5 μ F/phase, the T_I constants are less than 0.1 rad/s and tend to be zero.

The reason is that at high capacitances, the resistance does not significantly affect the oscillation damping in the phase insulation circuits. The leak is purely capacitive, and the insulation efficiency is sharply reduced. A phase current leak does not instantly reduce the phase voltage due to a sufficiently high charge potential of the insulation ground capacitance. In this case, the electric hazard increases dramatically [16–18].

In order to simulate the leakage with the human body equivalent circuit (Fig. 2), we specified the internal body resistance R_{hio} , skin resistance R_{hs} , and skin capacitance C_{hs} ($X_{hs} = 1/(\omega_0 C_{hs})$) and transformed the model as follows.

The equivalent resistances for the human body equivalent circuit are estimated as:

$$R_e = R_{hio} + \frac{R_{hs} X_{hs}^2}{X_{hs}^2 + R_{hs}^2}; X_e = R_{hio} + \frac{X_{hs} R_{hs}^2}{R_{hs}^2 + X_{hs}^2}. \quad (3)$$

Considering the inverse transformation of the $R_e C_e$ circuit, the human body impedance is:

$$R_h = \frac{X_e^2 + R_e^2}{R_e}; X_h = \frac{X_e^2 + R_e^2}{X_e}. \quad (4)$$

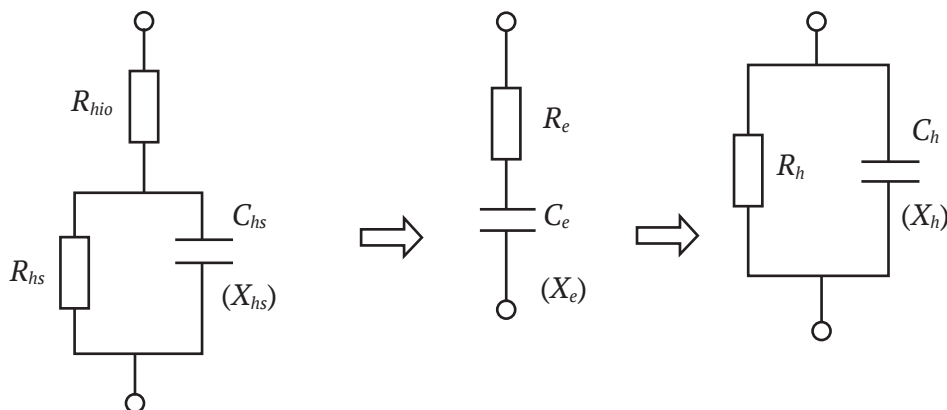


Fig. 2. Transformation of the human body equivalent circuit

Then phase resistance and capacitance for a circuit when a person comes into contact with a live component are estimated as:

$$R_{th} = \frac{R_I R_h}{R_I + R_h}; \quad X_{th} = \frac{X_I X_h}{X_I + X_h}. \quad (5)$$

The time constant of damped oscillations in the phase insulation circuit accounting for the human body properties is:

$$T_{th} = \frac{X_{th}}{R_{th}}. \quad (6)$$

In the case of skin breakdown, the human body resistance is equal to the internal body resistance $R_{hio} \approx 1$ kOhm. Therefore, the leakage circuit properties are:

$$R_{th} = \frac{R_I}{1 + R_I} \approx 1; \quad X_{th} = X_I; \quad T_{th} = \frac{X_I(1 + R_I)}{R_I}; \quad (7)$$

We found that in this case, the T_I constant (2.5...35 rad/s) is an order of magnitude greater than the similar values of the T_{th} constant (0.1...3 rad/s). The greatest increment of T_{IH} occurs when the insulation resistance is less than 31.5 kOhm/phase and the insulation capacitance is less than 0.3 μ F/phase. As the insulation resistance reaches $R_I > 31.5$ kOhm/phase, the T_{th} constants do not change and depend only on the phase insulation capacitance C_I .

The reason for this is that when a person touches a phase live wire, the resistance of the leakage path decreases sharply to 1 kOhm and is virtually independent of R_I . In this way, the insulation

resistance is shunted. The leakage current I_y and the constant T_{IH} depend only on the phase insulation ground capacitance.

In order to incorporate the low-frequency polarization into the phase insulation model, we added an RC circuit consisting of the capacitor C_{ab} and resistor R_{ab} with the absorption current i_{ab} (Fig. 1, d) [5, 7, 18].

For the analysis of the transient occurring in the insulation, direct incorporation of the differential link (R_{ab}, X_{ab}) leads to a more complicated simulation model. This is because the series RC circuit is a source of interference in the oscillatory circuit. The equivalent circuit of the phase insulation can be transformed to include the resistance and capacitance into the absorption current (Fig. 3).

The following relationship indicates the time constant of damped oscillations in a circuit representing the insulation resistance and capacitance:

$$T_{IF} = \frac{X_{IF}}{R_{IF}} = \frac{X_I (R_I R_{ab} + Z_{ab}^2)}{R_I (X_I X_{ab} + Z_{ab}^2)} = T_I \frac{R_I R_{ab} + Z_{ab}^2}{X_I X_{ab} + Z_{ab}^2}, \quad (8)$$

where R_{ab}, X_{ab}, Z_{ab} are the phase resistance, capacitance, and impedance; R_{IF}, X_{IF} are the insulation ground resistance and capacitance estimated as:

$$R_{IF} = \frac{R_I R_A}{R_I + R_A} = \frac{R_I Z_{ab}^2}{R_I R_{ab} + Z_{ab}^2}; \quad (9)$$

$$X_{IF} = \frac{X_I X_A}{X_I + X_A} = \frac{X_I Z_{ab}^2}{X_I X_{ab} + Z_{ab}^2}.$$

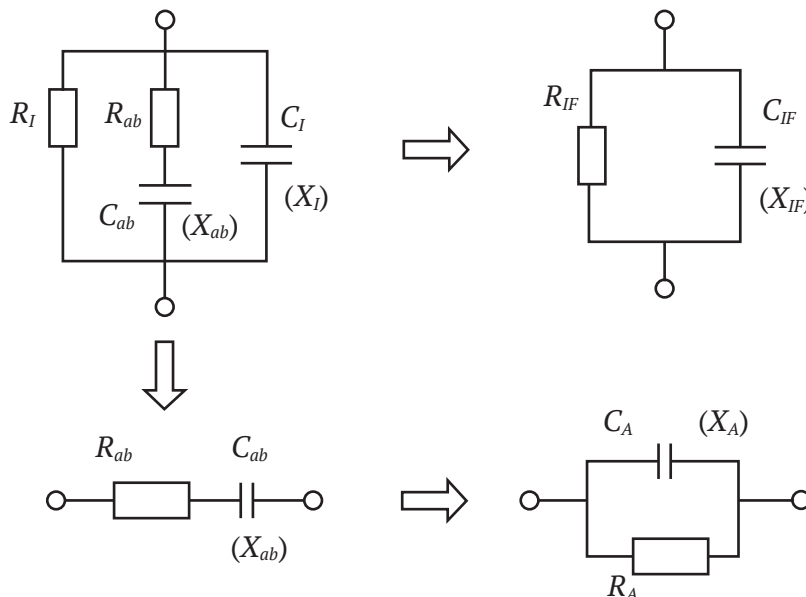


Fig. 3. Transformation of the equivalent circuit of the phase insulation to include the resistance and capacitance to the absorption current

Where R_I, X_I are the insulation ground resistance and capacitance for ion conductivity; R_A, X_A are the resistance and capacitance to the absorption current estimated as:

$$R_A = \frac{R_{ab}^2 + X_{ab}^2}{R_{ab}}; \quad X_A = \frac{R_{ab}^2 + X_{ab}^2}{X_{ab}}. \quad (10)$$

When C_{ab} is comparable to the insulation capacitance C_I, T_{IF} reaches its maximum [14].

With the above relationships, equivalent circuits of mine power distribution systems suitable for a wide range of applications can be generated.

Fig. 4 shows a *Simulink* simulation model of a mine power distribution system with an RC filter in the RCD circuit.

The simulation model functionality is as follows:

- simulation of current leakages through the phase insulation accounting for the presence of the RC filter in the RCD circuit;
- analysis of the low-frequency polarization effect on electrical safety in transient and steady-state current phase insulation leakages;

- analysis of transient and steady-state phase insulation leakages to assess the electric hazard when a person comes into contact with a live component;

- analysis of current and voltage variations in the filter and RCD tester circuits for various current leakage types.

As an example, Figs. 5 and 6 show oscilloscope patterns of the leakage currents and phase ground voltages for a single-phase leakage to a human body (contact with phase A, $R_h = 1 \text{ kOhm}$), symmetric insulation properties $R_I = 300 \text{ kOhm}$, $C_I = 0.03 \text{ }\mu\text{F}$, $R_{ab} = 1 \text{ MOhm}$, $C_{ab} = 0.01 \text{ }\mu\text{F}$, $U_L = 1140 \text{ V}$.

With the oscilloscope patterns, we could assess the instantaneous and effective currents and voltages in the equivalent circuit nodes, phase angle shifts, surge currents, and transient periods in case of a single-phase leakage through a human body.

A comparative analysis of the simulation results showed good agreement (more than 0.95) with similar research results [5, 7, 13]. The proposed simulation model applies to a wide range of insulation and emergency trip monitoring problems to ensure the electrical safety of mine power distribution systems.

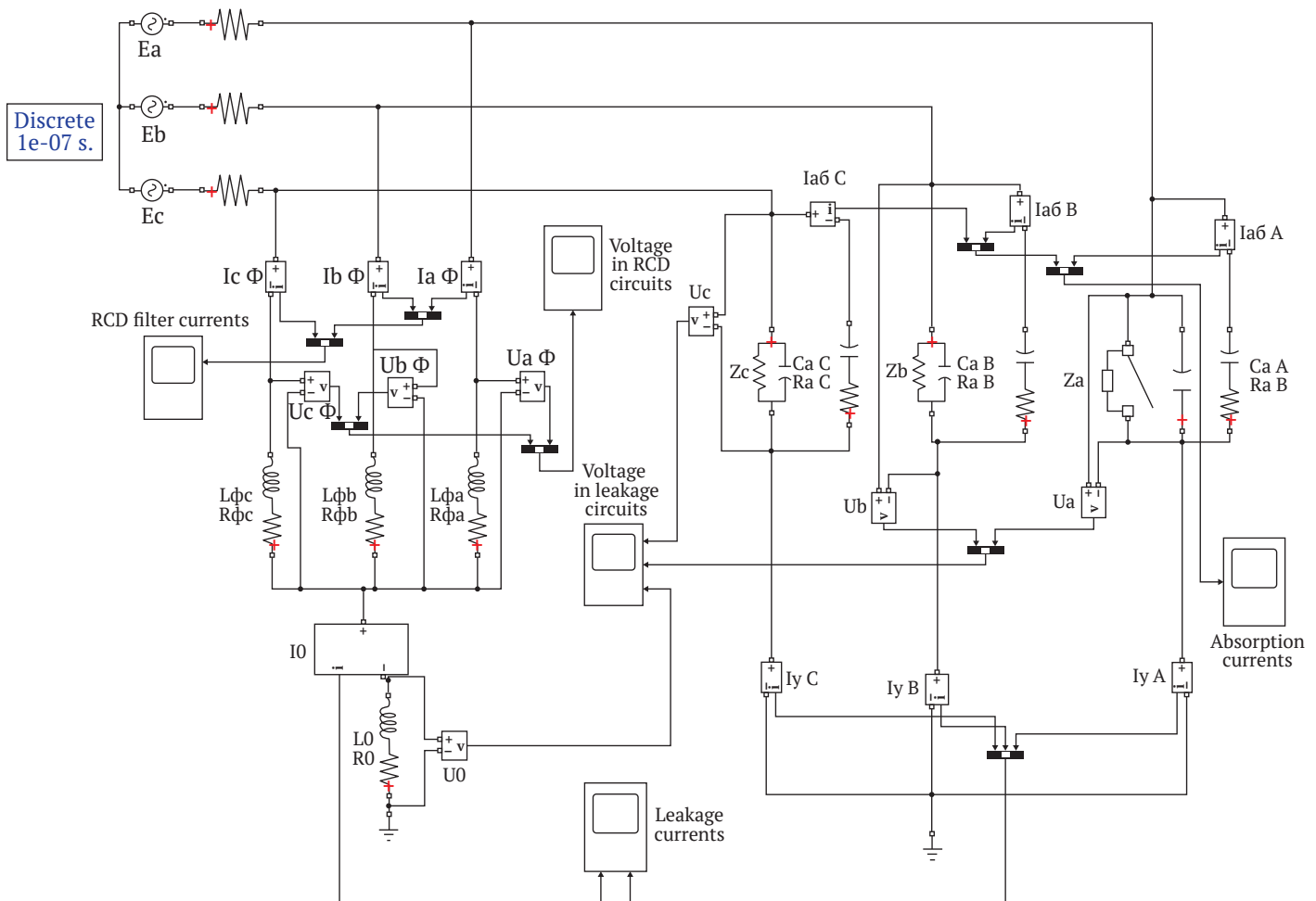


Fig. 4. Simulation model of a mine power distribution system with an RC filter in the RCD circuit



Fig. 5. Oscilloscope pattern of the leakage currents through insulation, human body, and RCD tester circuit with an RC filter

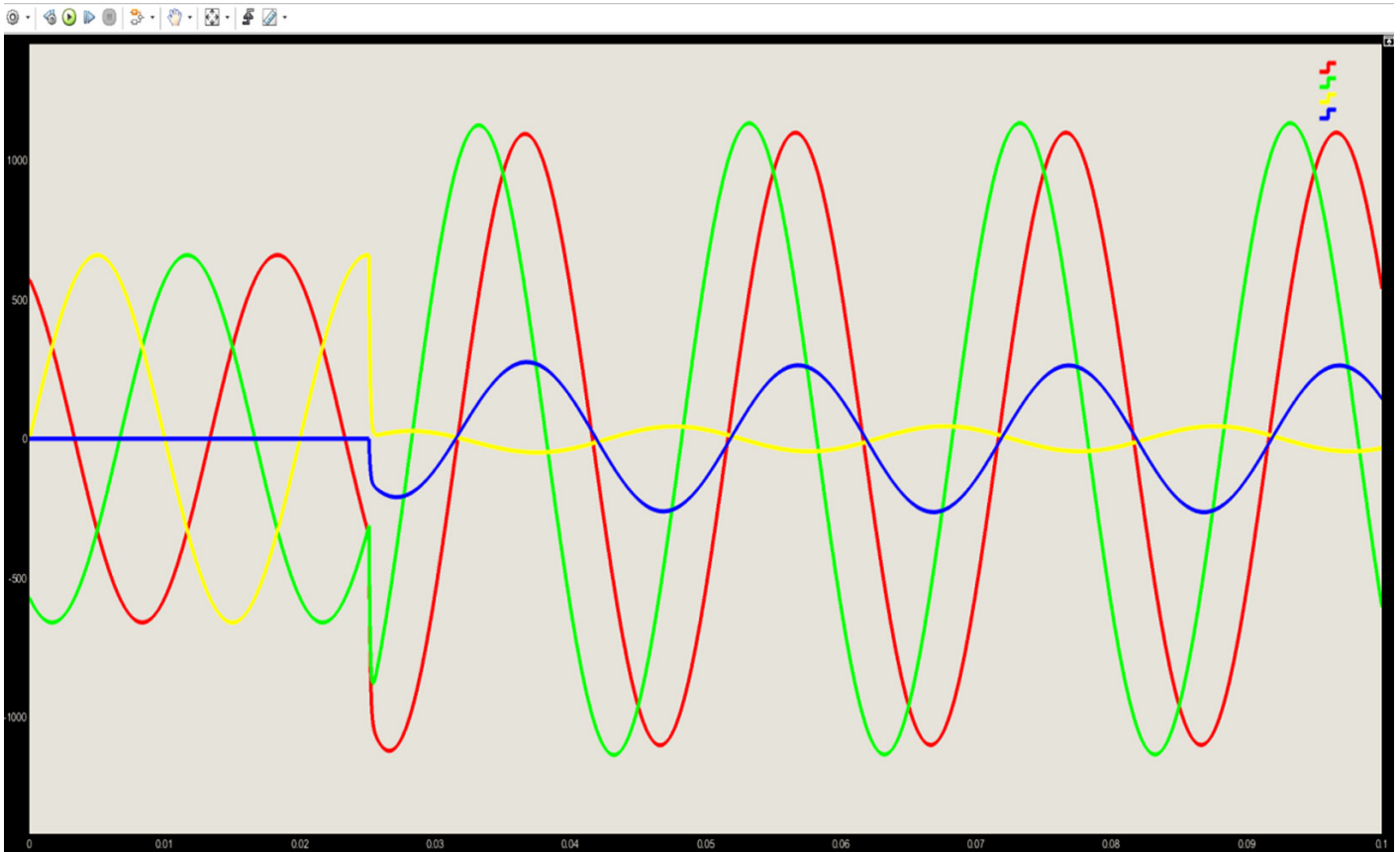


Fig. 6. Oscilloscope pattern of the phase voltages and zero sequence voltages before and after a person touches live phase A



Conclusions

The proposed equivalent circuit of a mine power distribution system can be used to analyze insulation currents and phase voltages as the insulation resistance changes under symmetric, single-phase, and two-phase leakages also caused by a person coming into contact with live components.

The equivalent circuit includes the EMF source, RCD, and insulation leakage paths. The model supports extensive ranges of its component properties including their critical values. The model gives a more accurate quantitative and qualita-

tive assessment of the RCD efficiency. It assesses the acceptable insulation resistance and current passing through the person, the contribution of low-frequency polarization to the required insulation resistance, and selects the insulating material, shunt-connected surge protection devices, and protective bypassing of damaged phases and residual current arrestors.

The equivalent circuit of the power distribution system addresses a range of problems related to insulation and trip monitoring in the mining industry.

References

1. Gladilin L.V., Shchutsky V.I., Batsezhev Yu.G. et al. *Electrical safety in the mining industry*. Moscow: Nedra; 1977. 327 p. (In Russ.)
2. Shchutsky V.I., Sidorov A.I., Sitchikhin Yu.V. et al. *Electrical safety in open-pit mining*. Moscow: Nedra; 1996. (In Russ.)
3. Pichuev A.V., Peturov V.I., Suvorov I.F. *Effects of non-stationary modes on electrical safety of mining electrical equipment*. Moscow: Gornaya kniga; 2011. 326 p. (In Russ.)
4. Klyuev R.V., Bosikov I.I., Gavrina O.A., Lyashenko V.I. Assessment of operational reliability of power supply to developing ore mining areas at a high-altitude mine. *Mining Science and Technology (Russia)*. 2021;6(3):211–220. (In Russ.) <https://doi.org/10.17073/2500-0632-2021-3-211-220>
5. Kim K.E. *Non-stationary modes in mine electrical networks up to 1,000 V and their impact on electrical safety*. [Ph.D. Thesis] Moscow: Moscow Mining University; 1975. (In Russ.)
6. Kolosyuk V.P. *Emergency tripping in mine electrical installations*. Moscow: Nedra; 1980. 334 p. (In Russ.)
7. Sidorov A.I., Peturov V.I., Pichuev A.V. et al. Electrical safety of power supply systems. *Advances in Current Natural Sciences*. 2010;(2):114. URL: <https://natural-sciences.ru/ru/article/view?id=7752> (In Russ.)
8. Peturov V.I. Method for measuring phase insulation properties in insulated neutral systems. *Elektrobezopasnost*. 1998;(1):9–12. (In Russ.)
9. Kano Murga J. *Electricity. The danger of its use and protection of people from electric shock*. MF. Per. GPNTB, “Instalador”. 1976;(106):75–78.
10. Pouvel I. Problems de protection dans les reseaux miniers. *Revue de l'industrie minerale*. 1983;25(7). (In French)
11. Kupfer J., Bastek R., Eggert S. Grenzwerte zur Vermeidung von unfällen durch elektrischen strom min tödlichem Ausgang. *Zeitschrift für die Gesamte Hygiene*. 1981;27(1):9–12. (In German)
12. Suvorov I.F. *Integrated electrical safety systems for electrical installations up to 1000 V*. Chita: Chita State University; 2005. 328 p. (In Russ.)
13. Khusainov Sh.N., Sidorov A.I., Khusainova N.A. Improved method for insulation conductivity estimation of a grid segment with a branch line from the electric parameter measurements. *Bulletin of South Ural State University. Series: Power Engineering*. 2002;(7):24–29. (In Russ.)
14. Pichuev A.V. Parametric relationships for the insulation resistance of mine electrical networks. *Mining Informational and Analytical Bulletin*. 2011;(4):398–400. (In Russ.)
15. Tsapenko E.F. Resonant overvoltages in mine networks caused by the use of UAKI, AZAK, AZSh, AZUR RCP Devices. *Mining Informational and Analytical Bulletin*. 2000;(3):106–109. (In Russ.)
16. Tsapenko E.F. Leakage current protection monitoring in mine networks up to 1,200 V. *Mining Informational and Analytical Bulletin*. 2003;(6):155–156. (In Russ.)
17. Pichuev A.V. Unsymmetrical current leakage through the insulation in mine electrical networks. *Elektrobezopasnost*. 2011;(2):28–33. (In Russ.)



18. Abderrezak H., Mizane A. Hybrid model for insulation active component control in an isolated neutral electrical network. In: *Proceedings of the 2012 International Conference on Industrial Engineering and Operations Management*. Istanbul, Turkey, July 3–6, 2012. Pp. 1961–1970. URL: <https://ieomsociety.org/ieom2012/pdfs/466.pdf>

Information about the authors

Alexandr V. Pichuev – Cand. Sci. (Eng.), Associate Professor of the Department of Energy and Energy Efficiency of Mining Industry, University of Science and Technology MISIS, Moscow, Russian Federation; ORCID [0000-0001-7457-5702](https://orcid.org/0000-0001-7457-5702), Scopus ID [57209798580](https://scopus.com/authid/detail.url?authorID=57209798580); e-mail allexstone@mail.ru

Vadim L. Petrov – Dr. Sci. (Eng.), Vice-Rector, Professor of the Department of Energy and Energy Efficiency of Industrial Enterprises, University of Science and Technology MISIS, Moscow, Russian Federation; ORCID [0000-0002-6474-5349](https://orcid.org/0000-0002-6474-5349), Scopus ID [8919065900](https://scopus.com/authid/detail.url?authorID=8919065900); e-mail petrovv@misis.ru

Received 07.01.2023

Revised 25.01.2023

Accepted 26.01.2023



EXPERIENCE OF MINING PROJECT IMPLEMENTATION

Review paper

<https://doi.org/10.17073/2500-0632-2022-08-16>

UDC 622.276:004.67



The assessment of the level of digitalization and digital transformation of oil and gas industry of the Russian Federation

V. V. Yurak^{1,2}   , I. G. Polyanskaya¹  , A. N. Malyshev^{1,2}  ¹ Institute of Economics of Ural Branch of RAS, Yekaterinburg, Russian Federation² Ural State Mining University, Yekaterinburg, Russian Federation vera_yurak@mail.ru

Abstract

Digitalization and digital transformation of companies have turned from global trends to an urgent need. Thanks to digitalization and digital transformation, organizations can overcome the times of crisis, the times of lockdowns with less losses and respond more effectively to any adverse changes in the external environment. The assessment of the level of digitalization and digital transformation allows to determine how fast the processes of introducing digital technologies and optimizing processes with digital solutions proceed, both in companies and across the industry as a whole. The article provides an analysis with the systematization of foreign and domestic methods, methodological approaches, methods for assessing the digitalization level and digital transformation, as well as reveals their positive and negative aspects. Based on a comparative analysis, an improved author-developed methodological toolkit is proposed for assessing the level of digitalization and digital transformation, alleviating the disadvantages of the existing methodological experience. The approbation of the author-developed methodological toolkit was performed using the oil and gas industry as an example; the following companies, being the industry leaders, were analysed: PJSC “Lukoil”, PJSC “NK “Rosneft”, PJSC “Gazprom”, and PJSC “Tatneft”. According to the results, the digitalization and digital transformation processes of the domestic oil and gas industry are insufficiently dynamic. It was found that in the period from 2016 to 2020, the Russian Federation industry leaders were in the following order from the most advanced to the least advanced in terms of the digitalization level and digital transformation: PJSC “Gazprom” topped the list; PJSC “NK “Rosneft” was second; PJSC “Lukoil” was the third largest company, and PJSC “Tatneft” held the fourth position.

Keywords

oil and gas industry, digitalization, digital transformation, assessment, methodological approaches, methodological toolkit, comparative approach, ranking, strategic development, comparative analysis, Russian Federation

For citation

Yurak V.V., Polyanskaya I.G., Malyshev A.N. The assessment of the level of digitalization and digital transformation of oil and gas industry of the Russian Federation. *Mining Science and Technology (Russia)*. 2023;8(1):87–110. <https://doi.org/10.17073/2500-0632-2022-08-16>

ОПЫТ РЕАЛИЗАЦИИ ПРОЕКТОВ В ГОРНОПРОМЫШЛЕННОМ СЕКТОРЕ ЭКОНОМИКИ

Обзорная статья

Оценка уровня цифровизации и цифровой трансформации нефтегазовой отрасли РФ

В. В. Юрак^{1,2}   , И. Г. Полянская¹  , А. Н. Малышев^{1,2}  ¹ Институт экономики УрО РАН, г. Екатеринбург, Российская Федерация² Уральский государственный горный университет, г. Екатеринбург, Российская Федерация vera_yurak@mail.ru

Аннотация

Цифровизация и цифровая трансформация компаний из мировых тенденций превратились в насущную необходимость. Организации благодаря цифровизации и цифровой трансформации могут с меньшими потерями преодолевать кризисные времена, времена локдаунов и наиболее эффективно отвечать на любые негативные изменения внешней среды. Оценка уровня цифровизации и цифровой трансформации позволяет определить: насколько быстро протекают процессы внедрения циф-



ровых технологий и оптимизации процессов цифровыми решениями как в компаниях, так и в отрасли в целом. В статье проведен анализ с систематизацией зарубежных и отечественных методов, методологических подходов, методик по оценке уровня цифровизации и цифровой трансформации; выявлены их положительные и отрицательные стороны. На базе сравнительного анализа предложены усовершенствованный авторский методический инструментарий по оценке уровня цифровизации и цифровой трансформации, нивелирующий недостатки существующего методического опыта. Апробация авторского методического инструментария была выполнена на примере нефтегазовой отрасли; анализу подлежали следующие компании – лидеры отрасли: ПАО «ЛУКОЙЛ», ПАО НК «Роснефть», ПАО «Газпром», а также ПАО «Татнефть». Результаты продемонстрировали недостаточную динамику процессов цифровизации и цифровой трансформации отечественной нефтегазовой отрасли. Было выявлено, что лидеры отрасли в период с 2016 по 2020 г. в РФ по уровню цифровизации и цифровой трансформации располагаются в следующем порядке от наиболее продвинутых к наименее продвинутым: ПАО «Газпром» на первом месте; на втором ПАО «НК «Роснефть»; на третьем ПАО «Лукойл»; на четвертом ПАО «Татнефть».

Ключевые слова

нефтегазовая отрасль, цифровизация, цифровая трансформация, оценка, методологические подходы, методический инструментарий, сравнительный подход, ранжирование, стратегическое развитие, сравнительный анализ, Российская Федерация

Для цитирования

Yurak V.V., Polyanskaya I.G., Malyshev A.N. The assessment of the level of digitalization and digital transformation of oil and gas industry of the Russian Federation. *Mining Science and Technology (Russia)*. 2023;8(1):87–110. <https://doi.org/10.17073/2500-0632-2022-08-16>

Introduction

The relevance of digitalization and digital transformation of the oil and gas industry is indicated by both the global situation associated with changing oil prices and the sanctions policy against Russia, and the need to develop hard-to-recover oil reserves in the conditions of depleting exploited fields, as well as the Arctic projects, using digital models [1–3]. The significance of the development of hard-to-recover reserves in Russia is associated “... with an increase in their share in the structure of hydrocarbon reserves (now it exceeds 65 % of the total volume), as well as with the forecasts of a decline in oil production by 44 % by 2035, approximately 310 million tons. In 2017, oil production from hard-to-recover reserves in Russia amounted to 39 million tons, and according to the forecast of the Ministry of Energy of the Russian Federation, by 2035 this index is expected to be 80 million tons per year” [4]. Under the current conditions, it is digital solutions¹ [5] that become priority lines in improving the performance efficiency of the companies² [6]. Currently, almost all leading oil and

gas companies of the world³ [7–9] establish their development strategy on the use of digital transformation as a major line [7–9]. Technological processes are being implemented in the industry since digital transformation is a significant competitive advantage, it contributes to the profitability of oil and gas companies and increases their market sustainability. The comprehensive digitalization of the companies' activities and the complete digital transformation

³ Siemens. Making the digital leap with Topsiders 4.0. URL: <https://assets.siemens-energy.com/siemens/assets/api/uuid:a0f97b62-5070-46a3-984f-1ed4144e398d/topsiders-whitepaper.pdf> (Accessed: 12.06.2022)

BP. BP Sustainability report 2018. Responding to the dual challenge. URL: <https://www.bp.com/content/dam/bp/business-sites/en/global/corporate/pdfs/sustainability/group-reports/bp-sustainability-report-2018.pdf> (Accessed: 12.06.2022)

Equinor. Equinor Sustainability report 2018. URL: <https://www.equinor.com/en/news/2019-03-15-annual-sustainability-reports-2018.html> (Accessed: 12.06.2022)

Chevron. Chevron Sustainability report 2018. Climate change resilience framework. URL: <https://www.chevron.com/-/media/shared-media/documents/climate-change-resilience.pdf> (Accessed: 12.06.2022)

Eni. Eni Sustainability report 2018. URL: <https://www.eni.com/assets/documents/EniFor-2018-eng.pdf> (Accessed: 12.08.2022)

ExxonMobil. ExxonMobil Sustainability report 2018. Highlights. URL: <https://corporate.exxonmobil.com/Community-engagement/Sustainability-Report> (Accessed: 12.06.2022)

Shell. Shell Energy transition report 2018. URL: https://www.shell.com/energy-and-innovation/the-energy-future/shell-energy-transition-report/_jcr_content/par/toptasks.steam/1524757699226/3f2ad7f01e2181c302cdc453c5642c77a4cb48ca3/web-shell-energy-transition-report.pdf (Accessed: 12.06.2022)

Sinopec. Sinopec Sustainability report 2018. URL: http://www.sinopec.com/listco/en/investor_centre/reports/2018/ (Accessed: 12.06.2022)

¹ INTERENERGO. On the digital transformation of Gazprom Neft and technological trends in the oil industry. URL: <https://ieport.ru/stat/325802-o-cifrovoj-transformacii-gazprom-nefti-i-technologicheskix-trendax-neftyanoj-otrasli.html> (Accessed: 12.06.2022)

Neftegaz-EXPO. Oil organizations. URL: <https://www.neftegaz-expo.ru/ru/ui/17160/> (Accessed: 12.06.2022)

² Oil and Gas Information Agency. LUKOIL introduces digital field models. URL: <https://www.angi.ru/news/2878022-LUKOIL-introduces-digital-field-models/> (Accessed: 12.06.2022)

Neftegaz.RU. Strategy “Rosneft-2022”. URL: <https://neftegaz.ru/tech-library/menedzhment/142430-strategiya-rosneft-2022/> (Accessed: 12.06.2022)



can allow them to become at least 20 % more efficient than they are these days [7].

Along with positive trends towards digitalization in the leading companies of the oil and gas industry in Russia, there are still unresolved problems hindering its transformation and the formation of digital platforms. The major problem is observed in the dependence of the industry on foreign technologies, equipment, software and investments, which is aggravated by sanctions and other restrictions. The level of import substitution remains insufficient. With regard to the Arctic shelf projects, they are scarcely being developed after the U.S. company ExxonMobil and the British company BP, possessing the necessary technology, withdrew from the joint projects. Shell Company also ceased its activities. Total Company transferred its share in the Bazhenov formation fields to Lukoil, and the latter transferred its share in Shtokman to Gazprom [10]. “Many Western oilfield services companies have also reduced the scale of their business in Russia” [1]. The situation is aggravated by the COVID-19 pandemic, which hinders the growth of financial performance of companies, which affects the amount of investment in R&D and various innovations.

Another significant challenge for the industry is the training of qualified personnel [11, 12]. This problem is typical for the entire mineral resource complex [13, 14]. Specialists “with digital competencies, such as analytics and big data, robotics, operation of unmanned aerial vehicles, programming, 3D modeling” [2], as well as with the competencies of new emerging professions in the industry related to digitalization are required [15].

The issues related to economic security and trade secrets upon the exchange of technical data remain to be the areas of concern. According to the experts’ opinion, the funding provided in the Digital Economy program for information security leaves much to be desired. In this connection, the Russian companies, unlike the foreign ones, are often afraid to share information. In turn, this can slow down the process of neural network prediction [16].

The success of the digitalization transformation in industry is largely hindered by the lack of an optimal level of management of the entire set of processes from a single control center in the companies.

There is also a problem of institutional support or legal regulation of the activities of digital platforms, covering a complex of various organizations, along with the parent one. The problem arises “due to the lack of a well-defined legal definition of a digital platform in the jurisdiction of most countries, including Russia” [17]. In the Russian legislation, “The Legal

Regulation of Digital Environment”, Federal Project developed as the follow-up of Decree of the President of the Russian Federation No. 204 “On the National Goals and Strategic Objectives of the Development of the Russian Federation for the Period up to 2024” of May 7, 2018, involves the elaboration of a list of regulations for the removal of obstacles hindering the development of the digital economy. The settlement addresses the relevant administrative, production and economic issues of enterprises in related industries that comprise the digital platform, including issues related to legal status, protection of rights, obligations and security.

Along with the identified problems, the issue of the development of methodological support for assessing the level of digitalization and digital transformation, as well as the economic assessment of the implementation of the achieved levels within the industry, which would be applicable for each industry enterprise (company), as well as digital transformation, requires further development. The availability of such methodological support will allow to perform a timely diagnosis of “constrictions” and effective management of digitalization and digital transformation.

Hence, *the purpose* of this research is to improve the management of digitalization and digital transformation of the oil and gas industry through the development of the author guidelines, mitigating the shortcomings of existing methods.

The purpose determines the importance of performing the following tasks:

1. The analysis of the theoretical foundations of digitalization and digital transformation.
2. The assessment of the current state of the digital transformation of the oil and gas industry.
3. The study, analysis and systematization of foreign and domestic general, industry and production methods (for individual enterprises and companies), methodological approaches, recommendations and methods for assessing digitalization and digital transformation.
4. The development of an improved author methodology for assessing the level of digitalization and digital transformation of the oil and gas industry, alleviating the disadvantages of existing methods.

Research Methods

The methodological basis of the research was composed of standard general scientific methods, as well as the method of content analysis upon the study and systematization of foreign and domestic general, industry and production methods (for individual enterprises and companies), methodological

approaches, recommendations and methods for assessing the level of digitalization and digital transformation. The methods of mathematical statistics and the foresight method were also used in the formation of the author methodology for assessing the level of digitalization and digital transformation of the oil and gas industry, alleviating the disadvantages of the existing methods.

Results and Discussion

The Analysis of the Theoretical Foundations of Digitalization and Digital Transformation

The digital transformation is characterized by the penetration of advanced technologies introduced in the process of digitalization into the entire complex of ongoing business processes of companies. Along with this, “digital transformation is increasingly understood as a controllable adaptation of companies in the context of advancing digitalization for the provision of sustainable value creation” [18]. In Russia, these processes are supposed to be implemented in a digital economy, which is defined by Decree of the President of the Russian Federation No. 204 of May 07, 2018 to be one of the national development goals of the Russian Federation until 2024 and highlighted among the priority national projects. One of the tasks, being set to achieve the goal, is formulated as the transformation of priority sectors of the economy, including industry, transport and energy infrastructure “through the introduction of digital technologies and platform solutions”⁴. Obviously, it is of direct relevance to subsurface resources management. The major lines of the development of the digital economy were previously approved in the relevant program by the Order of the Government of the Russian Federation No. 1632 of 28.07.2017⁵.

The relation of the main terms is shown in Fig. 1. The term “digital economy” was introduced in 1995 by Canadian scientist Don Tapscott, who described the digital form of representation of objects, the impact of information technology on business, public administration system, etc. [19]. Subsequently, the term “digital economy” was interpreted differently by other authors, meanwhile the interpretations were close in meaning [20–23].

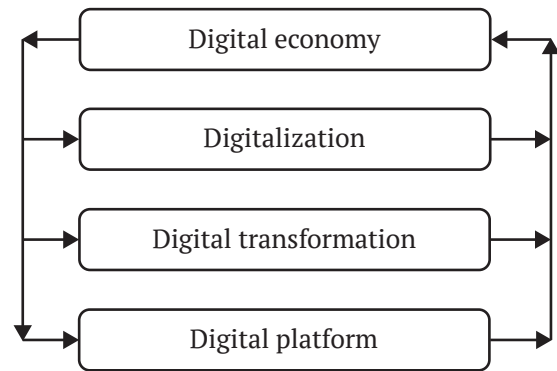


Fig. 1. The chronology of the development of the conceptual construct and the relationship between the concepts of the digital economy and digital transformation

According to Decree of the President of the Russian Federation No. 203 of May 9, 2017, the “digital economy” is defined as “economic activity in which digital data constitute a key factor of production, the processing of large volumes and the use of the results of the analysis of these data allow to significantly increase the efficiency of various types of production, technologies, equipment, storage, sale, delivery of goods and services compared to the traditional forms of management”⁶.

A key concept for understanding the terms “digital economy” and “digital transformation” is “digitalization”, which is commonly interpreted as “the process of introducing digital technologies for generating, processing, transmitting, storing and visualizing data in various fields of human activity” [24], as well as “integrating digital technologies into everyday life by digitizing everything that can be digitized”⁷.

The oil and gas industry is also one of the industries with a particular emphasis put on digitalization and digital transformation. The digitalization of the oil and gas complex as an integral part of the fuel and energy complex (FEC), its essence and development prospects are directly addressed within the framework of “Digital Energy” departmental program developed as a follow-up to the main federal regulations concerning digitalization.

“The digitalization of the oil and gas complex should be understood as the application of new advanced technologies within existing business

⁴ Decree of the President of the Russian Federation of 07.05.2018 No. 204 “On the national goals and strategic objectives of the development of the Russian Federation for the period up to 2024”. URL: <http://kremlin.ru/acts/bank/43027/page/1> (Accessed: 12.06.2022)

⁵ Decree of the Government of the Russian Federation of July 28, 2017 No. 1632-r “On Approval of the Digital Economy Program of the Russian Federation”. URL: <https://www.garant.ru/products/ipo/prime/doc/71634878/> (Accessed: 12.06.2022)

⁶ Decree of the President of the Russian Federation of May 9, 2017 No. 203 “On the Strategy for the Development of the Information Society in the Russian Federation for 2017–2030”. URL: <http://kremlin.ru/acts/bank/41919> (Accessed: 12.06.2022)

⁷ Growth people. Global digitalization. URL: https://ludirosta.ru/post/globalnaya-tsifrovizatsiya_2225 (Accessed: 12.06.2022)

processes without changing their principles and structure” [25]. Digital transformation involves the improvement and change of business processes by managing a complex of elements of digital technologies.

Overall, the scheme of the digital transformation of the oil and gas industry, including its impact on the final performance of companies, can be presented as follows (Fig. 2). According to Fig. 2, digital technologies based on the principles of artificial intelligence, being reinforced in the national strategy for its development up to 2030⁸, and implemented in the Russian oil industry, include big data, neural networks, digital twins, cognitive technologies, machine learning.

The assessment of the current state of the digital transformation of the oil and gas industry: the major lines of digital transformation of the largest Russian oil and gas companies

Digital transformation is now taking place in all large oil and gas companies [16]. This applies to both foreign and Russian companies. Foreign oil and gas

⁸ Decree of the President of the Russian Federation of October 10, 2019 No. 490 “On the development of artificial intelligence in the Russian Federation”. URL: <https://garant.ru/products/ipo/prime/doc/72738946/> (Accessed: 12.06.2022)

companies such as Equinor⁹, BP¹⁰, Shell¹¹, have a high level of digitalization and digital transformation for the achievement of which, along with digital technologies, they improve partnerships in the area of creating platforms for digital transformation¹² [7–9].

⁹ Equinor. Equinor Sustainability report 2018. URL: <https://www.equinor.com/en/news/2019-03-15-annual-sustainability-reports-2018.html> (Accessed: 12.06.2022)

¹⁰ BP. BP Sustainability report 2018. Responding to the dual challenge. URL: <https://www.bp.com/content/dam/bp/business-sites/en/global/corporate/pdfs/sustainability/group-reports/bp-sustainability-report-2018.pdf> (Accessed: 12.06.2022)

¹¹ Shell. Shell Energy transition report 2018. URL: https://www.shell.com/energy-and-innovation/the-energy-future/shell-energy-transition-report/_jcr_content/par/toptasks.stream/1524757699226/3f2ad7f01e2181c302cdc453c5642c77acb48ca3/web-shell-energy-transition-report.pdf (Accessed: 12.06.2022)

¹² Siemens. Making the digital leap with Topsiders 4.0. URL: <https://assets.siemens-energy.com/siemens/assets/api/uuid:a0f97b62-5070-46a3-984f-1ed4144e398d/topsiders-whitepaper.pdf> (Accessed: 12.06.2022)

Chevron. Chevron Sustainability report 2018. Climate change resilience framework. URL: <https://www.chevron.com/-/media/shared-media/documents/climate-change-resilience.pdf> (Дата обращения: 12.06.2022)

Eni. Eni Sustainability report 2018. URL: <https://www.eni.com/assets/documents/EniFor-2018-eng.pdf> (Accessed: 12.08.2022)

ExxonMobil. ExxonMobil Sustainability report 2018. Highlights. URL: <https://corporate.exxonmobil.com/Community-engagement/Sustainability-Report> (Accessed: 12.06.2022)

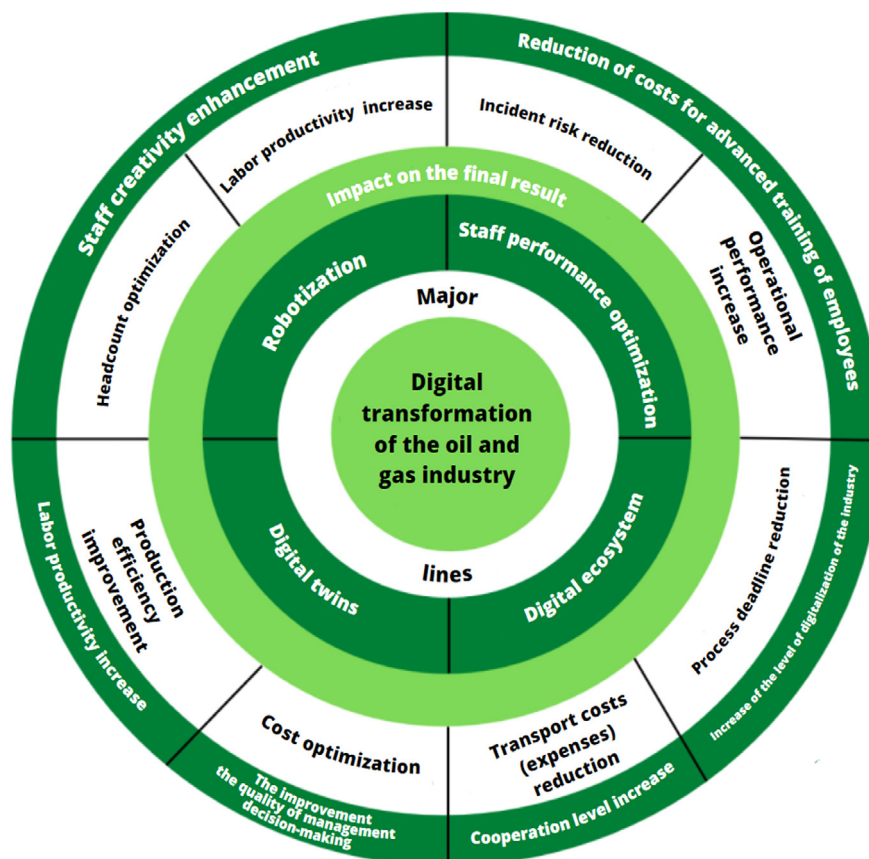


Fig. 2. The major lines of digital transformation of the oil and gas industry and their impact on the final result



In Russia, “the technological portfolio of oil companies consists of hundreds of projects aimed at maximizing oil recovery in conventional fields, as well as providing access and the possibility of efficient development of hard-to-recover reserves” [5]. At the same time, the complexity of digitalization in this very industry is higher than in other industries. “The business consists of managing complex physical and chemical processes, as well as a large number of complex manufacturing and oil extracting assets. The work is performed within the framework of a complex cyber-physical system, where real production is combined with its digital twin¹³. Among the oil organizations, we can highlight such large holdings as PJSC “Lukoil”, PJSC “NK “Rosneft”, PJSC “Gazprom”, which are the industry leaders in terms of digitalization and digital transformation¹⁴. PJSC “Tatneft” also demonstrates good performance. Let us discuss each company in detail.

PJSC “NK “Rosneft”. The company’s enterprises provide more than 35 % of liquid hydrocarbons production in Russia. Half of the produced raw materials are extracted from large fields: Priobskoye, Samotlorskoye, Prirazlomnoye and Malobalykskoye (the Khanty-Mansiysk Autonomous Area – Yugra), Vankorskoye (the Krasnoyarsk Territory), Verkhnechonskoye (the Irkutsk Region)¹⁵

The company’s comprehensive digitalization plan is an integral part of “Rosneft-2022” strategy approved in 2017. The plan includes such programs as “digital field”, “digital plant”, “digital supply chain”, “digital filling station”, the implementation of which will contribute to the transition to a higher level of business information service, reliability and efficiency of production, as well as to the reduction of losses. Upon that, the controllability and decision-making time along the entire production chain of the company will be improved. The strategy provides for the introduction of 78 proven technologies and obtaining effect of the implementation in the amount of more than 11 billion rubles¹⁶

At the Ilishevsky field (Bashkiria), there is an operating *Digital Field*, “an analogue of real production, where all processes, from oil production and

¹³ INTERENERGO. On the digital transformation of Gazprom Neft and technological trends in the oil industry. URL: <https://ieport.ru/stat/325802-o-cifrovoj-transformacii-gazprom-nefti-i-texnologicheskix-trendax-neftyanoj-otrasli.html> (Accessed: 12.06.2022)

¹⁴ Neftegaz-EXPO. Oil organizations. URL: <https://www.neftegaz-expo.ru/ru/ui/17160/> (Accessed: 12.06.2022)

¹⁵ State report “On the state and use of the mineral resource base of the Russian Federation in 2020”. Moscow: Ministry of Natural Resources and Ecology of Russia. Federal Agency for Subsoil Use (Rosnedra); 2021. Pp. 22–23.

¹⁶ Tadviser. State. Business. Technologies. Information technologies in Rosneft.

transportation to the movement of personnel and vehicles, are reflected on a digital platform. The process is performed on the basis of “*digital twins*” using a 3D visualization platform. A pipeline monitoring system using drones, which is based on machine learning and computer vision technologies, is allocated within a separate project”¹⁷.

The Digital Transformation Center and the Digital Cluster are the key mechanisms for the implementation of the digital programs. Based on the artificial intelligence algorithm, a computer vision technology has been introduced at the facility of PJSC “Var-yoganneftegaz”. “Detailed 3D models have been created for six producing assets (“RN-Uvatneftegaz”, “Slavneft-Krasnoyarskneftegaz”, “RN-Vankor”, “NK “Kondaneft”, “Verkhnechonskneftegaz” and “Vostsibneftegaz”). The 3D models will be used upon the creation of a unified information and technology environment for the monitoring the operation of oil fields using advanced visualization and a three-dimensional twin of the asset”¹⁸.

The company implements all its projects based on the introduction of innovative technologies, including the use of unique domestic drilling rigs in the northern version, as well as its own software¹⁹. The company is building a 770-kilometer pipeline to connect the Vankor and Payakh clusters with the oil loading terminal being under construction at the Bukhta Sever port²⁰.

PJSC “Gazprom Neft” develops fields in the largest oil and gas regions of the country, namely in the Khanty-Mansiysk and Yamalo-Nenets Autonomous Areas, as well as in the Irkutsk, Omsk, Orenburg, Tomsk Regions and on the shelf of the Barents Sea. The key asset of the company is the southern part of the Priobskoye field (LLC “Gazpromneft-Khantos”), where oil production amounted to 10 million tons in 2020. The company is actively working on the development of new major projects for the development of the Novoportovskoye, Prirazlomnoye and Vostochno-Messoyakhskoye fields²¹.

¹⁷ Tadviser. State. Business. Technologies. Information technologies in Rosneft.

¹⁸ Tadviser. State. Business. Technologies. Information technologies in Rosneft.

¹⁹ Ekb. Tsargrad. Checkmate in Taimyr: Vostok Oil will turn the oil industry around the world. URL: https://tsargrad.tv/articles/shah-i-mat-na-tajmyre-vostok-ojl-perevernjot-mirovujju-jenergetiku_592772 (Accessed: 01.08.2022)

²⁰ BFM. Rosneft has started development drilling at the Payakhskoye field of the Vostok Oil project.

²¹ State report “On the state and use of the mineral resource base of the Russian Federation in 2020”. Moscow: Ministry of Natural Resources and Ecology of Russia. Federal Agency for Subsoil Use (Rosnedra). 572 p.



The policy of digital transformation is performed at all stages of activities, starting from geological exploration and up to product sales. In 2013, the introduction of innovative was started in “Gazprom-neft-Khantos” Company, and a production control center (PCC) has been operating here since 2017²². Later, digital transformation is approved in the list of priority lines of the company’s activities, coordinated by the relevant directorate²³.

In 2019, PJSC “Gazprom Neft” “launched over 150 new digital initiatives and 10 digital transformation programs”²⁴.

The company “focuses on the implementation of digital technologies, including the early stages of working with assets, when the maximum value is created, because the uncertainties relating to the geological objects are still too great and making high-quality decisions is crucial”²⁵.

The following projects are being implemented: “*Cognitive Geologist*” project, which allows using the initial geological information “in order to provide a clear mathematical assessment of the probability of success in a particular case”²⁶; “*Digital Drilling*” project, which facilitates remote control from the Geo-Navigator Drilling Control Center (DCC); “*Smart Field*” project, which “allows online viewing of any information on the field development, i.e. well operation parameters, repair history and plans, the levels of fluid withdrawal compensation, conducted and planned studies”²⁷; “*Cognitive Engineering*” project that optimizes many field development schemes using machine intelligence.

²² Expert. Analytical Center. Digital fountain. URL: <http://www.acexpert.ru/archive/nomer-20-796/cifrovoy-fontan.html> (Accessed: 27.09.2021)

²³ Gazprom Neft. Digitization is a fundamental trend. URL: <https://www.gazprom-neft.ru/press-center/sibneft-online/archive/2018-may/1589542/> (Accessed: 23.07.2022)

²⁴ Comnews. The digital transformation of Gazprom Neft has produced an economic effect. URL: <https://www.comnews.ru/content/208475/2020-08-06/2020-w32/cifrovaya-transformaciya-gazprom-nefti-dala-ekonomicheskij-effekt> (Accessed: 23.08.2021)

²⁵ Gazprom Neft. On the digital transformation of Gazprom Neft and technological trends in the oil industry. URL: <https://www.gazprom-neft.ru/press-center/lib/4029430/> (Accessed: 19.09.2021)

²⁶ Gazprom Neft. Production in a digital format Gazprom Neft combines the entire cycle of field development with digital technologies. URL: <https://www.gazprom-neft.ru/press-center/sibneft-online/archive/2018-may/1589543/> (Accessed: 21.09.2021)

²⁷ Neftegaz.RU. The correspondent of Neftegaz.RU learned how digitalization helped Salym Petroleum Development to optimize the work of the production fund at Salym. URL: <https://neftegaz.ru/news/dobycha/512708-korrespondent-neftegaz-ru-uznal-kak-tsifrovizatsiya-pomogla-salym-petroleum-development-optimizirova/> (Accessed: 09.09.2021)

The development of the Novoportovskoye oil and gas field is performed using an integrated model, “including five hydrodynamic models of major development objects; the models of production and injection wells; the models of a land network for product gathering, including the models of pipelines from well-heads” [26]. In conjunction with subsidiary company “Gazpromneft-Angara”, a digital model of oil reservoirs, which will become the basis for the formation of a strategy for the development of hard-to-recover reserves by its “digital twin”²⁸. was developed. “The company has established competence centers for ML and AI, VR/AR, IoT, robotics, blockchain, video analytics and product service design”²⁹.

“The launch of a digital logistics management system in the Arctic, which allowed to optimize the cost of exporting ARCO and Novy Port oil by 10 %”, should not go unmentioned³⁰. “Prirazlomnaya” offshore ice-resistant fixed platform (OIRFP) was created, allowing performing all technological operations, such as drilling, oil production and storage, preparation and shipment of finished products³¹.

Virtually, PJSC “Gazprom Neft” is a “digital oil company” managed on the basis of big data and digital twins. The company produced the world’s first oil found using artificial intelligence, and it operates 40,000 “digitized” wells³². To implement the digital transformation strategy, it is planned to allocate up to 5 % of the total investment of Gazprom Neft. According to expert opinion, “the digital platform will allow to increase the base effect of digital transformation programs by 23 % due to faster project

²⁸ Neftegaz.ru. Gazprom Neft has created the industry’s first digital model of the Achimov formation. URL: <https://neftegaz.ru/news/Geological-exploration/197900-gazprom-neft-sozdala-pervuyu-v-otrasli-tsifrovuyu-model-achimovskoy-tolshchi/><https://neftegaz.ru/news/partnership/538597-achimovka-i-tsifrovizatsiya-gazprom-neft-i-halliburton-razrabotayut-programmu-tehnologicheskogo-sot/> (Accessed: 19.09.2021)

²⁹ Neftegaz.ru. Gazprom Neft has created the industry’s first digital model of the Achimov formation. URL: <https://neftegaz.ru/news/dobycha/512708-korrespondent-neftegaz-ru-uznal-kak-tsifrovizatsiya-pomogla-salym-petroleum-development-optimizirova/> (Accessed: 09.09.2021)

³⁰ Neftegaz.ru. Gazprom Neft has created the industry’s first digital model of the Achimov formation. URL: <https://neftegaz.ru/news/dobycha/512708-korrespondent-neftegaz-ru-uznal-kak-tsifrovizatsiya-pomogla-salym-petroleum-development-optimizirova/> (Accessed: 09.09.2021)

³¹ Pro-arctic. The record well of the Prirazlomnoye field has been put into operation. URL: <https://pro-arctic.ru/08/09/2021/news/44438#read> (Accessed: 25.07.2022)

³² Microsoft. How is a digital oil company built? URL: <https://news.microsoft.com/ru-ru/features/belevtsev/> (Accessed: 25.07.2022)



implementation”³³. The company also uses a digital approach in its procurement activities. The optimization of the procurement, supply and logistics system is performed through the introduction of “i-sourcing” system³⁴.

In relation to the personnel policy issues, PJSC “Gazprom Neft” acts as one of the founders of Scientific and Educational Center “Artificial Intelligence in Industry”, it is implementing “Business Thinking in Digital Reality” Program³⁵. Along with Equinor, BP, Shell, PJSC “Gazprom Neft”, is a member of International Consortium “Open Subsurface Data Universe” (OSDU) the subject of which is work with a large amount of geological data³⁶.

PJSC “NK “LUKOIL” produces oil in the Western Siberia (the Khanty-Mansiysk Autonomous Area – Yugra), the Perm Territory, the Nenets Autonomous Area, the Komi Republic, and on the continental shelf. About half of the oil production is performed by subsidiary company LLC “Lukoil-Western Siberia” at the Vatyegansky, Tevlinsko-Russkinsky, Povkhovsky and Yuzhno-Yakunsky fields. Approximately 37 % is produced by two enterprises of the holding, namely LLC “Lukoil-Perm” and LLC “Lukoil-Komi”. In 2020, the company’s production of liquid hydrocarbons (excluding its share in joint ventures) amounted to 73.4 mln t, having decreased by 10.6 % compared to the previous year³⁷. In 2021, the oil production increased by 2.7 % compared to 2020³⁸.

The digital development of the company is conducted under “The Information Strategy of LUKOIL

Group up to 2030”³⁹, including the following programs: digital twins, ecosystem, digital staff and robotics. The applied technologies include the following ones: “the industrial internet of things, interaction technologies, robots and drones, artificial intelligence, mobile devices, cloud technologies, Big Data”⁴⁰. Within the elaboration of the strategy, a “smart field” project is being implemented at the Vatyoganskoye field. “There are 12 facilities, 29 oil reservoirs and 156 deposits under development.” Within the framework of the project, “the following tasks are solved: updating the understanding of the geological structure, elaborating effective solutions for optimizing field development, detailing and implementing the prospects for increasing oil production”⁴¹. In the Bolshekhetskaya depression of the Yamal-Nenets Autonomous Area, the company is implementing a digital pilot project⁴². The intellectual field elements are present in the following subsidiaries of the company: “LUKOIL-Perm”, “LUKOIL-Western Siberia”, “LUKOIL-Nizhnevolzhskneft”, “LUKOIL-Komi”, RITEK. These ones include Integrated Operation Centers (ICOs).

At the Kokuyskoye field of “LUKOIL-Perm”, the introduction of digital technologies allowed to “manage production more efficiently”⁴³ by monitoring well operation parameters, pumping equipment, as well as controlling the emergence of dangerous situations.

The digital oil and gas production model was created on the basis of the Yuzhno-Yagunskoye and Vostochno-Ikilorskoye fields being developed by “LUKOIL-Western Siberia”. Here, there is an operating Integrated Operation Center, in which “new management approaches are embodied, including integrated planning, close cooperation with scientific institutions and a collective analysis of the technological process”⁴⁴. The automated systems of the

³³ Manufacturing control. How GAZPROM NEFT has already received 7.2 billion rubles. from digitalization. URL: https://up-pro.ru/library/information_systems/automation_management/mlrd-rub-ot-tsifrovizatsii/ (Accessed: 25.07.2022)

³⁴ Isource. How digital technologies are changing the procurement process of societies. URL: <https://isource.neftegaz.ru/chapter2> (Accessed: 26.07.2022)

³⁵ Neftgaz.ru. GazpromNeft has created the industry’s first digital model of the Achimov formation. URL: <https://neftegaz.ru/news/Geological-exploration/197900-gazprom-neft-sozdala-pervuyu-v-otrasli-tsifrovuyu-model-achimovskoy-tolshchi/> <https://neftegaz.ru/news/partnership/538597-achimovka-i-tsifrovizatsiya-gazprom-neft-i-halliburton-razrabotayut-programmu-tehnologicheskogo-sot/> (Accessed: 19.09.2021)

³⁶ Gazprom Neft. Gazprom Neft will make the development of digital solutions cheaper through an open industrial data platform. URL: <https://digital.gazprom-neft.ru/about-news?id=94> (Accessed: 21.09.2021)

³⁷ State report “On the state and use of the mineral resource base of the Russian Federation in 2020”. Moscow: Ministry of Natural Resources and Ecology of Russia. Federal Agency for Subsoil Use (Rosnedra); 2021. 572 p.

³⁸ Neftgaz.ru. LUKOIL’s hydrocarbon production in 2021 increased by 4.7 %, refining volume – by 7.4 %.

³⁹ Lukoil. Digitalization program. URL: <https://csr2018.lukoil.ru/strategy/digitalization-program> (Accessed: 04.08.2022)

⁴⁰ Expert. Analytical Center. Digital fountain. URL: <http://www.acexpert.ru/archive/nomer-20-796/cifrovoy-fontan.html> (Accessed: 27.09.2021)

⁴¹ Oil and Gas Information Agency. Lukoil introduces digital field models. URL: <https://www.angi.ru/news/2878022-ЛУКОЙЛ-внедряет-цифровые-модели-месторождений/> (Accessed: 28.10.2021)

⁴² Expert. Analytical Center. Measure oil with your mind. URL: <http://www.acexpert.ru/archive/nomer-12-13-792/izmerit-neft-umom.html> (Accessed: 28.10.2021)

⁴³ Association of independent oil and gas producing organizations. Oil with intelligence. URL: <http://www.assoneft.ru/activities/press-centre/tek/5164/> (Accessed: 27.07.2022)

⁴⁴ RBC. Companies that can quickly implement digital solutions become leaders. URL: <https://plus.rbc.ru/news/5ad2f7ba7a8aa94d53490a4f> (Accessed: 27.10.2020)



Advanced Process Control⁴⁵ are being implemented at all enterprises of the company for oil refining and petrochemistry.

PJSC “TATNEFT”. “The major region of activity of PJSC “Tatneft”, which extracts 4–5 % of the Russian oil, is conventionally the Republic of Tatarstan. The company’s largest fields are Romashkinskoye, Bavlinskoye, Novo-Elkhovskoye in the Republic of Tatarstan, the production at which amounted to 22.9 mln t in 2020”⁴⁶.

The beginning of the process of digital transformation in PJSC “Tatneft” dates back to 2014. Currently, digital technologies cover all processes, i.e. collection and processing of geological and technological information; creation and updating of geological and hydrodynamic models, decision-making on the choice of optimal geological and technical measures (GTM) as well as their implementation. Wells are designed on the basis of three-dimensional (3D) field models. Active work is being conducted to create artificial intelligence and digital “twins”. Digital twins have also been implemented “in the form of hydrodynamic models for oil assets that provide 80 % of oil production” at the Almetievskaya and Abrakhmanovskaya fields, as well as at the Romashkinskoye and Novoelkhovskoye fields.

There is an operating GTM Center (geological and technical measures), where the measures for oil recovery increase are modeled. “Mobile OGPW” Project (oil and gas production workshop) has been implemented as well, it allows to continuously monitor and coordinate the process of oil and gas production remotely from the workplace throughout the day. On the basis of the company, its own software is being developed, including the following: the software package of CIS ARMITS, CIS “Tatneft-Nefte dobycha”, Roxar, T-navigator. A software package based on neural network interpretation of the logging material has also been developed. NGT Smart software is being actively implemented to monitor and manage the development of oil fields.

In PJSC “Tatneft”, a significant role is assigned to the digital transformation of investment activities. In 2019, “the Automated Investment Management System (AIMS) was created”. The system constitutes a single bank of investment projects, being an analytical tool for managing the company’s investment activities. The system was developed as part of the software import substitution program based on 1C: Enter-

prise platform. Thus, the company was able to ensure information transparency, strengthen control over the implementation of its projects, apply neural network data analysis and obtain a significant economic effect of 1 billion rubles. Specialists of the company consider it promising to use the results of the Modeling Center to calculate the volume of production when choosing the optimal business projects.

The company’s relatively high level of digital transformation allows its specialists to work on the formation of a digital platform to coordinate a complex of activities in this line.

The analysis and systematization of foreign and domestic general, industry and production methods (for individual enterprises and companies), methodological approaches, recommendations and methods for assessing digitalization and digital transformation

The level of development of the methodological system for assessing the level of digitalization and digital transformation is evidenced by a significant number of the developed foreign and domestic methods related to global and country (regional) levels. Most of them have been analyzed, systematized and presented in a series of scientific researches⁴⁷ [23, 27–31]. The international methods for assessing the level of digitalization and digital transformation include: Digital Evolution Index (DEI) Rating, Information and Communication Technologies Development Index (ICT Development Index, IDI), Global Cybersecurity Index, PwC’s The Future is Coming Rating, Global Connectivity Index (GCI); International Digital Economy and Society Index (I-DESI); Boston Consulting Group’s Economy Digitalization Index (e-Intensity); World Digital Competitiveness Index (WDCI); e-Government Development Index (The UN Global E-Government Development Index – EGDI); Networked Readiness Index; E-Participation Index (EPART). In Russia, the following methods have been developed to determine the level of digitalization of the country: the rating of regions of the Russian Federation by the level of development of the information society (the Ministry of Digital Development, Telecommunications and Mass Media of the Russian Federation; “Digital Russia” Index (Skolkovo Information Center); Business Digitalization Index (Institute for Statistical Research and Economics of the National Research University Higher School of Economics); Ivanov Digital Index (PJSC “Sberbank”).

⁴⁵ RBC. Companies that can quickly implement digital solutions become leaders. URL: <https://plus.rbc.ru/news/5ad2f7ba7a8aa94d53490a4f> (Accessed: 27.10.2020)

⁴⁶ State report “On the state and use of the mineral resource base of the Russian Federation in 2020”. Moscow: Ministry of Natural Resources and Ecology of Russia. Federal Agency for Subsoil Use (Rosnedra); 2021. 572 p.

⁴⁷ Moscow School of Management “Skolkovo”. Center for Financial Innovation and Cashless Economy. Methodology for calculating the “Digital Russia” index of the constituent entities of the Russian Federation. URL: https://finance.skolkovo.ru/downloads/documents/FinChair/Research_Reports/SKOLKOVO_Digital_Russia_Methodology_2019-04_ru.pdf (Accessed: 12.06.2022)



A comparative analysis of the major methods and methodological approaches for assessing the level of digitalization and digital transformation at the level of sectors of the economy (industries) and individual enterprises is provided in Table 1.

The analyzed methodological approaches and techniques assess the level of digitalization and digital transformation of the industry (sectors of the economy) and individual enterprises from various perspectives using appropriate methods and indices upon that. The major methods include: questioning, analytical and comparative methods, the integral assessment method, economic and mathematical methods and financial and economic analysis methods, as well as the method of expert assessments, fuzzy (uncertain) sets, moving curves, etc. The indices of digital maturity, including innovative capacity, are assessed as well. Some of the proposed assessment methods have a significant error, which does not allow accurate assessment due to the use of extremely limited conditions and parameters.

With respect to the oil and gas industry, a comprehensive methodology for determining the level of digitalization is of interest, the application of the one can be attributed both to the level of a country, an industry, and an individual company. It was developed and successfully applied by EY (Ernst & Young, UK). EY has already conducted digital transformation readiness assessments for more than 3,800 companies in 44 countries. Pursuant to Order of the Ministry of Energy of the Russian Federation, such an assessment was also carried out for the domestic oil and gas industry⁴⁸. In accordance with the methodology, the readiness of the country's institutional environment, the degree of the penetration of digital solutions in the industry are determined; in particular, Digital DNA map is built for companies based on analytical data on the current level of implementation and the use of digital systems, as well as on the level of readiness of the company for digital transformation. The following areas are considered for calculations: strategy, innovation and development; interaction with clients; supply chain and operation management; information technologies; risks and cybersecurity; finance; legal support; taxation; leadership and organizational culture. The methodology allows to compare the results of assessing the levels of digitalization of the industry and individual companies, to identify their strengths and weaknesses. Deloitte Company offers a digital transformation model for

⁴⁸ State contract dated 21.08.2019. No. 0173100008319000044/K/02. Analysis of the level of implementation and use of digital information systems. URL: <https://in.minenergo.gov.ru/upload/iblock/971/971c417247ad76e15c6d3b910dc9dcca.pdf> (Accessed: 12.06.2022)

oil and gas exploration and production, which can be used to calculate the level of digitalization and digital transformation in these segments. However, the analysis revealed that there is no approved industry methodology, as well as a methodology for assessing digitalization and its transformation at the level of enterprises of the industry.

The improved author methodological toolkit for assessing the level of digitalization and digital transformation of the oil and gas industry

The author methodology implies a comprehensive assessment of the strategic level of digitalization and digital transformation of both an enterprise and the industry as a whole. Thanks to this assessment it is possible not only to calculate the aforesaid level, but also to determine the role of such phenomena as digitalization and digital transformation in the development strategy of the organization. The methodology of the author was developed based on the results of the study of foreign and domestic scientific publications, as well as the study of assessment methods used by consulting companies. The methodology of the author takes into account most of the advantages and disadvantages of existing methods, which were determined on the basis of a comparative analysis of 24 existing methodological recommendations and reflected in Table 1. Thus, taking into account the results of the comparative analysis, the list of indices being used has been reduced to three for the express assessment; it is recommended to obtain all indices used for the calculation from open sources of information.

The conditions/principles for the implementation of the author methodological toolkit for an express assessment of the level of digital transformation of companies in the industry, taking into account the shortcomings of existing methodological approaches to assessing the level of digitalization and digital transformation, will be as follows:

1. The assessment of the level of digital transformation is based on a comparative approach;
2. The selected leading companies of the analyzed and assessed industry are subject to the assessment of the level of digital transformation;
3. The selected indices of the assessment should concern digital transformation, they should characterize it and be publicly available;
4. The sources of information for the selected indices are exclusively official sources of information;
5. Based on the selected indices, the multipliers characterizing the level of digitalization and digital transformation are formed;
6. The multipliers are assigned certain weights, which are set on the basis of an expert survey.



Table 1

Comparative analysis of methodological approaches to the assessment of the level of digitalization and digital transformation of the industry and individual enterprises

Source	Method name, key assessment method	Indices in the methodology	Positive aspects	Negative aspects
Comprehensive methods and methodological approaches to assessing the level of digitalization and digital transformation (for industries and individual enterprises)				
Potetenko S. V. The assessment of the level of digitalization of enterprises (organizations) and industries. Belarus. OJSC "Giprosvyaz" [32]	The assessment of the level of digital development of enterprises, industries and functional areas	Automation, computerization, informatization, digitalization	Allows to obtain a generalized view of the assessment for the enterprise and industry, control measurement in the sphere of digitalization, identify and develop the prospects of growth points and determine the immediate prospects for the digital transformation of enterprises and the industry.	The document contains a very brief description of the assessment methodology
EY (Ernst & Young, Great Britain). The analysis of the level of implementation and use of digital information systems*	Methodology for the level of implementation and application of digital information systems	The readiness of the country's institutional environment, the degree of penetration of digital solutions in the industry, particularly for the companies, are determined, "Digital DNA" map based on the analytical data about the current level of implementation and application of digital systems, as well as the level of readiness for digital transformation is drawn. For calculations, the following areas are considered: strategy, innovation and development; interaction with customers; supply chain and operation management; information technologies; risks and cybersecurity; finance; legal support; taxation; leadership and organizational culture	The methodology allows to compare the assessment results of the levels of digitalization of the industry and individual companies, identifying their strengths and weaknesses	Difficulties in collecting data, in particular for the oil and gas industry
Deloitte: Digital transformation in oil and gas exploration and production – from bytes to barrels**	Digital transformation model	The digital transformation model represents a roadmap that includes 10 stages (mechanization, sensor installation, transfer, integration, analysis, visualization, addition, robotization, creation, virtualization) with detailed explanation of technologies for each stage. The current level of digital maturity, the desired level of transformation and lines for increasing the level of transformation are determined	The current and desired level of digital maturity and transformation is determined in the segments of exploration, development and production of hydrocarbon raw materials using the relevant technologies. The possibilities of digital transformation are assessed for each segment. It can be applied both to the industry as a whole and to enterprises in individual segments	A large number of assessment indices, cumbersome calculations
IBM Digital transformation of the oil and gas industry***	Digital transformation model	The areas that will benefit from digital transformation in the sectors of the oil and gas industry (exploration and assessment works, development and production) are specified	A wide range of assessment indices	Difficulty in obtaining statistical data when analyzing enterprises of the industries

* State contract dated 21.08.2019. No. 0173100008319000044/K/02. Analysis of the level of implementation and use of digital information systems. URL: <https://in.minenergo.gov.ru/upload/iblock/971/971c417247ad76e15c6d3b910dc9dcca.pdf> (Accessed: 12.06.2022)

** Deloitte. Digital transformation in oil and gas exploration and production – from bytes to barrels. URL: <https://nangs.org/analytics/deloitte-tsifrovaya-transformatsiya-v-sfere-razvedki-i-dobychi-nefti-i-gaza-ot-bajtov-k-barrelyam-fevral-2018-pdf> (Accessed: 26.08.2021)

*** IBM. Digital transformation of the oil and gas industry. URL: <https://www.ibm.com/downloads/cas/JLE286ZX> (Accessed: 27.08.2021)



Table 1 continued

Source	Method name, key assessment method	Indices in the methodology	Positive aspects	Negative aspects
Kuklina E.A., Mitselovskaya O.S. Methodological approach to assessing the level of innovative development of enterprises (exemplified by the sphere of housing and utility services) [33]	A methodological approach to assessing the level of innovative development of an industry and an enterprise using the methods of expert assessments, Innovation Scorecard (ISC), assessment of financial stability, ratios, etc.	The assessment of prospects for innovative development of the industry: the ratio of organizations implementing technological innovations in the total number of organizations, %; the volume and intensity of expenses for technological innovations; the volume and ratio of innovative goods, works, services in the total volume of shipped goods, works, services. The assessment of the innovation potential of an enterprise: innovation process, innovation strategy, innovation structure, innovation culture, provision of resources. The assessment of the level of innovative activity: intellectual property security ratio; R&D personnel ratio; coefficient of property intended for R&D; the rate of development of new technologies; the rate of introduction of new products; innovative growth rate	A comprehensive assessment using several recognized methods for each stage. The possibility of application in various areas	Difficulty in obtaining statistical data when analyzing enterprises of certain industries
Institute for Statistical Studies and Economics of Knowledge, National Research University Higher School of Economics [34]	The index of digitalization of economic sectors, social sphere and authorities, developed for an aggregate assessment of the distribution level of digital technologies	The index characterizes the rate of adaptation to digital transformation, the level of application of broadband Internet, cloud services, RFID technologies, ERP systems, and the involvement of business sector organizations in e-commerce. The index is calculated for Russia and the European countries, the Republic of Korea and Turkey	Calculated on the basis of small number of indicators	Cannot be considered optimal because of a small number of indicators being taken into account
Istomina E.A. The assessment of digitalization trends in industry [35]	Methodology for assessing digitalization in industry	Methods for assessing digitalization at the macro level and for a certain business entity are considered. Economic effect of investments in digitalization, percentage of labor productivity, profitability	The author indicates only 3 indices that are extremely important for an entrepreneur, in her opinion. The rest of indices is described as insignificant, therefore the assessment can be neglected.	The fragmentation of the methodological presentation. There is no link between the assessment of digitalization trends of individual enterprises and the industry as a whole
Methods for assessing the level of digitalization and digital transformation of individual enterprises and their innovative component				
Yashin S.N., Shchekoturova S.D. The application of the methodology for assessing the efficiency of the innovative development of an enterprise exemplified by PJSC "RUS-POLYMET" [36]	Moving curve method	<ul style="list-style-type: none"> • The ratio of employees engaged in R&D • The level of mastering of new technology • The degree of mastering of new products • The ratio of material resources for R&D • The degree of provision of the enterprise with intellectual property • The ratio of investment in innovative projects 	<ul style="list-style-type: none"> • The completeness of the assessment. The logical structure is ensured throughout the methodology • The assessment is focused on the analysis of a relatively small number of related indices. This simplifies the calculation and generalization • Developed on the basis of complementary methodologies • The assessment of innovative development is performed in conjunction with the economic status of the enterprise 	The company's strategic and tactical guidelines are not considered. There is no comparison with other companies in the industry



Table 1 continued

Source	Method name, key assessment method	Indices in the methodology	Positive aspects	Negative aspects
Kokhanova V.S. Fuzzy logic apparatus as a tool for assessing the effectiveness of a company's digitalization [37]	Fuzzy logic	The parameters vary depending on the need. One can enter both the simplest binary scale "good - bad", and a more complex one, in which the number of terms will reach 5, 7, or even 10	It is on par with other assessment systems; the assessment is performed in a more free form than upon formal logic. The comprehensive and applicable nature of fuzzy logic tools	There is still a portion of people who do not accept this method of assessment
Brusakova I.A. Methods and models for assessing the maturity of the innovation structure [38]	The production model of corporate knowledge about the enterprise readiness for digital transformations	Innovativeness of the infrastructure of an enterprise, innovative activity, innovative complexity of an enterprise	After assessing three macro parameters, one can talk about the readiness of the enterprise for digital transformations	Not the entire level of digitalization is determined, but only the innovative component, while taking into account the information component
Zakharova E.V., Mityakova O.I. The assessment of the innovative potential of an enterprise, taking into account the digitalization of the economy [39]	Methods for calculating the innovative potential of information potential indices (analytical method for calculating the system of indices, method for calculating an integral index based on the logistic regression model, method for financial and economic analysis, method for expert assessments, method for calculating the integral index based on the logistic regression model)	It covers 19 indices in 4 groups: production and technology, management and finance, the factors of innovative activity and the indices of information component	Relatively easy calculations due to the small number of indices. Due to the assessment of the information component, it is possible to determine the strengths and weaknesses of the enterprise's potential. The base is formed on methods for assessing innovative potential	Not the entire level of digitalization is determined, but only the innovative component, while taking into account the information component
Mityakova O.I. The assessment of the innovative potential of an industrial enterprise [40]	Analytical method for calculating the system of indices	The determination of the state of each component of the innovation potential by calculating a number of indices characterizing the innovation potential: 1. Staff 2. Production and technology 3. Scientific and technical 4. Financial and economic 5. Organizational and managerial potential	The calculations are based on the data reflected in the statement of financial and economic activity of the company, a high level of objectivity of the calculations, a comprehensive assessment of the potential	Not the entire level of digitalization is determined, but only the innovative component of the one
Deloitte: Digital Maturity Model Achieving digital maturity to drive growth*	Digital Maturity Model	5 key indices are highlighted, based on which the assessment is performed: consumers, strategy, technology, production, structure and culture of the organization (Customer, Strategy, Technology, Operations, Organization & Culture). In their turn, they have 28 sub-indicators, which are divided into 179 digital characteristics. The emphasis is put on the strategy (Business Strategy), which determines the focus of the transformation. The successive steps of strategy concretizing are the definition of a business model (Business Model) and an operating model (Operating Model), which determine the required level of digital maturity according to the selected measures	The assessment is performed based on a large number of indicators, which increases its accuracy and depth in the internal aspects	An example of the application of this assessment has not been found due to the closed nature of the data. One cannot perform a prompt assessment

* Deloitte. Digital Maturity Model Achieving digital maturity to drive growth. URL: <https://www2.deloitte.com/content/dam/Deloitte/global/Documents/Technology-Media-Telecommunications/deloitte-digital-maturity-model.pdf> (Accessed: 28.08.2021)



Table 1 continued

Source	Method name, key assessment method	Indices in the methodology	Positive aspects	Negative aspects
Merzlov I. Yu., Shilova E. V., Sannikova E. A., Sedinin M. A. A comprehensive methodology for assessing the level of digitalization of organizations [27]	A comprehensive methodology for assessing the level of digitalization of organizations	A step-by-step methodology for determining the digitalization of business processes has been developed. Six enlarged business processes are highlighted, each of which is itemized by a number of sub-processes: staff management, production, performance of work, provision of services, marketing, logistics, finance and accounting, general economic activity. A pyramid of the digitalization process has been developed, including five levels (primary, local, partial, complex digitalization; “smart” organization; digital ecosystem. Based on the final data, the sectoral and country level of digitalization can be determined, as well as the corresponding rating for the formation of various types	It is based on the methods of expert assessments and questionnaires. It is easy to understand and count the results	Public access to filling out the questionnaire due to the creation of the site, which can lead to errors in the calculation, as well as the possibility of the questionnaire being filled out by non-specialists from the organization
Babkin A. V., Pestova A. Yu. The assessment of the level of digitalization of an industrial enterprise (Peter the Great St. Petersburg Polytechnic University) [41, 42]	The assessment of the level of digitalization of an industrial enterprise	Labor resources, material and technical support, digital infrastructure of an enterprise, software, financial resources, organizational and managerial indicators / 19 indicators	Complex assessment using the statistical data of an enterprise and average market values for each of the assessed parameters	The complexity of the assessment. There is no comparison with other companies in the industry
Kozlov A. V. Teslia A. B. Digital potential of industrial enterprises: essence, definition and calculation methods [43]	The methodology for determining the digital potential of an industrial enterprise as a tool for managing digital transformation processes at an enterprise (expert assessments + to obtain a numerical assessment of the integral index – digital potential – other models, being more complex, can be used, for example, the parametric entropy method, Saaty method, the method of principal components)	The external environment index, the internal environment index, including 2 subgroups: reflecting the resources at the moment and reflecting the future capabilities of the enterprise for the implementation of digital technologies. 17 indicators	The proposed approach to assessing digital potential allows to analyze not only the current level of digitalization of business processes in an enterprise, but also the possibility of increasing digital potential	Not quite accurate assessment because of practical focus mainly on subjective assessments
MIT Center for Digital Business and Capgemini Consulting*	Digital transformation assessment	Customer experience, operational processes and business models / 9 indices	Relatively small number of indices and available calculations	Difficulty in collecting statistical data for assessment

* MIT Center for Digital Business and Capgemini Consulting. Assessment of digital transformation. URL: https://www.capgemini.com/wp-content/uploads/2017/07/The_Digital_Advantage_How_Digital_Leaders_Outperform_their_Peers_in_Every_Industry.pdf (Accessed: 27.08.2021)



Table 1 continued

Source	Method name, key assessment method	Indices in the methodology	Positive aspects	Negative aspects
Analytical Agency Arthur D. Little. Digital Transformation – How to Become Digital Leader*	Digital transformation index	When calculating the index, 23 indicators are used that characterize the development strategy and leadership; products and services; customer management; transactions and supply chains; corporate services and control; information technologies; workplace and culture	The result of the assessment of the indices allows to determine the level of the company, the efficiency of the transformation, and to predict the result of the company's development. Relatively straightforward calculations due to a small number of indices	Difficulty in collecting statistical data for assessment
KPMG Company. Are you ready for digital transformation? Measuring your digital business aptitude**	Model of digital aptitude assessment	Vision and strategy, digital talents, key digital processes, flexible sources and technologies, leadership – 5 major indices, 23 indices in total	Calibrated Risk Management, Digital Management, Architectural Discipline, Engagement, Agile Architecture, Infrastructure, Social Media, Mobile Interaction, Mobility, Strategic Partnerships, Measurement & Analytics, Optimized Platforms, Agile Development, Interface Design, Talent Development, Skill Optimization, Talent Development, Obtaining Talents, Strategy Implementation, Thought Leadership, Strategy is defined, goals are defined	An example of the application of this assessment has not been found due to the closed nature of the data. One cannot perform a prompt assessment
Global Center for Digital Business Transformation [27]	Digital piano	Business model, organizational structure, employees, processes, IT opportunities, offerings, interaction model	Based on the questions asked in the course of this assessment, the gap between the current state of affairs and the required level in each line can be determined, thus indicating the volume of changes required	Answering questions will be the key aspect. An inaccurate answer to them is equivalent to a fuzzy assessment
Ionology Company. Step by Step Guide to Digital Transformation***	Digital transformations	Strategy and culture, people and customers, processes and innovation, technology, data and analytics	The methodology is focused on the younger generation's interests	There is no total number of assessment indices, only the key lines are singled out. Therefore, there is no way to assess the positive points
National Academy of Sciences and Engineering of Germany. Industry Maturity Index 4.0. Management of the Digital Transformation of Companies. Acatech research***	Acatech Industrie 4.0 Maturity Index	Resources, information systems, culture and organizational structure	The processing of advantages, disadvantages and existing opportunities, the analysis of deficiencies, allowing subsequently to assess the degree of flexibility and continuous development of the established company	Complex methodology for assessment

* Analytical agency Arthur D. Little. Digital Transformation – How to Become Digital Leader. URL: https://www.adlittle.com/sites/default/files/viewpoints/ADL_HowtoBecomeDigitalLeader_02.pdf (Accessed: 05.09.2020)

** KPMG. Are you ready for digital transformation? Measuring your digital business aptitude. URL: <https://assets.kpmg/content/dam/kpmg/pdf/2016/04/measuring-digital-business-aptitude.pdf> (Accessed: 04.09.2021)

*** Ionology. Step by Step Guide to Digital Transformation. URL: <https://www.ionology.com/step-by-step-guide-to-digital-transformation> (Accessed: 05.10.2021)

*** National Academy of Sciences and Technology of Germany. Industry Maturity Index 4.0. Managing the digital transformation of Companies. Acatech research. URL: https://www.acatech.de/wp-content/uploads/2018/03/acatech_STUDIE_rus_Maturity_Index_WEB.pdf (Accessed: 04.09.2020)

Table 1 continued

Source	Method name, key assessment method	Indices in the methodology	Positive aspects	Negative aspects
Komanda-A Company (KMDA). The assessment of strategic transformations in the process of digital transformation*	The assessment of strategic transformations in the process of digital transformation	Customer centricity, collaboration, data, innovation, value, people	Link to strategy. Customer-oriented approach	Offered by the developer for assessment. Lack of any document where one could go through the methodology in detail
DMA Pulse. A digital solution for assessing the potential and dynamics of changes in your company during digital transformation**	Digital maturity assessments	Digital infrastructure, HR and human capital development, product creation and value management, digitalization of business processes, data use, customer experience management	More than 40 blocks of questions of different levels of depth, allowing to identify the areas of underdevelopment and development potential	Lack of any document where one could go through the methodology in detail

* Team-A Company (KMDA). Assessment of strategic transformations in the process of digital transformation. URL: <https://komanda-a.pro/transformation> (Accessed: 02.09.2020)

** DMA Pulse. A digital solution for assessing the potential and dynamics of changes in your company in the process of digital transformation. URL: <https://komanda-a.pro/audit> (Accessed: 09.08.2021)

The stages of implementation of the author methodological toolkit for assessing the level of digital transformation of enterprises (companies) and the industry as a whole are shown in Fig. 3.

Stage I. The approbation of the author methodological toolkit was performed in the context of the oil and gas industry. Annual reports of the selected enterprises (PJSC “Gazprom”, PJSC “NK “Rosneft”, PJSC “Tatneft” and PJSC “Lukoil”) constituted the information base of the research.

The key indices characterizing the level of digitalization and digital transformation were as follows: profit, intangible assets, R&D costs, company market value. To calculate the market value of the company, financial Internet resources⁴⁹ were used as the sources of information concerning the stock quotes and their number.

⁴⁹ Finanz.ru. Share quotes. URL: <https://www.finanz.ru/aktsii> (Accessed: 12.06.2022)

InvestFunds. Independent data source for private investment in Russia. Share quotes. URL: <https://investfunds.ru/stocks/> (Accessed: 12.06.2022)

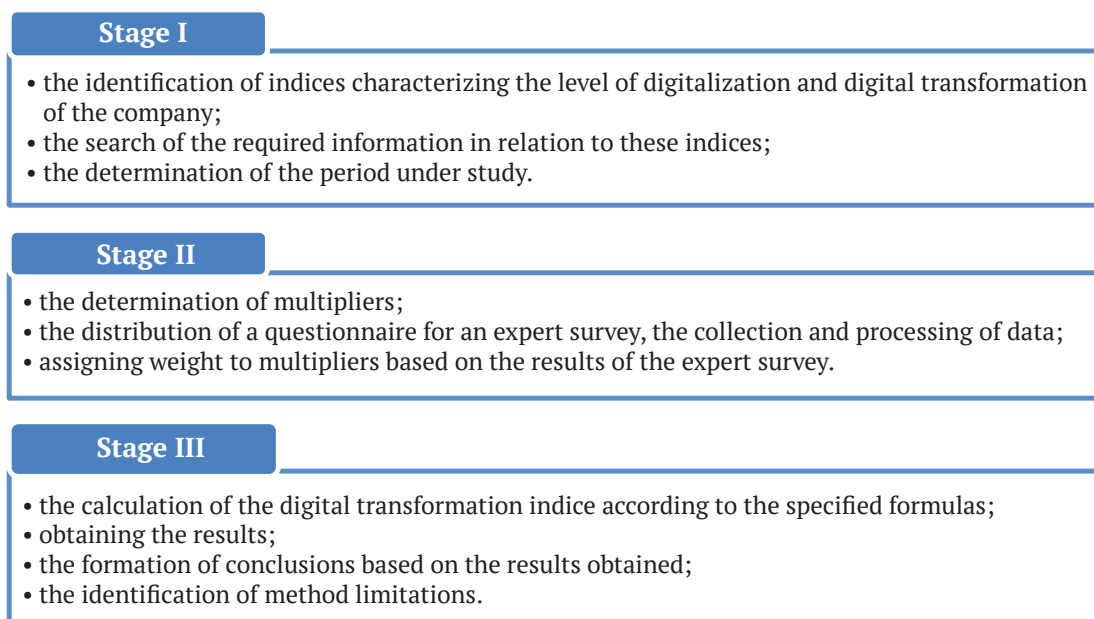


Fig. 3. The stages of implementation and approbation of the author methodology toolkit under the conditions of the oil and gas industry of the Russian Federation



Excluding economically unrepresentative time periods, three periods were selected for the research:

- 2008. The Year of the global economic crisis;
- 2010–2011. The period of recovery, economic rehabilitation;

– 2016–2020. The period of design, development, formation and implementation of digital technologies and platform solutions in the Russian Federation. The period under consideration has been increased from 2 to 4 years due to the extremely rapid development of the line under investigation.

All indices are presented in a comparable form. Some of the indices were missing in the 2008 reports, while another part was reported in dollars, not in rubles. Dollars were converted into rubles at the average rate for each year⁵⁰. Below are the tables for each company with the selected indices. Dashes indicate no publicly available data.

Stage II. The application of the cost approach allowed to distinguish the following multipliers characterizing the level of digitalization and digital transformation:

⁵⁰ Ministry of Finance. Currency Converter. URL: <https://minfin.com.ua/currency/converter/> (Accessed: 12.06.2022)

1. The multiplier of the ratio of intangible assets and the market value of the company

$$A = \frac{HA}{P}, \tag{1}$$

where *HA* stands for intangible assets of the company; *P* stands for the market value of a company, obtained by multiplying the value of a share by the number of shares.

2. The multiplier of the ratio of R&D activities and the market value of the company

$$B = \frac{RDC}{P}, \tag{2}$$

where *RDC* stands for the company’s R&D expenses.

3. The multiplier of the ratio of the net profit of the company and the market value of the company

$$C = \frac{Pt}{P}, \tag{3}$$

where *Pt* stands for net profit of the company.

Thus,

$$DL = (x_1A + x_2B + x_3C)100 \%, \tag{4}$$

where *DL* stands for the indicator of the level of digitalization and digital transformation; *x*₁ stands for the weight of multiplier *A*; *x*₂ stands for the weight of multiplier *B*; *x*₃ stands for the weight of multiplier *C*.

Table 2

Selected indices for PJSC “Gazprom”

Indices	Year							
	2008	2010	2011	2016	2017	2018	2019	2020
Intangible assets, RUB	3.2·10 ⁸	3.7·10 ⁸	3.7·10 ⁸	1.49·10 ¹⁰	2.009·10 ¹⁰	1.93·10 ¹⁰	1.71·10 ¹⁰	1.474·10 ¹⁰
R&D expenses, RUB	2.67·10 ⁹	2.62·10 ⁹	3.2·10 ⁹	2.89·10 ¹⁰	1.61·10 ¹⁰	1.359·10 ¹⁰	1.92·10 ¹⁰	1.807·10 ¹⁰
Net profit, RUB	1.73·10 ¹¹	7.8·10 ¹¹	1.307·10 ¹²	9.516·10 ¹¹	7.143·10 ¹¹	1.456·10 ¹²	1.203·10 ¹²	1.35·10 ¹¹
Share price, RUB	108.6	193.5	171.3	154.55	130.5	153.5	256.4	212.98
Number of shares outstanding, pcs.	2.367·10 ¹⁰	2.367·10 ¹⁰	2.367·10 ¹⁰	2.367·10 ¹⁰	2.367·10 ¹⁰	2.367·10 ¹⁰	2.367·10 ¹⁰	2.367·10 ¹⁰

Table 3

Selected indices for PJSC “NK “Rosneft”

Indices	Year							
	2008	2010	2011	2016	2017	2018	2019	2020
Intangible assets, RUB	1.83·10 ¹⁰	2.3·10 ¹⁰	2.2·10 ¹⁰	5.9·10 ¹⁰	7.5·10 ¹⁰	7.5·10 ¹⁰	6.9·10 ¹⁰	8·10 ¹⁰
R&D expenses, RUB	2.05·10 ⁹	2.9·10 ⁹	8.55·10 ⁹	2.02·10 ¹⁰	2.99·10 ¹⁰	3.21·10 ¹⁰	3·10 ¹⁰	2.68·10 ¹⁰
Net profit, RUB	1.43·10 ¹¹	3.47·10 ¹¹	3.84·10 ¹¹	1.74·10 ¹¹	3.83·10 ¹¹	8.28·10 ¹¹	9.17·10 ¹¹	3.24·10 ¹¹
Share price, RUB	112.34	218.85	214.55	402.8	291.5	432.5	454	435.1
Number of shares outstanding, pcs.	1.0598·10 ¹⁰	1.0598·10 ¹⁰	1.0598·10 ¹⁰	1.0598·10 ¹⁰	1.0598·10 ¹⁰	1.0598·10 ¹⁰	1.0598·10 ¹⁰	1.0598·10 ¹⁰

Table 4

Selected indices for PJSC “Lukoil”

Indices	Year							
	2008	2010	2011	2016	2017	2018	2019	2020
Intangible assets, RUB	$2.42 \cdot 10^{10}$	$4.407 \cdot 10^{10}$	$4.34 \cdot 10^{10}$	$4.313 \cdot 10^{10}$	$4.13 \cdot 10^{10}$	$4.18 \cdot 10^{10}$	$4.31 \cdot 10^{10}$	$5 \cdot 10^{10}$
R&D expenses, RUB	$2.3 \cdot 10^9$	$3.65 \cdot 10^9$	$4.11 \cdot 10^9$	$5.8 \cdot 10^9$	$5.8 \cdot 10^9$	$6.2 \cdot 10^9$	$5.7 \cdot 10^9$	$5.2 \cdot 10^9$
Net profit, RUB	$2.674 \cdot 10^{11}$	$2.743 \cdot 10^{11}$	$3.345 \cdot 10^{11}$	$3.038 \cdot 10^{11}$	$3.994 \cdot 10^{11}$	$6.192 \cdot 10^{11}$	$6.402 \cdot 10^{11}$	$1.52 \cdot 10^{10}$
Share price, RUB	948	1742	1702.5	3449	3345.5	4997	6169	5169.5
Number of shares outstanding, pcs.	$6.93 \cdot 10^8$	$6.93 \cdot 10^8$	$6.93 \cdot 10^8$	$6.93 \cdot 10^8$	$6.93 \cdot 10^8$	$6.93 \cdot 10^8$	$6.93 \cdot 10^8$	$6.93 \cdot 10^8$

Table 5

Selected indices for PJSC “Tatneft”

Indices	Year							
	2008	2010	2011	2016	2017	2018	2019	2020
Intangible assets, RUB	$2.2 \cdot 10^8$	$2 \cdot 10^8$	$1.9 \cdot 10^8$	$4.6 \cdot 10^8$	$8.8 \cdot 10^8$	$1.5 \cdot 10^9$	$1.85 \cdot 10^9$	$2.05 \cdot 10^9$
R&D expenses, RUB	–	$9 \cdot 10^7$	$6 \cdot 10^7$	$6.3 \cdot 10^8$	$6 \cdot 10^8$	$1 \cdot 10^9$	$2.5 \cdot 10^9$	$2.4 \cdot 10^9$
Net profit, RUB	$3.43 \cdot 10^{10}$	$3.89 \cdot 10^{10}$	$5.488 \cdot 10^{10}$	$1.05 \cdot 10^{11}$	$1 \cdot 10^{11}$	$1.98 \cdot 10^{11}$	$1.56 \cdot 10^{11}$	$8.16 \cdot 10^{10}$
Share price, RUB	56	148.7	160.69	427	478.8	737.9	759.7	513.7
Number of shares outstanding, pcs.	$2.18 \cdot 10^9$	$2.18 \cdot 10^9$	$2.18 \cdot 10^9$	$2.18 \cdot 10^9$	$2.18 \cdot 10^9$	$2.18 \cdot 10^9$	$2.18 \cdot 10^9$	$2.18 \cdot 10^9$

It is recommended that the weight of each of the multipliers be determined by an expert survey of specialists in a given field of activity. Within the implementation of the author methodological toolkit, the experts were offered a questionnaire. According to the results of a survey of 35 experts from the Institute of Economics of the Ural Branch of the RAS, the Mining Institute of the Ural Branch of the RAS, Tomsk Polytechnic University, and Tyumen Industrial University, it was established that the weights of multipliers A and B are the same and equal to 0.4 c.u. accordingly, the weight of multiplier C is assigned at the level of 0.2 c.u. The weight was calculated by determining the arithmetic mean. Hence, the formula (4) is as follows:

$$DL = (A \times 0,4 + B \times 0,4 + C \times 0,2)100 \%. \quad (5)$$

Stage III

According to the data obtained at the stage I of the implementation of the author methodological toolkit, Tables 6–9 provide for the calculations and the assessment of the final level of digitalization and digital transformation of the companies in annual terms. There are no values in some cells of the table, and that is associated with the above mentioned factor, namely the closed data, the impossibility of performing the calculation.

In the Russian context, a satisfactory level of digitalization and digital transformation is recommended to consider more than 5 %; if the indicator is below this value, the level is considered unsatisfactory, therefore, the company is not focused on digital development in the long run.

The values of the calculated multipliers and the level of digitalization and digital transformation for PJSC “Gazprom”

Table 6

Multipliers	Year							
	2008	2010	2011	2016	2017	2018	2019	2020
HA / P , c.u.	0.00012	0.00009	0.00009	0.00407	0.00650	0.00531	0.00282	0.00292
RDC , c.u.	0.00104	0.00057	0.00079	0.00790	0.00521	0.00374	0.00316	0.00358
Pt / P , c.u.	0.06729	0.17019	0.32230	0.26009	0.23121	0.40067	0.19819	0.02678
DL , %	1.39	3.43	6.48	5.68	5.09	8.38	4.20	0.80



Table 7

The values of the calculated multipliers and the level of digitalization and digital transformation for PJSC “NK “Rosneft”

Multipliers	Year							
	2008	2010	2011	2016	2017	2018	2019	2020
HA / P, c.u.	0.01537	0.00992	0.00968	0.01382	0.02428	0.01636	0.01434	0.01735
RDC, c.u.	0.00172	0.00125	0.00376	0.00473	0.00968	0.00700	0.00623	0.00581
Pt / P, c.u.	0.12011	0.14961	0.16888	0.04076	0.12397	0.18064	0.19058	0.07026
DL, %	3.09	3.44	3.91	1.56	3.84	4.55	4.63	2.33

Table 8

The values of the calculated multipliers and the level of digitalization and digital transformation for PJSC “Lukoil”

Multipliers	Year							
	2008	2010	2011	2016	2017	2018	2019	2020
HA / P, c.u.	0.03684	0.03651	0.03679	0.01805	0.01782	0.01207	0.01008	0.01396
RDC, c.u.	0.00350	0.00302	0.00348	0.00243	0.00250	0.00179	0.00133	0.00145
Pt / P, c.u.	0.40704	0.22725	0.28360	0.12713	0.17231	0.17884	0.14978	0.00424
DL, %	9.75	6.13	7.28	5.00	3.36	4.26	4.13	3.45

Table 9

The values of the calculated multipliers and the level of digitalization and digital transformation for PJSC “Tatneft”

Multipliers	Year							
	2008	2010	2011	2016	2017	2018	2019	2020
HA / P, c.u.	0.00180	0.00062	0.00054	0.00049	0.00084	0.00093	0.00112	0.00183
RDC, c.u.	–	0.00028	0.00017	0.00068	0.00058	0.00062	0.00151	0.00214
Pt / P, c.u..	0.28113	0.12016	0.15676	0.11265	0.09586	0.12285	0.09425	0.07291
DL, %	–	2.44	3.16	2.30	1.97	2.52	1.99	1.62

According to Tables 6–9, a final table of the levels of digitalization and digital transformation was compiled for each selected company and the industry as a whole (Table 10).

Conclusions: based on the obtained screening of the companies and the results of the approbation of the author methodological toolkit for assessing the level of digitalization and digital transformation (Table 10, Fig. 4), we can conclude that, in general, the situation with digital transformation of the oil and gas industry of the Russian Federation is unsatisfactory. The rates of change in the level of digitalization and digital transformation of the selected companies for the considered time periods are shown in Fig. 4. PJSC “Gazprom” exhibits the most stable and satis-

factory development dynamics. PJSC “Lukoil” has a similar trend, but only in 2008, 2010 and 2011, after 2016 the index decreases to an unsatisfactory level. Besides, during the period of development and implementation of digital technologies and platform solutions in the Russian Federation, a trend towards increasing digitalization and digital transformation can be observed at PJSC “NK “Rosneft”.

The lowest values of the level of digitalization and digital transformation in the considered time periods were recorded at PJSC “Tatneft”. Upon that, each of the selected companies declares an ever-increasing rates of digitalization of all processes in its reports. Based on the data obtained, the observed situation can be characterized either by a slowdown in the rate

of implementation of digitalization and digital transformation processes due to the already achieved high level, or by the deterioration of the situation and the presence of not entirely reliable information in the reports of the companies. The year 2020 is characterized by a slowdown in growth in all companies due to the COVID-19 pandemic. Although it was noted in work [8] that companies with a high level of implementation of digital processes suffered the least from this pandemic.

Based on Fig. 4, we can present the following ranking of industry companies for the implementation of digital processes in their activities: PJSC “Gazprom” and PJSC “Lukoil” are among the leaders in terms of digitalization and digital transformation, PJSC “NK “Rosneft” is in second place and PJSC “Tatneft” closes the rating.

Conclusions

The developed author methodological toolkit for assessing the level of digitalization and digital transformation allows to perform an express analysis of both the enterprise (company) and the industry as a whole with regard to introducing digital processes and identifying their role in the strategic development. However, like any other toolkit, the methods have a number of minor limitations. Firstly, the methodological toolkit provides for the application of major key indices of digital transformation (intangible assets, R&D costs and net profit), but the narrower ones, for example, such as the number of patents in the field of digitalization, the introduction and use of digital twins of fields, etc. are not taken into account. The reasoning behind this is that the purpose was not to assess the digital platform, nor to consider

Table 10

A final table of the digitalization levels and digital transformation was compiled for each selected company and the industry as a whole, %

Company name	Year								The average DT for the analyzed periods
	2008	2010	2011	2016	2017	2018	2019	2020	
PJSC “Gazprom”	3.01	6.77	11.56	4.87	5.09	6.64	5.30	0.87	5.51
PJSC “NK “Rosneft”	3.09	3.44	3.91	1.56	3.84	4.55	4.63	2.33	3.41
PJSC “Tatneft”	–	2.44	3.16	2.30	1.97	2.52	1.99	1.62	2.28
PJSC “Lukoil”	9.75	6.13	7.28	3.36	4.26	4.13	3.45	0.70	4.88
Industry level	3.9625	4.695	6.4775	3.0225	3.79	4.46	3.8425	1.38	4.02

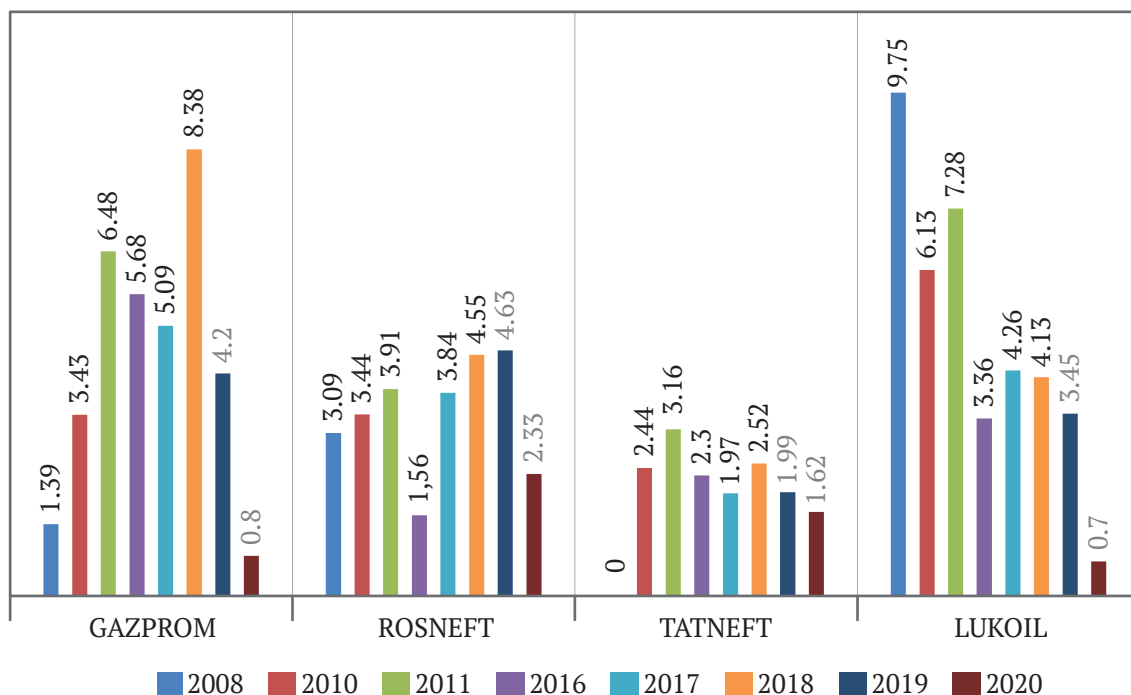


Fig. 4. The dynamics of changes in the level of digitalization and digital transformation of each company, %



the level of digitalization and digital transformation of the companies' suppliers and consumers. Secondly, the methodological toolkit is very dependent on the openness and completeness of the collected data, despite a small number of indices. Thirdly, there is no possibility of assessing the companies that are not listed on the stock exchange. Fourthly, the weight of the multipliers was determined on the basis of an expert survey, the results of which largely depend on the experts.

It has been established that the industry leaders of the Russian Federation in the period from 2016 to 2020 in terms of the level of digitalization and digital transformation range in the following order from the most advanced to the least advanced: PJSC "Gazprom" is in the first place ($DL_{av} - 4.82\%$); PJSC "NK "Rosneft" is in the second place ($DL_{av} - 3.38\%$); PJSC "Lukoil" is in the third place ($DL_{av} - 3.18\%$); PJSC "Tatneft" is in the fourth place ($DL_{av} - 2.08\%$). According to Table 10, the values were obtained by determining the arithmetic average of the levels of digitalization (DL_{av}) and digital transformation for each company for the periods under review.

The average index of the digitalization level and digital transformation by industry over the past 5 years is 3.36 %, which is extremely unsatisfactory in terms of a comprehensive digital transformation.

A further line of the research is observed in assessing and comparing the levels of digitalization and digital transformation of foreign oil and gas industries of the leading oil and gas producing countries with the domestic ones applying the author methodological toolkit.

Thus, *the goal* of this research has been achieved, since the system for managing digitalization and digital transformation of the oil and gas industry has been improved through the development of author methodological toolkit for assessing the level of digitalization and digital transformation of both an individual enterprise and the oil and gas industry as a whole, based on a comparative analysis of existing methods.

The research provides for the analysis of the theoretical foundations of digitalization and digital transformation; foreign and domestic general, industry and production methodological toolkits (for individual enterprises and companies), methodological approaches, recommendations and methods for assessing digitalization, digital transformation have been studied and systematized; the current state of the digital transformation of the oil and gas industry has been identified by approbation of the author methodological toolkit for assessing the level of digitalization and digital transformation.

References

1. Gordina V. *Difficulties in exploration oil projects in the Arctic*. URL: <http://pro-arctic.ru/17/04/2018/resources/31616#read> (Accessed: 12.06.2022)
2. Nasibulin M.M. Fuel and energy complex of Russia: digitization. *Neftegaz.RU*. 2020;(4):19–24. (In Russ.) URL: <https://magazine.neftegaz.ru/upload/iblock/59c/59ce2d2f0ca1e25d1f29c1daadebb2c4.pdf> (Accessed: 12.06.2022)
3. Kashirsky A.S., Kirichenko Y.V. World ocean as the last reserve of mankind. *Mining Science and Technology (Russia)*. 2017;(1):67–76. (In Russ.) <https://doi.org/10.17073/2500-0632-2017-1-67-74>
4. Alifirova E. *Gazprom Neft created the industry's first digital model of the Achimov formation*. URL: <https://neftegaz.ru/news/Geological-exploration/197900-gazprom-neft-sozdala-pervuyu-v-otraslitsifrovuyu-model-achimovskoy-tolshchi/> (Accessed: 12.06.2022)
5. Kovalenko A. Oil with intelligence. *Expert Ural*. 2018;(38). (In Russ.) URL: <http://www.assoneft.ru/activities/press-centre/tek/5164/> (Accessed: 12.06.2022)
6. Khamidullin M., Sakharova K. Digital transformation of investment activity in PJSC Tatneft. *Neftegaz.RU*. 2021;(8):28–33. (In Russ.) URL: <https://magazine.neftegaz.ru/articles/tsifrovizatsiya/694505-tsifrovaya-transformatsiya-investitsionnoy-deyatelnosti-v-pao-tatneft/> (Accessed: 12.06.2022)
7. Ileby M., Knutsen E. Data-driven remote condition monitoring optimizes off-shore maintenance, reduces costs. *WorldOil*. 2017:60–62. URL: <https://assets.siemens-energy.com/siemens/assets/api/uuid:d8274ee1-a0ea-4858-b203-9b6e4ea33b9a/wo-1217-offshore-technology.pdf> (Accessed: 12.06.2022)
8. Hawash B., Abuzawayda Y.I., Mokhtar U.A. et al. Digital transformation in the oil and gas sector during COVID-19 Pandemic. *International Journal of Management*. 2020;11(12):725–735. <https://doi.org/10.34218/IJM.11.12.2020.067>



9. Daneeva Yu., Glebova A., Daneev O., Zvonova E. Digital transformation of oil and gas companies: energy transition. *Advances in Economics, Business and Management Research*. 2020;(148):199–205. <https://doi.org/10.2991/aebmr.k.200730.037>
10. Larchenko L.V., Vorobeva L.G. Oil and gas complex of Russia: development scenario. *Innovations*. 2020;(7):12–18. (In Russ.) <https://doi.org/10.26310/2071-3010.2020.261.7.003>
11. Martynov V.G., Koshelev V.N., Mayer V.V., Tumanov A.A. Oil and gas education in Russia: yesterday, today, tomorrow. *Vysshie Obrazovanie v Rossii*. 2021;30(8–9):144–157. (In Russ.) <https://doi.org/10.31992/0869-3617-2021-30-8-9-144-157>
12. Martynov V.G., Koshelev V.N., Dushin A.V. Modern challenges for oil and gas education. *Vysshie Obrazovanie v Rossii*. 2021;29(12):9–20. (In Russ.) <https://doi.org/10.31992/0869-3617-2020-29-12-9-20>
13. Petrov V.L. Analytical review of the training system for mining engineers in Russia. *Mining Science and Technology (Russia)*. 2022;7(3):240–259. <https://doi.org/10.17073/2500-0632-2022-3-240-259>
14. Vercheba A.A. Personnel training for the mining and geological sector of Russia. *Mining Science and Technology (Russia)*. 2021;6(2):144–153. <https://doi.org/10.17073/2500-0632-2021-2-144-153>
15. Vavenkov M.V. VR/AR technologies and staff training for mining industry. *Mining Science and Technology (Russia)*. 2022;7(2):180–187. <https://doi.org/10.17073/2500-0632-2022-2-180-187>
16. Vasilkov A. *Digitalization of the oil and gas industry*. URL: <https://dx.media/articles/how-it-works/tsifrovaya-transformatsiya-neftegazovoy-otrasli/> (Accessed: 12.06.2022)
17. Altukhov A.V., Gostilovich A.O., Kashkin S. Yu. Legal aspects of digital platforms for the sharing consumption economy. *Economics and Management*. 2021;27(2):102–110. (In Russ.) <https://doi.org/10.35854/1998-1627-2021-2-102-110>
18. Aturin V.V., Moga I.S., Smagulova S.M. Digital transformation management: Scientific approaches and economic policy. *Upravlenets*. 2020;11(2):67–76. (In Russ.) <https://doi.org/10.29141/2218-5003-2020-11-2-6>
19. Tapscott D. *The digital economy by Don tapscott. Promise and Peril in the age of networked intelligence*. New York: McGraw-Hill; 1995. 376 p.
20. Osterwalder A., Pigneur Y., Tucci C.L. Clarifying business models: origins, present, and future of the concept. *Communications of the Association for Information Systems*. 2005;16(1):1–26. <https://doi.org/10.17705/1CAIS.01601>
21. Babkin A.V., Burkaltseva D.D., Vorobey D.G., Kosten Yu.N. Formation of digital economy in russia: essence, features, technical normalization, development problems. *St. Petersburg State Polytechnical University Journal. Economics*. 2017;10(3):9–25. (In Russ.) URL: https://economy.spbstu.ru/userfiles/files/articles/2017/3/01_babkin_burkaltseva_kosten_vorobev.pdf
22. Keshelava A.V., Budanov V.G., Dmitrov I.D. et al. *Introduction to the Digital Economy. On the threshold of the “digital” future. Book 1*. VNIIGeosystem; 2017. 28 p. (In Russ.) URL: <https://spkurdyumov.ru/uploads/2017/07/vvedenie-v-cifrovuyu-ekonomiku-na-poroze-cifrovogo-budushhego.pdf>
23. Kokh L.V., Kokh Yu.V. Analysis of existing approaches to measurement. *St. Petersburg State Polytechnical University Journal. Economics*. 2019;12(4):78–89. (In Russ.) <https://doi.org/10.18721/JE.12407>
24. Plotnikov V.A. Digitalization of production: the theoretical essence and development prospects in the Russian economy. *Izvestiya Sankt-Peterburgskogo Gosudarstvennogo Ekonomicheskogo Universiteta*. 2018;(4):16–24. (In Russ.) URL: https://unecon.ru/sites/default/files/izvestiya_no_4-2018.pdf
25. Suloeva S.B., Martynatov V.S. The features of the digital transformation of oil and gas enterprises. *Organizator Proizvodstva*. 2019;27(2):27–36. (In Russ.) <https://doi.org/10.25987/VSTU.2019.26.70.003>
26. Apasov R.T., Chameev I.L., Varavva A.I. et al. Integrated modeling: a tool to improve quality of design solutions in development of oil rims of multi-zone oil-gas-condensate fields. *Oil Industry Journal*. 2018;(12):46–49. (In Russ.) <https://doi.org/10.24887/0028-2448-2018-12-46-49>
27. Merzlov I. Yu., Shilova E.V., Sannikova E.A., Sedinin M.A. Comprehensive methodology for assessing the level of digitalization in the organizations. *Ekonomika, Predprinimatelstvo i Pravo*. 2020;10(9):2379–2396. (In Russ.) <https://doi.org/10.18334/epp.10.9.110856>



28. Soloveva I. P., Kupriianova M. V. A review of foreign and national approaches for evaluating the level of digitization. In: *II International Scientific Conference "Actual Problems of Management, Economics and Economic Security"*. September 28, 2020, Kostanay. Cheboksary: Publ. House "Sreda"; 2020. Pp. 125–130. (In Russ.) <https://doi.org/10.31483/r-96267>
29. Gileva T. A. Digital maturity of the enterprise: methods of assessment and management. *Bulletin USPTU. Science, Education, Economy. Series Economy*. 2019;(1):38–52. (In Russ.) <https://doi.org/10.17122/2541-8904-2019-1-27-38-52>
30. Lapidus L. V. Analysis of methods for assessing the level of digitalization in the context of priority tasks for Russian regions. In: *Scientific and Practical Conference "Regional Dimension of the Digital Economy"*. April 23, 2019, Moscow. Pp. 6–9. URL: http://larisalapidus.ru/wp-content/uploads/2020/04/Lapidus_LV_LCh_2019_tezisyi-1-1.pdf (Accessed: 12.06.2022)
31. Kupriianova M. V., Simikova I. P. Methodology of evaluating the level of digitalization in the sphere of industrial production. In: *All-Russian Scientific and Practical Conference with International Participation "Law, Economics and Management: Topical Issues"*. December 13, 2019, Cheboksary. Cheboksary: Publ. House "Sreda"; 2019. Pp. 28–34. (In Russ.) <https://doi.org/10.31483/r-74149>
32. Potetetnko S. V. *Assessment of the level of digitalization of enterprises (organizations) and industries*. Belarus. JSC "Giprosvyaz". URL: https://www.itu.int/en/ITU-D/Regional-Presence/CIS/Documents/Events/2020/03_Minsk/Presentations/ITU%20Workshop%204%20March%202020%20-%20Sergey%20Potetenko.pdf (Accessed: 26.08.2021)
33. Kuklina E. A., Mitselovskaya O. S. Methodological approach in assessing the level of innovative development of an enterprise (on the example of housing and communal services sphere). *Administrative Consulting*. 2020;(6):110–122. (In Russ.) <https://doi.org/10.22394/1726-1139-2020-6-110-122>
34. Ledneva O. V. Statistical study of the Russian economy digitalization level: problems and prospects. *Voprosy Innovatsionnoy Ekonomiki*. 2021;11(2):455–470. (In Russ.) <https://doi.org/10.18334/vinec.11.2.111963>
35. Istomina Ye. A. Methodology assessment of trends in the digital economy of industry. *Bulletin of Chelyabinsk State University*. 2018;(12):108–116. (In Russ.) <https://doi.org/10.24411/1994-2796-2018-11212>
36. Yashin S. N., Shchekoturova S. D. Applying the methodology for assessment of enterprise innovative development efficiency: evidence from PAO Ruspolymet. *Finance and Credit*. 2016;(47):27–46. (In Russ.) URL: <https://www.fin-izdat.ru/journal/fc/detail.php?ID=70222> (Accessed: 12.06.2022)
37. Kokhanova V. S. Fuzzy logic apparatus as a tool for assessing the effectiveness of digitalization of a company. *Vestnik Universiteta*. 2021;(2):36–41. (In Russ.) <https://doi.org/10.26425/1816-4277-2021-2-36-41>
38. Brusakova I. A. Methods and models for estimating the maturity of the innovation structure. *Management Sciences*. 2019;9(3):56–62. (In Russ.) <https://doi.org/10.26794/2304-022X-2019-9-3-56-62>
39. Zakharova E. V., Mityakova O. I. Assessment of the innovative potential of the enterprise taking into account the digitalization of the economy. *Voprosy Innovatsionnoy Ekonomiki*. 2020;10(3):1653–1666. (In Russ.) <https://doi.org/10.18334/vinec.10.3.110601>
40. Mityakova O. I. Evaluation of the innovative potential of an industrial enterprise. *Finance and Credit*. 2004;(13):69–74. (In Russ.)
41. Babkin A. V., Pestova A. Yu. Algorithm of the assessment of level of digitalization of the industrial enterprise. In: Babkin A. V. (ed.) *Collection of Proceedings of the Scientific and Practical Conference with Foreign Participation "Digital Transformation of the Economy and Industry"*. June 20–22, 2019, St. Petersburg. St. Petersburg: POLYTECH-PRESS; 2019. Pp. 683–680. <https://doi.org/10.18720/IEP/2019.3/74>
42. Babkin A. V., Pestova A. Yu. Indicators for assessing the level of digitalization of an industrial enterprise. In: *Materials of the XIV International Scientific-Practical Conference "Actual Problems of Development of Economic Entities, Territories and Systems of Regional and Municipal Government"*. June 01–02, 2019, Kursk. Kursk: Southwestern State University. 2019;(3):38–41.
43. Kozlov A. V., Teslya A. B. Digital potential of industrial enterprises: essence, determination and calculation methods. *Transbaikal State University Journal*. 2019;25(6):101–110. (In Russ.) <https://doi.org/10.21209/2227-9245-2019-25-6-101-110>



Information about the authors

Vera V. Yurak – Cand. Sci. (Econ.), Associate Professor, Senior Researcher, Institute of Economics of the Urals Branch of the Russian Academy of Sciences; Associate Professor of the Department of Economics and Management, Ural State Mining University, Yekaterinburg, Russian Federation; ORCID [0000-0003-1529-3865](https://orcid.org/0000-0003-1529-3865), Scopus ID [57190411535](https://scopus.com/authid/detail.url?authorID=57190411535), ResearcherID [J-7228-2017](https://orcid.org/J-7228-2017); e-mail vera_yurak@mail.ru

Irina G. Polyanskaya – Cand. Sci. (Econ.), Associate Professor, Head of the Sector, Scientific Secretary, Institute of Economics of the Urals Branch of the Russian Academy of Sciences; Associate Professor of the Department of Economics and Management, Ural State Mining University, Yekaterinburg, Russian Federation; ORCID [0000-0002-0073-2821](https://orcid.org/0000-0002-0073-2821), Scopus ID [55764050500](https://scopus.com/authid/detail.url?authorID=55764050500); e-mail irina-pol2004@mail.ru

Alexander N. Malyshev – Economist, Institute of Economics of the Urals Branch of the Russian Academy of Sciences; Laboratory Researcher of the Research Laboratory for the Reclamation of Disturbed Lands and Man-Made Objects, Ural State Mining University, Yekaterinburg, Russian Federation; ORCID [0000-0002-3104-1687](https://orcid.org/0000-0002-3104-1687), Scopus ID [57223099993](https://scopus.com/authid/detail.url?authorID=57223099993); e-mail malyshev.k1b@gmail.com

Received 12.08.2022

Revised 13.10.2022

Accepted 15.12.2022